THE DESIGN AND SYNTHESIS OF GROUP VII-BASED MOLECULAR CATALYSTS FOR CO_2 REDUCTION

by

CHARLES JOHN STANTON III

(Under the Direction of George Majetich and Henry Schaefer)

ABSTRACT

The efficient chemical conversion of carbon dioxide (CO_2) to useful fuels remains an unsolved and intriguing scientific problem. One promising approach that has emerged in the past 30 years is to leverage electrocatalysts in the conversion of CO_2 to commodity chemicals. If the requisite electrons for this process are obtained from renewable sources (e.g., solar, wind, hydroelectric, etc.), a carbon-neutral process may be envisioned. The feasibility of large-scale systems that can facilitate electrocatalytic conversion depends on the development of active, selective, and affordable catalysts. Many electrocatalysts have been developed that can mediate these processes, including heterogeneous and homogenous transition-metal compounds. In the latter group, several first-row transition metal catalysts have been reported with manganese, iron, cobalt, nickel and copper metal centers. Recent work focused on Mn(I)-centered catalysts is discussed here. Utilizing the extensively-investigated MnBr(2,2'-bipyridine)$(CO)_3$ system as a template, several modifications within the primary coordination sphere have recently been reported, which include: 1) replacement of one pyridine in the 2,2'-bipyridine (bpy) backbone of MnBr(bpy)$(CO)_3$ with an *N*-heterocyclic carbene (NHC) moiety; 2) substitution of the axial

bromine ligand with other pseudo-halogen ligands, including CN and NCS; and 3) modulation of the ligand π-acidity. The impact and efficacy of these modifications is reviewed.

INDEX WORDS: Carbon Dioxide, Carbon Monoxide, Electrocatalyst, *N*-Heterocyclic Carbene, Manganese, Catalyst, Green Chemistry

THE DESIGN AND SYNTHESIS OF GROUP VII-BASED MOLECULAR CATALYSTS FOR CO_2 REDUCTION

by

CHARLES JOHN STANTON III

BS, University of Florida, 2000

MS, University of Georgia, 2004

A Dissertation Submitted to the Graduate Faculty of The University of Georgia in Partial Fulfillment of the Requirements for the Degree

DOCTOR OF PHILOSOPHY

ATHENS, GEORGIA

2016

THE DESIGN AND SYNTHESIS OF GROUP VII-BASED MOLECULAR CATALYSTS FOR CO_2 REDUCTION

by

CHARLES JOHN STANTON III

Major Professors:	George Majetich Henry Schaefer III
Committee:	Jay Agarwal Robert Phillips Vladimir Popik

Electronic Version Approved:

Suzanne Barbour
Dean of the Graduate School
The University of Georgia
December 2016

DEDICATION

For my Family: Nicole, Maximillian, Amelia, Samuel, Janet, Charles, Matthew, Steven, Robert, Diana, Noreen, and Pepper.

ACKNOWLEDGEMENTS

To Nicole, my Mom, my brothers, my children and Noreen, I thank you for your inspiration, encouragement and love throughout both my academic and non-academic pursuits. To Robert and Diana, I appreciate your guidance, and for being positive role models for me to aspire to. I also acknowledge Mike and Geza for their unwavering support and unconditional friendship throughout the past ten years. Without the help and love from these friends and family, none of this would have been possible.

To my undergraduate research advisor, Dr. Tomas Hudlicky, thank you for providing the opportunity to begin learn synthetic organic chemistry. I am also grateful to my master's advisor, Dr. Geert Jan Boons for the many opportunities and help you provided while I was in your laboratory. To my committee members, Drs. Robert Phillips and Vladimir Popik, I appreciate your time and mentorship. To Dr. Eric Ferreira, thank you for always making the time to meet with me, and for allowing me to learn alongside your students. I also thank the many faculty and staff members at the University of Georgia who supported me over the past four years: Dr. I. Jon Amster, Dr. John Stickney, Dr. Ryan Hili, Dr. Jeff Urbauer, Dr. Richard Hubbard, Dr. Norbert Pienta, Dr. Pingrong Wei, Ms. Lauren Bowman, Ms. Sybil Zimmerman, Ms. Kathryn Juras, and Ms. Kristie Huff. To my fellow friends and colleagues that have been in and out of the trenches with me, I wish you the best: Ms. Delaney Hook, Ms. Apoorva Srivastava, Ms. Roshini Ramachandran, Dr. Brian Knight, Dr. Dewey Sutton, Dr. Tom Irvin, Dr. Suzie Stevenson, Mr. Christopher McNitt, Mr. Josh Valencia, Mr. Phil Knutson, Mr. Francisco Sarabia, Dr. Khoi Huynh, Mr. Anthony Prudden, Mr. Jonathon Vandezande, Mr. Jeff Costello, Ms. Sheneika Jackson, Ms.

Cailen McCloskey, Mr. Jake Rothbaum and Dr. Qiankun Li.

To my advisors, Dr. Schaefer and Dr. Majetich; I am indebted to you for your continuous teaching and support as I pursued my Ph.D. I am also extremely grateful for the financial support you provided for me so that I could efficiently spend my time pursuing chemistry with no distractions. Thank you for allowing me to be an independent researcher, and for your ever-helpful guidance as I shifted research topics.

Lastly, I would like to acknowledge the person who has influenced me the most while at UGA, Dr. Jay Agarwal. In terms of science and teaching, I have met few people that possess comparable passion and motivation. I will treasure our time solving problems together (both chemistry and non-chemistry), many of which I would have been unable to solve alone. Thank you for your daily inspiration to be a better chemist, a more productive collaborator, and a stronger problem-solver – I am honored to have you as a friend, and as part of my family.

TABLE OF CONTENTS

Page

LIST OF TABLES

Page

LIST OF FIGURES

Page

LIST OF SCHEMES

Page

CHAPTER 1

INTRODUCTION

CURRENT ENERGY DEMAND AND FUTURE OUTLOOK

Energy consumption has significantly increased with the advancement of society; it is projected to double by 2050 and triple by 2100. As a result, scientists have been presented with a challenging goal that will impact generations to come: develop new, green technologies for the storage of energy. Indeed, several carbon-neutral technologies are being explored to accommodate future energy demands, including wind, nuclear, geothermal, solar, and hydroelectric.[1, 2] However, these solutions are subject to inconsistent input that is difficult to mate with fluctuating demand. Nonetheless, these resources are plentiful and systems able to harness and convert these renewable sources to energy are becoming more affordable.[1] Despite these efforts, the combustion of fossil fuels remains a major source of present-day energy,[3] leading to an alarming increase in the amount of atmospheric CO_2. Therefore, reducing the production of CO_2 and/or converting it to useful materials would impact the global carbon balance.[4]

Carbon dioxide (CO_2) is a fully oxidized form of carbon and a thermodynamically stable molecule that is produced by both natural (respiration) and artificial processes, as highlighted above.[4, 5] Ideally, the CO_2 produced by artificial processes is balanced by plant consumption, resulting in a constant atmospheric CO_2 concentration.[6] Unfortunately, industrial activities and urban development have disrupted this balance; production outpaces fixation to a large degree. To make matters worse, CO_2 also functions as a greenhouse gas. Specifically, it raises the atmospheric

temperature by efficiently absorbing incident solar radiation.[7] The impact of this effect is grievous, contributing to polar ice cap reduction, rising sea levels, and increased precipitation.[8] Thus, robust systems that chemically reduce CO_2 to lower the concentration of this principle greenhouse gas is a major environmental objective for the 21st century. Note that, commercial interest also exists due to the low material cost and abundance of CO_2.

The transformation of CO_2 requires a large amount of energy because of its inherent inertness. The electrochemical reduction of CO_2 is a potentially viable method for energy storage by replacing C−O bonds with C−H and C−C bonding.[9] In this model CO_2 can be converted into useful fuels and chemical feedstocks using an electrical bias. Since the requisite electricity may be obtained from renewable sources, including solar, wind, nuclear, and hydroelectric energy, a carbon-neutral process may be realized.[2, 6, 10]

$$CO_2 + 2H^+ + 2e^- \longrightarrow CO + H_2O \qquad E^0 = -0.53\ V \quad (E1.1)$$

$$CO_2 + 2H^+ + 2e^- \longrightarrow HCO_2H \qquad E^0 = -0.61\ V \quad (E1.2)$$

$$CO_2 + 4H^+ + 4e^- \longrightarrow HCHO + H_2O \qquad E^0 = -0.53\ V \quad (E1.3)$$

$$CO_2 + 6H^+ + 6e^- \longrightarrow CH_3OH + H_2O \qquad E^0 = -0.38\ V \quad (E1.4)$$

$$CO_2 + 8H^+ + 8e^- \longrightarrow CH_4 + 2H_2O \qquad E^0 = -0.24\ V \quad (E1.5)$$

$$CO_2 + e^- \longrightarrow CO^{\bullet -} \qquad E^0 = -1.90\ V \quad (E1.6)$$

Table 1.1: Thermodynamic Potentials for Various CO_2 Reduction Products (pH 7 in aqueous solution vs NHE, 25 ˚C, 1 atmosphere gas pressure, and 1 M for the other solutes).

The reduction of CO_2 to "synthesis gas" (CO/H_2) is more favorable when proton-coupled, multi-electron steps are employed rather than single electron reductions, as thermodynamically

less stable molecules are formed (see Table 1.1, E1.1-E1.6).[5, 11, 12] Once CO_2 and H_2O have been converted to CO and H_2, the "syn gas" can be utilized in well-developed Fischer-Tröpsch technologies to make plastics, waxes and oils.[5]

The feasibility of large-scale systems that can facilitate the electrochemical reduction of CO_2 to useful chemicals depends on the development of active, selective, and affordable catalysts.[10] Many electrocatalysts have been developed that can help promote these processes, ranging from heterogeneous metals or alloys to homogenous transition-metal complexes..[2, 6, 10, 13] However, these two catalyst classes generally have different reaction mechanisms and require distinct electrochemical cell designs and experimental protocols. The focus of this dissertation is the synthesis and design of group-VII molecular catalysts that can be employed as electrocatalysts for the reduction of CO_2 to carbon monoxide (CO). To this end, a literature summary of group-VII electrocatalysts is presented.

GROUP VII-ELECTROCATALYSTS: THE *fac*-[ReX(bpy-R)(CO)$_3$] FAMILY

The most commonly explored electrocatalysts for CO_2 reduction are based on transition-metals. These metals often possess partially filled *d*-orbitals that facilitate CO_2 bonding,[6] and a myriad of accessible redox couples. Of known homogenous catalysts, the *fac*-ReCl(bpy)(CO)$_3$ (bpy = 2,2′-bipyridine) system reported by Hawecker, Lehn and Ziessel in 1984 (Figure 1.1) is among the most efficient for CO_2 reduction to CO.[14] The cyclic voltammetry (CV) of *fac*-[ReCl(bpy)(CO)$_3$] (*fac* = *facial*) displays two one-electron reductions spaced 390 mV apart; the first appears at −1.34 V vs. saturated calomel electrode (SCE), while the second occurs at −1.73 V vs. SCE.[14] A Faradiac efficiency greater than 90% was reported, with excellent selectivity for CO_2 reduction over the reduction of protons to H_2, even in the presence of water.[14] These seminal results

led to further work on ReX(diim)$(CO)_3$-type electrocatalysts (diim = diimine), including many contributions by Meyer,[15-18] Deronzier,[19-21] Abruña,[22, 23] Fujita,[24-26] Ishitani,[27] Wong,[28] and Kubiak.[10, 29-31] Highlights of these studies are discussed in the following sections.

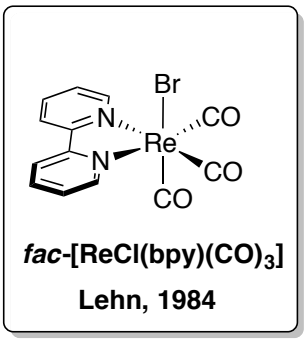

Figure 1.1: The *fac*-[ReCl(bpy)$(CO)_3$] System[14]

Meyer *et al.* investigated the electrochemical reduction of CO_2 using *fac*-ReCl(bpy)$(CO)_3$ and reported two reductions waves in acetonitrile (CH_3CN).[17] The first reduction was described to be quasireversible, leading to electron loading in the π* molecular orbital of the bipyridine ligand. The second reduction involves electron addition to Re center, which results in the loss of chloride and forms anion, $[Re(bpy)(CO)_3]^-$. When bulk electrolysis of ReCl(bpy)$(CO)_3$ was run at the first reduction potential (*ca.* −1.55 V vs SCE) in CH_3CN saturated with CO_2, CO and carbonate (CO_3^{2-}) were observed as the products. When the bulk electrolysis of either ReCl(bpy)$(CO)_3$ or $[Re(bpy)(CO)_3]_2$ was run past the metal-based reduction (i.e., at second reduction potential, ca. −1.8 V vs SCE), CO was found to be the primary product, with a small amount of tributylamine *N*-(*n*-Bu_3) also formed.

Results from the electrochemical studies by Meyer and co-workers suggest that ReCl(bpy)$(CO)_3$ can reduce CO_2 by two different routes. The one-electron pathway can proceed after the first reduction, resulting in a reductive disproportionation of CO_2 to yield CO and CO_3^{2-}.

The two-electron pathway can be accessed at the second reduction, where catalysis is observed to be much faster. Meyer postulated that an oxide acceptor (i.e., a proton) was necessary for the two-electron pathway, and previous work by Hadai and co-workers[32] and Meyer and co-workers[33] has indicated that the amine [i.e., *N*-(*n*-Bu_3)] generated during electrocatalytic CO_2 reduction is a result of the Hofmann degradation of the quaternary ammonium salt used as supporting electrolyte, tetrabutylammonium hexafluorophosphate (TBAH).

In 1998, Wong *et al.* examined the effect of four weak Brønsted acids on the electroreduction of CO_2 catalyzed by [ReCl(bpy)$(CO)_3$(py)](OTf) (OTf = CF_3SO_3): H_2O, methanol (MeOH), phenol (PhOH), and 2,2,2-trifluoroethanol (TFE).[28] Previous discussed studies on the electrocatalytic reduction of CO_2 have focused on the efficiency of the metal catalysts; Wong's study focused on the synergistic action of the metal catalysts with "co-catalysts". The addition of Brønsted acids enhanced the rate of the catalytic process and improved the lifetime of the catalyst. The efficiency of the reduction of CO_2 improved as the acidity of the Brønsted acid increased; the acids with lower pK_as (i.e., TFE and phenol, ca. 12.5 and 10, respectively) had the greatest effect and required a lower concentration to achieve the maximum effect. Although the acidity of water and methanol is comparable (i.e., the pK_a for water and methanol is 15.7 and 16, respectively), water was found to have a much lower efficiency in enhancing the catalytic current. Wong postulated that in addition to serving as a proton source, water also functions as a relatively strong Lewis base that may compete with CO_2 for the open binding site on rhenium.

In order to probe the mechanism, Kubiak and co-workers conducted a systematic study of the electrochemical reduction of CO_2 catalyzed by five different ReCl(bpy-R)$(CO)_3$ complexes, where bpy-R was: 1) bpy; 2) 4,4'-dimethyl-bpy (dmbpy); 3) 4,4'-di-*t*-butyl-bpy (bpy-*t*-Bu); 4) 4,4'-dicarboxyl-bpy (bpy-COOH); and 5) 4,4'-dimethoxy-bpy (bpy-OMe) (Figure 1.2).[29]

Electrochemical studies of this series indicated that the reduction potentials of these complexes were affected by the bpy ligand substituents. Specifically, the trend in ligand acidity (4-carboxylpyridine pK_a = 3.10, pyridine pK_a = 5.17, 4-methylpyridine pK_a = 5.94, 4-*t*-butylpyridine pK_a = 5.99, and 4-methoxypyridine pK_a = 6.62), is reflected in the reduction potentials of these substrates; i.e., the more acidic the ligand, the more negative the reduction potentials. However, no trend was observed with regard to catalytic current enhancement under CO_2 at the second reduction potential. Results of catalyst performance (in order of ligand acidity) was as follows: 1) ReCl(bpy-COOH)$(CO)_3$ (no current enhancement at −1.73 V vs SCE; 2) ReCl(bpy)$(CO)_3$ (3.4× at −1.73 V vs SCE); 3) ReCl(dmbpy)$(CO)_3$ (ca. 3.4× at −1.77 V vs SCE); 4) ReCl(bpy-*t*-Bu)$(CO)_3$ (18.4× at −1.83 V vs SCE; 5) ReCl(bpy-COOH)$(CO)_3$ (no current enhancement at −1.86 V vs SCE. As noted in their report, the catalytic activity for CO_2 reduction is not solely dependent on the electrocatalyst reduction potential.

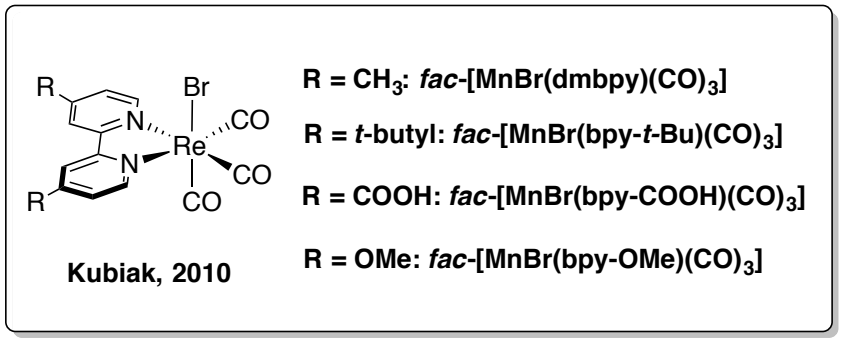

Figure 1.2: ReCl(bpy-R)$(CO)_3$ Complexes for Electrocatalytic CO_2 Reduction[29]

When ReCl(bpy)$(CO)_3$ and ReCl(bpy-*t*-Bu)$(CO)_3$ were compared at the same reduction potential (i.e., −1.83 V vs SCE), ReCl(bpy-*t*-Bu)$(CO)_3$ showed more than 3.5× more catalytic current enhancement than Lehn's catalyst, ReCl(bpy)$(CO)_3$. When compared to the

$ReCl(bpy)(CO)_3$ complex, IR-SEC studies show that the $ReCl(bpy\text{-}t\text{-}Bu)(CO)_3$ complex forms a stable Re(0) radical, and much less dimer is formed during electrolysis. It was proposed that this may be the cause of the enhanced catalytic activity of $ReCl(bpy\text{-}t\text{-}Bu)(CO)_3$.

MANGANESE: THE SWITCH TO A FIRST-ROW ALTERNATIVE

Our research has focused on the use of valence-isoelectronic manganese(I)-centered electrocatalysts. Manganese is preferred to rhenium because of the lower material cost, as a result of greater earth abundance (*ca.* 1 million times more abundant than rhenium),[10] and positively-shifted redox potentials; the latter yields a decreased overpotential for CO_2 reduction. Only five first-row transition metals have been employed as metal centers in molecular catalysts for the conversion of CO_2 to date: manganese,[34-51] iron,[52-57] nickel,[58-60] cobalt,[61-63] and copper.[64] These catalysts generally yield CO as the major product of the reduction of CO_2. The use of Ni- and Co-centered electrocatalysts were reported in 1974, while Cu- and Fe-centered catalysts have been studied since the 1990s.

The use of manganese as an electrocatalyst appeared more recently: Bourrez *et al.* reported the use of $MnBr(bpy)(CO)_3$ and $MnBr(dmbpy)(CO)_3$ as efficient electrocatalysts for CO_2 reduction catalyst in 2011 (Figure 1.3).[34] This pioneering study showed that these manganese catalysts were capable of reducing CO_2 at a significantly lower overpotential (*ca*. 0.4 V), with selectivity and Faradaic efficiency (FE_{CO} ~85% during preparative electrolysis) comparable to the $ReCl(bpy)(CO)_3Cl$ system studied by Lehn.[14] CVs of $MnBr(bpy)(CO)_3$ and $MnBr(dmbpy)(CO)_3$ showed two one-electron reductions separated by ca. 300mV. It was also observed that the inclusion of H_2O was needed to produce a current enhancement. When a solution of $MnBr(bpy)(CO)_3$ in acetonitrile was saturated with CO_2, no significant difference was detected for

either of the first two reduction peaks. However, the addition of 5% H_2O induced a large increase at the two electron reduction, verifying a Brønsted acid was necessary for catalysis to occur. For rhenium, Wong *et al.* noted that the addition of weak Brønsted acids, such as water, helps to stabilize the [Re−CO_2] intermediate through protonation, which facilitates the cleavage of one of the C−O bonds of CO_2, releasing H_2O and forming CO.[28]

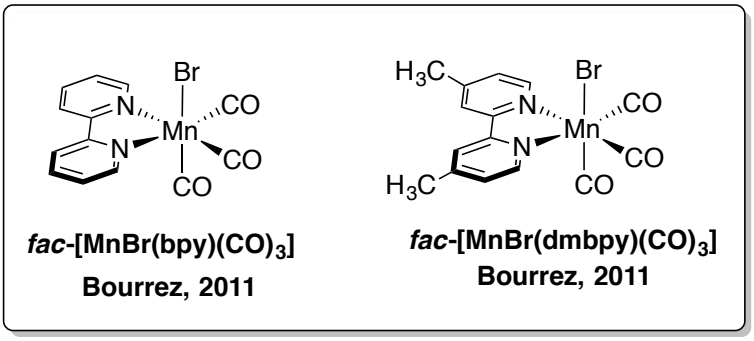

***fac*-[MnBr(bpy)(CO)$_3$]**
Bourrez, 2011

***fac*-[MnBr(dmbpy)(CO)$_3$]**
Bourrez, 2011

Figure 1.3: First Reported Mn(I)-Bipyridine Based CO_2 Electrocatalysts[34]

In 2013 Kubiak and co-workers reported a study of two new Mn(I) electrocatlaysts (Figure 1.4): MnBr(bpy-*t*-Bu)$(CO)_3$ and Mn(bpy-*t*-Bu)$(CO)_3(CH_3CN)](OTf)$.[36] The CV of MnBr(bpy-*t*-Bu)$(CO)_3$ in dry acetonitrile under argon was similar to the CV reported by Bourrez *et al.* for MnBr(bpy)$(CO)_3$:[34] the first reduction wave appeared at −1.39 V vs SCE (−1.77 V vs Fc/Fc^+) and the second reduction appeared at −1.57 V vs SCE (−1.95 V vs Fc/Fc^+). The second reduction formed the catalytically active anion, $[Mn(bpy\text{-}t\text{-}Bu)(CO)_3]^-$. A significant oxidation wave was observed at −0.30 V vs SCE (−0.68 V vs Fc/Fc^+), which was assigned to the oxidative cleavage of the Mn dimer, $[Mn(bpy\text{-}t\text{-}Bu)(CO)_3]_2$, formed at the first reduction potential.

It has been hypothesized in their report that addition of a Brønsted acid was necessary for catalyst turnover due to the 300 mV anodic shift for the two electron reduction of MnBr(bpy-*t*-

Bu)$(CO)_3$ when compared to ReBr(bpy-*t*-Bu)$(CO)_3$. The necessity of Brønsted acids suggests that catalysis will not transpire unless protonation of the [Mn−CO_2] intermediate occurs. As mentioned for rhenium systems, the addition of Brønsted acids increases catalytic current and stabilizes the [Re−CO_2] intermediate through protonation. Unlike Mn systems, catalysis can still occur without the addition of Brønsted acids for Re; the necessary protons can be furnished from degradation of the electrolyte (or solvent) since catalysis occurs at more negative potential. Three different weak Brønsted acids were examined in Kubiak's report: H_2O, MeOH, and TFE. Results from this study show that the catalytic current increases as the acid strength increases. In the course of their study, infrared spectroelectrochemistry (IR-SEC) and rotating disk electrochemistry were used as tools to elucidate key intermediates in the mechanistic process of CO_2 reduction. It was verified that at the potential of the first reduction, the manganese catalyst quickly dimerizes after the immediate loss of bromide. Dimerization of MnBr(bpy)$(CO)_3$ after the first reduction was observed by IR-SEC in an earlier report by Hartl *et al*.[65] Further reduction breaks apart the dimer to afford the catalytically active species $[Mn(bpy\text{-}t\text{-}Bu)(CO)_3]^-$. The activity of these catalysts was comparable to the corresponding Re(I) catalysts tested under similar experimental conditions. More importantly, these catalysts demonstrated excellent selectivity for the reduction of CO_2 to CO; no H_2 was detected during bulk electrolysis.

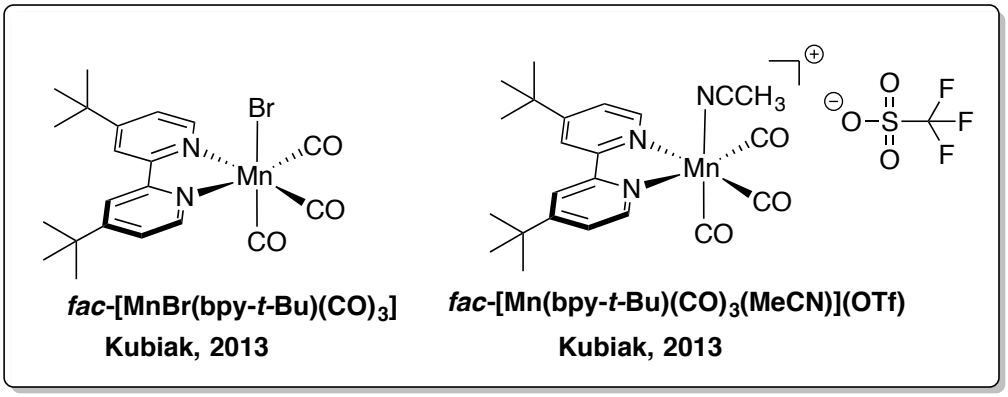

Figure 1.4: Mn(I)-Bipyridine Based CO_2 Electrocatalysts[36]

In 2014 Bourrez *et al.* investigated the mechanism of CO_2 reduction using pulsed electron-paramagnetic-resonance (EPR) spectroscopy and density functional theory (DFT) computations.[35] A catalytic cycle where two equivalents of $[Mn(bpy\text{-}R)(CO)_3](CH_3CN)$ are reduced by two electrons to form a Mn(0)-dimer, $[Mn(bpy)(CO)_3]_2$ (Figure 1.5) was proposed. The Mn(0)-dimer, coupled with a Brønsted acid, can undergo a two-electon oxidative addition with CO_2 to form the observed Mn(II)-hydroxycarbonyl low-spin intermediate. Finally, the Mn(II)-complex was further reduced (at the reduction potential of the electrocatalysis and production of CO occurs) in the presence of a Brønsted acid to complete the catalytic cycle and regenerate the Mn(I) species, $[Mn(bpy\text{-}R)(CO)_3](CH_3CN)$. Electrocatalytic experiments were also performed with $^{13}CO_2$ and gas chromatography mass spectrometry (GCMS) to verify that the production of CO comes directly from CO_2 and not through catalyst decomposition.

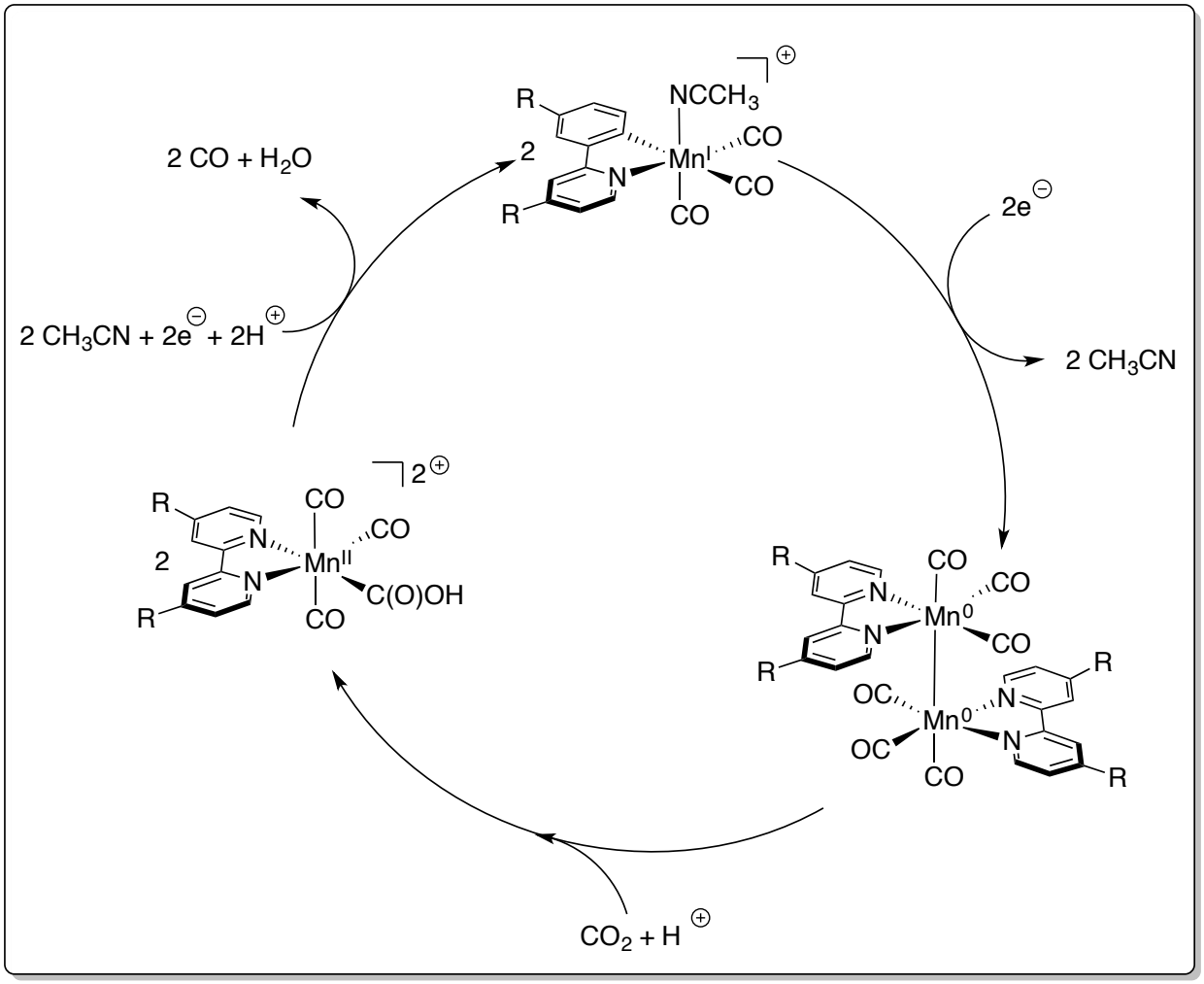

Figure 1.5: Proposed Mechanism of CO_2 Reduction Using Pulsed-EPR Spectroscopy and DFT Computations[35]

As discussed earlier, manganese catalysts can reduce CO_2 at lower over potentials than their rhenium analogs.[34-36] However, Mn catalysts have also been shown to easily dimerize after one−electron reduction. This dimerization occurs much slower for Re catalysts, and limits the catalytic activity for Mn catalyst. To help eliminate this unwanted dimerization, two new Mn catalysts were synthesized by Kubiak and co-workers in 2014 (Scheme 1.1): $MnBr(mesbpy)(CO)_3$ and $[Mn(mesbpy)(CO)_3(MeCN)](OTf)$, where mesbpy = 6,6'-dimesityl-2,2'-bipyridine. Each complex contained bulky mesityl groups in the 6,6'-positions on the bpy skeleton.[39] The synthesis

of the mesbpy ligand was achieved by treatment 6,6'-dibromo-2,2'-bipyridine with an 2,4,6-trimethylphenylboronic acid, sodium carbonate and a catalytic amount of tetrakis(triphenylphosphine)palladium(0) (*Suzuki coupling*) to afford the desired ligand in 71% yield (Scheme 1.1).[66] The mesbpy ligand was then treated with bromopentacarbonylmanganese(I) in refluxing diethylether to give MnBr(mesbpy)$(CO)_3$, in 69% yield. Treatment of MnBr(mesbpy)$(CO)_3$ with silver trifluoromethanesulfonate in CH_3CN gave the Mn(I)-cationic complex, [Mn(mesbpy)$(CO)_3$(MeCN)](OTf), in 69% yield.

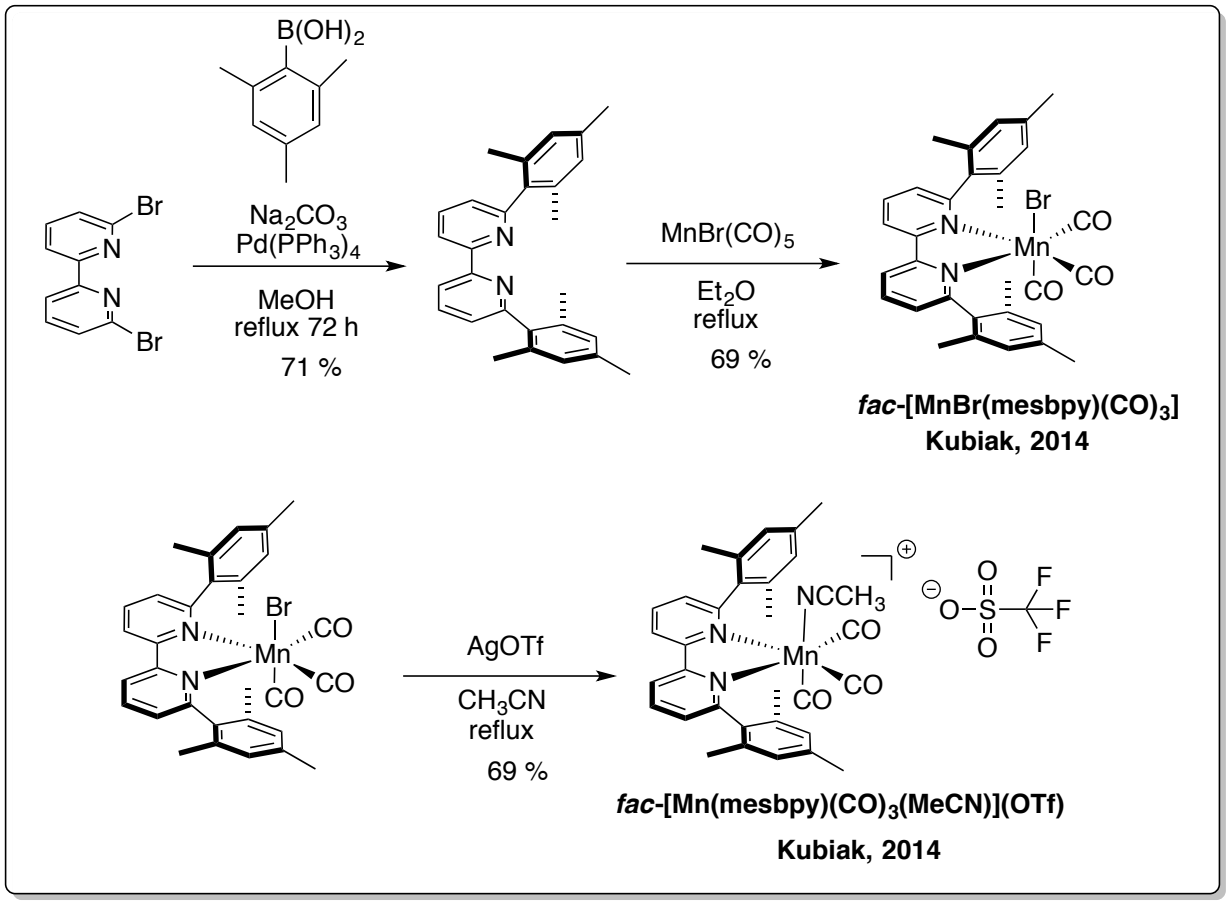

Scheme 1.1: Synthesis of MnBr(mesbpy)$(CO)_3$ and [Mn(mesbpy)$(CO)_3$(MeCN)](OTf)[39]

The electrochemistry of $MnBr(mesbpy)(CO)_3$ and $[Mn(mesbpy)(CO)_3(MeCN)](OTf)$ showed no evidence of dimerization, confirming that the bulky mesbpy ligand provided enough steric hindrance. When these complexes were studied electrochemically, unusual CVs were observed. As discussed earlier, $MnX(bpy\text{-}R)(CO)_3$ complexes show two one-electron reductions which are separated by 200-300 mV, depending on the bpy substitution.[34, 36] When $MnBr(mesbpy)(CO)_3$ and $[Mn(mesbpy)(CO)_3(MeCN)](OTf)$ were analyzed, a single, reversible two-electron reduction wave was observed under N_2 at −1.6 V Fc/Fc^+. This reduction generates the anion, $[Mn(mesbpy)(CO)_3]^-$, at a potential more positive (ca. 300 mV) than found for typical Mn bpy catalysts. IR-SEC of $MnBr(mesbpy)(CO)_3$ under N_2 indicates that both a singly reduced species $[Mn(mesbpy)(CO)_3]^0$ and the anionic complex $[Mn(mesbpy)(CO)_3]^-$ form at the same potential. It was concluded that since a singly reduced species is observed during IR-SEC experiments, the single, reversible two-electron reduction for $MnBr(mesbpy)(CO)_3$ and $[Mn(mesbpy)(CO)_3(MeCN)](OTf)$ is the result of two one-electron reductions instead of a direct two-electron reduction.

Kubiak and co-workers proposed a catalytic mechanism (Figure 1.6) for the reduction of CO_2 using the $MnBr(mesbpy)(CO)_3$. First, reduction of $MnBr(mesbpy)(CO)_3$ to $[Mn(mesbpy)(CO)_3]^-$ is generated at −1.6 V Fc/Fc^+. This anion can then bind with CO_2 in the presence of a Brønsted acid to form $Mn(I)(mesbpy)(CO)_3(CO_2H)$. There is clear evidence that this 18-e^- intermediate can bind to CO_2/H^+; however, catalysis does not occur until the species $Mn(I)(mesbpy)(CO)_3(CO_2H)$ is "over-reduced". This 18e^- Mn(I)−CO_2H intermediate is "over-reduced" at −2.0 V Fc/Fc^+ to form a short-lived 19-e^- species which rapidly reacts with available acid to eliminate water and form $[Mn(mesbpy)(CO)_4]^0$. Further reduction of the tetracarbonyl species regenerates catalytically active species $[Mn(mesbpy)(CO)_3]^-$.

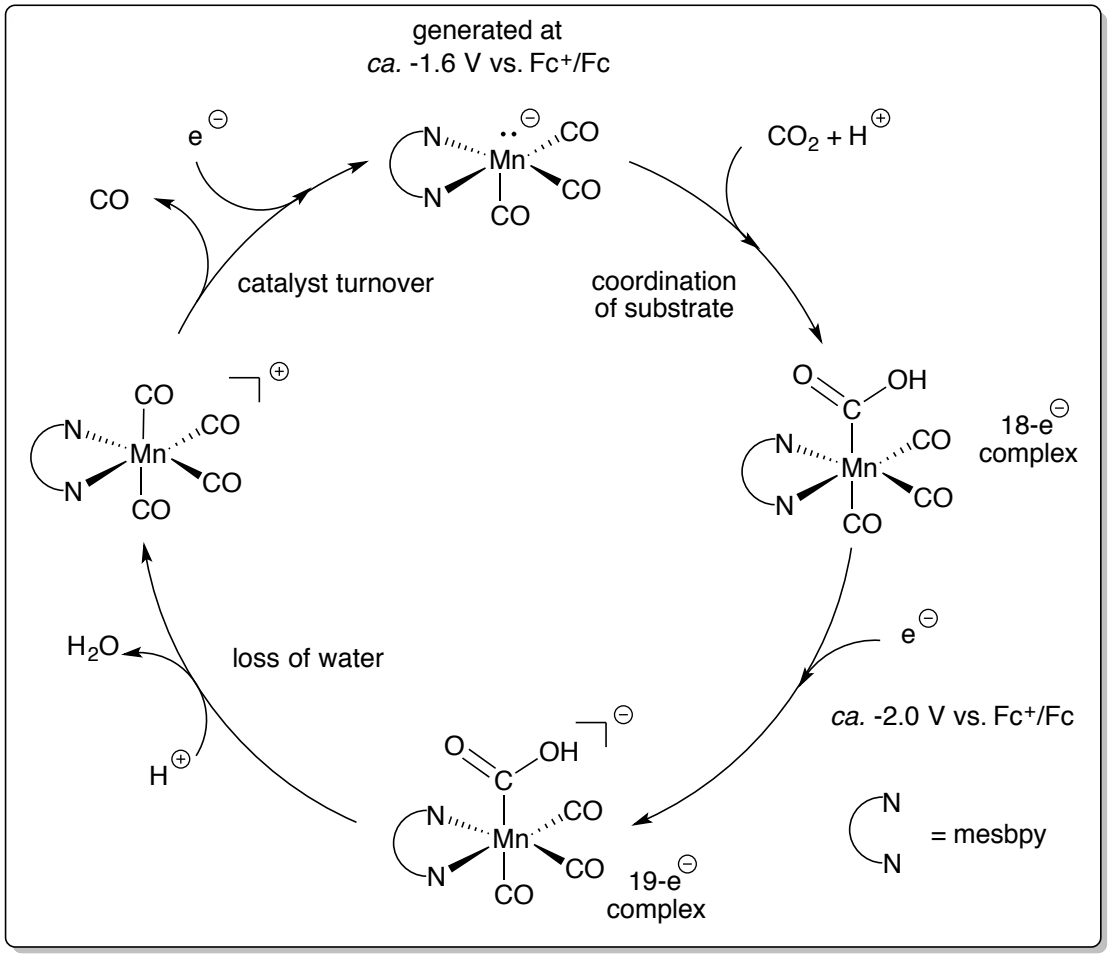

Figure 1.6: Proposed Catalytic Mechanism the Reduction of CO_2 Using the Complex $MnBr(mesbpy)(CO)_3$[39]

In 2015, Agarwal *et al.* utilized the addition of a phenolic group in the second coordination sphere embedded on a bpy ligand to probe the effects of catalysis.[44] This strategy was similar to that reported by Savéant and co-workers in 2012 whereby the addition of phenolic groups on iron porphyrin catalysts modulated current enhancement at the potential of CO_2 reduction through increased local proton concentration.[56, 57] Synthesis of the key 6-(2-methoxyphenyl)-bpy intermediate was achieved by treating 2,2'-bipyridine with 2-lithioanisole (prepared by treatment of 2-bromoanisole with lithium metal), followed by rearomatization with potassium permanganate (Scheme 1.2).[67] Conversion of the methoxy group to the phenol was accomplished by

demethylation with molten pyridinium hydrochloride to afford 6-(2-hydroxyphenyl)-bpy in 90% yield. To form the Mn(I)-complexes, either 6-(2-methoxyphenyl)-bpy or 6-(2-hydroxyphenyl)-bpy were treated with $MnBr(CO)_5$ and refluxed in methanol to give both desired products: $MnBr(MeOPh\text{-}bpy)(CO)_3$ in 82% yield and $MnBr(HOPh\text{-}bpy)(CO)_3$ in 98% yield.

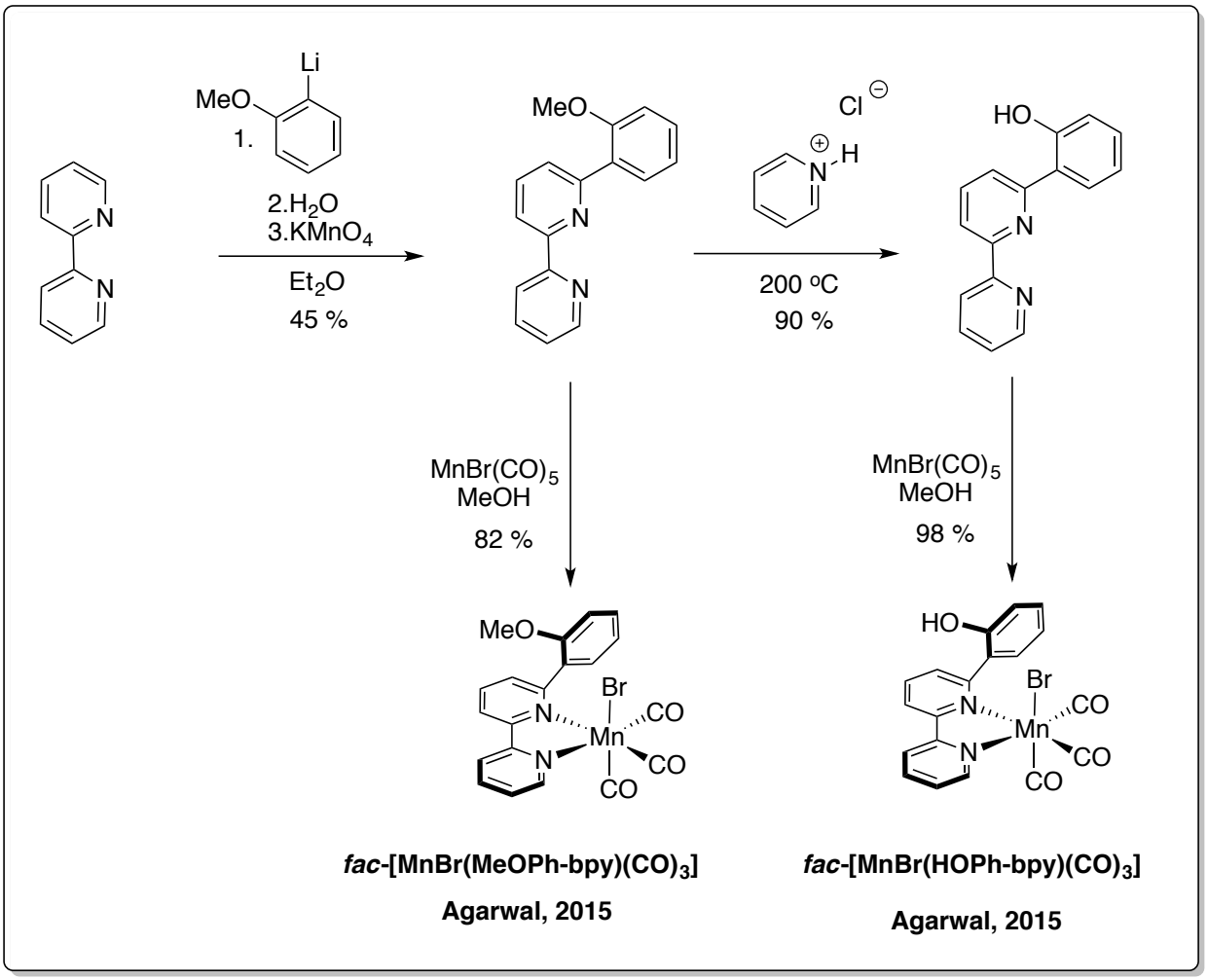

Scheme 1.2: Introduction of an Ancillary Phenol on Mn(I)-bpy Based CO_2 Electrocatalysts[44]

Electrochemical analysis showed that $MnBr(HOPh\text{-}bpy)(CO)_3$ reduces CO_2 at nearly the same potential as unmodified $MnBr(bpy)(CO)_3$ but showed seven times the catalytic current

density. When MnBr(MeOPh-bpy)$(CO)_3$ was analyzed, there was only a marginal difference in the two electron reduction potentials and catalytic current density when compared to that of MnBr(bpy)$(CO)_3$. These results suggest that the strategically placed phenolic proton was responsible for the increased catalytic current. In addition, the phenolic moiety embedded on the bpy framework was found to stabilize the Mn-CO_2 intermediate via hydrogen bonding between the proton associated with the phenol (a Brønsted acid) and the oxygen atom of CO_2 (a Brønsted base). Theoretical work also indicated that the increased catalytic activity could be attributed to an intramolecular mechanism for proton-assisted dehydration of MnBr(HOPh-bpy)$(CO)_3$COOH.

In 2016, Sampson *et al.* coupled the use of bulky molecular catalysts, such as MnBr(mesbpy)$(CO)_3$ and [Mn(mesbpy)$(CO)_3$(MeCN)](OTf), with a Lewis acid, $Mg(OTf)_2$.[42] Although these catalysts bind to CO_2 at very low potentials, they showed little to no reactivity for CO_2 reduction with weak Brønsted acids at −1.6 V Fc/Fc^+. In fact, "over-reduction" of a Mn(I)-COOH complex at −2.0V Fc/Fc^+ was required to achieve fast catalytic rates.[39] An earlier study in 1991 conducted by Savéant and co-workers described the use of Mg^{2+} cations, as well as other Lewis acids, to increase the rate of CO_2 reduction and improve the stability of catalysis for iron tetraphenylporphyrins.[52] It was found that a Lewis acid could facilitate the breaking of one C−O bond of a bound CO_2 ligand to afford CO. To that end, the rate of catalysis for MnBr(mesbpy)$(CO)_3$ and [Mn(mesbpy)$(CO)_3$(MeCN)](OTf) was increased by over 10-fold by using Mg^{2+} cations instead of TFE.

Several electrochemical experimental studies verified that the electrocatalysis with Mg^{2+} proceeded through a reductive disproportionation mechanism (Figure 1.7). First, the active catalyst $[MnBr(mesbpy)(CO)_3]^-$ is formed at −1.5V Fc/Fc^+, followed by binding with CO_2. A Mg^{2+} cation then can coordinate with the CO_2 ligand where it aids in the weakening of a C−O bond

of the bound CO_2 molecule; a second CO_2 molecule can then complete the breaking of the C−O bond, which releases CO_3^{2-} as a product and forms [Mn(mesbpy)$(CO)_4$]. The cationic Mn(I) tetracarbonyl complex is then reduced by two electrons to release CO and regenerates the active catalytic complex.

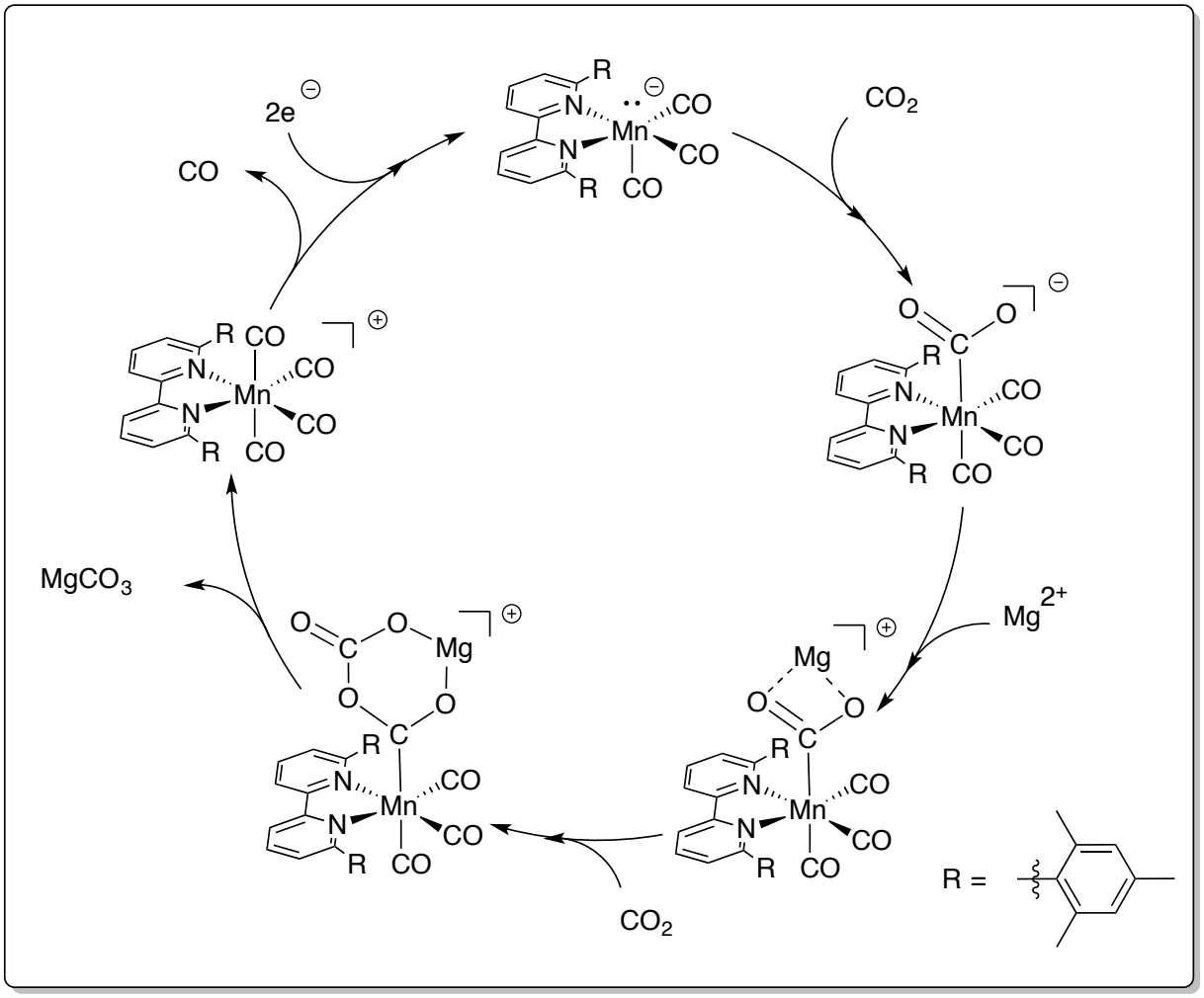

Figure 1.7: Proposed Catalytic Mechanism for CO_2 Reduction with Added Lewis Acid[42]

A molecular manganese catalyst immobilized on mesoporous TiO_2 was reported by Rosser *et al.* in 2016.[49] It has been previously reported that the maximum turnover number (TON) for the $MnX(bpy\text{-}R)(CO)_3$ class of compounds is 24 after 18 h,[34] and 36 after 6 h.[42] In this report, a novel Mn(I) CO_2 reduction catalyst was equipped with a phosphonate functionality (MnP) that allowed for anchoring and direct wiring between the Mn center (catalytic center) and the titanium oxide surface.[68] The authors chose a mesoporous TiO_2 electrode for these reasons: 1) long-term stability and conductivity under reducing conditions;[69] 2) a three-dimensional morphology for high catalyst loading and to facilitate close inter-molecular interactions;[49] and 3) transparency for spectroelectrochemical characterization of catalytic intermediates.[70]

The TiO_2|MnP catalyst was shown to efficiently reduce CO_2 to CO at −1.7V Fc/Fc^+; after 2 h of bulk electrolysis, a high Faradaic efficiency for CO production was observed (FE_{CO} ~67%). Trace H_2 was also produced (FE_{H2} ~12%); however, no formate was detected during analysis. Notably, the TiO_2|MnP cathode reached an impressive TON of 112 after 2 h of bulk electrolysis, far superior to other Mn(I) catalyst systems described previously. During the reduction process a formed Mn−Mn dimer species was detected, the first reported formation of active catalytic dimers on a surface. Rosser remarked that this finding may provide a strategy for retaining homogeneous reaction mechanisms while also gaining the advantages of heterogeneous catalysis. Lastly, it was demonstrated that the TiO_2|MnP cathode could be used for solar-driven CO_2 reduction when assembled in a photoelectrochemcial (PEC) cell with a CdS-sensitized photoanode. Immobilization of a catalyst on TiO_2 surface coupled with implementation of a PEC cell showcases the advancement of moving molecular electrocatalytic CO_2 reduction towards a full artificial photosynthetic system.

To summarize, several key findings have been revealed since Bourrez *et al.* reported the use of $MnBr(bpy)(CO)_3$ and $MnBr(dmbpy)(CO)_3$ as efficient electrocatalysts for CO_2 reduction in 2011. All of these catalysts offer improvements over their rhenium counterparts, including a decreased overpotential for CO_2 conversion and a decreased material cost. Most of the manganese(I) complexes that have been reported for the electrochemical reduction of CO_2 employ a bpy backbone, which limits structural and electronic modifications to a large degree. We believed that replacing a pyridine ring in bpy with an *N*-heterocyclic carbene (NHC) would take advantage of the versatility of NHCs. The next sections briefly describe NHCs and their use as ligands in group VII-complexes.

N-HETEROCYCLIC CARBENES (NHCs)

NHCs are electron–rich nucleophillic ligands in which the reactive carbene center is stabilized by both the σ-electron–withdrawing and π-electron–donating character of adjacent nitrogen atoms (Figure 1.8).[71, 72] Most NHCs exist as five-membered rings, but several "ring-expanded" cores have also been reported, including six-membered (tetrahydropyrimidine), seven-membered (diazepane) and eight-membered (diazocane) heterocyclic constructs.[73-75] The isolation of the NHCs has revolutionized organometallic chemistry, because: 1) most NHCs are based around imidazolium salt precursors, which are synthetically easy to prepare and handle,[71] 2) NHCs have both strong σ-donor, and π-acceptor properties, which allow them to form strong bonds with metal centers through σ and π interaction;[76-83] 3) the strong binding of an electron–rich carbene to the metal center helps the metal retain the NHC ligand during the course of the reaction, which leads to a longer catalyst lifetime and consistent reactivity throughout the transformation,[84] 4) NHC ligand frameworks can offer considerable steric protection to the metal associated to it in the

complex, and 5) the electronic and steric nature of NHCs can be modulated through functionalization of the backbone and the *N*-bound substituents.[71]

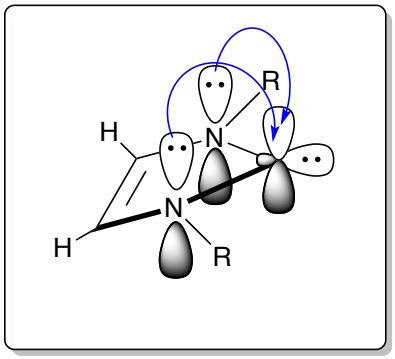

Figure 1.8: Stabilization of NHC via π-Electron Donation From Adjacent Heteroatoms

N-HETEROCYCLIC CARBENES AND GROUP VII-METALS

The first Re(I)-tricarbonyl complex with a supporting NHC ligand was reported by Herrmann *et al.* in 1992.[85] This report generated considerable interest in this field, with the majority of reports published since 2010.[86-113] Recent work has focused on the photophysical properties of Re(I)-tricarbonyl complexes that are bound to diimine (diim) π-conjugated ligands, such as bpy or 1,10-phenanthroline (phen), and how chemical variations of these systems can be used to tune the photophysical properties of the complexes. Investigations where an NHC ligand is based around a pyridyl-, or a pyrimidal-substitued imidazole, or a benzimidazole ring have indicated that these types of ligands are able to tune MLCT transitions through their π* system.[98, 102, 103, 107] For example, these complexes have shown a blue-shifted emission when compared to bpy and phen analogs which can be explained in a decreased overall conjugation from the bpy or phen to the NHC ligand.[103] In addition, it has been observed that in the case of tricarbonyl Re(I) complexes the pyridyl-NHC ligands are photoactive upon irradiation whereas the pyrimdyl-NHC ligand is photostabile.[103]

Several recent reviews focus on rhenium and NHCs as supporting ligands, further illustrating the broad interest in this research area.[110, 114-120] Only two groups had investigated the catalytic ability of rhenium-NHC complexes (Figure 1.9),[92, 113] as noted by Kühn in a 2016 review which was focused on cationic rhenium complexes ligated with NHCs.[108] In 2009, Berke and co-workers disclosed a report where several new five-coordinated rhenium(I) hydride NHC complexes of the type [Re(Br)(H)(NO)(PR_3)(NHC)] were synthesized. These Re(I) complexes were shown to be effective catalysts for both the dehydrocoupling of $Me_2NH{\cdot}BH_3$ and for transfer hydrogenation reactions of olefins, where $Me_2NH{\cdot}BH_3$ was the hydrogen donor to produce alkanes.[92] In 2013, Liu and co-workers synthesized several Re(I) NHC carbonyl complexes and tested the catalytic activity in the insertion reaction of terminal alkynes into 2-methylacetoacetates to give substituted 5-oxo-2-hexenoates.[113]

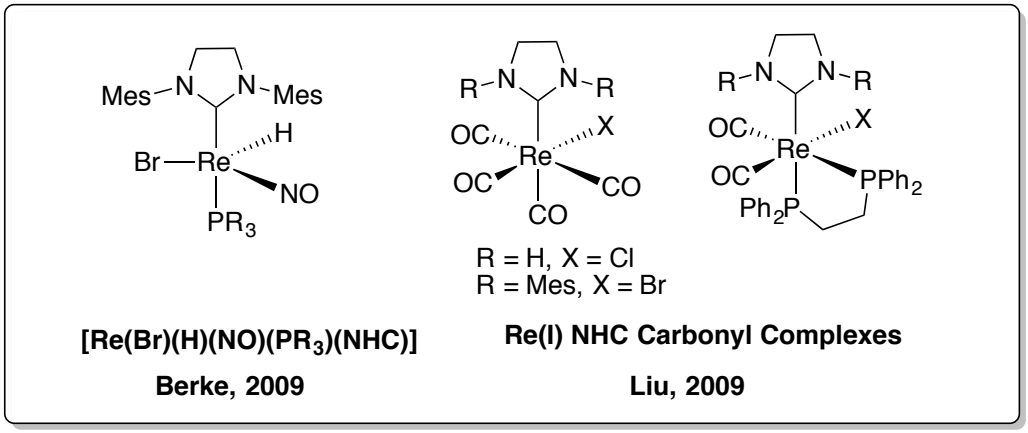

Figure 1.9: Catalytic Rhenium NHC Complexes[92, 113]

In late 2015, Delcamp and co-workers reported a series of Re(I) pyridyl NHC complexes (NHC imidazole) that were examined in the photocatalytic reduction of CO_2.[109] Synthesis of the ReBr(PyNHC-CH_3)$(CO)_3$ complex (Scheme 1.3) began with a copper−catalyzed coupling with

imidazaole and 2-bromopyridine (*Ullmann Coupling*) to produce the desired imidazole-pyridine heterocycle in 68% yield. Alkylation of the imidazole ring with methyl iodide, followed by salt metathesis with sodium hexafluorophosphate gave rise to the imidazolium salt in 70% yield over 2 steps. Finally, the imidazolium salt was chelated with $ReBr(CO)_5$ in refluxing toluene with trimethylamine to give the desired catlalyst $ReBr(PyNHC\text{-}CH_3)(CO)_3$ albeit in a low, 6% yield.

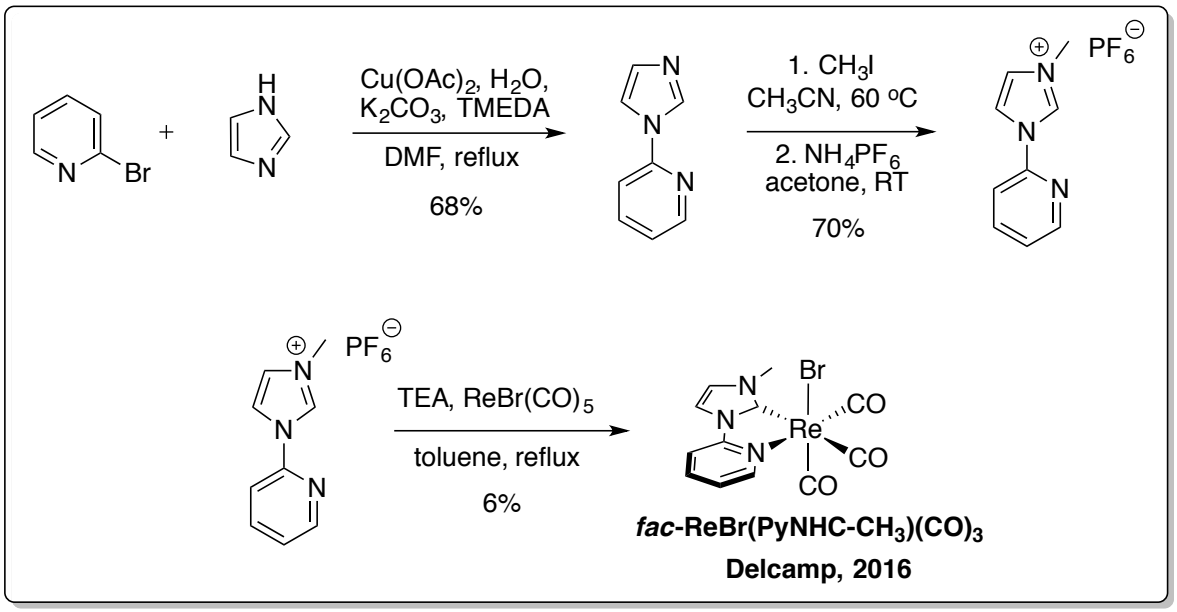

Scheme 1.3: Synthesis of $ReBr(PyNHC\text{-}CH_3)(CO)_3$[109]

The synthesis of the arylated NHC catalysts began with a copper(I)-catalyzed coupling with imidazole and the respective aryl bromide (*Ullmann Coupling*) to give the targeted *N*-arylated imidazoles (Scheme 1.4). Heating the *N*-arylated imidazoles with 2-bromopyridine afforded the arylated imidazolium salts which were chelated with $ReCl(CO)_5$ in refluxing toluene with trimethylamine to give the targeted Re(I)-NHC complexes, namely: $ReX(PyNHC\text{-}Ph)(CO)_3$, $ReX(PyNHC\text{-}PhOC_6H_{13})(CO)_3$ and $ReX(PyNHC\text{-}PhCF_3)(CO)_3$, where X = Cl or Br. Both the Re-chloride and Re-bromide complexes could be accessed by a single reaction when using

mismatched halides for the NHC-proligand and the metal source. These complexes could then be purified via flash chromatography.

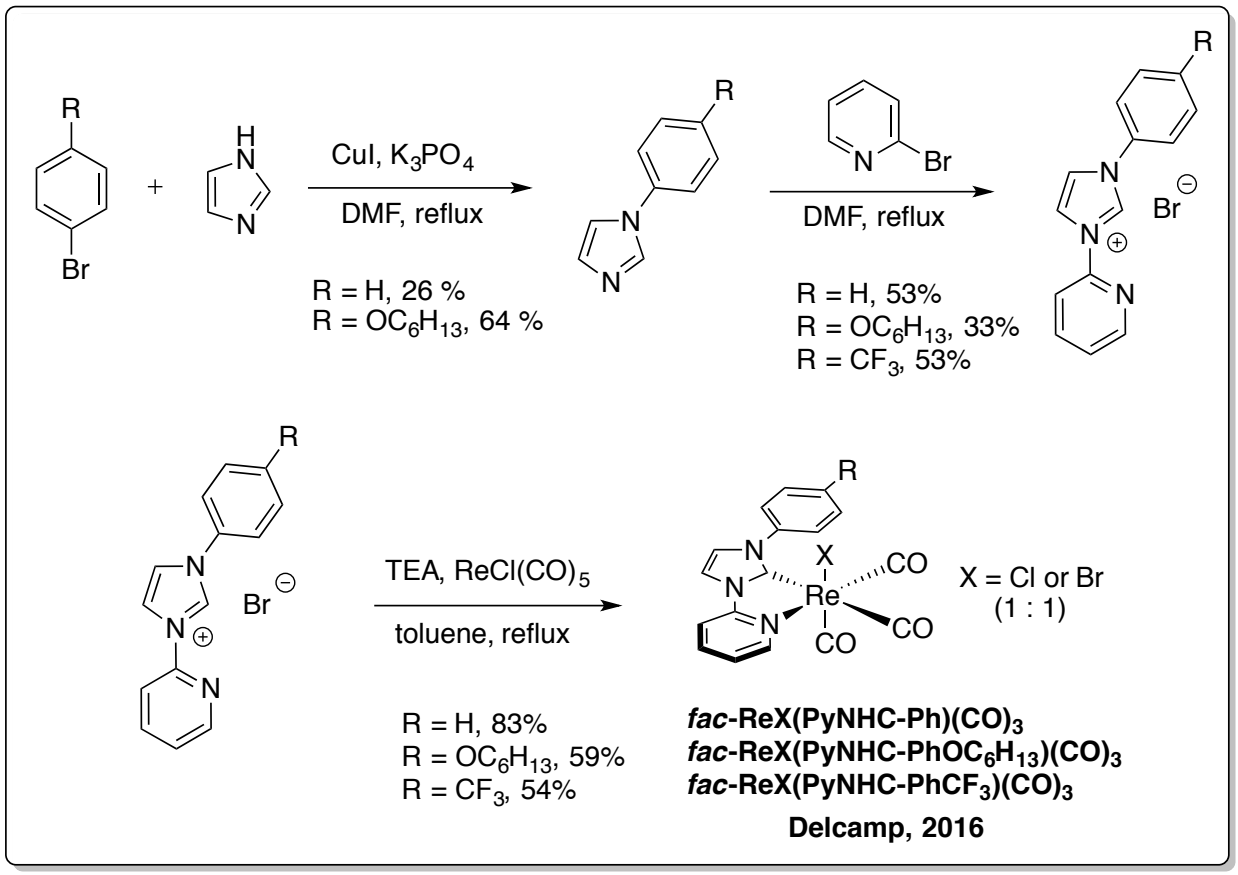

Scheme 1.4: Synthesis of the Arylated Re(I)-NHC catalysts[109]

The reported Re(I)-complexes were subsequently evaluated for their ability to reduce CO_2 electrochemically. Under a N_2 atmosphere, the Re(I)-NHC complexes showed two irreversible reductions and an irreversible oxidation. Switching the atmosphere to CO_2 lead to a catalytic current enhancement at the first reduction wave with a larger current increase at the second reduction wave. The current increases were similar for all the complexes with ReX(PyNHC-$PhCF_3$)$(CO)_3$ showing the highest enhancement at each reduction wave. The Re(I)-NHC

complexes were also examined in the photocatalytic reduction of CO_2 using a simulated solar spectrum, and compared with the benchmark catalyst, $ReBr(bpy)(CO)_3$. All of the complexes functioned as CO_2 reduction catalysts in the presence of the photosensitizer *fac*-$Ir(ppy)_3$ (ppy = phenylpyridine) and the strong electron donor BIH (BIH = 1,3-dimethyl-2-phenyl-2,3-dihydro-1*H*-benzo[d]imidazole). The $ReBr(PyNHC\text{-}PhCF_3)(CO)_3$ complex performed much better than the benchmark $ReBr(bpy)(CO)_3$ complex in each set of reactions using a solar simulated spectrum. In the presence of *fac*-$Ir(ppy)_3$ and BIH, both $ReBr(PyNHC\text{-}PhCF_3)(CO)_3$ and $ReBr(bpy)(CO)_3$ produced good turnover numbers (55 TON and 33 TON, respectively). More importantly, the $ReBr(PyNHC\text{-}PhCF_3)(CO)_3$ catalyst retained good turnover numbers (32 TON) with no photosensitizer, while the $ReBr(bpy)(CO)_3$ was less effective (14 TON). As discussed by Delcamp, very few catalysts are capable of nonphotosensitized CO_2 catalytic reduction with visible light, suggesting future possibilities for additional Group VII-NHC complexes in terms of catalysis.

After reporting that an electron–withdrawing group improved photocatalysis and reduced the overpotential, Delcamp and co-workers reported a follow-up study in 2016, where four electron–deficient-substituted Re(I)-NHC complexes were synthesized and examined for their efficiency to reduce CO_2 electrocatalytically.[111] The synthesis of the electron–deficient Re(I)-NHC complexes (Scheme 1.5) started with a copper(I)-catalyzed coupling of imidazole with the appropriate phenyl bromide to give 1-(4-cyanophenyl)-1*H*-imidazole and 1-(3,5-bis(trifluoromethy)lphenyl)-1*H*-imidazole in 14% and 88% yields, respectively (Note: both 1-(4-trifluoromethylphenyl)-1*H*-imidazole and 1-(4-nitrophenyl)-1*H*-imidazole are commercially available). Heating the arylated-imidazoles with neat 2-bromopyridine afforded the arylated imidazolium salts. It was noted that this procedure lowered the yields of the trifluoromethyl

imidazolium salts (due to product sublimation), which was circumvented with the addition of a solvent (DMF). Finally, deprotonation of the imidazolium salts with trimethylamine, followed by an *in situ* chelation to $ReCl(CO)_5$, gave the final products in varying yields: $ReBr(PyNHC\text{-}PhCF_3)(CO)_3$ (56%), $ReBr(PyNHC\text{-}PhNO_2)(CO)_3$ (40%), $ReBr(PyNHC\text{-}PhCN)(CO)_3$ (95%), and $ReBr(PyNHC\text{-}Ph(bis\text{-}CF_3)(CO)_3$ (36%).

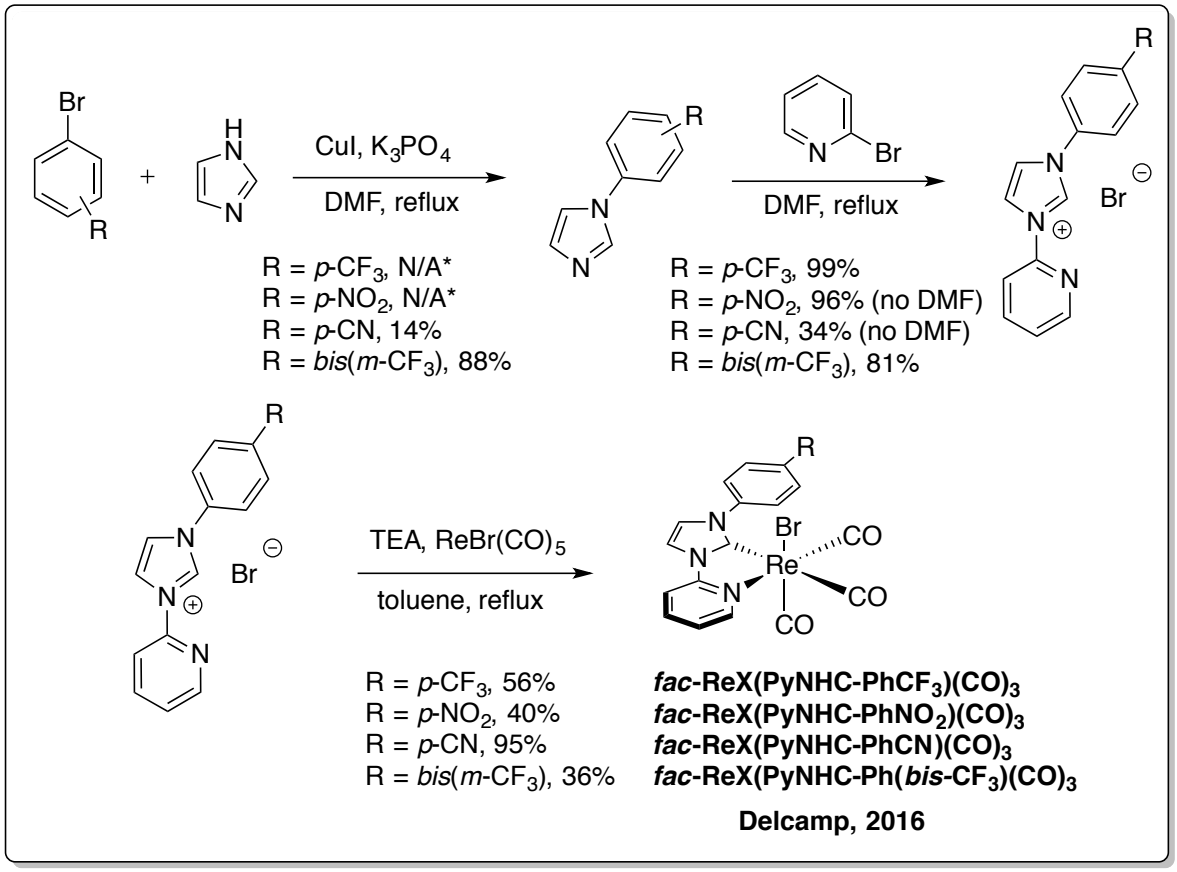

Scheme 1.5: Synthesis of Electron-Deficient Arylated Re(I)-NHC Catalysts[111]

Cyclic voltammetry was performed under N_2 on all new arylated Re(I)-NHC systems and compared to the benchmark bpy catalyst, $ReBr(bpy)(CO)_3$. The solution stable catalysts (i.e., $ReBr(PyNHC\text{-}PhNO_2)(CO)_3$ were found to decompose in solution before CV could be obtained)

all showed two reduction waves, and each was 300-350 mV more negative relative to $ReBr(bpy)(CO)_3$. Although there are relatively small shifts in reduction potentials across the electron−deficient arylated Re(I)-NHC series, CVs performed under CO_2 showed catalytic enhancement which varied significantly based on NHC substitution. In addition, the difference in overpotential where catalysis occurs is very similar for the Re(I)-NHC complexes when compared to the $ReBr(bpy)(CO)_3$ system. This result was because all of the Re(I)-NHC complexes showed a large catalytic current increase at the first reduction potential, whereas $ReBr(bpy)(CO)_3$ only showed significant catalytic increase at the second potential. Of the new Re(I)-NHC catalysts, $ReBr(PyNHC\text{-}PhCF_3)(CO)_3$ performed the best, and was selected for additional electrochemical analyses.

The electrocatalytic performance of $ReBr(PyNHC\text{-}PhCF_3)(CO)_3$ was evaluated by CV and bulk electrolysis using three Brønsted acids: PhOH, TFE, and H_2O. With the addition of H_2O, both the rate of catalysis and catalytic current enhancement improved dramatically. Bulk electrolysis of $ReBr(PyNHC\text{-}PhCF_3)(CO)_3$ revealed that catalysis with the addition of PhOH was nonselective, and substantial H_2 was produced. It is important to note that when either TFE or H_2O were used as the Brønsted acid, CO was the major product and only trace amounts of H_2 was formed. In addition, when H_2O was used as the proton source during preparative electrolysis, $ReBr(PyNHC\text{-}PhCF_3)(CO)_3$ showed a higher Faradaic efficiency for CO production (FE_{CO} ~92%) than did $ReBr(bpy)(CO)_3$ (FE_{CO} ~61%).

CONCLUSIONS

With the discovery of the *fac*-$ReCl(bpy)(CO)_3$ system reported by Lehn and co-workers in 1984,[14] the field of electrochemical CO_2 reduction to CO using molecular catalysts has been the

subject of much research. In 2011, Bourrez reported the use of valence-isoelectronic Mn(I) species, i.e., $MnBr(bpy)(CO)_3$, as an efficient electrocatalysts for CO_2 reduction catalyst. This study showed that these manganese catalysts reduced CO_2 to CO at a significantly lower overpotential while retaining a similar selectivity and Faradaic efficiency. The most investigated manganese catalysts to date are of the type $MnBr(bpy\text{-}R)(CO)_3$, where bpy has been modified with *t*-butyl, mestiyl, or phenolic moieties. We have focused on modifying the supporting bidentate ligand with an *N*-heterocyclic carbene. NHC ligands provide a framework that can be modified sterically and electronically easier and more effectively than bpy. Rationally designing NHC ligands has the potential to enhance the catalytic activity and increase the stability of Mn(I)-catalyst systems. The next four sections of this dissertation focus on the progress we have made towards achieving these goals during the past four years.

REFERENCES:

1. Ibrahim, H.; Ilinca, A.; Perron, J., Energy Storage Systems—Characteristics and Comparisons. *Renewable and Sustainable Energy Reviews* **2008**, *12* (5), 1221-1250.

2. Appel, A. M.; Bercaw, J. E.; Bocarsly, A. B.; Dobbek, H.; DuBois, D. L.; Dupuis, M.; Ferry, J. G.; Fujita, E.; Hille, R.; Kenis, P. J.; Kerfeld, C. A.; Morris, R. H.; Peden, C. H.; Portis, A. R.; Ragsdale, S. W.; Rauchfuss, T. B.; Reek, J. N.; Seefeldt, L. C.; Thauer, R. K.; Waldrop, G. L., Frontiers, Opportunities, and Challenges in Biochemical and Chemical Catalysis of CO_2 Fixation. *Chemical Reviews* **2013**, *113* (8), 6621-6658.

3. Song, C., Global Challenges and Strategies for Control, Conversion and Utilization of CO_2 for Sustainable Development Involving Energy, Catalysis, Adsorption and Chemical Processing. *Catalysis Today* **2006**, *115* (1–4), 2-32.

4. Kumar, B.; Llorente, M.; Froehlich, J.; Dang, T.; Sathrum, A.; Kubiak, C. P., Photochemical and Photoelectrochemical Reduction of CO_2. *Annual Review of Physical Chemistry* **2012**, *63*, 541-569.

5. Benson, E. E.; Kubiak, C. P.; Sathrum, A. J.; Smieja, J. M., Electrocatalytic and Homogeneous Approaches to Conversion of CO_2 to Liquid Fuels. *Chemical Society Reviews* **2009**, *38* (1), 89-99.

6. Qiao, J.; Liu, Y.; Hong, F.; Zhang, J., A Review of Catalysts for the Electroreduction of Carbon Dioxide to Produce Low-Carbon Fuels. *Chemical Society Reviews* **2014**, *43* (2), 631-675.

7. Li, K.; An, X.; Park, K. H.; Khraisheh, M.; Tang, J., A Critical Review of CO_2 Photoconversion: Catalysts and Reactors. *Catalysis Today* **2014**, *224*, 3-12.

8. Khatib, H., IEA World Energy Outlook 2011—A Comment. *Energy Policy* **2012**, *48*, 737-743.

9. Hori, Y., CO_2 Reduction Using Electrochemical Approach. In *Solar to Chemical Energy Conversion*, Springer: 2016; pp 191-211.

10. Grice, K. A.; Kubiak, C. P., Recent Studies of Rhenium and Manganese Bipyridine Carbonyl Catalysts for the Electrochemical Reduction of CO_2. *CO_2 Chemistry* **2013**, *66*, 163-188.

11. Halmann, M. M.; Steinberg, M., *Greenhouse Gas Carbon Dioxide Mitigation: Science and Technology*. CRC press: 1998.

12. Sutin, N.; Creutz, C.; Fujita, E., Photo-Induced Generation of Dihydrogen and Reduction of Carbon Dioxide Using Transition Metal Complexes. *Comments on Inorganic Chemistry* **1997**, *19* (2), 67-92.

13. Lu, Q.; Rosen, J.; Zhou, Y.; Hutchings, G. S.; Kimmel, Y. C.; Chen, J. G.; Jiao, F., A Selective and Efficient Electrocatalyst for Carbon Dioxide Reduction. *Nature Communications* **2014**, *5*, 3242.

14. Hawecker, J.; Lehn, J.-M.; Ziessel, R., Electrocatalytic Reduction of Carbon Dioxide Mediated by Re(bipy)$(CO)_3$Cl (bipy= 2,2′-bipyridine). *Journal of the Chemical Society, Chemical Communications* **1984**, (6), 328-330.

15. Sullivan, B. P.; Meyer, T. J., Photoinduced Irreversible Insertion of CO_2 Into a Metal–Hydride Bond. *Journal of the Chemical Society, Chemical Communications* **1984**, (18), 1244-1245.

16. Sullivan, B. P.; Meyer, T. J., Kinetics and Mechanism of Carbon Dioxide Insertion Into a Metal-Hydride Bond. A Large Solvent Effect and an Inverse Kinetic Isotope Effect. *Organometallics* **1986**, *5* (7), 1500-1502.

17. Sullivan, B. P.; Bolinger, C. M.; Conrad, D.; Vining, W. J.; Meyer, T. J., One-and Two-Electron Pathways in the Electrocatalytic Reduction of CO_2 by *fac*-Re(bpy)$(CO)_3$Cl (bpy= 2,2′-bipyridine). *Journal of the Chemical Society, Chemical Communications* **1985**, (20), 1414-1416.

18. O'Toole, T. R.; Margerum, L. D.; Westmoreland, T. D.; Vining, W. J.; Murray, R. W.; Meyer, T. J., Electrocatalytic Reduction of CO_2 at a Chemically Modified Electrode. *Journal of the Chemical Society, Chemical Communications* **1985**, (20), 1416-1417.

19. Cosnier, S.; Deronzier, A.; Moutet, J.-C., Electrochemical Coating of a Platinum Electrode by a Poly(Pyrrole) Film Containing the *fac*-Re(2,2′-bipyridine)$(CO)_3$Cl System Application to Electrocatalytic Reduction of CO_2. *Journal of Electroanalytical Chemistry and Interfacial Electrochemistry* **1986**, *207* (1), 315-321.

20. Cosnier, S.; Deronzier, A.; Moutet, J.-C., Electrocatalytic Reduction of CO_2 on Electrodes Modified by *fac*-Re(2,2′-bipyridine)$(CO)_3$Cl Complexes Bonded to Polypyrrole Films. *Journal of Molecular Catalysis* **1988**, *45* (3), 381-391.

21. Cosnier, S.; Deronzier, A.; Moutet, J.-C., Substitution Effects on the Electrochemical Behaviour of the (2,2′-bipyridine) Tricarbonylchlororhenium(I) Complex in Solution or in Polymeric Form and Their Relation to the Catalytic Reduction of Carbon Dioxide. *New Journal of Chemistry* **1990**, *14* (11), 831-839.

22. Breikss, A. I.; Abruña, H. D., Electrochemical and Mechanistic Studies of $Re(CO)_3$(dmbpy)CI] and Their Relation to the Catalytic Reduction of CO_2. *Journal of Electroanalytical Chemistry and Interfacial Electrochemistry* **1986**, *201* (2), 347-358.

23. Cabrera, C. R.; Abruna, H. D., Electrocatalysis of CO_2 Reduction at Surface Modified Metallic and Semiconducting Electrodes. *Journal of Electroanalytical Chemistry and Interfacial Electrochemistry* **1986**, *209* (1), 101-107.

24. Hayashi, Y.; Kita, S.; Brunschwig, B. S.; Fujita, E., Involvement of a Binuclear Species with the Re−C(O)O−Re Moiety in CO_2 Reduction Catalyzed by Tricarbonyl Rhenium(I)

Complexes with Diimine Ligands: Strikingly Slow Formation of the Re−Re and Re−C(O)O−Re Species from Re(dmb)$(CO)_3$S (dmb= 4,4′-Dimethyl-2,2′-bipyridine), S= Solvent). *Journal of the American Chemical Society* **2003**, *125*, 11976-11987.

25. Fujita, E.; Muckerman, J. T., Why Is Re-Re Bond Formation/Cleavage in $[Re(bpy)(CO)_3]_2$ Different from That in $[Re(CO)_5]_2$? Experimental and Theoretical Studies on the Dimers and Fragments. *Inorganic Chemistry* **2004**, *43* (24), 7636-7647.

26. Fujita, E., Photochemical Carbon Dioxide Reduction with Metal Complexes. *Coordination Chemistry Reviews* **1999**, *185–186*, 373-384.

27. Takeda, H.; Koike, K.; Inoue, H.; Ishitani, O., Development of an Efficient Photocatalytic System for CO_2 Reduction Using Rhenium(I) Complexes Based on Mechanistic Studies. *Journal of the American Chemical Society* **2008**, *130* (6), 2023-2031.

28. Wong, K.-Y.; Chung, W.-H.; Lau, C.-P., The Effect of Weak Brönsted Acids on the Electrocatalytic Reduction of Carbon Dioxide by a Rhenium Tricarbonyl Bipyridyl Complex. *Journal of Electroanalytical Chemistry* **1998**, *453* (1), 161-170.

29. Smieja, J. M.; Kubiak, C. P., Re(bipy-*t*-Bu)$(CO)_3Cl^-$ Improved Catalytic Activity for Reduction of Carbon Dioxide: IR-Spectroelectrochemical and Mechanistic Studies. *Inorganic Chemistry* **2010**, *49* (20), 9283-9289.

30. Smieja, J. M.; Benson, E. E.; Kumar, B.; Grice, K. A.; Seu, C. S.; Miller, A. J.; Mayer, J. M.; Kubiak, C. P., Kinetic and Structural Studies, Origins of Selectivity, and Interfacial Charge Transfer in the Artificial Photosynthesis of CO. *Proceedings of the National Academy of Sciences* **2012**, *109* (39), 15646-15650.

31. Grice, K. A.; Gu, N. X.; Sampson, M. D.; Kubiak, C. P., Carbon Monoxide Release Catalysed by Electron Transfer: Electrochemical and Spectroscopic Investigations of [Re(bpy-R)$(CO)_4$](OTf) Complexes Relevant to CO_2 Reduction. *Dalton Transactions* **2013**, *42* (23), 8498-8503.

32. Tezuka, M.; Yajima, T.; Tsuchiya, A.; Matsumoto, Y.; Uchida, Y.; Hidai, M., Electroreduction of Carbon Dioxide Catalyzed by Iron-Sulfur Cluster Compounds $[Fe_4S_4(SR)_4]^{2-}$. *Journal of the American Chemical Society* **1982**, *104* (24), 6834-6836.

33. Bolinger, C. M.; Sullivan, B. P.; Conrad, D.; Gilbert, J. A.; Story, N.; Meyer, T. J., Electrocatalytic Reduction of CO_2 Based on Polypyridyl Complexes of Rhodium and Ruthenium. *Journal of the Chemical Society, Chemical Communications* **1985**, (12), 796-797.

34. Bourrez, M.; Molton, F.; Chardon-Noblat, S.; Deronzier, A., [Mn(bipyridyl)$(CO)_3$Br]: An Abundant Metal Carbonyl Complex as Efficient Electrocatalyst for CO_2 Reduction. *Angewandte Chemie International Edition* **2011**, *123* (42), 10077-10080.

35. Bourrez, M.; Orio, M.; Molton, F.; Vezin, H.; Duboc, C.; Deronzier, A.; Chardon-Noblat, S., Pulsed-EPR Evidence of a Manganese(II) Hydroxycarbonyl Intermediate in the

Electrocatalytic Reduction of Carbon Dioxide by a Manganese Bipyridyl Derivative. *Angewandte Chemie International Edition* **2014**, *53* (1), 240-243.

36. Smieja, J. M.; Sampson, M. D.; Grice, K. A.; Benson, E. E.; Froehlich, J. D.; Kubiak, C. P., Manganese as a Substitute for Rhenium in CO_2 Reduction Catalysts: The Importance of Acids. *Inorganic Chemistry* **2013**, *52* (5), 2484-2491.

37. Takeda, H.; Koizumi, H.; Okamoto, K.; Ishitani, O., Photocatalytic CO_2 Reduction Using a Mn Complex as a Catalyst. *Chemical Communications* **2014**, *50* (12), 1491-1493.

38. Compain, J.-D.; Bourrez, M.; Haukka, M.; Deronzier, A.; Chardon-Noblat, S., Manganese Carbonyl Terpyridyl Complexes: Their Synthesis, Characterization and Potential Application as CO-Release Molecules. *Chemical Communications* **2014**, *50* (19), 2539-2542.

39. Sampson, M. D.; Nguyen, A. D.; Grice, K. A.; Moore, C. E.; Rheingold, A. L.; Kubiak, C. P., Manganese Catalysts with Bulky Bipyridine Ligands for the Electrocatalytic Reduction of Carbon Dioxide: Eliminating Dimerization and Altering Catalysis. *Journal of the American Chemical Society* **2014**, *136* (14), 5460-5471.

40. Grills, D. C.; Farrington, J. A.; Layne, B. H.; Lymar, S. V.; Mello, B. A.; Preses, J. M.; Wishart, J. F., Mechanism of the Formation of a Mn-Based CO_2 Reduction Catalyst Revealed by Pulse Radiolysis with Time-Resolved Infrared Detection. *Journal of the American Chemical Society* **2014**, *136* (15), 5563-5566.

41. Agarwal, J.; Shaw, T. W.; Stanton, C. J.; Majetich, G. F.; Bocarsly, A. B.; Schaefer, H. F., NHC-Containing Manganese(I) Electrocatalysts for the Two-Electron Reduction of CO_2. *Angewandte Chemie International Edition* **2014**, *53* (20), 5252-5255.

42. Sampson, M. D.; Kubiak, C. P., Manganese Electrocatalysts with Bulky Bipyridine Ligands: Utilizing Lewis Acids To Promote Carbon Dioxide Reduction at Low Overpotentials. *Journal of the American Chemical Society* **2016**, *138* (4), 1386-1393.

43. Franco, F.; Cometto, C.; Vallana, F. F.; Sordello, F.; Priola, E.; Minero, C.; Nervi, C.; Gobetto, R., A Local Proton Source in a [Mn(bpy-R)$(CO)_3$Br]-Type Redox Catalyst Enables CO_2 Reduction Even in the Absence of Brønsted Acids. *Chemical Communications* **2014**, *50* (93), 14670-14673.

44. Agarwal, J.; Shaw, T. W.; Schaefer III, H. F.; Bocarsly, A. B., Design of a Catalytic Active Site for Electrochemical CO_2 Reduction with Mn(I)-Tricarbonyl Species. *Inorganic Chemistry* **2015**, *54* (11), 5285-5294.

45. Machan, C. W.; Stanton III, C. J.; Vandezande, J. E.; Majetich, G. F.; Schaefer III, H. F.; Kubiak, C. P.; Agarwal, J., Electrocatalytic Reduction of Carbon Dioxide by Mn(CN)(2,2′-bipyridine)$(CO)_3$: CN Coordination Alters Mechanism. *Inorganic Chemistry* **2015**, *54* (17), 8849-8856.

46. Rawat, K. S.; Mahata, A.; Choudhuri, I.; Pathak, B., *N*-Heterocylic Carbene-Based Mn Electrocatalyst for Two-Electron CO_2 Reduction over Proton Reduction. *The Journal of Physical Chemistry C* **2016**, *120* (16), 8821-8831.

47. Zeng, Q.; Tory, J.; Hartl, F., Electrocatalytic Reduction of Carbon Dioxide with a Manganese(I) Tricarbonyl Complex Containing a Nonaromatic α-Diimine Ligand. *Organometallics* **2014**, *33* (18), 5002-5008.

48. Cheung, P. L.; Machan, C. W.; Malkhasian, A. Y.; Agarwal, J.; Kubiak, C. P., Photocatalytic Reduction of Carbon Dioxide to CO and HCO_2H Using *fac*-$Mn(CN)(bpy)(CO)_3$. *Inorganic Chemistry* **2016**, *55* (6), 3192-3198.

49. Rosser, T. E.; Windle, C. D.; Reisner, E., Electrocatalytic and Solar-Driven CO_2 Reduction to CO with a Molecular Manganese Catalyst Immobilized on Mesoporous TiO_2. *Angewandte Chemie International Edition* **2016**, *55* (26), 7388-7392.

50. Stanton III, C. J.; Vandezande, J. E.; Majetich, G. F.; Schaefer III, H. F.; Agarwal, J., Mn-NHC Electrocatalysts: Increasing π Acidity Lowers the Reduction Potential and Increases the Turnover Frequency for CO_2 Reduction. *Inorganic Chemistry* **2016**, *55* (19), 9509-9512.

51. Walsh, J. J.; Smith, C. L.; Neri, G.; Whitehead, G. F.; Robertson, C. M.; Cowan, A. J., Improving the Efficiency of Electrochemical CO_2 Reduction Using Immobilized Manganese Complexes. *Faraday Discussions* **2015**, *183*, 147-160.

52. Hammouche, M.; Lexa, D.; Momenteau, M.; Saveant, J. M., Chemical Catalysis of Electrochemical Reactions. Homogeneous Catalysis of the Electrochemical Reduction of Carbon Dioxide by Iron("0") Porphyrins. Role of the Addition of Magnesium Cations. *Journal of the American Chemical Society* **1991**, *113* (22), 8455-8466.

53. Bhugun, I.; Lexa, D.; Saveant, J.-M., Ultraefficient Selective Homogeneous Catalysis of the Electrochemical Reduction of Carbon Dioxide by an Iron(0) Porphyrin Associated with a Weak Broensted Acid Cocatalyst. *Journal of the American Chemical Society* **1994**, *116* (11), 5015-5016.

54. Grodkowski, J.; Behar, D.; Neta, P.; Hambright, P., Iron Porphyrin-Catalyzed Reduction of CO_2. Photochemical and Radiation Chemical Studies. *The Journal of Physical Chemistry A* **1997**, *101* (3), 248-254.

55. Dhanasekaran, T.; Grodkowski, J.; Neta, P.; Hambright, P.; Fujita, E., *p*-Terphenyl-Sensitized Photoreduction of CO_2 with Cobalt and Iron Porphyrins. Interaction Between CO and Reduced Metalloporphyrins. *The Journal of Physical Chemistry A* **1999**, *103* (38), 7742-7748.

56. Costentin, C.; Drouet, S.; Robert, M.; Savéant, J.-M., A Local Proton Source Enhances CO_2 Electroreduction to CO by a Molecular Fe Catalyst. *Science* **2012**, *338* (6103), 90-94.

57. Costentin, C.; Passard, G.; Robert, M.; Savéant, J.-M., Pendant Acid–Base Groups in Molecular Catalysts: H-Bond Promoters or Proton Relays? Mechanisms of the Conversion of

CO_2 to CO by Electrogenerated Iron(0) Porphyrins Bearing Prepositioned Phenol Functionalities. *Journal of the American Chemical Society* **2014**, *136* (33), 11821-11829.

58. Meshitsuka, S.; Ichikawa, M.; Tamaru, K., Electrocatalysis by Metal Phthalocyanines in the Reduction of Carbon Dioxide. *Journal of the Chemical Society, Chemical Communications* **1974**, (5), 158-159.

59. Beley, M.; Collin, J. P.; Ruppert, R.; Sauvage, J. P., Electrocatalytic Reduction of Carbon Dioxide by Nickel Cyclam^{2+} in Water: Study of the Factors Affecting the Efficiency and the Selectivity of the Process. *Journal of the American Chemical Society* **1986**, *108* (24), 7461-7467.

60. Thoi, V. S.; Chang, C. J., Nickel *N*-Heterocyclic Carbene–Pyridine Complexes that Exhibit Selectivity for Electrocatalytic Reduction of Carbon Dioxide Over Water. *Chemical Communications* **2011**, *47* (23), 6578-6580.

61. Fisher, B. J.; Eisenberg, R., Electrocatalytic Reduction of Carbon Dioxide by Using Macrocycles of Nickel and Cobalt. *Journal of the American Chemical Society* **1980**, *102* (24), 7361-7363.

62. Fujita, E.; Szalda, D. J.; Creutz, C.; Sutin, N., Carbon Dioxide Activation: Thermodynamics of Carbon Dioxide Binding and the Involvement of Two Cobalt Centers in the Reduction of Carbon Dioxide by a Cobalt(I) Macrocycle. *Journal of the American Chemical Society* **1988**, *110* (14), 4870-4871.

63. Matsuoka, S.; Yamamoto, K.; Ogata, T.; Kusaba, M.; Nakashima, N.; Fujita, E.; Yanagida, S., Efficient and Selective Electron Mediation of Cobalt Complexes with Cyclam and Related Macrocycles in the *p*-Terphenyl-Catalyzed Photoreduction of Carbon Dioxide. *Journal of the American Chemical Society* **1993**, *115* (2), 601-609.

64. Haines, R. J.; Wittrig, R. E.; Kubiak, C. P., Electrocatalytic Reduction of Carbon Dioxide by the Binuclear Copper Complex $[Cu_2(6\text{-(diphenylphosphino-2,2'-bipyridyl})_2(MeCN)_2][PF_6]_2$. *Inorganic Chemistry* **1994**, *33* (21), 4723-4728.

65. Hartl, F.; Rossenaar, B. D.; Stor, G. J.; Stufkens, D. J., Role of an Electron-Transfer Chain Reaction in the Unusual Photochemical Formation of Five-Coordinated Anions $[Mn(CO)_3(\alpha\text{-diimine})]^-$ From *fac*-$[Mn(X)(CO)_3(\alpha\text{-diimine})]$ (X= halide) at Low Temperatures. *Recueil des Travaux Chimiques des Pays-Bas* **1995**, *114* (11-12), 565-570.

66. Schmittel, M.; Ganz, A.; Schenk, W. A.; Hagel, M., Synthesis and Coordination Properties of 6,6′-Dimesityl-2,2′-Bipyridine. *Zeitschrift für Naturforschung B* **1999**, *54* (4), 559-564.

67. Jeffery, J.; Schatz, E.; Ward, M., The Co-ordination Chemistry of Mixed Pyridine-Phenol Ligands; Synthesis of 6-(2-Hydroxyphenyl)-2,2′-Bipyridine (HL) and the Crystal Structures of $[Cu_2L_2(\mu\text{-}MeCO_2)][PF_6] \cdot 1.5\ CH_2Cl_2$ and $[CoL_2][PF_6] \cdot MeCN$. *Journal of the Chemical Society, Dalton Transactions* **1992**, (12), 1921-1927.

68. Willkomm, J.; Orchard, K. L.; Reynal, A.; Pastor, E.; Durrant, J. R.; Reisner, E., Dye-Sensitised Semiconductors Modified with Molecular Catalysts for Light-Driven H_2 Production. *Chemical Society Reviews* **2016**, *45* (1), 9-23.

69. Rosser, T. E.; Gross, M. A.; Lai, Y.-H.; Reisner, E., Precious-Metal Free Photoelectrochemical Water Splitting with Immobilised Molecular Ni and Fe Redox Catalysts. *Chemical Science* **2016**, *7* (7), 4024-4035.

70. Neri, G.; Walsh, J. J.; Wilson, C.; Reynal, A.; Lim, J. Y. C.; Li, X.; White, A. J. P.; Long, N. J.; Durrant, J. R.; Cowan, A. J., A Functionalised Nickel Cyclam Catalyst for CO_2 Reduction: Electrocatalysis, Semiconductor Surface Immobilisation and Light-Driven Electron Transfer. *Physical Chemistry Chemical Physics* **2015**, *17* (3), 1562-1566.

71. Benhamou, L.; Chardon, E.; Lavigne, G.; Bellemin-Laponnaz, S. p.; César, V., Synthetic Routes to *N*-Heterocyclic Carbene Precursors. *Chemical Reviews* **2011**, *111* (4), 2705-2733.

72. de Frémont, P.; Marion, N.; Nolan, S. P., Carbenes: Synthesis, Properties, and Organometallic Chemistry. *Coordination Chemistry Reviews* **2009**, *253* (7), 862-892.

73. Binobaid, A.; Iglesias, M.; Beetstra, D. J.; Kariuki, B.; Dervisi, A.; Fallis, I. A.; Cavell, K. J., Expanded Ring and Functionalised Expanded Ring *N*-Heterocyclic Carbenes as Ligands in Catalysis. *Dalton Transactions* **2009**, (35), 7099-7112.

74. Lu, W. Y.; Cavell, K. J.; Wixey, J. S.; Kariuki, B., First Examples of Structurally Imposing Eight-Membered-Ring (Diazocanylidene) *N*-Heterocyclic Carbenes: Salts, Free Carbenes, and Metal Complexes. *Organometallics* **2011**, *30* (21), 5649-5655.

75. Makhloufi, A.; Frank, W.; Ganter, C., Diamino-and Mixed Amino-Amido-*N*-Heterocyclic Carbenes Based on Triazine Backbones. *Organometallics* **2012**, *31* (5), 2001-2008.

76. Dröge, T.; Glorius, F., The Measure of All Rings—*N*-Heterocyclic Carbenes. *Angewandte Chemie International Edition* **2010**, *49* (39), 6940-6952.

77. Clavier, H.; Nolan, S. P., Percent Buried Volume for Phosphine and *N*-Heterocyclic Carbene Ligands: Steric Properties in Organometallic Chemistry. *Chemical Communications* **2010**, *46* (6), 841-861.

78. Kühl, O., Sterically Induced Differences in *N*-Heterocyclic Carbene Transition Metal Complexes. *Coordination Chemistry Reviews* **2009**, *253* (21), 2481-2492.

79. Díez-González, S.; Nolan, S. P., Stereoelectronic Parameters Associated with *N*-Heterocyclic Carbene (NHC) Ligands: A Quest for Understanding. *Coordination Chemistry Reviews* **2007**, *251* (5), 874-883.

80. Díez-González, S.; Marion, N.; Nolan, S. P., *N*-Heterocyclic Carbenes in Late Transition Metal Catalysis. *Chemical Reviews* **2009**, *109* (8), 3612-3676.

81. Nelson, D. J.; Nolan, S. P., Quantifying and Understanding the Electronic Properties of *N*-Heterocyclic Carbenes. *Chemical Society Reviews* **2013**, *42* (16), 6723-6753.

82. Marion, N.; Nolan, S. P., Well-Defined *N*-Heterocyclic Carbenes− Palladium(II) Precatalysts for Cross-Coupling Reactions. *Accounts of Chemical Research* **2008**, *41* (11), 1440-1449.

83. Glorius, F., *N-Heterocyclic Carbenes in Transition Metal Catalysis*. Springer: 2007; Vol. 21.

84. Valente, C.; Çalimsiz, S.; Hoi, K. H.; Mallik, D.; Sayah, M.; Organ, M. G., The Development of Bulky Palladium NHC Complexes for the Most-Challenging Cross-Coupling Reactions. *Angewandte Chemie International Edition* **2012**, *51* (14), 3314-3332.

85. Herrmann, W. A.; Mihalios, D.; Öfele, K.; Kiprof, P.; Belmedjahed, F., Metallcarbonyl-Synthesen, XXI. Einfache Synthese Eines Präparativ Nützlichen Alkoxy (Carbonyl) Metallats. *Chemische Berichte* **1992**, *125* (8), 1795-1799.

86. Liu, C.-Y.; Chen, D.-Y.; Lee, G.-H.; Peng, S.-M.; Liu, S.-T., Synthesis of Cyclic Diamino-Substituted Metal Carbene Complexes. *Organometallics* **1996**, *15* (3), 1055-1061.

87. Xue, W.-M.; Chan, M. C.-W.; Su, Z.-M.; Cheung, K.-K.; Liu, S.-T.; Che, C.-M., Spectroscopic and Excited-State Properties of Luminescent Rhenium(I) *N*-Heterocyclic Carbene Complexes Containing Aromatic Diimine Ligands. *Organometallics* **1998**, *17* (8), 1622-1630.

88. Huertos, M. A.; Pérez, J.; Riera, L. a.; Menéndez-Velázquez, A., From *N*-Alkylimidazole Ligands at a Rhenium Center: Ring Opening or Formation of NHC Complexes. *Journal of the American Chemical Society* **2008**, *130* (41), 13530-13531.

89. Flores-Figueroa, A.; Kaufhold, O.; Feldmann, K.-O.; Hahn, F. E., Synthesis of NHC Complexes by Template Controlled Cyclization of β-Functionalized Isocyanides. *Dalton Transactions* **2009**, (42), 9334-9342.

90. Kaufhold, O.; Stasch, A.; Pape, T.; Hepp, A.; Edwards, P. G.; Newman, P. D.; Hahn, F. E., Metal Template Controlled Formation of [11]ane-P_2C^{NHC} Macrocycles. *Journal of the American Chemical Society* **2008**, *131* (1), 306-317.

91. Hiltner, O.; Herdtweck, E.; Drees, M.; Herrmann, W. A.; Kühn, F. E., Synthesis and Characterization of Two New *fac*-Tricarbonylrhenium(I) Biscarbene Complexes. *European Journal of Inorganic Chemistry* **2009**, *2009* (13), 1825-1831.

92. Jiang, Y.; Blacque, O.; Fox, T.; Frech, C. M.; Berke, H., Development of Rhenium Catalysts for Amine Borane Dehydrocoupling and Transfer Hydrogenation of Olefins. *Organometallics* **2009**, *28* (18), 5493-5504.

93. Huertos, M. A.; Pérez, J.; Riera, L.; Díaz, J.; López, R., Effect of the Nature of the Substituent in *N*-Alkylimidazole Ligands on the Outcome of Deprotonation: Ring Opening

versus the Formation of *N*-Heterocyclic Carbene Complexes. *Chemistry–A European Journal* **2010**, *16* (28), 8495-8507.

94. Huertos, M. A.; Pérez, J.; Riera, L. a.; Díaz, J.; López, R., From Bis(*N*-Alkylimidazole) to Bis(NH–NHC) in Rhenium Carbonyl Complexes. *Angewandte Chemie International Edition* **2010**, *49* (36), 6409-6412.

95. Hiltner, O.; Boch, F. J.; Brewitz, L.; Härter, P.; Drees, M.; Herdtweck, E.; Herrmann, W. A.; Kühn, F. E., Bridged *fac*-Tricarbonylrhenium(I)–Biscarbene Complexes: Synthesis, Characterization, and Molecular Dynamics. *European Journal of Inorganic Chemistry* **2010**, *2010* (33), 5284-5293.

96. Blase, V.; Pape, T.; Hahn, F. E., Template Synthesis of a Macrocycle with a Mixed NHC/Phosphine Donor Set. *Journal of Organometallic Chemistry* **2011**, *696* (21), 3337-3342.

97. Chen, C.-H.; Liu, Y.-H.; Peng, S.-M.; Chen, J.-T.; Liu, S.-T., Synthesis of *N*-Heterocyclic Carbene Rhenium(I) Carbonyl Complexes. *Dalton Transactions* **2012**, *41* (9), 2747-2754.

98. Casson, L. A.; Muzzioli, S.; Raiteri, P.; Skelton, B. W.; Stagni, S.; Massi, M.; Brown, D. H., *N*-Heterocyclic Carbenes as π*-Acceptors in Luminescent Re(I) Triscarbonyl Complexes. *Dalton Transactions* **2011**, *40* (44), 11960-11967.

99. Martin, T. A.; Ellul, C. E.; Mahon, M. F.; Warren, M. E.; Allan, D.; Whittlesey, M. K., Neutral and Cationic Mono-and Bis-*N*-Heterocyclic Carbene Complexes Derived From Manganese and Rhenium Carbonyl Precursors. *Organometallics* **2011**, *30* (8), 2200-2211.

100. Li, X.-W.; Li, H.-Y.; Wang, G.-F.; Chen, F.; Li, Y.-Z.; Chen, X.-T.; Zheng, Y.-X.; Xue, Z.-L., Blue-Green Luminescent Rhenium(I) Tricarbonyl Complexes with Pyridine-Functionalized *N*-Heterocyclic Carbene Ligands. *Organometallics* **2012**, *31* (10), 3829-3835.

101. Canella, D.; Hock, S. J.; Hiltner, O.; Herdtweck, E.; Herrmann, W. A.; Kühn, F. E., Synthesis and Characterization of Propylene and Butylene Bridged *fac*-Tricarbonylrhenium(I) Biscarbene Complexes. *Dalton Transactions* **2012**, *41* (7), 2110-2121.

102. Wang, G.-F.; Liu, Y.-Z.; Chen, X.-T.; Zheng, Y.-X.; Xue, Z.-L., Synthesis, Structure and Luminescent Properties of Rhenium(I) Carbonyl Complexes Containing Pyrimidine-Functionalized *N*-Heterocyclic Carbenes. *Inorganica Chimica Acta* **2013**, *394*, 488-493.

103. Vaughan, J. G.; Reid, B. L.; Ramchandani, S.; Wright, P. J.; Muzzioli, S.; Skelton, B. W.; Raiteri, P.; Brown, D. H.; Stagni, S.; Massi, M., The Photochemistry of Rhenium(I) Tricarbonyl *N*-Heterocyclic Carbene Complexes. *Dalton Transactions* **2013**, *42* (39), 14100-14114.

104. Ng, C.-O.; Yiu, S.-M.; Ko, C.-C., Synthesis, Characterization, and Photophysical Study of Luminescent Rhenium(I) Diimine Complexes with Various Types of *N*-Heterocyclic Carbene Ligands. *Inorganic Chemistry* **2014**, *53* (6), 3022-3031.

105. Hock, S. J.; Schaper, L.-A.; Pöthig, A.; Drees, M.; Herdtweck, E.; Hiltner, O.; Herrmann, W. A.; Kühn, F. E., Synthesis and Characterisation of Chelated Cationic $Re(I)(CO)_3$bis(NHC)(WCA) Complexes. *Dalton Transactions* **2014**, *43* (5), 2259-2271.

106. Chan, C. Y.; Pellegrini, P. A.; Greguric, I.; Barnard, P. J., Rhenium and Technetium Tricarbonyl Complexes of *N*-Heterocyclic Carbene Ligands. *Inorganic Chemistry* **2014**, *53* (20), 10862-10873.

107. Vaughan, J. G.; Reid, B. L.; Wright, P. J.; Ramchandani, S.; Skelton, B. W.; Raiteri, P.; Muzzioli, S.; Brown, D. H.; Stagni, S.; Massi, M., Photophysical and Photochemical Trends in Tricarbonyl Rhenium(I) *N*-Heterocyclic Carbene Complexes. *Inorganic Chemistry* **2014**, *53* (7), 3629-3641.

108. Hille, C.; Kühn, F. E., Cationic Rhenium Complexes Ligated with *N*-Heterocyclic Carbenes–An Overview. *Dalton Transactions* **2016**, *45* (1), 15-31.

109. Huckaba, A. J.; Sharpe, E. A.; Delcamp, J. H., Photocatalytic Reduction of CO_2 with Re-Pyridyl-NHCs. *Inorganic Chemistry* **2015**, *55* (2), 682-690.

110. Visbal, R.; Gimeno, M. C., *N*-Heterocyclic Carbene Metal Complexes: Photoluminescence and Applications. *Chemical Society Reviews* **2014**, *43* (10), 3551-3574.

111. Liyanage, N. P.; Dulaney, H. A.; Huckaba, A. J.; Jurss, J. W.; Delcamp, J. H., Electrocatalytic Reduction of CO_2 to CO With Re-Pyridyl-NHCs: Proton Source Influence on Rates and Product Selectivities. *Inorganic Chemistry* **2016**, *55* (12), 6085-6094.

112. Stanton III, C. J.; Machan, C. W.; Vandezande, J. E.; Jin, T.; Majetich, G. F.; Schaefer III, H. F.; Kubiak, C. P.; Li, G.; Agarwal, J., Re(I) NHC Complexes for Electrocatalytic Conversion of CO_2. *Inorganic Chemistry* **2016**, *55* (6), 3136-3144.

113. Su, T. C.; Liu, Y. H.; Peng, S. M.; Liu, S. T., Rhenium Complexes with a Pyridinyl-Naphthyridine Ligand: Synthesis, Characterization, and Catalytic Activity. *European Journal of Inorganic Chemistry* **2013**, *2013* (13), 2362-2367.

114. Hahn, E. M.; Casini, A.; Kuehn, F. E., Re(VII) and Tc(VII) Trioxo Complexes Stabilized by Tridentate Ligands and Their Potential Use as Radiopharmaceuticals. *Coordination Chemistry Reviews* **2014**, *276*, 97-111.

115. Bellemin-Laponnaz, S. p.; Dagorne, S., Group 1 and 2 and Early Transition Metal Complexes Bearing *N*-Heterocyclic Carbene Ligands: Coordination Chemistry, Reactivity, and Applications. *Chemical Reviews* **2014**, *114* (18), 8747-8774.

116. Jürgens, S.; Herrmann, W. A.; Kühn, F. E., Rhenium and Technetium Based Radiopharmaceuticals: Development and Recent Advances. *Journal of Organometallic Chemistry* **2014**, *751*, 83-89.

117. Hock, S. J.; Schaper, L.-A.; Herrmann, W. A.; Kühn, F. E., Group 7 Transition Metal Complexes with *N*-Heterocyclic Carbenes. *Chemical Society Reviews* **2013**, *42* (12), 5073-5089.

118. Schaper, L. A.; Hock, S. J.; Herrmann, W. A.; Kuehn, F. E., Synthesis and Application of Water-Soluble NHC Transition-Metal Complexes. *Angewandte Chemie International Edition* **2013**, *52* (1), 270-289.

119. Kuninobu, Y.; Takai, K., Organic Reactions Catalyzed by Rhenium Carbonyl Complexes. *Chemical Reviews* **2010**, *111* (3), 1938-1953.

120. Hahn, F. E.; Jahnke, M. C., Heterocyclic Carbenes: Synthesis and Coordination Chemistry. *Angewandte Chemie International Edition* **2008**, *47* (17), 3122-3172.

CHAPTER 2

MANGANESE(I)-NHC ELECTROCATALYSTS FOR THE REDUCTION OF CO_2 TO CO

INTRODUCTION

In 2011 Bourrez and co-workers disclosed the first report where manganese was first used as an electrocatalyst for the reduction of CO_2 to CO, i.e., *fac*-MnBr(bpy)$(CO)_3$.[1] Since the publication of this seminal report, several studies have focused on modifications of the bipyridyl backbone or replacement of the axial halogen in order to improve the electrocatalytic process. Our research group has incorporated an *N*-heterocyclic carbene onto the supporting ligand. We hypothesized several advantages to this approach, including; ease of synthetic manipulation (i.e., sterically and electronically) of the NHC vs bipyridine backbone, and stronger binding of the electron–rich carbene to the metal center could potentially lead to a longer catalyst lifetime and more consistent reactivity throughout the catalytic process. In 2014 we reported the replacement of one pyridine ring in Bourrez's *fac*-MnBr(bpy)$(CO)_3$ catalyst with a NHC moiety to afford a *fac*-[MnBr(N-C)$(CO)_3$]-type catalyst (Figure 2.1).[2] This was the first report of a catalytic manganese organometallic complex supported by a NHC ligand. A followup study was performed in 2015 where the effects of axial ligand substitution were explored to gain insight on the photodecompostion and electrochemical activity of Mn(I)-NHC complexes.[3] Results from these studies follow.

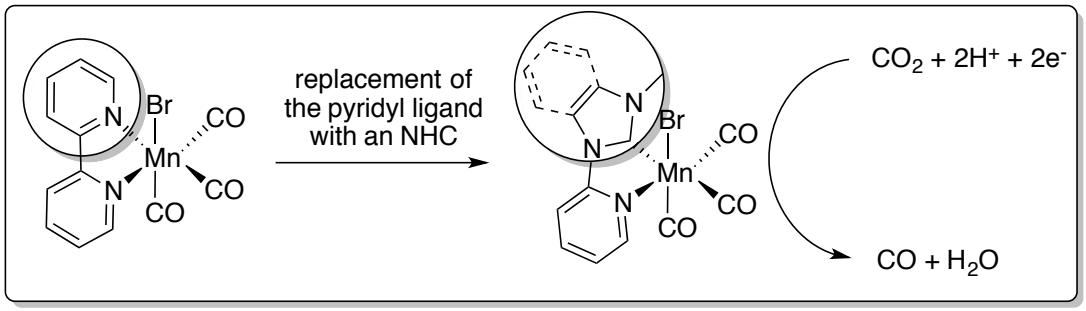

Figure 2.1: Replacement of Pyridine with NHC to Afford $MnBr(N\text{-}C)(CO)_3$-Type Catalysts

RESULTS AND DISCUSSION

In our first study, *N*-methyl-*N*′-2-pyridylbenzimidazolium (**L2.1**) and *N*-Methyl-*N*′-2-pyridylimidazolium (**L2.2**) were chosen as the model NHC-pyridyl ligands to replace bpy. Proligand **L2.1** and related proligands had been previously coordinated to rhenium(I) tricarbonyl compounds for photochemical studies,[4-6] however, neither **L2.1** nor **L2.2** have been reported in similar manganese(I) complexes.[7] Synthesis of **L2.1** (Scheme 2.1) and **L2.2** (Scheme 2.2) began with the *N*-arylation of either benzimidazole or imidazole with 2-bromopyridine.[8] The resulting 2-pyridyl hetereocycles were then alkylated with methyl iodide, and the corresponding iodo salts underwent salt metathesis with ammonium hexafluorophosphate to afford proligands [*N*-methyl-*N*′-2-pyridylbenzimidazolium]$^{+}PF_6^{-}$ and [*N*-methyl-*N*′-2-pyridylimidazolium]$^{+}PF_6^{-}$, **L2.1** and **L2.2** respectively.[9] The hexafluorophosphate salts were then chelated to $MnBr(CO)_5$, in the absence of light, using potassium carbonate in refluxing tetrahydrofuran[6] to give desired the Mn(I) complexes **L1.1** and **L1.2** in 4 steps with poor overall yields, 10% and 22%, respectively.

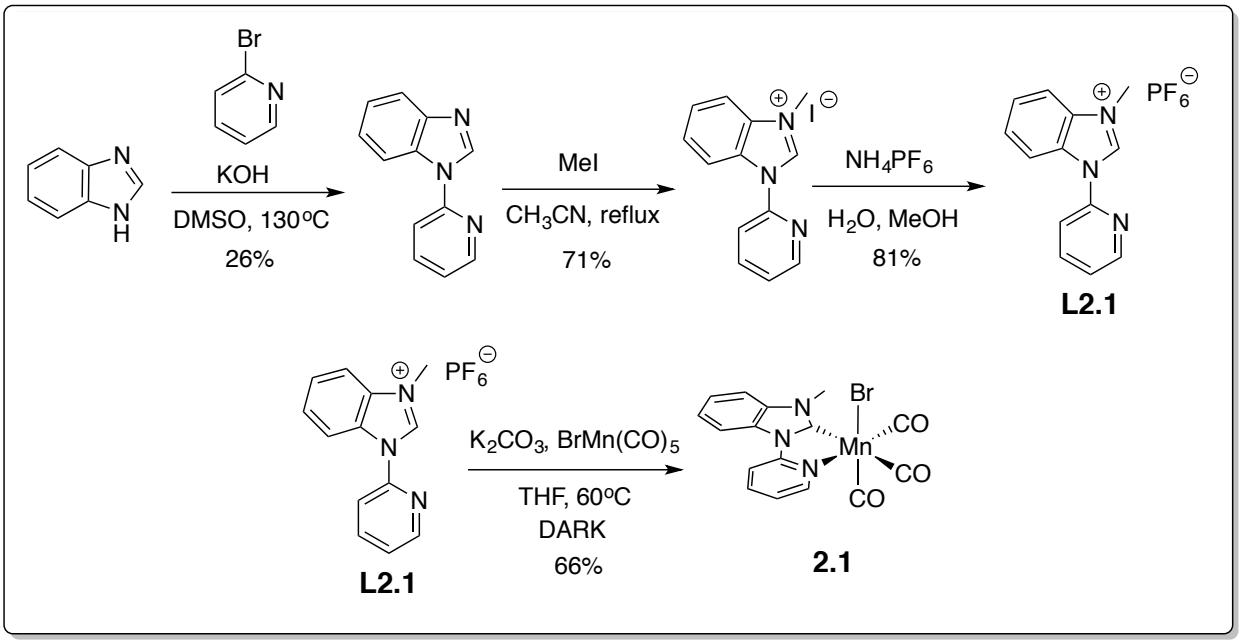

Scheme 2.1: Synthesis of Benzimidazole Substituted Proligand and NHC, **L2.1** and **2.1**

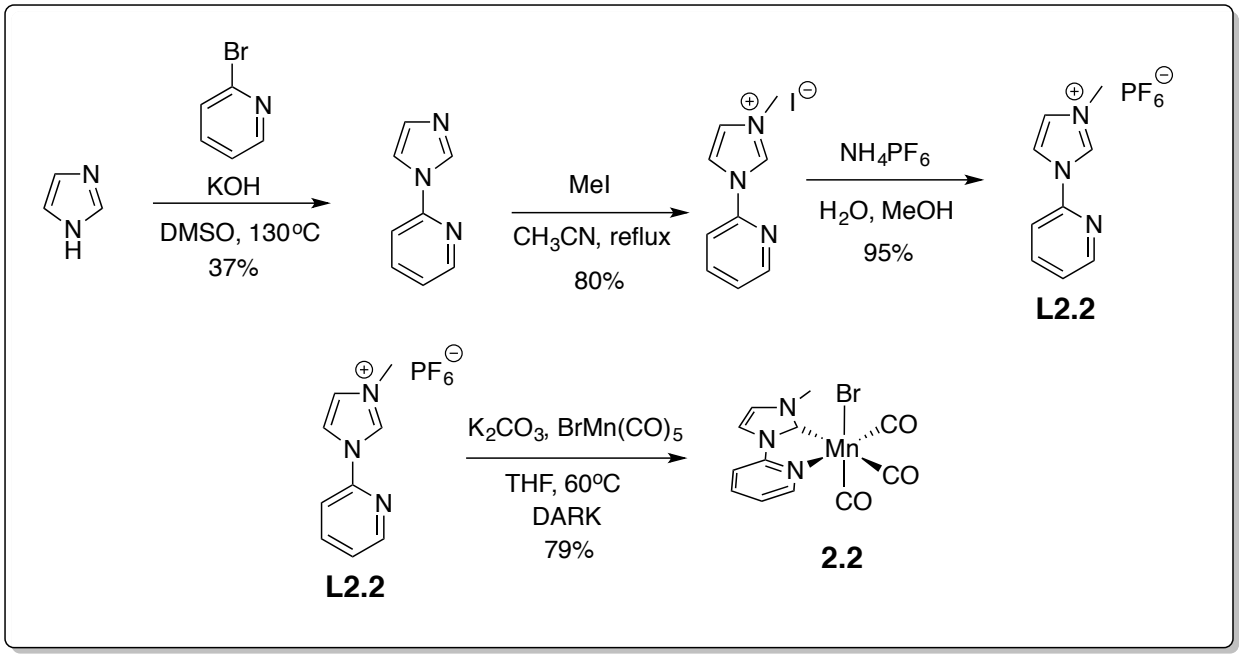

Scheme 2.2: Synthesis of Imidazole Substituted Proligand and NHC, **L2.2** and **2.2**

To address the low yields and the compromised purity of **2.1** and **2.2**, an improved synthetic strategy was realized (Scheme 2.3). The *N*-arylation of benzimidazole or imidazole with 2-bromopyridine and potassium carbonate were melted together, without solvent, to give the desired products in high yield (>90%).[10] The purity of the final products after metal chelation was improved by exploiting the solubility of the starting proligands **L2.3** and **L2.4**. Using a halogenated salt (which is H_2O soluble) instead of a PF_6 salt (which is insoluble in H_2O, and has increased organic solubility), allowed the removal of any unreacted ligand from the product mixture merely by an aqueous wash. To this end, chelation of **L2.3** and **L2.4** with $MnBr(CO)_5$ in the absence of light using potassium *t*-butoxide in refluxing tetrahydrofuran, yielded the desired compounds **2.1** and **2.2**, free of impurity after an aqueous work-up. The synthesis of complexes **2.1** and **2.2** was reduced to three steps with improved overall yields of 83% and 85%, respectively. When the iodo salts of **L2.3** and **L2.4** were used for chelation, a partial halogen exchange at the metal center was observed during ligation. This exchange was previously reported for Re(I)-tricarbonyl NHC compounds,[6] and mitigated by employing the bromo salt, obtained from methylation with MeBr. Compounds **2.1** and **2.2** were characterized by FTIR, ^{1}H NMR, and ^{13}C NMR (see S2.SI, pp 73-78). Single crystals of **2.1** were grown by slow diffusion and the structure was verified by X-ray analysis (Figure 2.2).

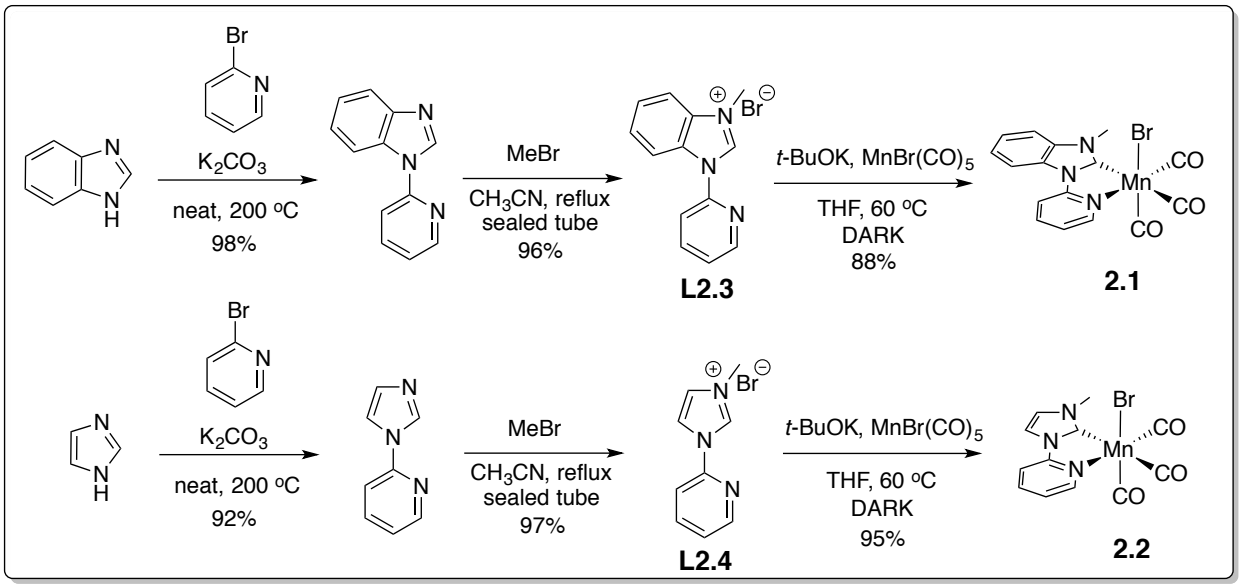

Scheme 2.3: An Improved Synthesis of Mn(I)-NHC Catalysts **2.1** and **2.2**

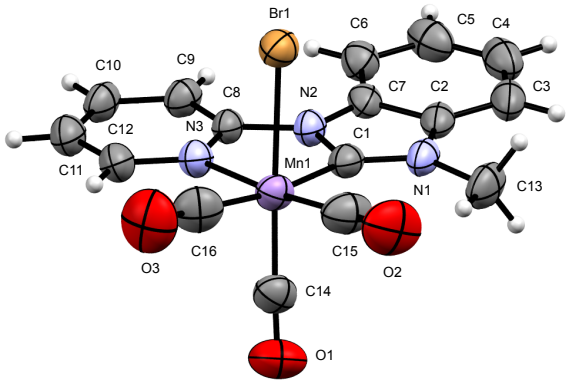

Figure 2.2: X-Ray Structure of Mn(I)-NHC Complex **2.1**

The cyclic voltammetry (CV) of **2.1** under Ar in wet CH_3CN (5% H_2O), shows two irreversible redox processes at −1.35 V and −1.64 V vs. SCE (Figure 2.3). The reduction wave at −1.64 V is attributed to a dimeric species formed during the first reduction $[Mn(N\text{-}C)(CO)_3]_2$, and no other reductive processes were observed when the CV was expanded to −3.0 V vs. SCE (i.e., solvent reduction). When the CV for **2.1** was run under an atmosphere of CO_2, the current doubles (2×) at the first reduction wave, indicating catalytic current enhancement. Note, H_2O or another

weak Brønsted acid is needed for catalytic activity.[1] When the CV was recorded in dry CH_3CN, there was no observed difference between Ar and CO_2 saturated electrolytes.

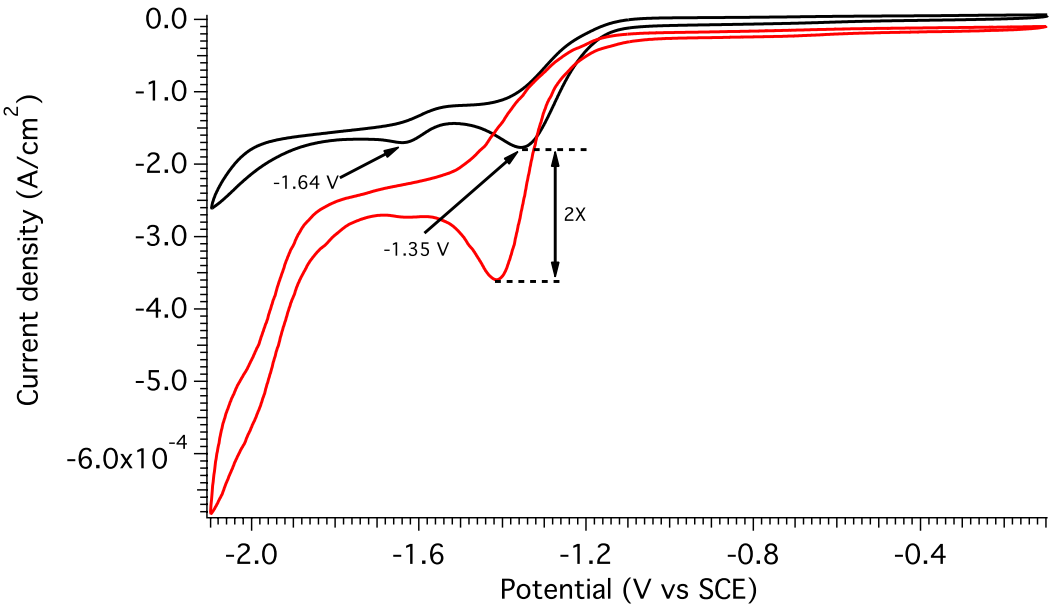

Figure 2.3: CV of **2.1** under Ar (black trace) and CO_2 (red trace) in wet (5% H_2O) CH_3CN with 0.1 TBAP supporting electrolyte at 10 mV/s. Complex was loaded at a concentration of 1 mM, and the pH adjusted to 3.7 ($HClO_4$) in the case of Ar.

The CV of complex **2.2** (Figure 2.4) under Ar in wet CH_3CN (5% H_2O) showed similar redox behavior, although the two reductions are shifted cathodically (more negative) to −1.46 V and −1.72 V vs SCE. Removal of the annulated benzene ring from complex **1.1** leads to an increased electron density at the metal center which results in the cathodic shift presumably by increasing bonding character and raising the LUMO energy.[11] This change is evident when comparing the symmetric CO frequencies for **2.1** (2015 cm^{-1}) and **2.2** (2012 cm^{-1}); increased electron density at the metal center weakens the CO bond, thus reducing the frequency.[12] When the CV for **2.2** was run under an atmosphere of CO_2, the current increases by 1.9× at the first

reduction wave. Both catalysts **2.1** and **2.2** fall below the 2.7× reduction enhancement previously found with Bourrez's catalyst, $MnBr(bpy)(CO)_3$.[1, 13] Electrocatalytic conversion of CO_2 to CO was also verified by the reduction of **2.1** (−1.35 V) in the presence of $^{13}CO_2$. Analysis of the headspace of the electrolysis cell after reduction indicated the presence of ^{13}CO, which was confirmed by FTIR analysis. In addition, these catalysts were selective for the reduction of CO_2 to CO; no H_2 production was observed at any point during electrolysis.

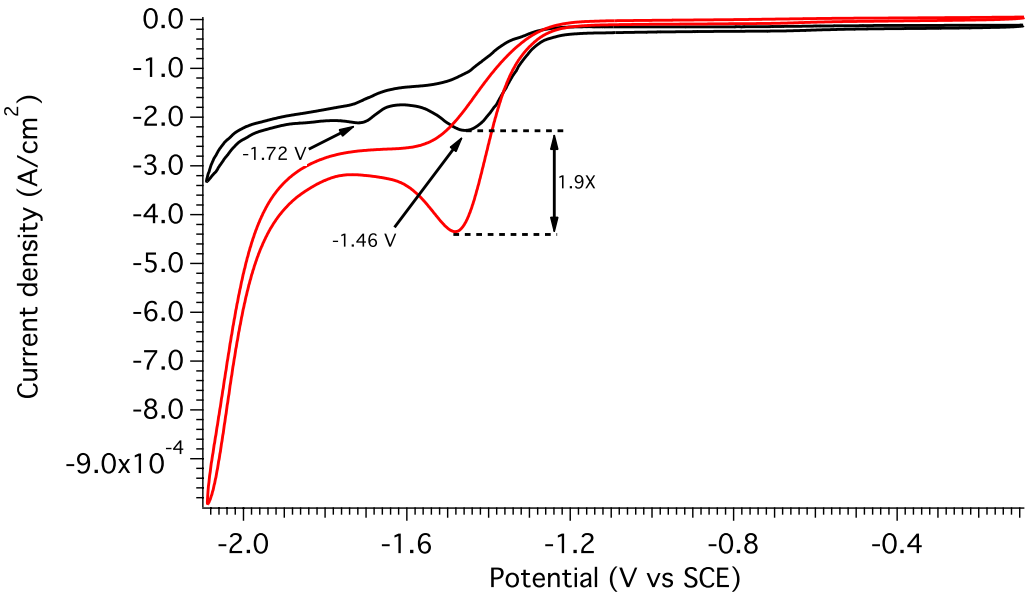

Figure 2.4: CV of **2.2** under Ar (black trace) and CO_2 (red trace) in wet (5% H_2O) CH_3CN with 0.1 TBAP supporting electrolyte at 10 mV/s. Complex was loaded at a concentration of 1 mM, and the pH adjusted to 3.7 ($HClO_4$) in the case of Ar.

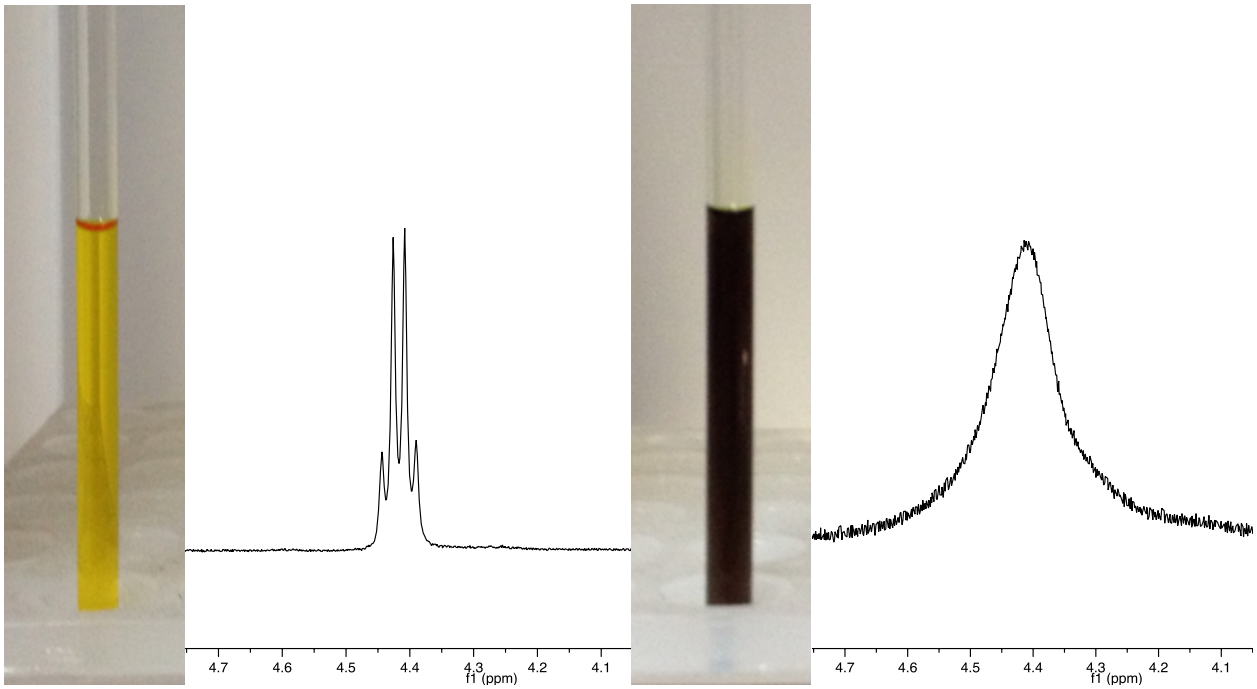

Figure 2.5: ^{1}H NMR of [MnBr(*N*-ethyl-*N*′-2-pyridylimidazol-2-ylidine)(CO)$_3$] **(2.4)** before exposure to laboratory light (left) and after ca. 30 minutes of exposure to laboratory light (right).

Manganese-centered tricarbonyl catalysts are well-known to be sensitive to ultraviolet and visible light.[14-25] The mechanism of photodissociation for *fac*-Mn(X)(bpy)(CO)$_3$ (X = halide) has been described by Stufkens and co-workers in 1996.[20] Upon irradiation, the *fac*-Mn(X)(bpy)(CO)$_3$ complex releases a carbonyl ligand, as determined by flash photolysis and low temperature IR spectroscopy.[20] The axial halogen of the CO dissociated product can then rearrange to fill the equatorial void, and the resulting axial position can then be coordinated with a solvent molecule.[20] In our laboratory, we observed a rapid color change (i.e., yellow to brown) in solution when our Mn(I)-NHC complexes are exposed (ca. 30 min) to ambient laboratory light (Figure 2.5). The ^{1}H NMR spectrum of the exposed complex shows significant broadening (Figure 2.5), however, the peaks retain the identical chemical shifts and integration as the non-exposed complex. In order to address this shortcoming, we chose to explore the effect of substituting the axial bromine ligand with other monoanionic ligands in the spectrochemical series.[3] The two ligands that were chosen

were: isothiocyanate (-NCS), and cyanide (-CN). The synthesis of these compounds (Scheme 2.4) began with the *N*-arylation of benzimidazole or imidazole with 2-bromopyridine, as previously described (Scheme 2.3). *N*-Alkylation with ethylbromide was chosen to increase the solubility of the catalysts. Furthermore, ethylbromide (a liquid) was preferred to working with methylbromide (a gas). Chelation of **L2.5** and **L2.6** with $MnBr(CO)_5$ yielded the desired Mn(I)-NHC catalysts **2.3** and **2.4**. Substitution of the axial bromide with isothiocyanate or cyanide was achieved by refluxing complexes **2.3** and **2.4** in methanol with an excess (100 eq.) of either sodium isothiocyanate or potassium cyanide to afford complexes **2.5**-**2.7**.[26, 27] All new complexes were characterized by FTIR, ^{1}H NMR,^{13}C NMR, and UV/vis (see S2.SI, pp 86-105). Single crystals of each were grown by slow diffusion of hexanes into a solution of the complex dissolved in dichloromethane and their structure were verified by X-ray analysis (Figures 2.6-2.8).

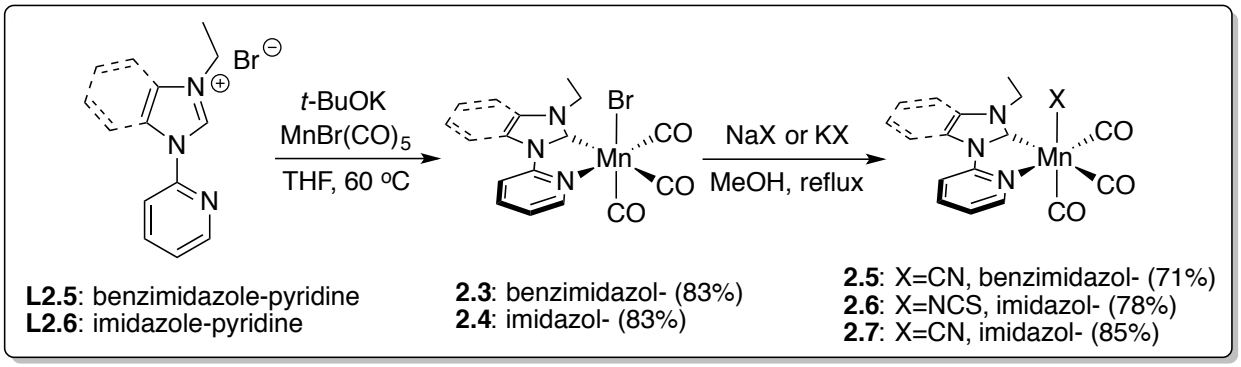

Scheme 2.4: Ligand Substitution at Metal Center of $[MnX(NHC\text{-}Py)(CO)_3]$ Complexes

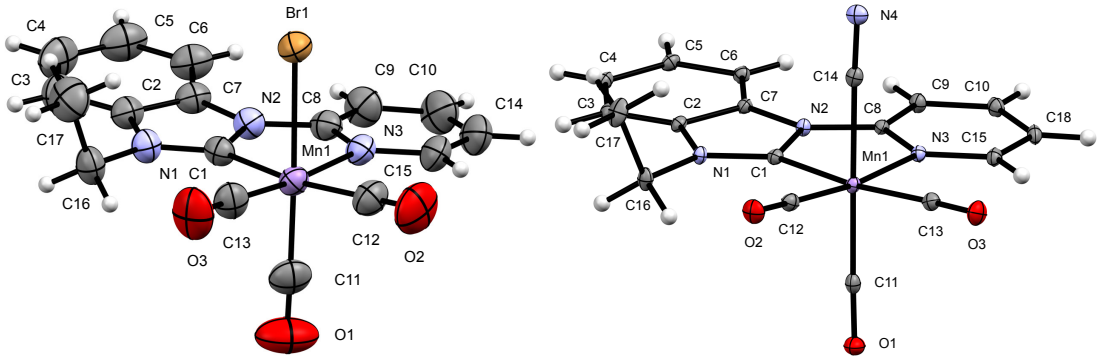

Figure 2.6: X-Ray Structure of Mn(I)-NHC Complexes **2.3** (left) and **2.5** (right)

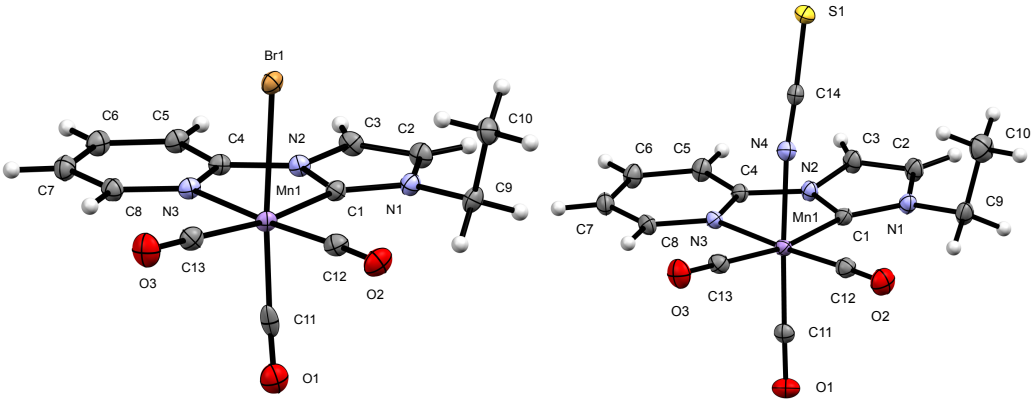

Figure 2.7: X-Ray Structures of Mn(I)-NHC Complexes **2.4** (left) and **2.6** (right)

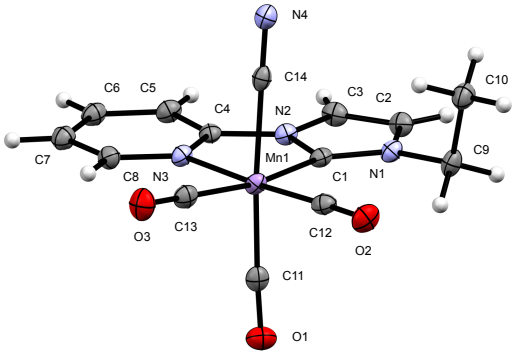

Figure 2.8: X-Ray Structures of Mn(I)-Complex **2.7**

The UV/Vis absorbance spectrum for the Et-Im-Pyr series indicates that the metal-to-ligand charge transfer (MLCT) band was blue-shifted from **2.4** (-Br, 398 nm) to **2.6** (-NCS, 368

nm) to **2.7** (-CN, 338 nm), while the $\pi \rightarrow \pi^*$ remained unchanged for the series, 266 nm (Figure 2.9). In the Et-BIm-Py series, **2.5** (-CN) exhibits a slightly red-shifted $\pi \rightarrow \pi^*$ band at 275 nm, while the MLCT band at 333 nm agrees well with **2.7** (338 nm).

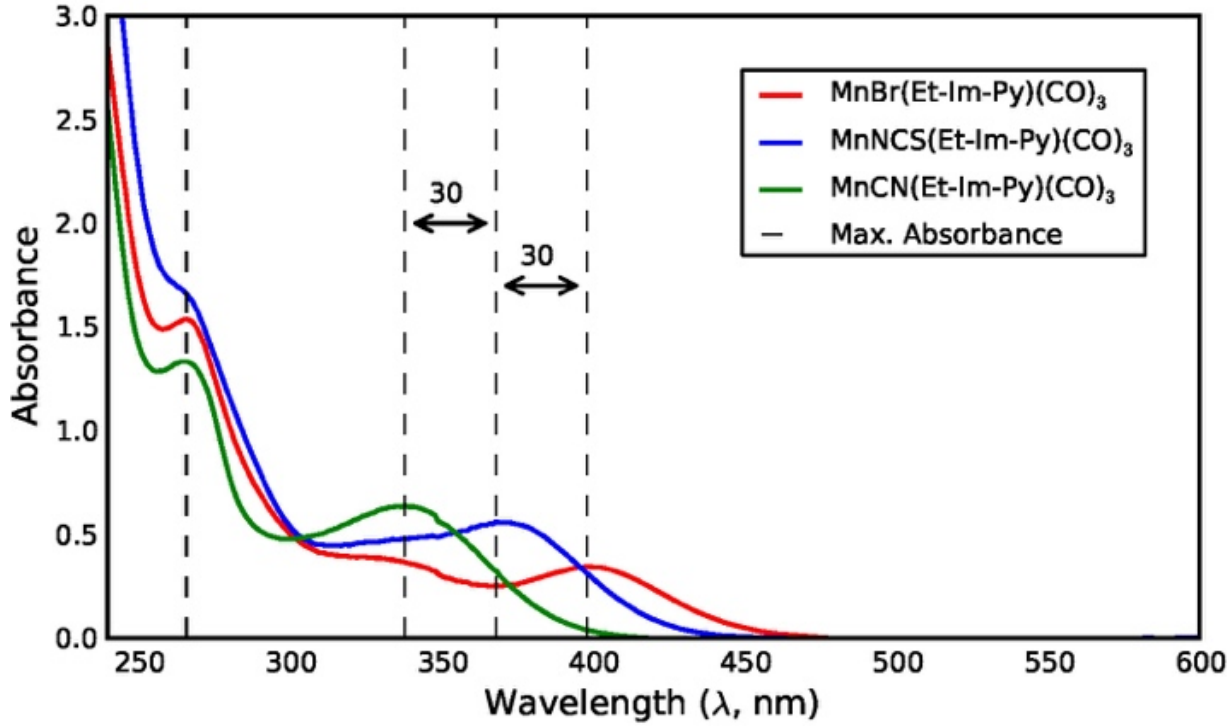

Figure 2.9: UV/Vis Spectra For the Et-Im-Pyr Series (**2.4, 2.6, 2.7**)

To measure the relative rates of photodecompostion of the Et-Im-Pyr series, each compound was irradiated with 350 nm or 420 nm light for known time intervals and monitored by UV-vis spectrophotometry. The data for this experiment for each compound are shown in Figures 2.9-2.14.

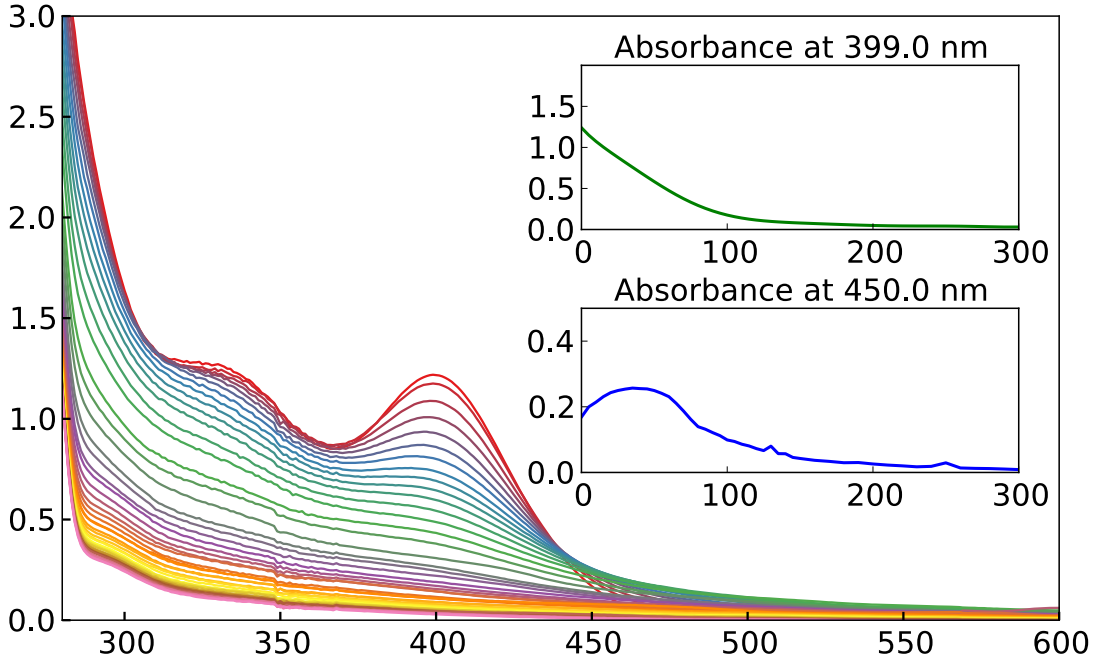

Figure 2.10: [MnBr(Et-Im-Py)$(CO)_3$] (**2.4**) Irradiated at 350nm

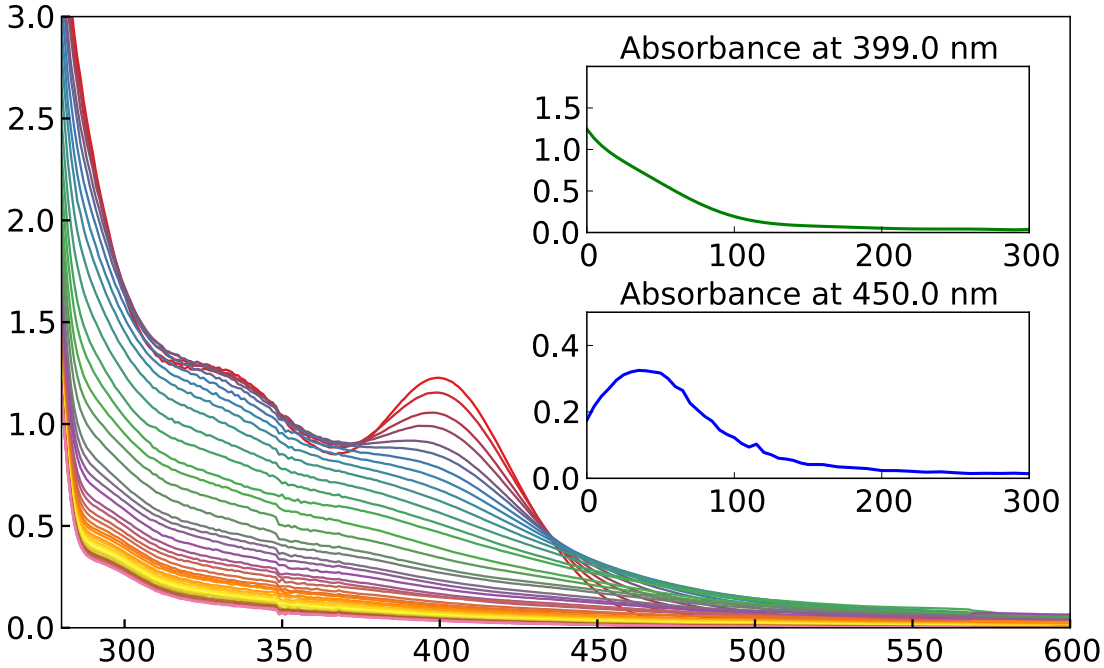

Figure 2.11: [MnBr(Et-Im-Py)$(CO)_3$] (**2.4**) Irradiated at 420nm

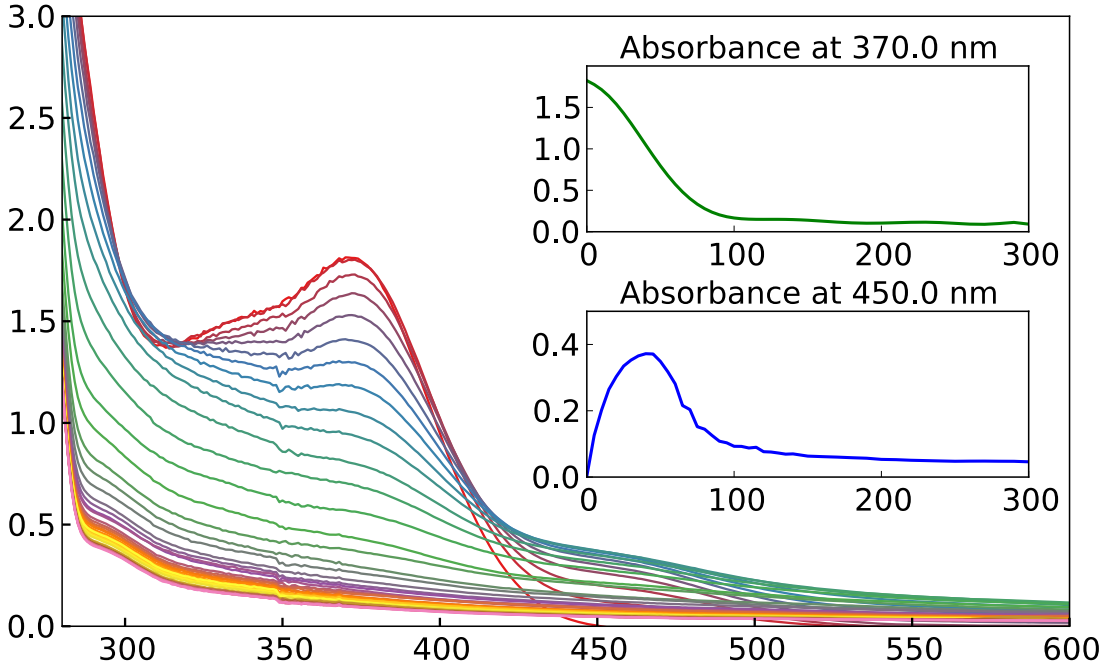

Figure 2.12: [MnNCS(Et-Im-Py)$(CO)_3$] (**2.6**) Irradiated at 350 nm

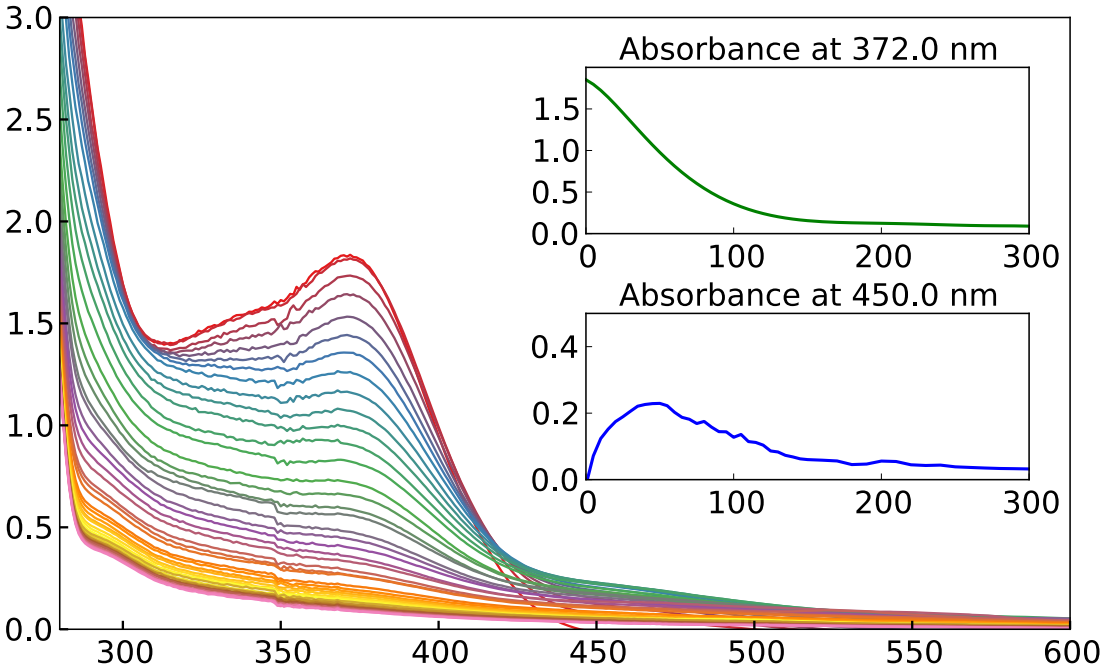

Figure 2.13: [MnNCS(Et-Im-Py)$(CO)_3$] (**2.6**) Irradiated at 420 nm

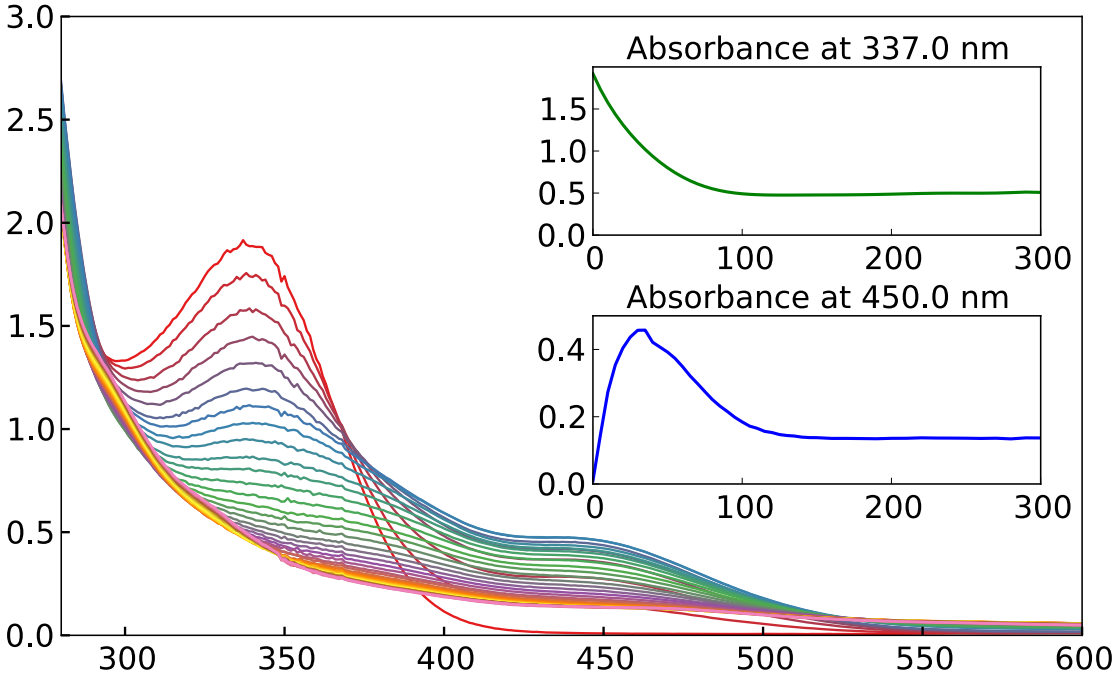

Figure 2.14: [MnCN(Et-Im-Py)$(CO)_3$] (**2.7**) Irradiated at 350 nm

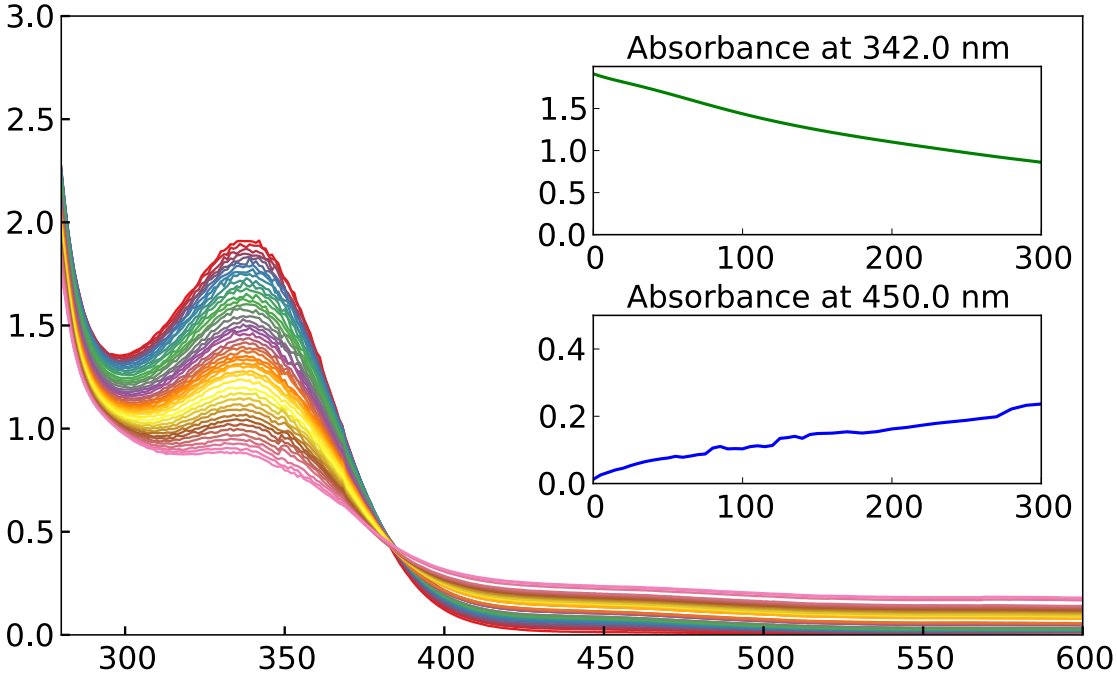

Figure 2.15: [MnCN(Et-Im-Py)$(CO)_3$] (**2.7**) Irradiated at 420 nm

The Et-Im-Pyr series revealed a rational trend expected from analysis of the MLCT bands. Irradiation with 350 nm light led to a faster decomposition of the NCS-ligand **2.6** (8%, Figure 2.12) and the CN-ligand **2.7** (23%, Figure 2.14) when compared to the Br-ligand **2.4** (Figure 2.10), as the maximum absorbance of the MLCT band of the NCS- and CN-complexes move closer to 350 nm. Conversely, irradiation with 420 nm light led to a slower decomposition of the NCS-ligand **2.6** (13%, Figure 2.13) and the CN-ligand **2.7** (423%, Figure 2.15) when compared to the Br-ligand **2.4** (Figure 2.11), due to the decreased absorption at 420 nm. This trend agreed with observations from a NMR experiment that indicated that the CN-substituted ligands were significantly more photostable than the Br-substituted ligands upon exposure to ambient laboratory light.

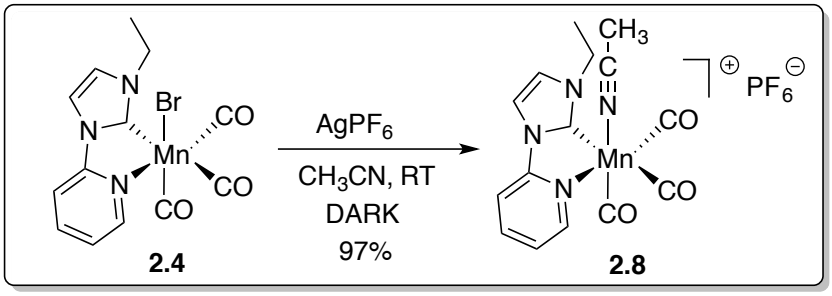

Scheme 2.5: Synthesis of $[Mn(Et\text{-}Im\text{-}Py)(CO)_3MeCN]^+$ (**2.8**)

In most cases, an intermediate species formed that was found to absorb at 450 nm. Initially, the decrease in the absorbance of the MLCT is approximately first order (i.e., near linear plot of $\ln([A]/[A_0])$ vs total irradiation time). After approximately 40 seconds of irradiation the absorbance at 450 nm begins to dissipate. Based on previous rhenium studies, it was hypothesized that the intermediate at 450 nm may be $[Mn(N\text{-}C)(CO)_3MeCN]^+$, resulting from the ligand exchange between the solvent and the axial bromide, while the final photoproduct may include

loss of a CO ligand. To that end, $[Mn(Et\text{-}Im\text{-}Py)(CO)_3MeCN]^+$ was synthesized from the reaction of $[MnBr(Et\text{-}Im\text{-}Py)(CO)_3]$ and silver hexafluorophosphate in acetonitrile to afford the desired cationic complex **2.8** (Scheme 2.5). The UV/vis of $[Mn(Et\text{-}Im\text{-}Py)(CO)_3MeCN]^+$ shows a $\pi \rightarrow \pi^*$ transition at 260 nm and a MLCT band at 355 nm (Figure 2.16), which is blue shifted from $[MnBr(Et\text{-}Im\text{-}Py)(CO)_3]$ (Figure 2.9, MLCT band at 398) by 43 nm. Because no significant absorbance appears at 450 nm, $[Mn(Et\text{-}Im\text{-}Py)(CO)_3MeCN]^+$ was eliminated as a possibility for the observed intermediate.

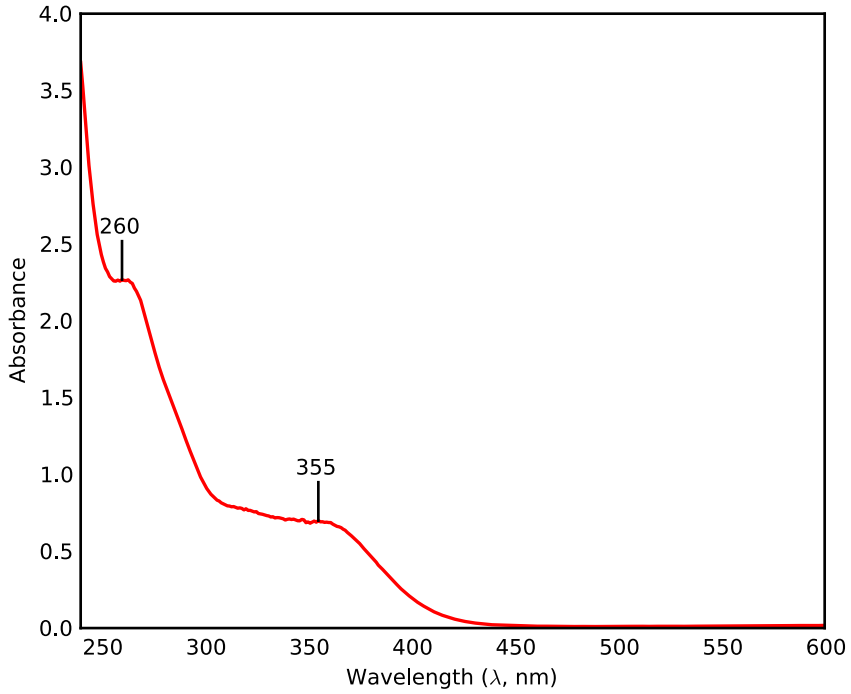

Figure 2.16: UV/vis of $[Mn(Et\text{-}Im\text{-}Py)(CO)_3MeCN]^+$ (**2.8**)

To further investigate the possibility of $[Mn(Et\text{-}Im\text{-}Py)(CO)_3MeCN]^+$ **2.8** as a photoproduct, the FTIR spectrum of this complex was compared to the spectrum of $[MnBr(Et\text{-}Im\text{-}Py)(CO)_3]$ (**2.4**) before and after irradiation at 350 and 420 nm. The initial FTIR spectrum of complex **2.4** (Figure 2.17, black trace) shows three CO stretches: a symmetric CO stretch at 2011

cm^{-1} and two asymmetric CO stretches at 1901 cm^{-1} and 1861 cm^{-1}. When irradiated with either 350 nm or 420 nm light for 5 min, the resulting photodecomposition product retains the symmetric CO stretch found in the starting complex **2.4** (Figure 2.16, yellow and red traces). We noted that the asymmetric CO stretch no longer displays a shoulder stretch at 1861 cm^{-1} which suggests the dissociation of a CO ligand from catalyst **2.4** upon irradiation, regardless of wavelength. Comparison of **2.4** with $[Mn(Et\text{-}Im\text{-}Py)(CO)_3MeCN]^+$ (Figure 2.16, grey trace) eliminates this species as a photoproduct since the observed transitions differ by ca. 20 cm^{-1}.

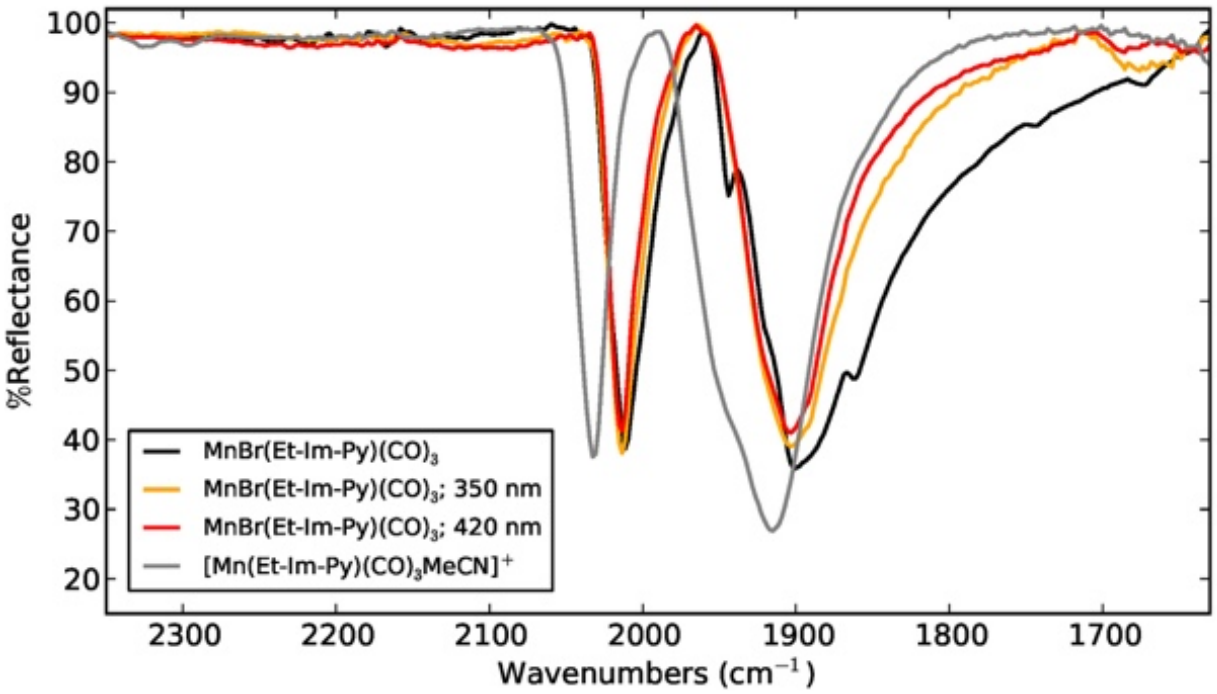

Figure 2.17: Infrared spectra of $[MnBr(Et\text{-}Im\text{-}Py)(CO)_3]$ (**2.4**, black) after five minutes of irradiation with 350 nm (orange) or 420 nm (red) light. The infrared spectrum of $[Mn(Et\text{-}Im\text{-}Py)(CO)_3MeCN]^+$ (gray) is shown for reference.

In a similar experiment, the photoproducts of complex $[MnCN(Et\text{-}Im\text{-}Py)(CO)_3]$ **2.7** were investigated. The initial FTIR spectrum of complex **2.7** (Figure 2.18, black trace) shows a CN stretch at 2109 cm^{-1}, a symmetric CO stretch at 2011 cm^{-1} and two asymmetric CO stretches at

1905 cm^{-1} and 1880 cm^{-1}. When the CN-complex **2.7** was irradiated with 420 nm light, the CN stretch and all three CO stretches persisted after 5 min, although the asymmetric stretch at 1880 cm^{-1} had significantly diminished (Figure 2.18, blue trace). Further irradiation for 20 min showed almost complete loss of this asymmetric stretch suggesting that CO dissociation occurs much slower for this compound when exposed to 420 nm light (Figure 2.18, green trace). FTIR analysis also indicates that the CN stretch remains unaffected throughout the experiment, thus indicating that the CN-ligand does not dissociate or rearrange during the course of irradiation

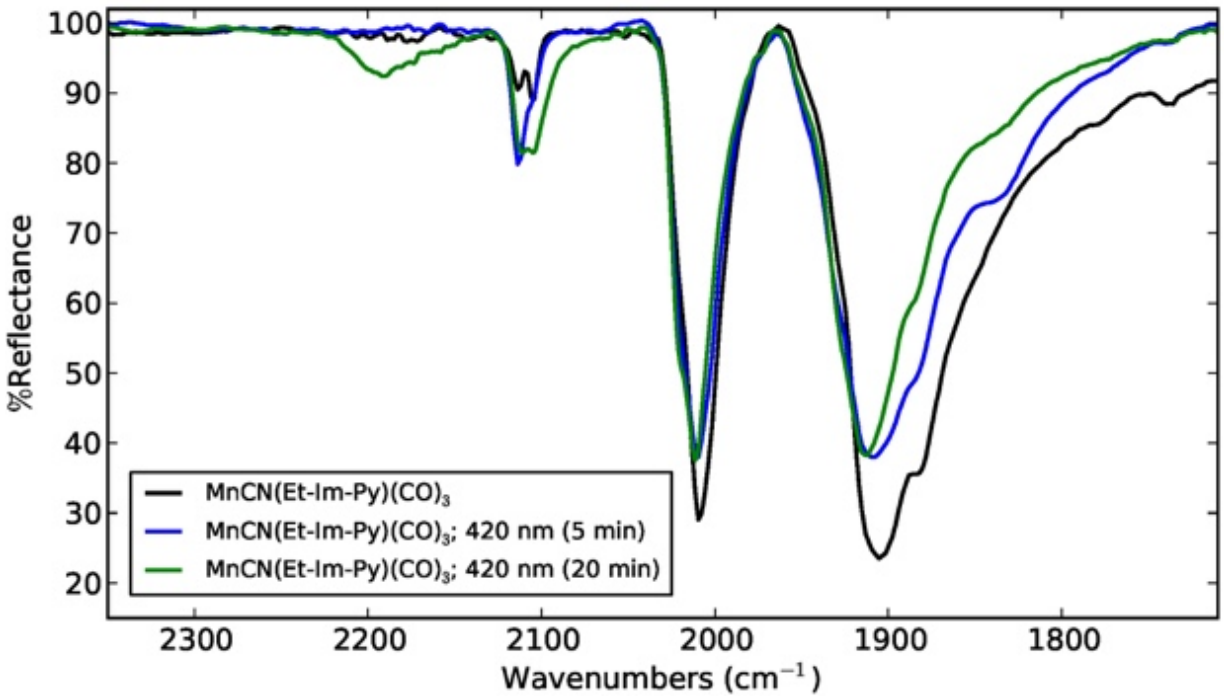

Figure 2.18: Infrared spectra of $MnCN(Et\text{-}Im\text{-}Py)(CO)_3$ (**2.7**, black) after five minutes (blue) and twenty minutes (green) of irradiation with 420 nm light.

In order to measure the electrocatalytic efficacy of the new MnX-NHC catalysts, CVs of compounds **2.4-2.7** were run under atmospheres of Ar and CO_2 in CH_3CN containing 5% H_2O using tetrabutylammonium perchlorate (TBAP) as the supporting electrolyte. The CV for Mn(I)-

catalyst **2.4** (Br-ligand) showed two reduction waves (Figure 2.19) under Ar, consistent with our first report of [MnBr(N-C)$(CO)_3$]-catalysts.[2] The first wave was reported at -1.53 V vs. SCE, which corresponded to the two-electron reduction of afford anion $[Mn(N\text{-}C)(CO)_3]^-$. The second reduction wave was at −1.82 V vs. SCE corresponding to the Mn−Mn dimer $[Mn(N\text{-}C)(CO)_3]_2$, and the oxidation of the formed dimer species is observed at −0.25 V vs SCE. Under an atmosphere of CO_2, the catalyst **2.4** displayed a catalytic current enhancement that increased by 2.1× at the first reduction wave, the result of the catalytic conversion of CO_2 to CO.

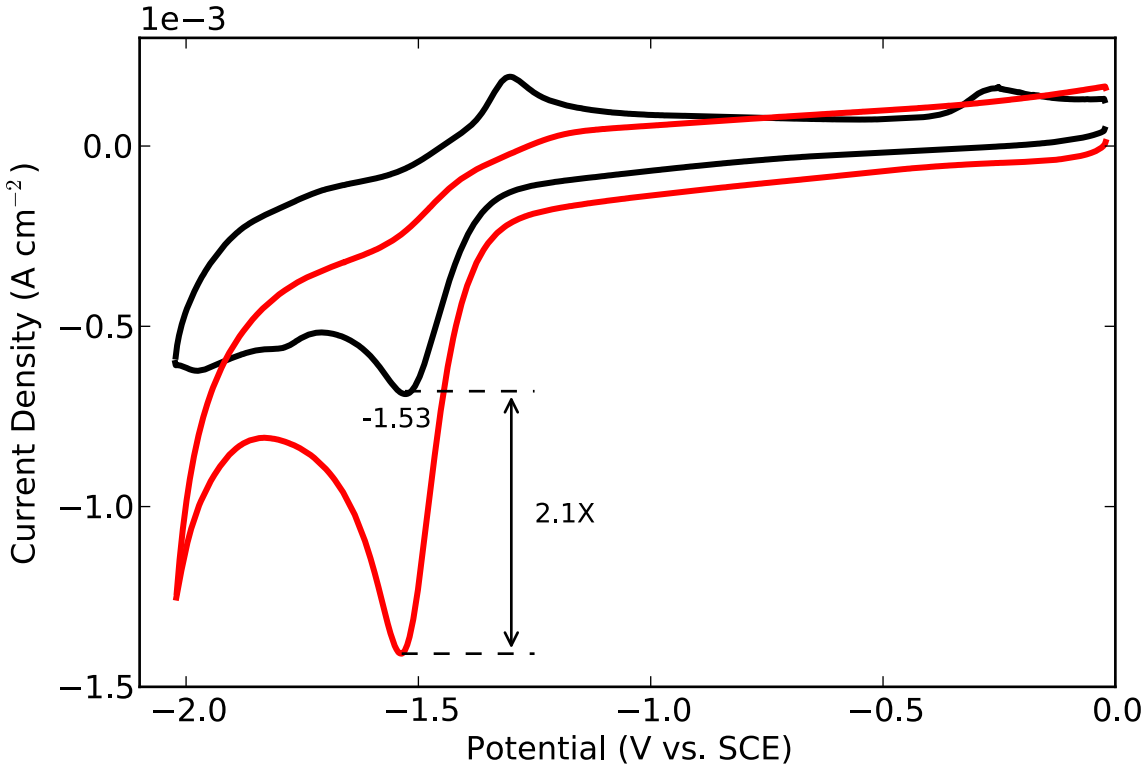

Figure 2.19: Cyclic voltammetry of **2.4** under Ar (black) and CO_2 (red) in MeCN with 5% H_2O and 0.1 M TBAP supporting electrolyte at 100 mV s^{-1}. The complex was loaded at a concentration of 1 mM, and the pH adjusted to 3.7 ($HClO_4$) for the Ar scan to match the proton content for CO_2

The CVs for the remaining complexes were run in identical fashion, and the two-electron reduction waves were observed as follows (Figure 2.20): −1.63 V vs SCE for **2.6** (NCS-ligand)

and −1.96 V vs SCE for **2.7** (CN-ligand). Reductions of **2.6** and **2.7** were shifted cathodic compared to **2.4** (Br-ligand), 100 mV and 430 mV respectively. MnCN(Et-BI-Py)$(CO)_3$, **2.5**, was reduced at -1.85 V vs. SCE which was shifted more positively by 110 mV when compared to **2.7**, MnCN(Et-Im-Py)$(CO)_3$. This shift for **2.5** vs **2.7** is not surprising; a similar shift was observed when MnBr(BI-Py)$(CO)_3$ **2.1** and **2.2** MnBr(Im-Py)$(CO)_3$ 2.2 were compared; the removal of the annulated benzene ring from the complex produced a cathodic shift of 100 mV.[2] Current enhancements at the two-electron reduction wave were lower for all other Mn(I)-compounds when compared to catalyst **2.4**, and are as follows: **2.6** (1.6×), **2.7** (1.4×), and **2.5** (1.2×). These limited catalytic efficiencies have been attributed to poor dissociation of the axial psuedohalogen (NCS or CN).

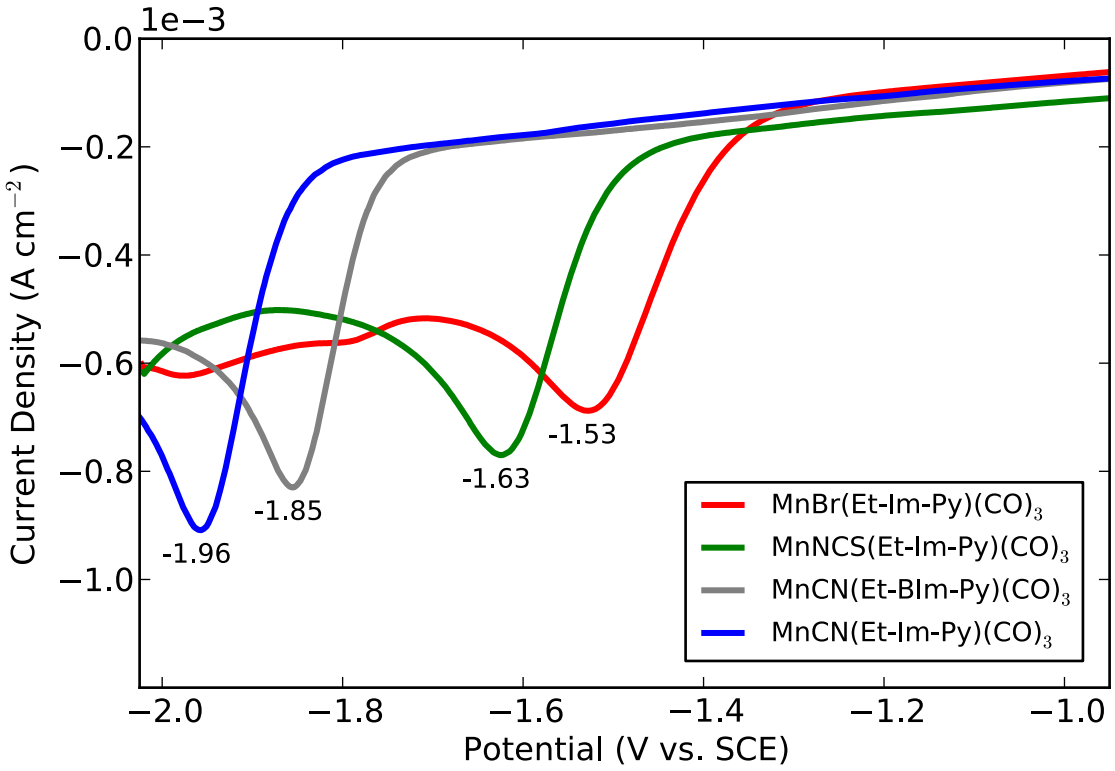

Figure 2.20: Linear sweep voltammetry of complexes **2.4-2.7** under Ar in MeCN with 5% H_2O and 0.1 M TBAP supporting electrolyte at 100 mV s^{-1}. The complex was loaded at a concentration of 1 mM, and the pH adjusted to 3.7 ($HClO_4$).

Current enhancements at the two-electron reduction wave were lower for all other Mn(I)-compounds when compared to catalyst MnBr(Et-Im-Py)$(CO)_3$ **2.4**, and are as follows: MnNCS(Et-Im-Py)$(CO)_3$ **2.6** (1.6×), MnCN(Et-Im-Py)$(CO)_3$ **2.7** (1.4×), and MnCN(Et-BI-Py)$(CO)_3$ **2.5** (1.2×). Br-Im-substituted complex **2.4** showed the highest TOF (0.86 s^{-1}), as a result of a 2.1× current enhancement under CO_2 compared to Ar, followed by: NCS-Im-substituted complex **2.6** (0.50 s^{-1}), CN-Im-substituted complex **2.7** (0.38 s^{-1}), NCS-Im-substituted complex **2.5** (0.28 s^{-1}). These limited catalytic efficiencies and TOFs have been attributed to the poor dissociation of the axial psuedohalogen (NCS or CN). Bulk electrolysis was performed on all compounds and the average faradaic efficiencies (FE_{CO}) from these experiments are reported in Table 1. Catalyst MnBr(Et-Im-Py)$(CO)_3$ **2.4** displayed the highest Faradaic efficiency (FE_{CO} = 66.8%), and was found to have excellent selectivity for CO_2 over available protons; thus precluding hydrogen production. In contrast, the NCS- and CN-catalysts were not selective for CO_2 to CO reduction, as substantial H_2 production was observed for catalysts **2.5-2.7**. As expected from the selectivity issue, the Faradiac efficiencies for CO production were also compromised for these catalysts as shown below.

Table 2.1. Turnover Frequencies (TOFs) and faradaic efficiencies (FE_{CO}s) for compounds **2.4-2.7** from cyclic voltammetry and bulk electrolysis experiments

Complex	**TOF**	**Avg. FE_{CO}**
MnBr(Et-Im-Py)$(CO)_3$, **2.4**	0.86 s^{-1}	66.8%
MnNCS(Et-Im-Py)$(CO)_3$, **2.6**	0.50 s^{-1}	27.0%
MnCN(Et-Im-Py)$(CO)_3$, **2.7**	0.38 s^{-1}	20.6%
MnCN(Et-BI-Py)$(CO)_3$, **2.5**	0.28 s^{-1}	29.7%

In summary a new series of [MnX(N-C)$(CO)_3$]-type CO_2 complexes were synthesized and characterized. These are the first catalytic manganese(I) *N*-heterocyclic carbene complexes that

have been reported.[2, 3] Catalytic CO production was observed for all compounds. However, when X = CN or NCS, substantial H_2 production was observed. UV studies indicate that all compounds undergo photodecomposition under 350 nm and 420 nm light, but CN-substituted complexes decomposed more slowly under 420 nm light, with five times longer lifetimes. The data from these studies indicate that Mn(I)-NHC based catalysts can be tuned by ligand substitution, either by structural modifications of the NHC or axial ligand substitution. Future work in our laboratory will explore how other substitutions can tune electron density around the Mn-center and perhaps prevent photodecomposition, lower reduction potential and/or increase catalytic current enhancement.

EXPERIMENTAL METHODS

General

All reagents were obtained from commercial suppliers and used as received unless otherwise noted. All reactions were performed using standard Schlenk-line techniques under an atmosphere of argon with minimal exposure to light. Tetrahydrofuran (THF) and methanol were dried and distilled prior to use; THF from Na/benzophenone and methanol from CaH_2. ^{1}H NMR and ^{13}C NMR spectra were recorded on a Varian Mercury Plus 400 MHz spectrometer or a Varian Unity Inova 500 MHz spectrometer. Chemical shifts were referenced to the residual protio signal of the deuterated solvent. FTIR spectra were recorded on a ThermoNicolet 6700 spectrophotometer running OMNIC software. X-Ray diffraction data were collected on a Bruker SMART APEX II system with graphite-monochromated Mo Kα radiation (λ = 0.71073 ˚A)

Electrochemical Testing

All electrochemical experiments and reactions were performed under rigorous air and moisture free conditions with 0.1 M tetrabutylammonium perchlorate (TBAP) in acetonitrile as the electrolyte unless otherwise noted. TBAP was synthesized by the dropwise addition concentrated perchloric acid into an equimolar solution of tetrabutylammonium bromide in water. The precipitated TBAP was collected, recrystallized three times from ethyl acetate/hexanes, and dried under reduced pressure (<0.1 Torr) for several hours over P_2O_5. Acetonitrile (MeCN) was bubble degassed and passed through two columns of activated alumina prior to use. Electrolyte solutions were prepared by dissolving TBAP in acetonitrile and passing the solution through a column of activated alumina in a fritted Schlenk filter directly into a Schlenk flask under an atmosphere of nitrogen. Manganese complexes were always loaded at a concentration of 1 mM and handled under red light at all times except during weighing. A 3 mm glassy carbon disk working electrode and a Ag/AgCl reference electrode (BASi model # MF-2012 and MF-2052, respectively) and a platinum mesh counter electrode were used in all electrochemical experiments except for bulk electrolysis where a 3.5 cm^2 glassy carbon plate was employed as the working electrode. A 15 mL three-necked round-bottom flask was used as the electrochemical cell and all electrodes were secured using "mini" #7 Ace-thread adaptors from Ace-glass in all experiments except bulk electrolysis where a 25 mL three-necked round-bottom flask was employed. Electrochemical measurements were performed on a CHI 760D electrochemical workstation (CH Instruments, Austin, TX). For all electrochemical experiments, the electrolyte was bubbled with the desired gas (Ar or CO_2) for 15 minutes. A scan of the electrolyte was performed to ensure a featureless background from 0 to −2.0 V vs. SCE. After adding the desired complex, the electrolyte was bubbled for 5 more minutes before collecting experimental data. Voltammograms were referenced to Fc^+/Fc at the end of the

experiment and then later reference to SCE by adding 380 mV.[28] FTIR spectra of electrolysis cell headspace were collected on a Nicolet 730 spectrometer running OMNIC software. Carbon monoxide and hydrogen production was measured using an HP 5980 gas chromatograph (GC) with a TCD analyzer and analog integrator. An Agilent CP7538 molecular sieve column was used to separate CO and H_2 from CO_2 at a column head pressure of 12 psi, oven temperature of 70 ˚C, injection temperature of 200 ˚C, and a detector temperature of 250 ˚C.

Synthesis

Preparation of [*N*-methyl-*N′*-2-pyridylbenzimidazolium]$^+$Br$^-$ (L2.3).

i. Coupling benzimidazole and pyridine:

Under an atmosphere of argon, a flask was charged with benzimidazole (10.00 g, 84.6 mmol), potassium carbonate (7.79 g, 56.4 mmol), and 2-bromopyridine (2.74 mL, 28.6 mmol). The reaction mixture was stirred at 205 ˚C for 18 hours, then cooled to room temperature. The resulting solution was diluted with water (200 mL) and extracted with DCM (3 x 200 mL). The combined organic extracts were washed with saturated Na_2CO_3 (3 x 200 mL) and brine (200 mL) then dried over anhydrous $MgSO_4$ before filtration to remove the drying agent. Concentration under reduced pressure using a rotary evaporator gave *N*,*N*′-2-pyridylbenzimidazolium as a light red oil (5.45 g, 96 %).

ii. Methylating benzimidazole:

Bromomethane (0.53 mL, 15.2 mmol) was collected at -78 ˚C and added to a sealed tube containing *N*,*N*′-2-pyridylbenzimidazolium (1.70 g, 8.7 mmol) dissolved in 7 mL of CH_3CN. After sealing the reaction flask under an argon atmosphere, the reaction mixture was stirred at reflux overnight (11 h). The solution was then allowed to cool to room temperature before being concentrated under reduced pressure using a rotary evaporator. Subsequent recrystallization from

CH_3CN/Et_2O gave [*N*-methyl-*N*′-2-pyridylbenzimidazolium]$^+Br^-$ as a white solid that was collected by vacuum filtration (2.42 g, 96 %). ^{1}H NMR (DMSO-d_6, 20 ˚C): δ 10.56 (1H, s), 8.78 (1H, d, J = 4Hz), 8.48-8.46 (1H, m), 8.31-8.26 (1H, m), 8.15-8.13 (1H, m), 8.06 (1H, d, J = 8Hz), 7.81-7.75 (2H, m), 7.72-7.69 (1H, m), 4.20 (3H, s).

Preparation of MnBr(*N*-methyl-*N*′-2-pyridylbenzimidazol-2-ylidine)(CO)$_3$ (2.1).

$MnBr(CO)_5$ (1.15 g, 4.2 mmol) was suspended in 25 mL of THF and sparged with argon for 30 minutes. While stirring, potassium *t*-butoxide (0.20 g, 1.8 mmol) was added, then [*N*-methyl-N′-2-pyridylbenzimidazolium]$^+Br^-$ (**L2.3**, 0.41 g, 1.4 mmol) was added slowly over one hour while heating at 60 ˚C under argon. The reaction mixture was heated overnight (11 h) at 60 ˚C before being allowed to cool to room temperature. THF was removed under reduced pressure using a rotary evaporator, and the resulting residue was triturated with Et_2O (4 x 25 mL) before being dissolved in DCM (100 mL). This solution was washed with water (100 mL) and brine (100 mL) to remove unreacted proligand and other water soluble impurities. The organic extract was dried over anhydrous $MgSO_4$ before filtration to remove the drying agent. Concentration under reduced pressure using a rotary evaporator afforded the product as a yellow-orange powder (0.53 g, 88 %). IR ν_{CO} (ATR, cm^{-1}): 2015 (s), 1927 (m, sh), 1897 (s). ^{1}H NMR (DMSO- d_6, 25 ˚C): δ 9.05 (1H, d, J = 10Hz), 8.53 (1H, d, J = 10Hz), 8.45 (1H, d, J = 5Hz), 8.28-8.25 (1H, m), 7.95 (1H, d, J = 5Hz), 7.62-7.52 (3H, m), 4.33 (3H, s). ^{13}C NMR (DMSO-d_6, 25 ˚C): δ 225.24, 221.15, 217.38, 216.30, 154.40, 153.49, 142.00, 137.24, 130.71, 125.29, 125.20, 123.07, 113.72, 112.96, 112.36, 35.32. In select cases, further trituration with EtOAc/hexanes and washing with Et_2O was required to remove trace impurities. Crystals suitable for single-crystal X-ray analysis were grown from the slow diffusion of hexanes into a solution of **2.1** in DCM.

Preparation of [*N*-methyl-*N*′-2-pyridylimidazolium]$^+Br^-$ (L2.4).

i. Coupling imidazole and pyridine:

Under an atmosphere of argon, a flask was charged with imidazole (5.76 g, 84.6 mmol), potassium carbonate (7.79 g, 56.4 mmol), and 2-bromopyridine (2.74 mL, 28.6 mmol). The reaction mixture was stirred at 190 ˚C for 18 hours, then allowed to cool to room temperature. The resulting solution was diluted with water (200 mL) and extracted with DCM (3 x 200 mL). The combined organic extracts were washed with saturated Na_2CO_3 (3 x 200 mL) and brine (200 mL), dried over anhydrous $MgSO_4$, and filtered to remove the drying agent. Concentration under reduced pressure using a rotary evaporator gave *N*,*N*′-2-pyridylimidazolium as a light yellow solid (3.80 g, 92%).

ii. Methylating imidazole:

See procedure for **L2.3**. Starting material: bromomethane (0.91 mL, 16.5 mmol) and *N*,*N*′-2-pyridylimidazolium (2.17 g, 15.0 mmol). Yield: 3.50 g, 97 %. ^{1}H NMR (DMSO-d_6, 20 ˚C): δ 10.08 (1H, s), 8.64 (1H, d, J = 8Hz), 8.51 (1H, s), 8.23-8.19 (1H, m), 8.03 (1H, d, J = 8Hz), 7.98 (1H, s), 7.65-7.62 (1H, m), 3.97 (3H, s).

Preparation of MnBr(*N*-methyl-*N*′-2-pyridylimidazol-2-ylidine)(CO)$_3$ (2.2).

$MnBr(CO)_5$ (0.48 g, 1.8 mmol) was suspended in 25 mL of THF and sparged with argon for 30 minutes. While stirring, potassium *t*-butoxide (0.20 g, 1.8 mmol) was added, then [*N*-methyl-*N*′-2-pyridylimidazolium]$^+$Br$^-$ (**L2.4**, 0.34 g, 1.4 mmol) was added slowly over one hour while heating at 60 ˚C under argon. The reaction mixture was heated overnight (11 h) at 60 ˚C before being allowed to cool to room temperature. THF was removed under reduced pressure using a rotary evaporator, and the resulting residue was triturated with Et_2O (4 x 25 mL) before being dissolved in DCM (100 mL). This solution was washed with water (100 mL) and brine (100 mL) to remove unreacted ligand and other water soluble impurities. The organic extract was dried over anhydrous $MgSO_4$ before filtration to remove the drying agent. Concentration under reduced

pressure using a rotary evaporator to afford the product as a yellow-orange powder (0.32 g, 60 %). IR ν_{CO} (ATR, cm^{-1}): 2012 (s), 1906 (br). ^{1}H NMR (DMSO-d_6, 25 ˚C): δ 8.92 (1H, d, J = 5Hz), 8.46 (1H, s), 8.23-8.21 (1H, m), 8.14 (1H, d, J = 10Hz), 7.72 (1H, s), 7.49-7.46 (1H, m), 4.05 (3H, s). ^{13}C NMR (DMSO-d_6, 25 ˚C): δ 225.93, 221.73, 217.64, 201.78, 153.79, 152.96, 141.67, 127.09, 123.33, 117.37, 112.57, 38.06. Further trituration with EtOAc/hexanes and washing with Et_2O was often required to remove additional impurities.

Preparation of [MnBr(*N*-ethyl-*N′*-2-pyridylimidazol-2-ylidine)$(CO)_3$] (2.4).

$MnBr(CO)_5$ (0.48 g, 1.8 mmol) and [*N*-ethyl-*N*′-2-pyridylimidazolium]$^{+}Br^{-}$ (**L2.6**) (0.36 g, 1.4 mmol) were suspended in 25 mL of THF and sparged with argon for 30 minutes. Potassium *t*-butoxide (0.20 g, 1.8 mmol) was added to the reaction mixture, with stirring, which was then heated to 60 ˚C under argon for 15 hours. After cooling to room temperature, the solvent was removed under reduced pressure using a rotary evaporator. The resulting solid residue as triturated with Et_2O before being dissolved in DCM and washed with water (100 mL) and brine (100 mL) to remove water-soluble impurities. The combined organic extracts were dried over anhydrous $MgSO_4$, filtered to remove the drying agent, and concentrated to afford the desired product as an orange-yellow powder (0.46 g, 83%). IR (ATR, cm^{-1}) ν_{CO}: 2011 (s), 1901 (s), 1862 (sh). ^{1}H NMR (DMSO- d_6, 20 ˚C): δ 8.92–8.91 (1H, m), 8.48 (1H, d, J = 4 Hz), 8.21–8.13 (2H, m), 7.79 (1H, d, J = 4 Hz), 7.49–7.45 (1H, m), 4.42 (2H, q, J = 8 Hz), 1.52 (3H, t, J = 8 Hz). ^{13}C NMR (DMSO-d_6, 25 ˚C): δ 225.39, 221.34, 217.10, 200.24, 153.26, 152.36, 141.17, 125.07, 122.80, 117.19, 112.04, 45.53, 16.29.

Preparation of [MnNCS(*N*-ethyl-*N′*-2-pyridylimidazol-2-ylidine)$(CO)_3$] (2.6).

[MnBr(*N*-ethyl-*N*′-2-pyridylimidazol-2-ylidine)$(CO)_3$] (**2.4**) (0.50 g, 1.3 mmol) and NaSCN (10.29 g, 127.0 mmol) were suspended in 100 mL of MeOH and stirred at 60 ˚C under argon for

15 hours. After cooling to room temperature, the reaction mixture was diluted with H_2O (50 mL) and extracted with DCM (3 x 50 mL). The combined organic extracts were washed with H_2O (100 mL) and brine (100 mL) then dried over anhydrous $MgSO_4$ followed by filtration to remove the drying agent. Concentration under reduced pressure using a rotary evaporator gave the desired product as a light yellow solid, which was further purified via recrystallization with acetone–Et_2O (0.37 g, 78%). IR (ATR, cm−1) ν_{CO}: 2014 (s), 1902 (s); ν_{CN}: 2109 (m). ^{1}H NMR (DMSO-d_6, 20 ˚C): δ 8.89–8.87 (1H, m), 8.55 (1H, d, J = 4 Hz), 8.32–8.20 (2H, m), 7.87 (1H, d, J = 4 Hz), 7.57–7.53 (1H, m), 4.43 (2H, q, J = 8 Hz), 1.51 (3H, t, J = 8 Hz). ^{13}C NMR (DMSO-d_6, 25 ˚C): δ 223.53, 217.81, 214.99, 197.04, 153.29, 152.28, 141.96, 138.16, 125.46, 123.60, 117.74, 112.36, 45.74, 16.61.

Preparation of [MnCN(*N*-ethyl-*N*′-2-pyridylimidazol-2-ylidine)(CO)$_3$] (2.7).

[MnBr(*N*-ethyl-*N*′-2-pyridylimidazol-2-ylidine)(CO)$_3$] (**2.4**) (0.90 g, 2.3 mmol) and KCN (14.87 g, 228.3 mmol) were suspended in 100 mL of MeOH and stirred at 60 under argon for 15 hours. After cooling to room temperature, the reaction mixture was diluted with H_2O (50 mL) and extracted with DCM (3 x 50 mL). The combined organic extracts were washed with H_2O (100 mL) and brine (100 mL) then dried over anhydrous $MgSO_4$ before filtration to remove the drying agent. Concentration under reduced pressure using a rotary evaporator gave the desired product as an off-white solid (0.66 g, 85%). IR (ATR, cm−1) ν_{CO}: 2009 (s), 1905 (s), 1882 (sh); ν_{CN}: 2109 (w). ^{1}H NMR (DMSO- d_6, 20 ˚C): δ 8.77–8.76 (1H, m), 8.51 (1H, s), 8.24–8.14 (2H, m), 7.81 (1H, s), 7.48–7.45 (1H, m), 4.34 (1H, q, J = 8 Hz), 1.50 (3H, t, J = 8 Hz). ^{13}C NMR (DMSO- d_6, 25 ˚C): δ 224.17, 218.19, 214.64, 199.52, 153.07, 151.95, 146.28, 141.01, 125.46, 122.85, 117.42, 112.19, 45.51, 16.05.

Preparation of [MnBr(*N*-ethyl-*N*′-2-pyridylbenzimidazol-2-ylidine)(CO)$_3$] (2.3).

See procedure for **2.4**. Starting materials: [$MnBr(CO)_5$] (0.48 g, 1.8 mmol), [*N*-ethyl-*N*′-2 pyridylbenzimidazolium]$^+Br^-$ (0.43 g, 1.4 mmol) and potassium *t*-butoxide (0.20 g, 1.8 mmol). Yield: 0.52 g, 83%. IR (ATR, cm−1) ν_{CO}: 2012 (s), 1913 (s), 1875 (sh). ^{1}H NMR (DMSO- d_6, 20 ˚C): δ 9.06–9.04 (1H, m), 8.52 (1H, d, J = 8 Hz), 8.44 (1H, d, J = 8 Hz), 8.27–8.23 (1H, m), 7.99 (1H, d, J = 8 Hz), 7.61–7.51 (3H, m), 4.83 (2H, q, J = 8 Hz), 1.60 (3H, t, J = 8 Hz). ^{13}C NMR (DMSO- d_6, 25 ˚C): δ 224.59, 220.76, 216.83, 214.92, 153.91, 152.91, 141.52, 135.55, 130.41, 124.90, 124.75, 122.59, 113.25, 112.69, 111.62, 43.06, 14.85.

Preparation of [MnCN(*N*-ethyl-*N*′-2-pyridylbenzimidazol-2-ylidine)$(CO)_3$] (2.5).

See procedure for **2.7**. Starting materials: **2.3** (0.48 g, 1.1 mmol) and KCN (7.05 g, 108.3 mmol). Yield: 0.30 g, 71%. IR (ATR, cm^{-1}) ν_{CO}: 2018 (s), 1919 (s), 1891 (sh); ν_{CN}: 2112 (m). ^{1}H NMR (DMSO-d_6, 20 ˚C): δ 8.90–8.88 (1H, m), 8.54 (1H, d, J = 8 Hz), 8.44 (1H, d, J = 8 Hz), 8.28–8.24 (1H, m), 7.99 (1H, d, J = 8 Hz), 7.62–7.50 (3H, m), 4.74 (2H, q, J = 8 Hz), 1.57 (3H, t, J = 8 Hz). ^{13}C NMR (DMSO- d_6, 25 ˚C): δ 223.33, 217.86, 214.54, 214.15, 153.62, 152.52, 145.68, 141.30, 135.68, 130.48, 124.92, 124.68, 122.59, 113.34, 112.68, 111.49, 42.99, 14.57.

Preparation of [Mn(*N*-ethyl-*N*′-2-pyridylimidazol-2-ylidine)$(CO)_3$MeCN](PF_6) (2.8).

$AgPF_6$ (0.13 g, 0.51 mmol) was dissolved in 5 mL of CH_3CN and the added to a solution of [MnBr(*N*-ethyl-*N*′-2 pyridylimidazol-2-ylidine)$(CO)_3$] (**2.4**) (0.20 g, 0.51 mmol) which was dissolved in 20 mL of CH_3CN. The mixture was stirred at room temperature for 1 h before filtration through Celite to remove the silver bromide precipitate. Concentration of the filtrate under reduced pressure using a rotary evaporator afforded the product as a yellow solid (0.25 g, 97%). IR (ATR, cm^{-1}) ν_{CO}: 2032 (s), 1916 (s). ^{1}H NMR (CD_3CN, 20 ˚C): δ 8.85 (1H, d, J = 4 Hz), 8.20–8.16 (1H, m), 8.00 (1H, s), 7.83 (1H, d, J = 8 Hz), 7.50–7.46 (2H, m), 4.49–4.44 (2H, m), 1.59–1.55 (3H, m).

REFERENCES:

1. Bourrez, M.; Molton, F.; Chardon-Noblat, S.; Deronzier, A., [Mn(bipyridyl)$(CO)_3$Br]: An Abundant Metal Carbonyl Complex as Efficient Electrocatalyst for CO_2 Reduction. *Angewandte Chemie International Edition* **2011**, *123* (42), 10077-10080.

2. Agarwal, J.; Shaw, T. W.; Stanton, C. J.; Majetich, G. F.; Bocarsly, A. B.; Schaefer, H. F., NHC-Containing Manganese(I) Electrocatalysts for the Two-Electron Reduction of CO_2. *Angewandte Chemie International Edition* **2014**, *53* (20), 5252-5255.

3. Agarwal, J.; Stanton III, C. J.; Shaw, T. W.; Vandezande, J. E.; Majetich, G. F.; Bocarsly, A. B.; Schaefer III, H. F., Exploring the Effect of Axial Ligand Substitution (X= Br, NCS, CN) on the Photodecomposition and Electrochemical Activity of [MnX(N–C)$(CO)_3$] Complexes. *Dalton Transactions* **2015**, *44* (5), 2122-2131.

4. Vaughan, J. G.; Reid, B. L.; Ramchandani, S.; Wright, P. J.; Muzzioli, S.; Skelton, B. W.; Raiteri, P.; Brown, D. H.; Stagni, S.; Massi, M., The Photochemistry of Rhenium(I) Tricarbonyl *N*-Heterocyclic Carbene Complexes. *Dalton Transactions* **2013**, *42* (39), 14100-14114.

5. Li, X.-W.; Li, H.-Y.; Wang, G.-F.; Chen, F.; Li, Y.-Z.; Chen, X.-T.; Zheng, Y.-X.; Xue, Z.-L., Blue-Green Luminescent Rhenium (I) Tricarbonyl Complexes with Pyridine-Functionalized N-Heterocyclic Carbene Ligands. *Organometallics* **2012**, *31* (10), 3829-3835.

6. Casson, L. A.; Muzzioli, S.; Raiteri, P.; Skelton, B. W.; Stagni, S.; Massi, M.; Brown, D. H., *N*-Heterocyclic Carbenes as π*-Acceptors in Luminescent Re(I) Triscarbonyl Complexes. *Dalton Transactions* **2011**, *40* (44), 11960-11967.

7. Díez-González, S.; Marion, N.; Nolan, S. P., *N*-Heterocyclic Carbenes in Late Transition Metal Catalysis. *Chemical Reviews* **2009**, *109* (8), 3612-3676.

8. Cano, R.; Ramón, D. J.; Yus, M., Transition-Metal-Free *O*-, *S*-, and *N*-Arylation of Alcohols, Thiols, Amides, Amines, and Related Heterocycles. *The Journal of Organic Chemistry* **2010**, *76* (2), 654-660.

9. Barbante, G. J.; Francis, P. S.; Hogan, C. F.; Kheradmand, P. R.; Wilson, D. J.; Barnard, P. J., Electrochemiluminescent Ruthenium(II) *N*-Heterocyclic Carbene Complexes: A Combined Experimental and Theoretical Study. *Inorganic Chemistry* **2013**, *52* (13), 7448-7459.

10. Raba, A.; Anneser, M. R.; Jantke, D.; Cokoja, M.; Herrmann, W. A.; Kühn, F. E., Facile and Scalable Preparation of 2-Imidazolylpyridines. *Tetrahedron Letters* **2013**, *54* (26), 3384-3387.

11. Back, O.; Henry-Ellinger, M.; Martin, C. D.; Martin, D.; Bertrand, G., ^{31}P NMR Chemical Shifts of Carbene–Phosphinidene Adducts as an Indicator of the π-Accepting Properties of Carbenes. *Angewandte Chemie International Edition* **2013**, *52* (10), 2939-2943.

12. Kühl, O., *Functionalised N-Heterocyclic Carbene Complexes*. John Wiley & Sons: 2010.

13. Smieja, J. M.; Kubiak, C. P., Re(bipy-*t*-Bu)$(CO)_3Cl^-$ Improved Catalytic Activity for Reduction of Carbon Dioxide: IR-Spectroelectrochemical and Mechanistic Studies. *Inorganic Chemistry* **2010**, *49* (20), 9283-9289.

14. Staal, L.; Oskam, A.; Vrieze, K., The Syntheses and Coordination Properties of $M(CO)_3X(DAB)$ (M= Mn, Re; X= Cl, Br, I; DAB= 1, 4-Diazabutadiene). *Journal of Organometallic Chemistry* **1979**, *170* (2), 235-245.

15. Stor, G. J.; Morrison, S. L.; Stufkens, D. J.; Oskam, A., The Remarkable Photochemistry of *fac*-$XMn(CO)_3$(α-diimine) (X= Halide): Formation of $Mn_2(CO)_6$(α-diimine)$_2$ via the *mer* Isomer and Photocatalytic Substitution of X^- in the Presence of PR_3. *Organometallics* **1994**, *13* (7), 2641-2650.

16. Stor, G.; Stufkens, D.; Vernooijs, P.; Baerends, E.; Fraanje, J.; Goubitz, K., X-ray Structure of *fac*-$IMn(CO)_3$(bpy) and Electronic Structures and Transitions of the Complexes *fac*-$XMn(CO)_3$(bpy) (X= Cl, I) and *mer*-$ClMn(CO)_3$(bpy). *Inorganic Chemistry* **1995**, *34* (6), 1588-1594.

17. Kleverlaan, C. J.; Hartl, F.; Stufkens, D. J., Real-Time Fourier Transform IR (FTIR) Spectroscopy in Organometallic Chemistry: Mechanistic Aspects of the *fac* to *mer* photoisomerization of *fac*-[$Mn(Br)(CO)_3$(R-DAB)]. *Journal of Photochemistry and Photobiology A: Chemistry* **1997**, *103* (3), 231-237.

18. Hartl, F.; Rossenaar, B. D.; Stor, G. J.; Stufkens, D. J., Role of an Electron-Transfer Chain Reaction in the Unusual Photochemical Formation of Five-Coordinated Anions $[Mn(CO)_3$(α-diimine)$]^-$ From *fac*-[$Mn(X)(CO)_3$(α-diimine)] (X= halide) at Low Temperatures. *Recueil des Travaux Chimiques des Pays-Bas* **1995**, *114* (11-12), 565-570.

19. Rossenaar, B. D.; Stufkens, D. J.; Oskam, A.; Fraanje, J.; Goubitz, K., Alkyl-Dependent Photochemistry of $Mn(R)(CO)_3$(R′-DAB) (R= Me, Bz; R′= iPr, pTol): Homolysis of the Mn-R Bond for R= Bz and Release of CO for R= Me. *Inorganica Chimica Acta* **1996**, *247* (2), 215-229.

20. Rosa, A.; Ricciardi, G.; Baerends, E. J.; Stufkens, D. J., Metal-to-Ligand Charge Transfer (MLCT) Photochemistry of *fac*-$Mn(Cl)(CO)_3$(H-DAB): A Density Functional Study. *The Journal of Physical Chemistry* **1996**, *100* (38), 15346-15357.

21. Kleverlaan, C. J.; Hartl, F.; Stufkens, D. J., Mechanistic Aspects of the Thermal *mer*-to-*fac* Isomerization of *mer*-[$Mn(X)(CO)_3$(α-diimine)] (X= Cl, Br, I). *Journal of Organometallic Chemistry* **1998**, *561* (1), 57-65.

22. Gonzalez, M. A.; Yim, M. A.; Cheng, S.; Moyes, A.; Hobbs, A. J.; Mascharak, P. K., Manganese Carbonyls Bearing Tripodal Polypyridine Ligands as Photoactive Carbon Monoxide-Releasing Molecules. *Inorganic Chemistry* **2011**, *51* (1), 601-608.

23. Gonzalez, M. A.; Carrington, S. J.; Fry, N. L.; Martinez, J. L.; Mascharak, P. K., Syntheses, Structures, and Properties of New Manganese Carbonyls as Photoactive CO-

Releasing Molecules: Design Strategies that Lead to CO Photolability in the Visible Region. *Inorganic Chemistry* **2012**, *51* (21), 11930-11940.

24. Govender, P.; Pai, S.; Schatzschneider, U.; Smith, G. S., Next Generation PhotoCORMs: Polynuclear Tricarbonylmanganese(I)-Functionalized Polypyridyl Metallodendrimers. *Inorganic Chemistry* **2013**, *52* (9), 5470-5478.

25. Yempally, V.; Kyran, S. J.; Raju, R. K.; Fan, W. Y.; Brothers, E. N.; Darensbourg, D. J.; Bengali, A. A., Thermal and Photochemical Reactivity of Manganese Tricarbonyl and Tetracarbonyl Complexes with a Bulky Diazabutadiene Ligand. *Inorganic chemistry* **2014**, *53* (8), 4081-4088.

26. Takeda, H.; Ishitani, O., Development of Efficient Photocatalytic Systems for CO_2 Reduction Using Mononuclear and Multinuclear Metal Complexes Based on Mechanistic Studies. *Coordination Chemistry Reviews* **2010**, *254* (3), 346-354.

27. Leasure, R.; Sacksteder, L.; Nesselrodt, D.; Reitz, G.; Demas, J.; DeGraff, B., Excited-State Acid-Base Chemistry of (α-Diimine)cyanotricarbonylrhenium(I) Complexes. *Inorganic Chemistry* **1991**, *30* (19), 3722-3728.

28. Connelly, N. G.; Geiger, W. E., Chemical Redox Agents for Organometallic Chemistry. *Chemical Reviews* **1996**, *96* (2), 877-910.

S2. SUPPORTING INFORMATION

S2.1 SELECTED SPECTRA

S2.1.1 ^{1}H NMR of [*N*-methyl-*N*′-2-pyridylbenzimidazolium]$^{+}$Br^{-} (L2.3)

Temperature: 20 ˚C
Solvent: DMSO-d_6

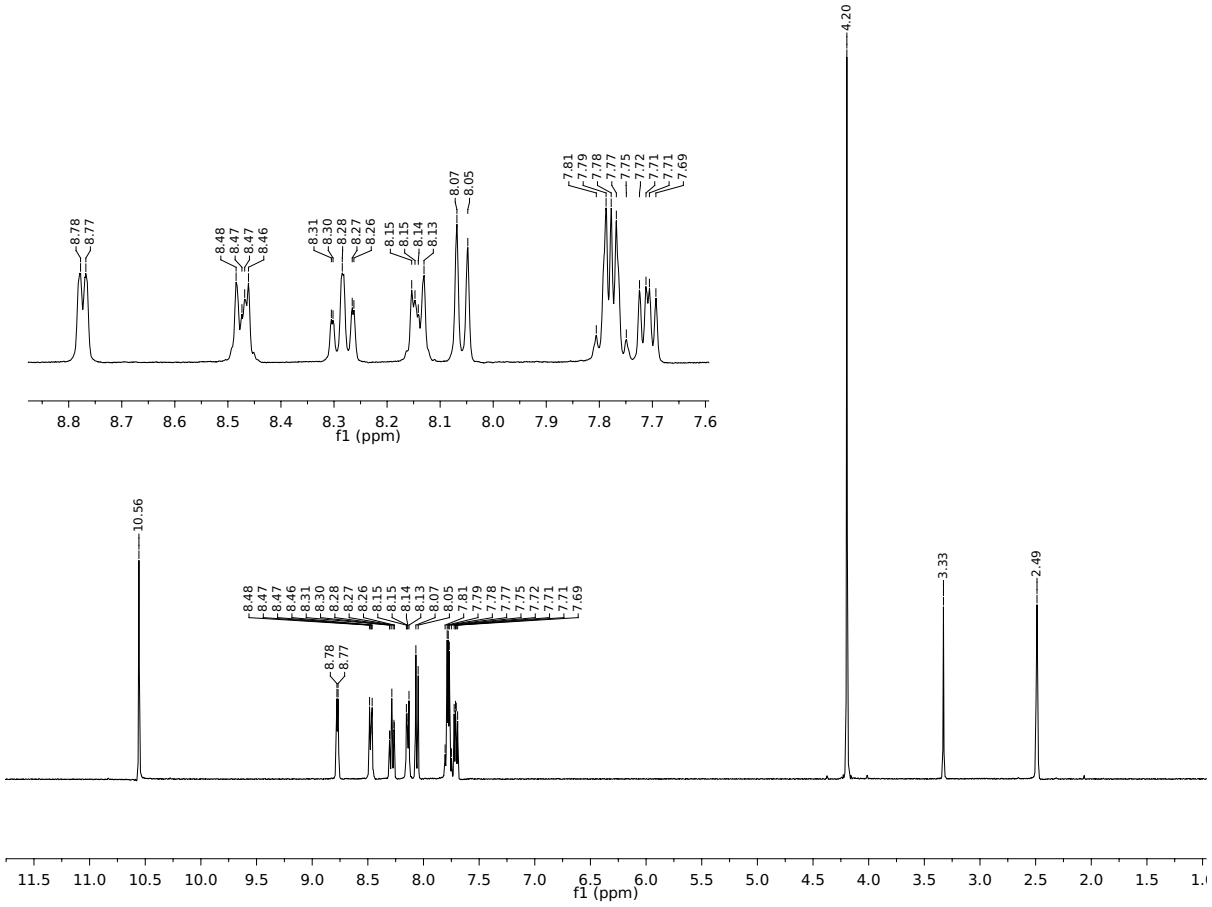

Note: The peak at 3.33 ppm is assigned to water and the peak at 2.49 ppm to dimethyl sulfoxide.

S2.1.2 ^{1}H NMR of [*N*-methyl-*N*′-2-pyridylimidazolium]$^{+}$Br^{-} (L2.4)

Temperature: 20 ˚C
Solvent: DMSO-d_6

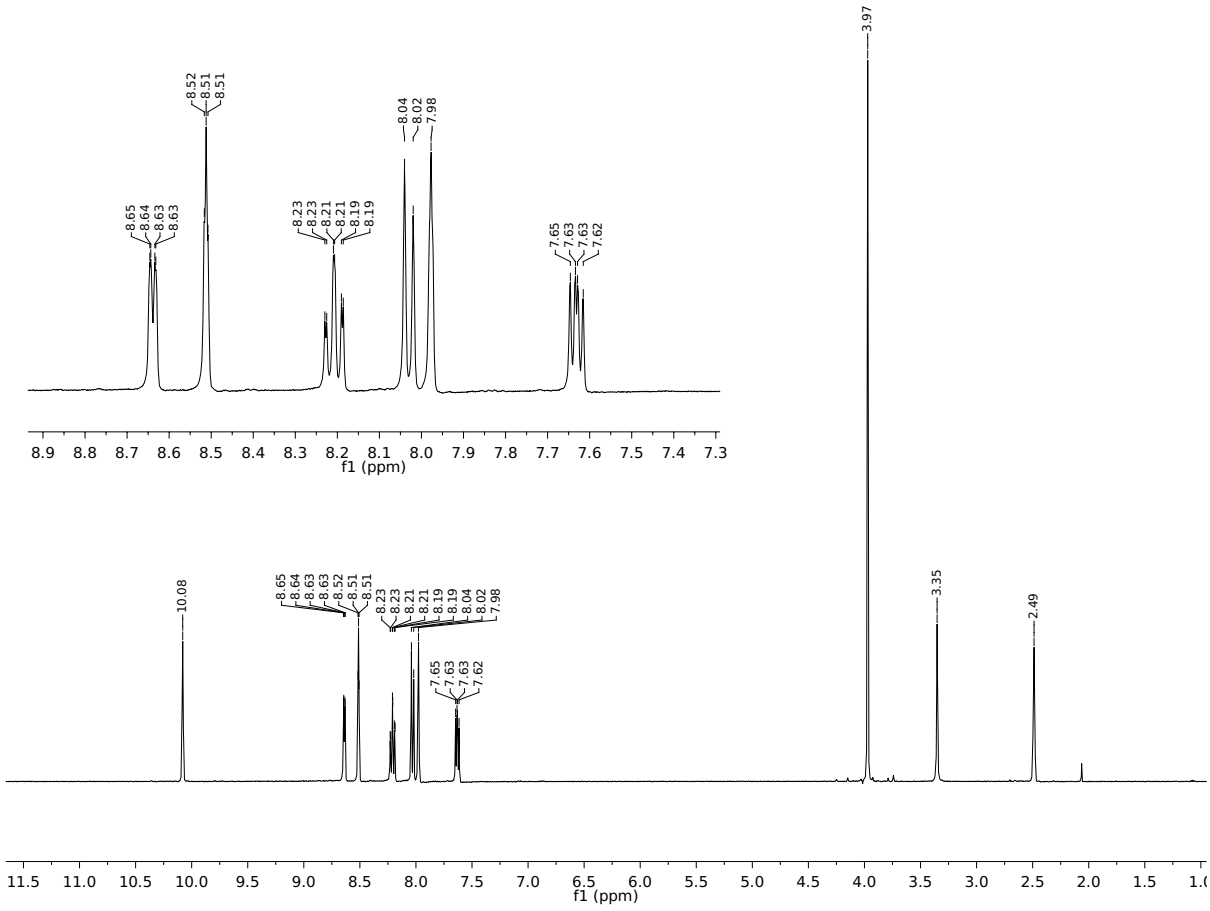

Note: The peak at 3.35 ppm is assigned water, the peak at 2.49 ppm to dimethyl sulfoxide, and the peak at roughly 2.0 ppm to residual acetone.

S2.1.3 ^{1}H NMR of MnBr(*N*-methyl-*N*′-2-pyridylbenzimidazol-2-ylidine)$(CO)_3$ (2.1)

Temperature: 25 ˚C
Solvent: DMSO-d_6

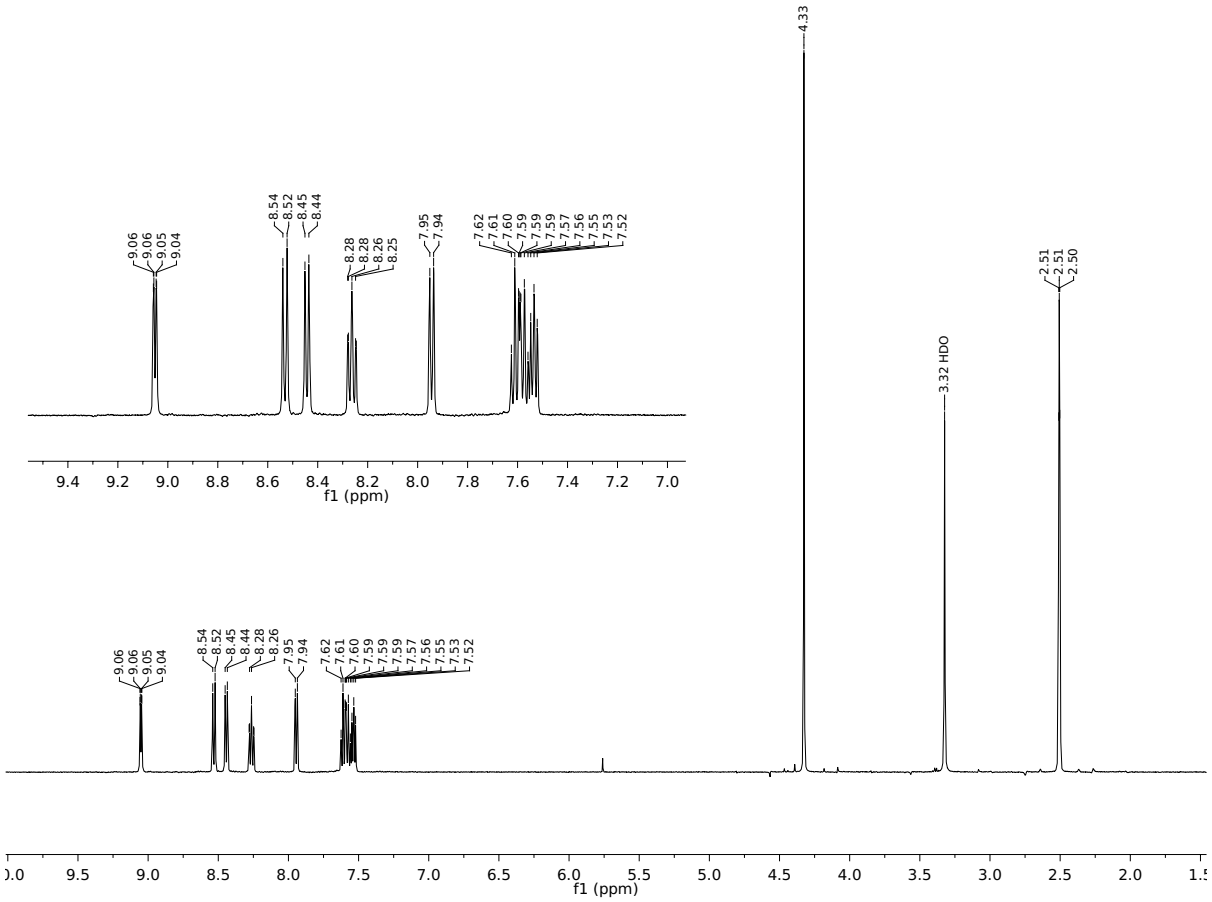

Note: The peak at roughly 5.7 ppm is assigned to residual dichloromethane, the peak at 3.32 ppm to water, and the peak at 2.51 ppm to dimethyl sulfoxide.

S2.1.4 ^{13}C NMR of MnBr(*N*-methyl-*N*′-2-pyridylbenzimidazol-2-ylidine)$(CO)_3$ (2.1)

Temperature: 25 ˚C
Solvent: DMSO-d_6

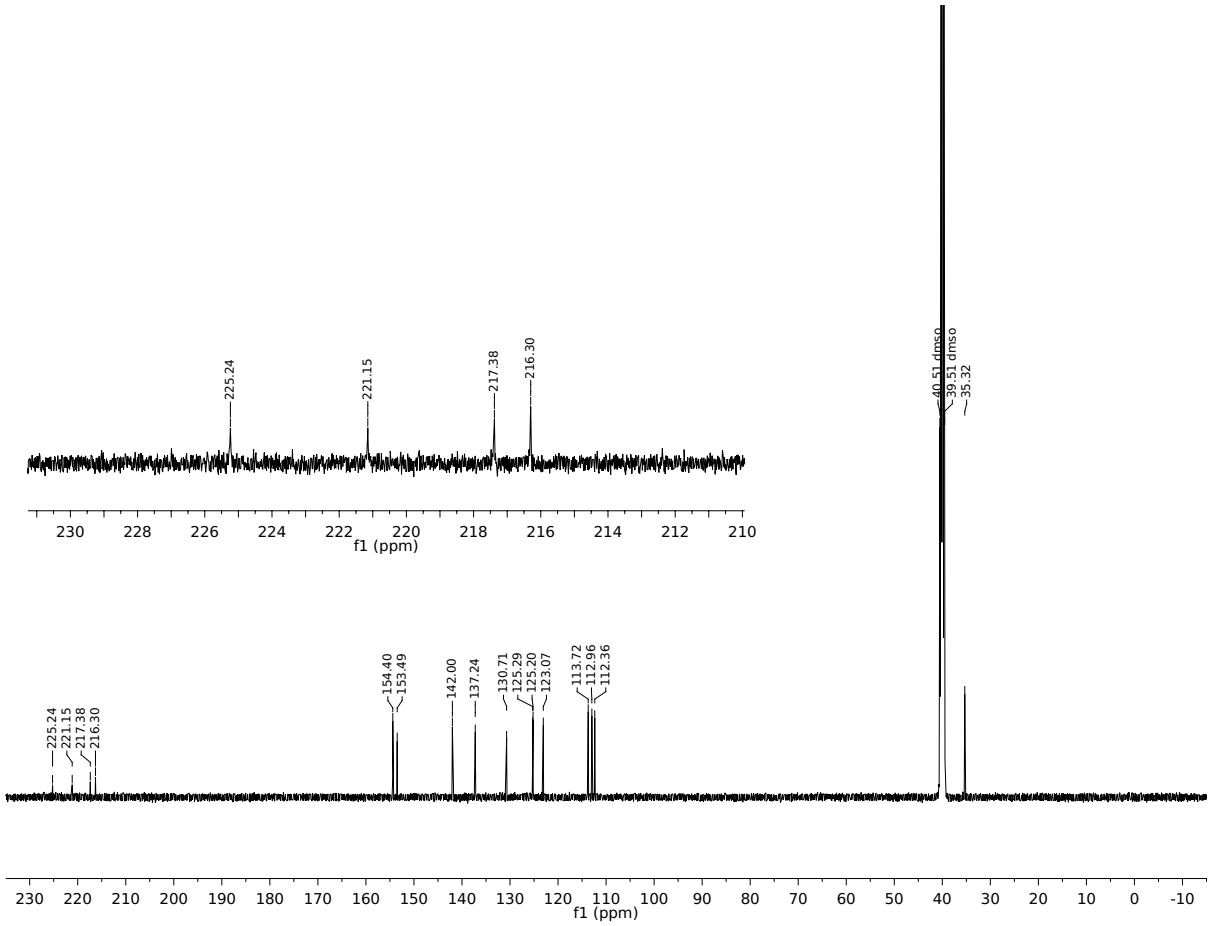

S2.1.5 FTIR of MnBr(*N*-methyl-*N*′-2-pyridylbenzimidazol-2-ylidine)$(CO)_3$ (2.1)

Method: ATR

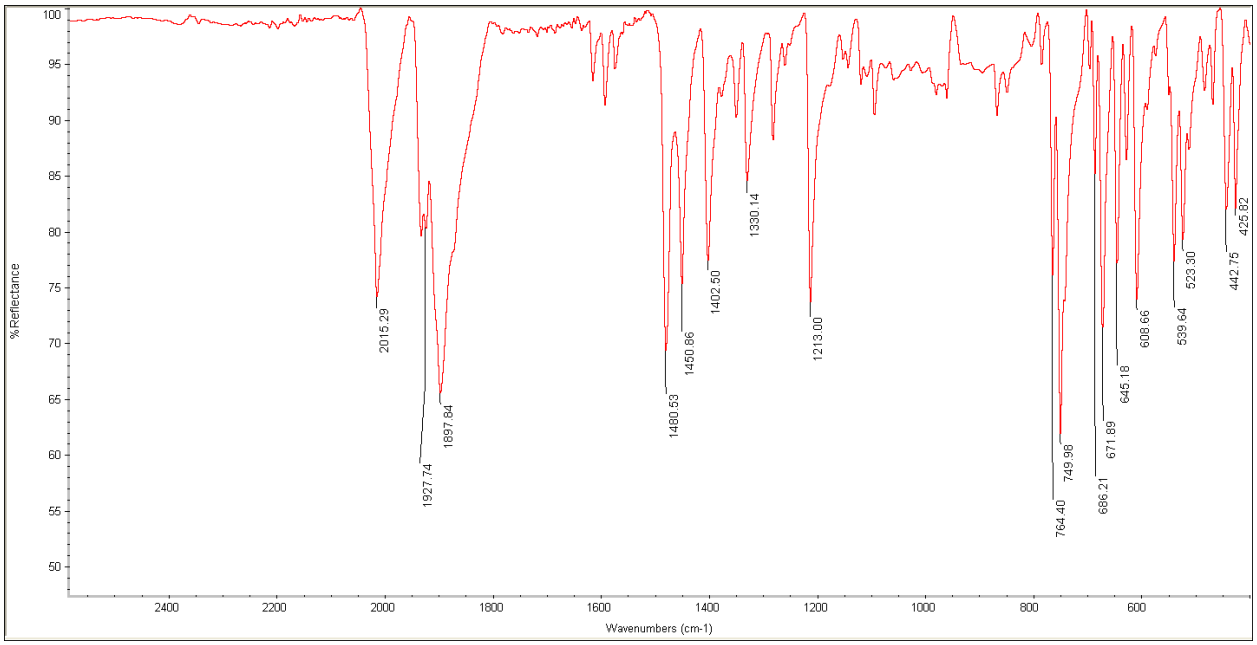

S2.1.6 ^{1}H NMR of MnBr(*N*-methyl-*N*′-2-pyridylimidazol-2-ylidine)$(CO)_3$ (2.2)

Temperature: 25 ˚C
Solvent: DMSO-d_6

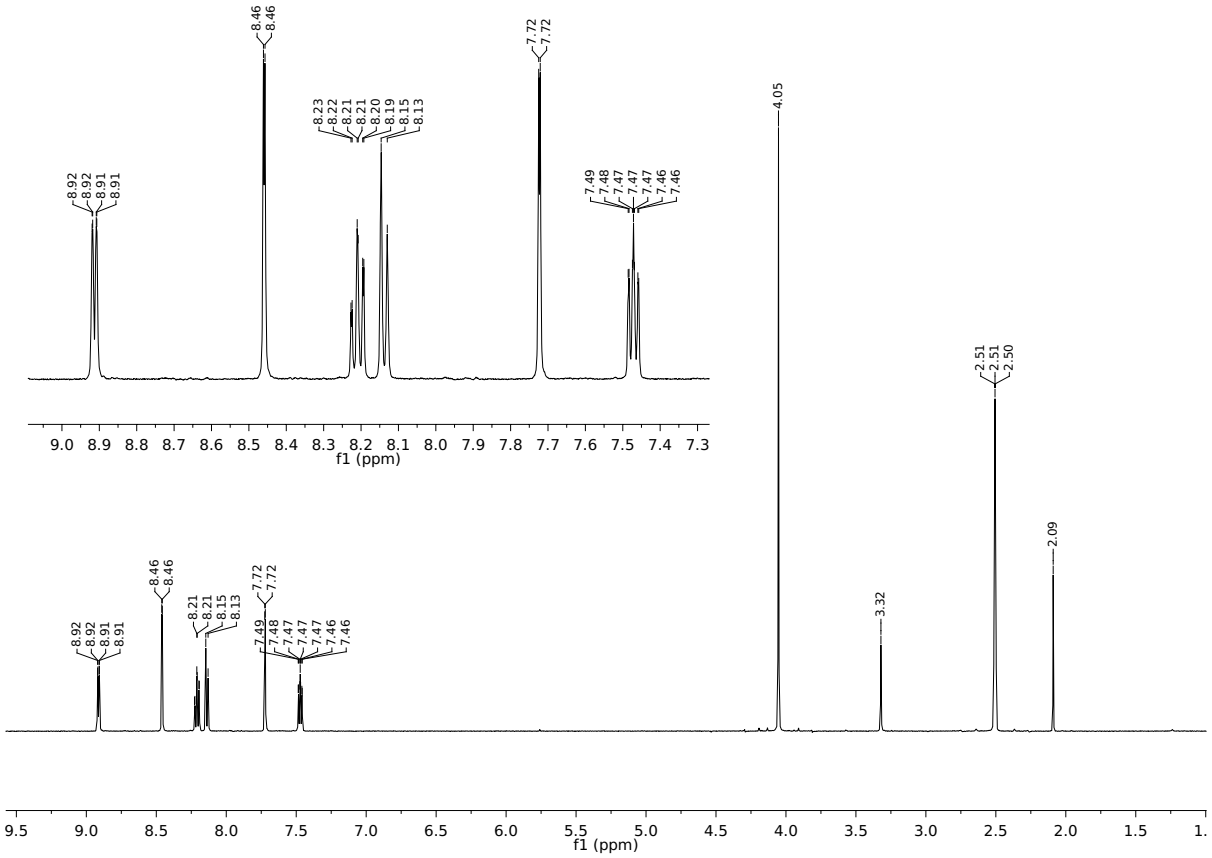

Note: The peak at 3.32 ppm is assigned to water, the peak at 2.51ppm to dimethyl sulfoxide, and the peak at 2.09 ppm to acetone.

S2.1.7 ^{13}C NMR of MnBr(*N*-methyl-*N*′-2-pyridylimidazol-2-ylidine)$(CO)_3$ (2.2)

Temperature: 25 ˚C
Solvent: DMSO-d_6

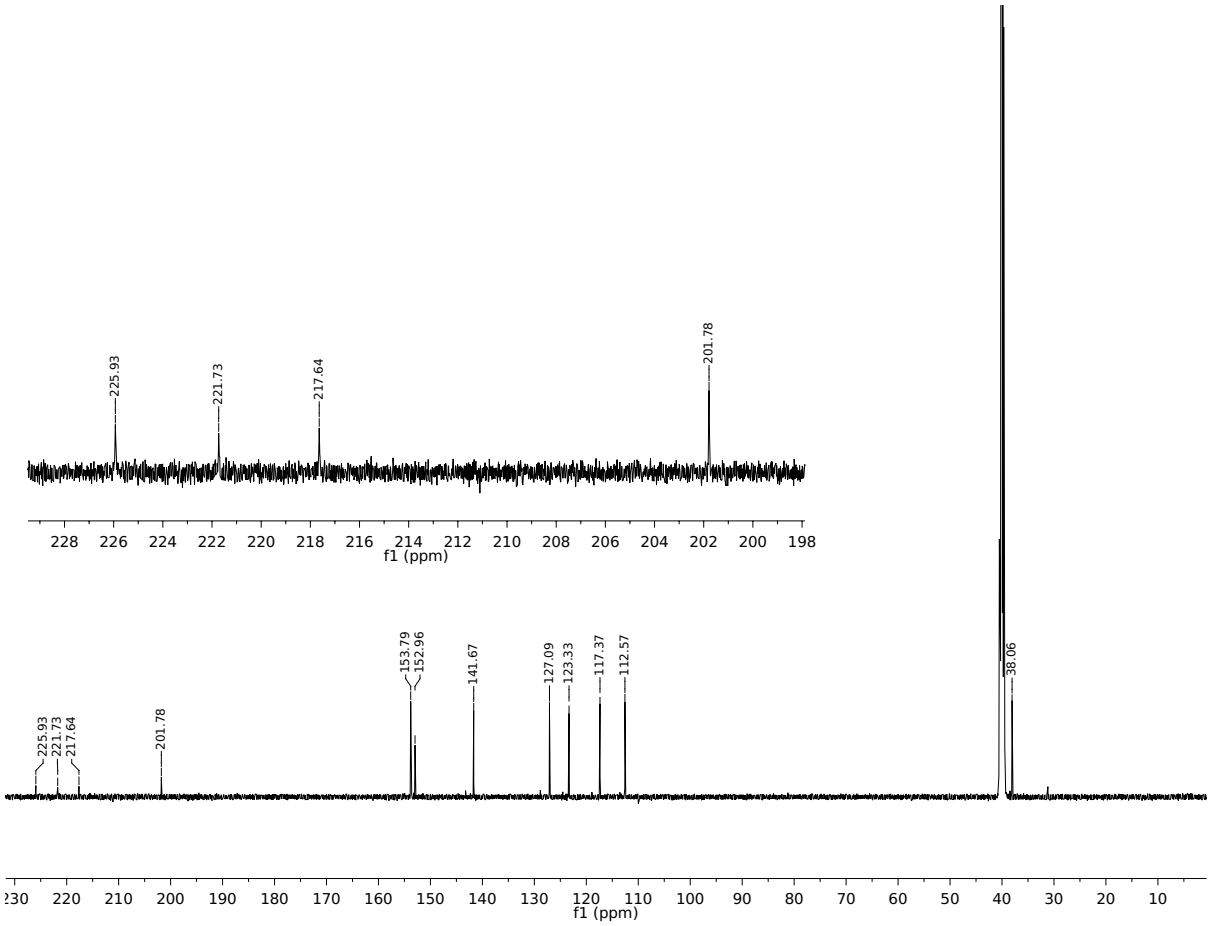

S2.1.8 FTIR of MnBr(*N*-methyl-*N*′-2-pyridylimidazol-2-ylidine)$(CO)_3$ (2.2)

Method: ATR

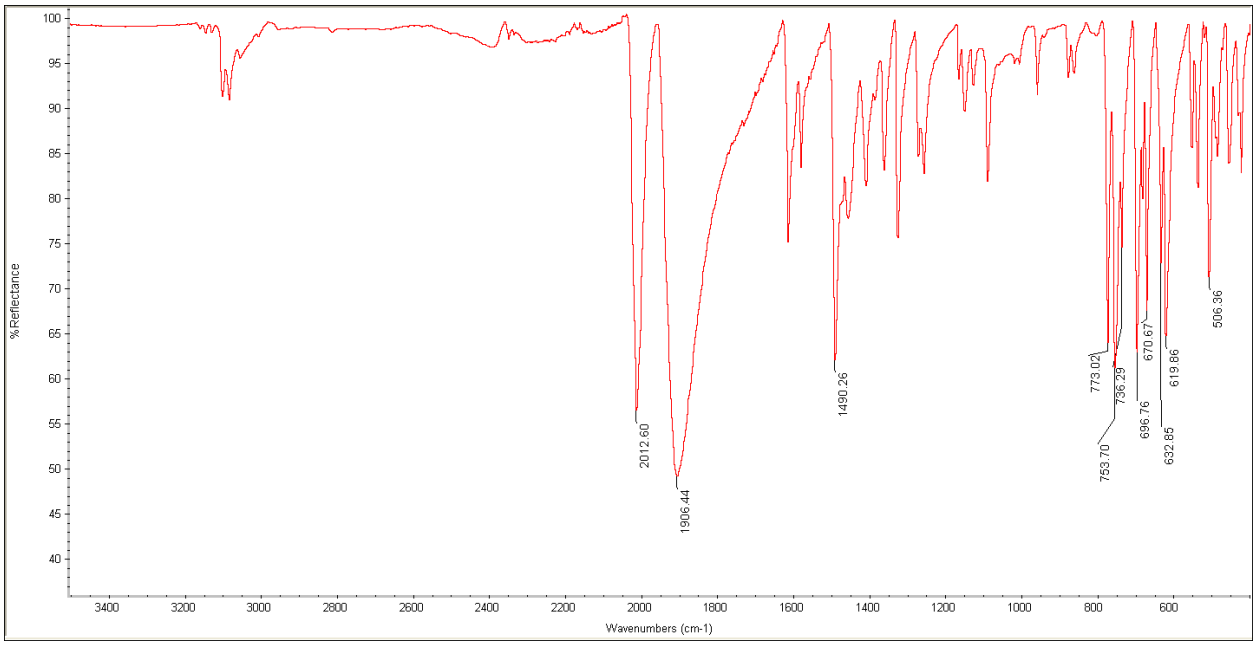

S2.1.9 Cyclic voltammetry of (2.1) (First scan)

Atmosphere: Argon
Catalyst Concentration: 1 mM
Solvent: CH_3CN
Electrolyte: 0.1 M TBAP

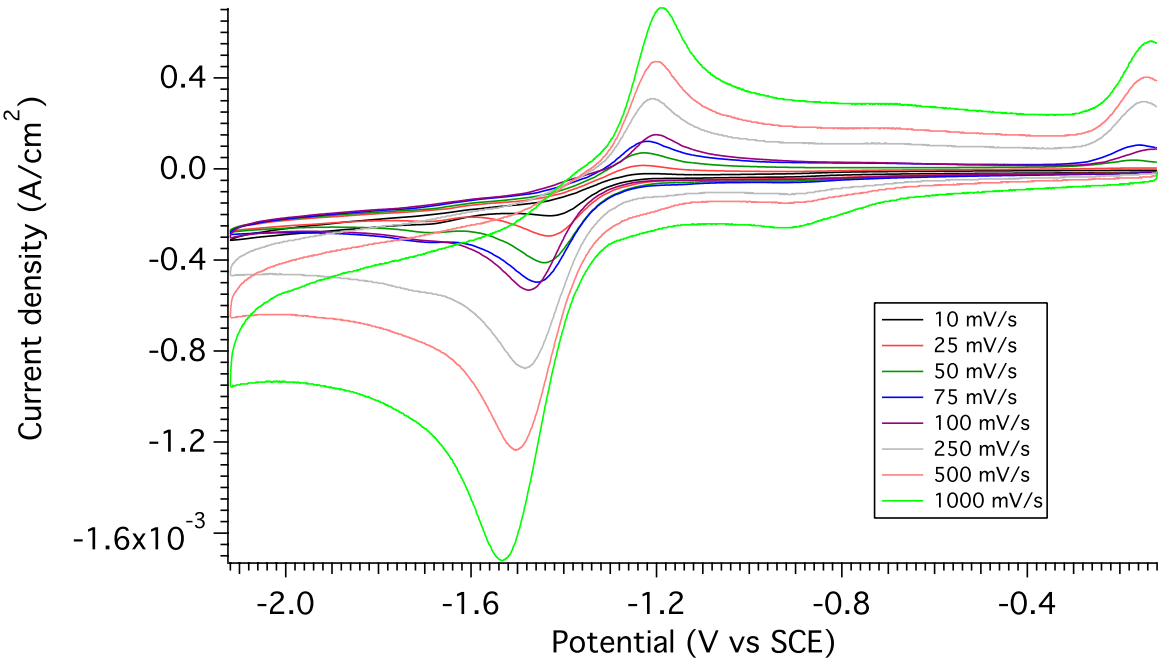

S2.1.10 Scan Rate Dependence of the First Peak Current of (2.1)

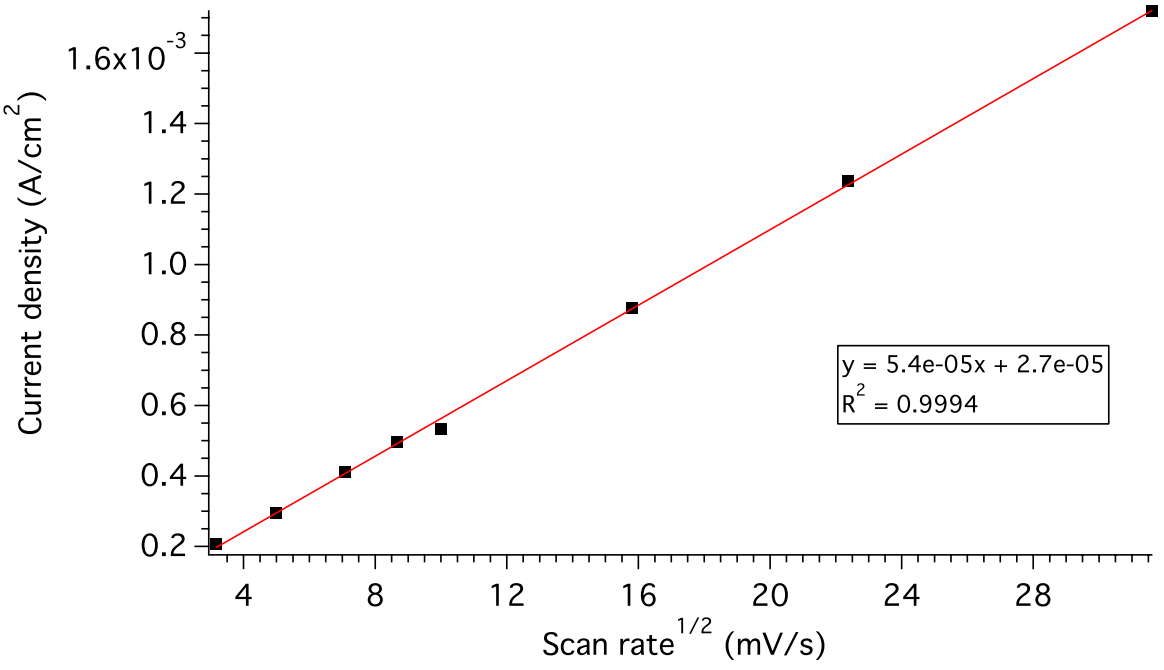

S2.1.11 Cyclic voltammetry of (2.1) (Second scan)

Atmosphere: Argon
Catalyst Concentration: 1 mM
Solvent: CH_3CN
Electrolyte: 0.1 M TBAP

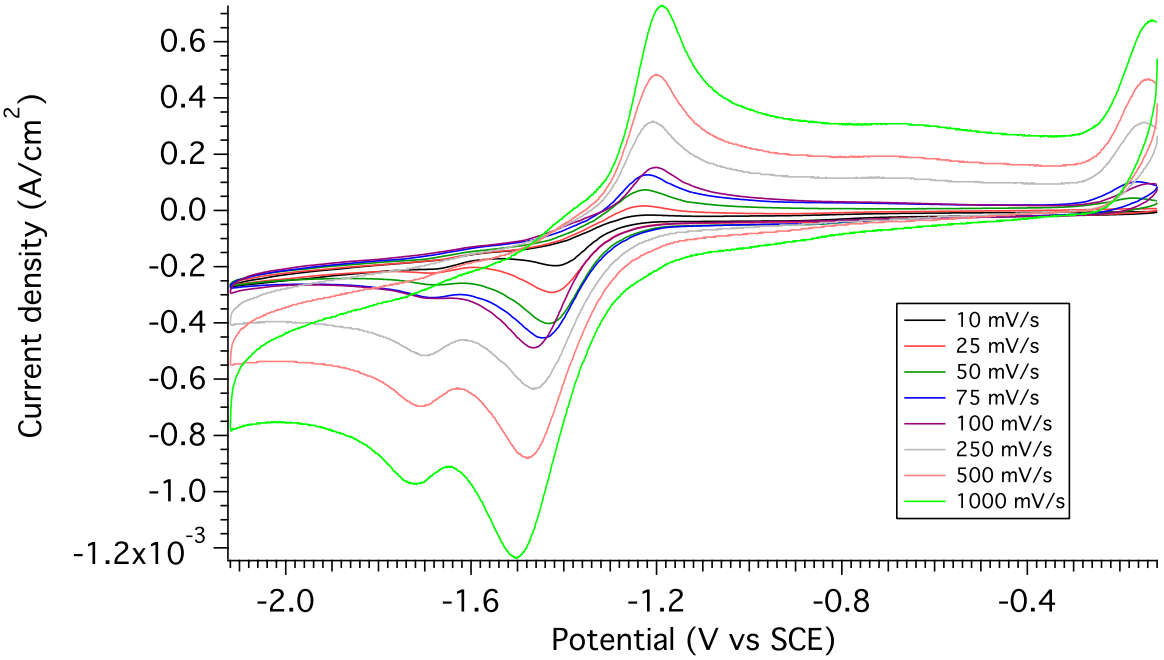

S2.1.12 Cyclic voltammetry of (2.2) (First scan)

Atmosphere: Argon
Catalyst Concentration: 1 mM
Solvent: CH_3CN
Electrolyte: 0.1 M TBAP

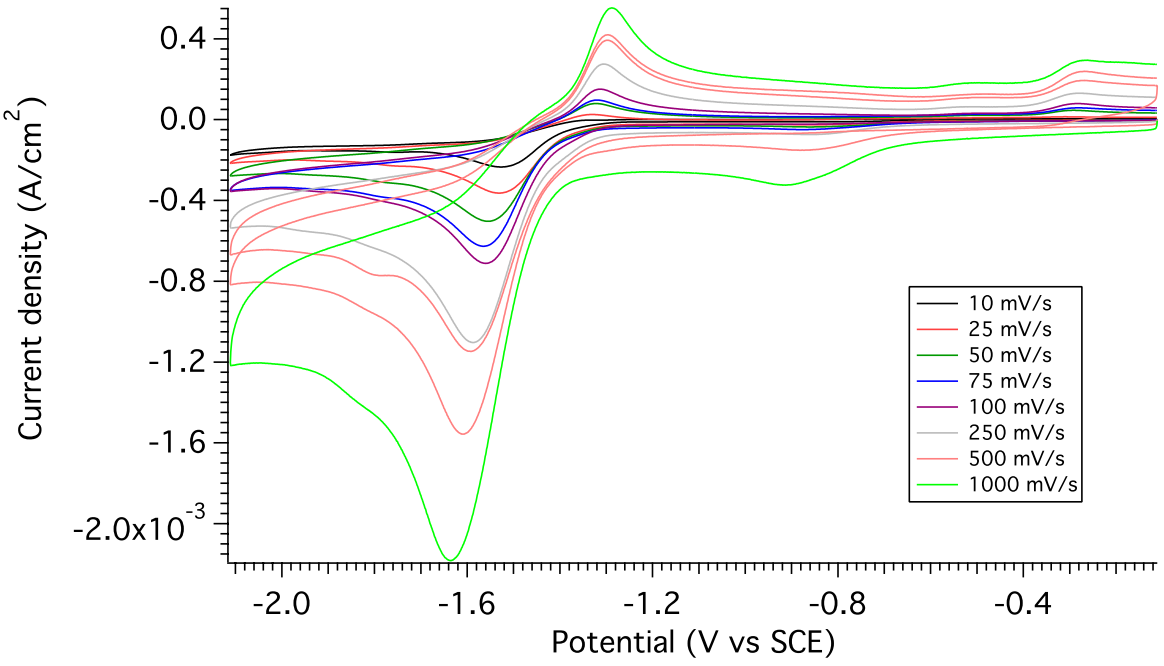

S2.1.13 Scan Rate Dependence of the First Peak Current of (2.2)

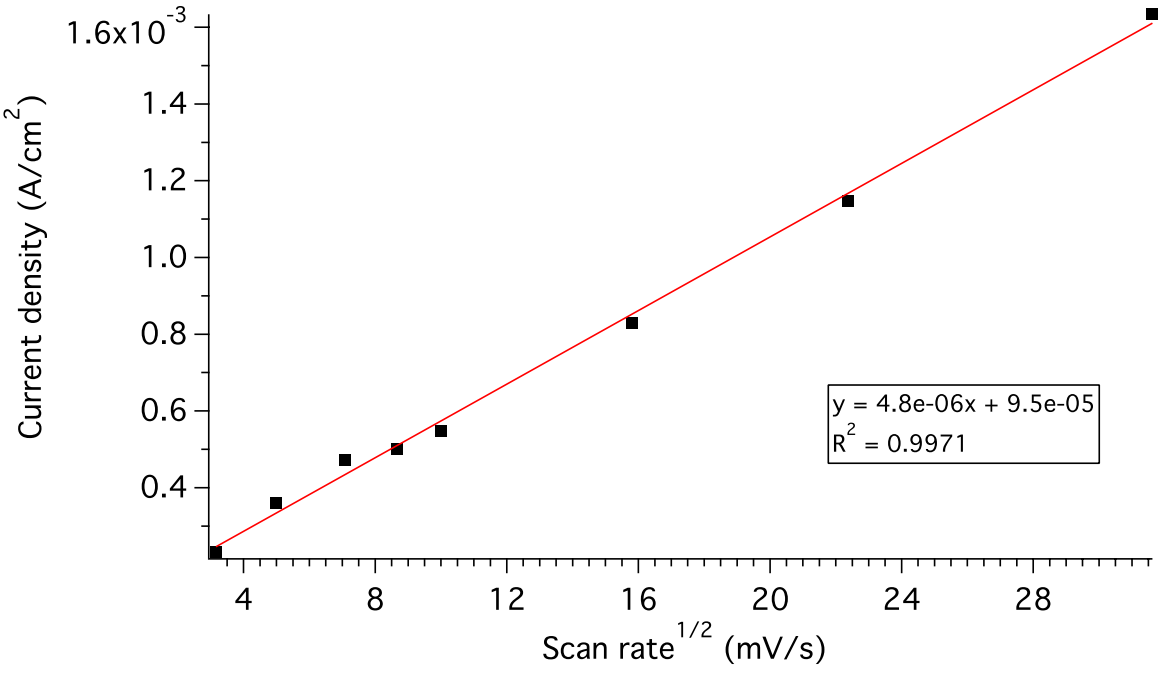

S2.1.14 Cyclic voltammetry of (2.2) (Second scan)

Atmosphere: Argon
Catalyst Concentration: 1 mM
Solvent: CH_3CN
Electrolyte: 0.1 M TBAP

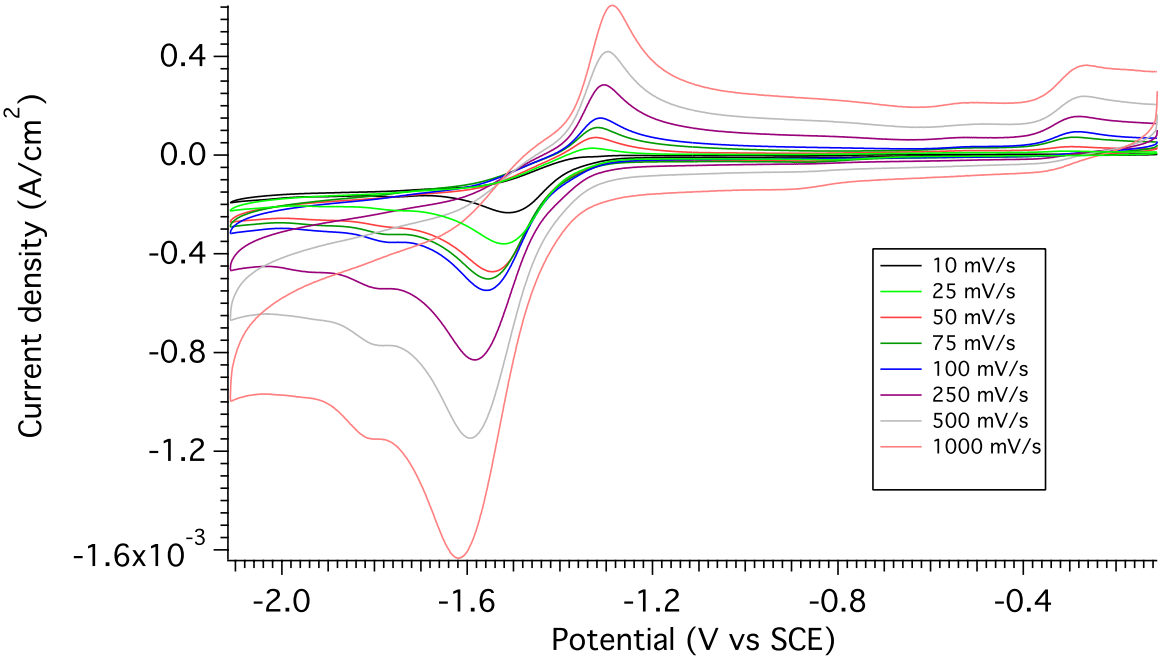

S2.1.15 FTIR from $^{13}CO_2$ labeling

Atmosphere: $^{13}CO_2$
Catalyst Concentration: 1 mM
Solvent: CH_3CN, 5 % H_2O
Electrolyte: 0.1 M TBAP

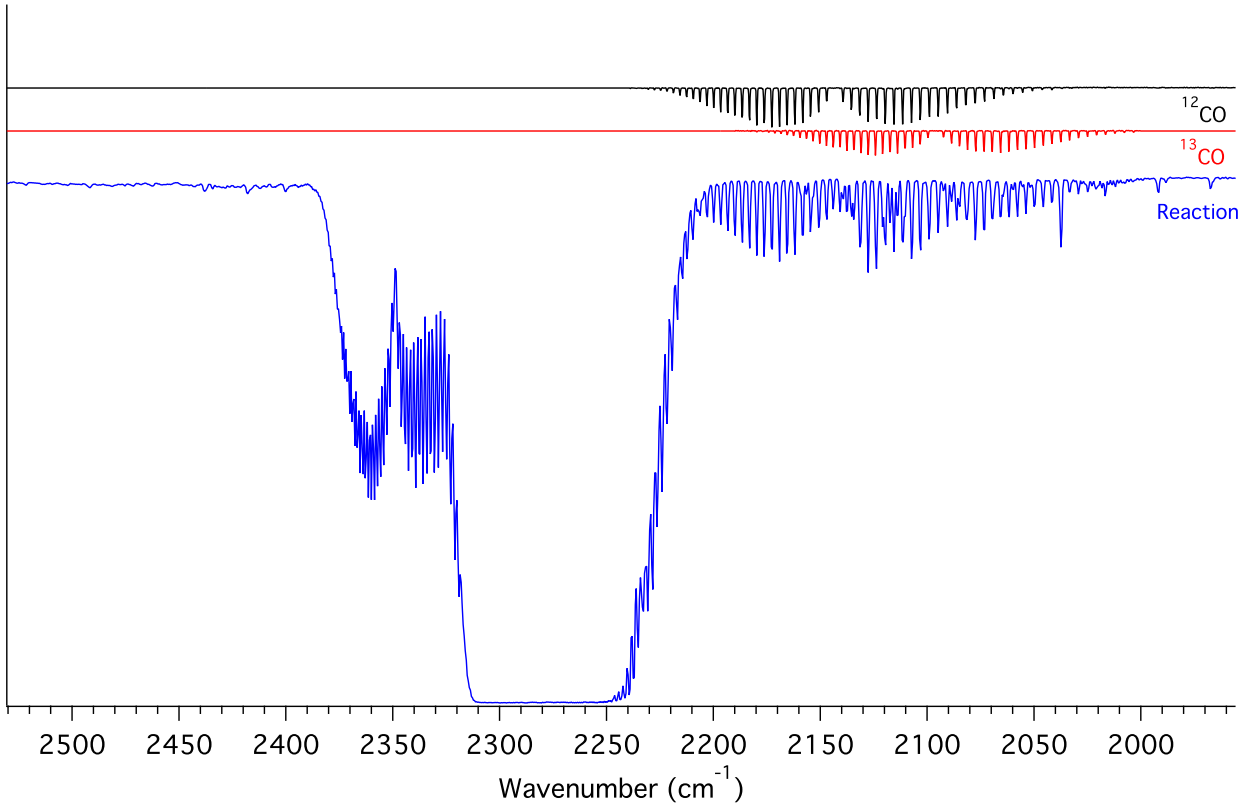

S2.1.16 2.4 ^{1}H NMR of [MnBr(*N*-ethyl-*N*′-2-pyridylimidazol-2-ylidine)$(CO)_3$] (2.4)

Temperature: 20 ˚C
Solvent: DMSO-d_6

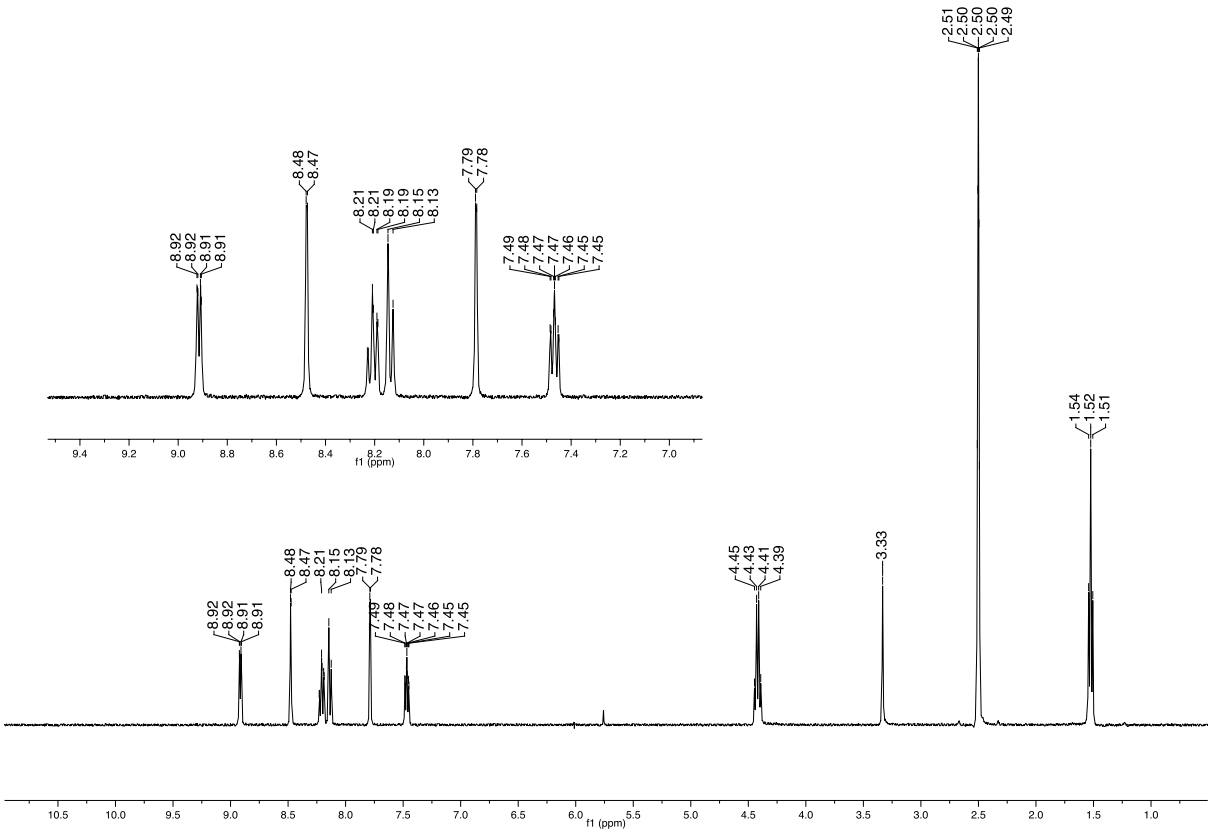

Note: The peak at roughly 5.7 ppm is assigned to residual dichloromethane, the peak at 3.33 ppm to water, and the peak at 2.50 ppm to dimethyl sulfoxide.

S2.1.17 ^{13}C NMR of [MnBr(*N*-ethyl-*N′*-2-pyridylimidazol-2-ylidine)$(CO)_3$] (2.4)

Temperature: 25 ˚C
Solvent: DMSO-d_6

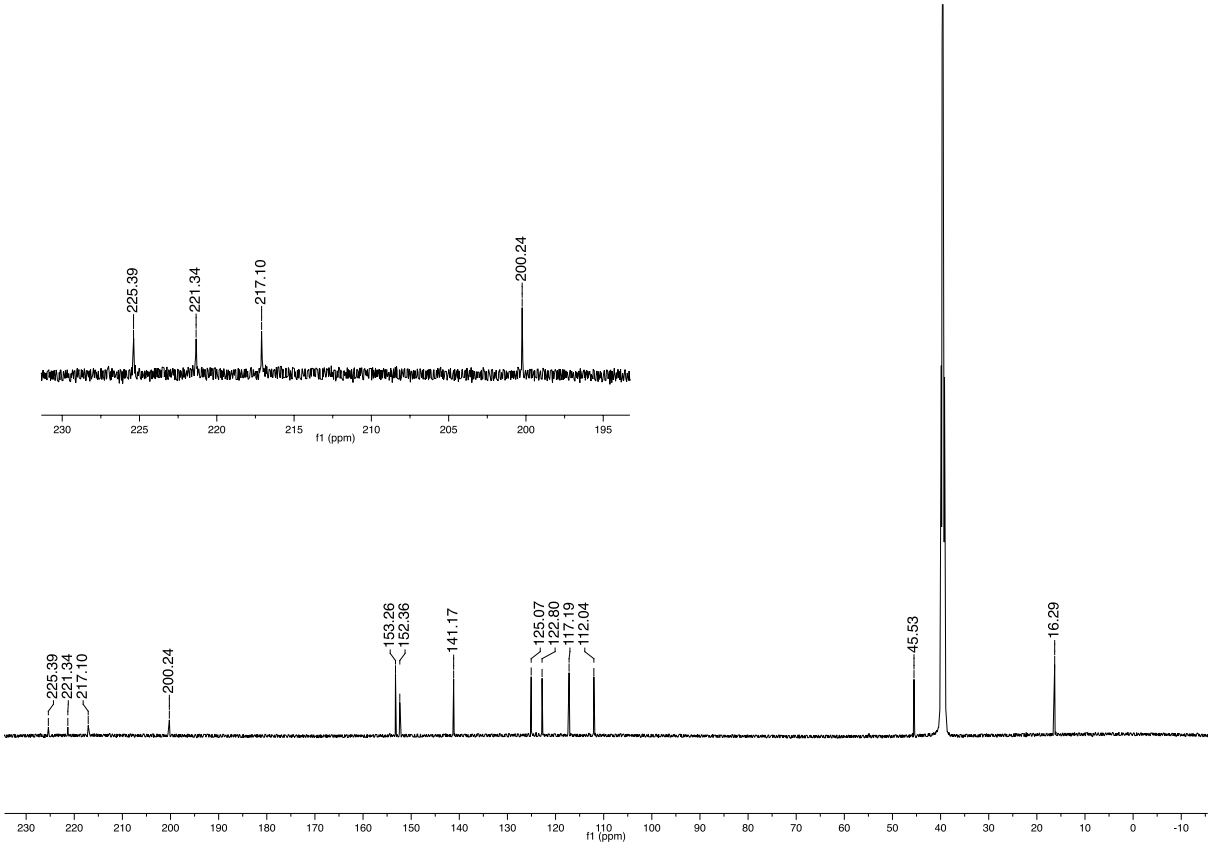

Note: The peak at 39.52 ppm is assigned to dimethyl sulfoxide.

S2.1.19 FTIR of [MnBr(*N*-ethyl-*N*′-2-pyridylimidazol-2-ylidine)$(CO)_3$] (2.4)

Method: ATR

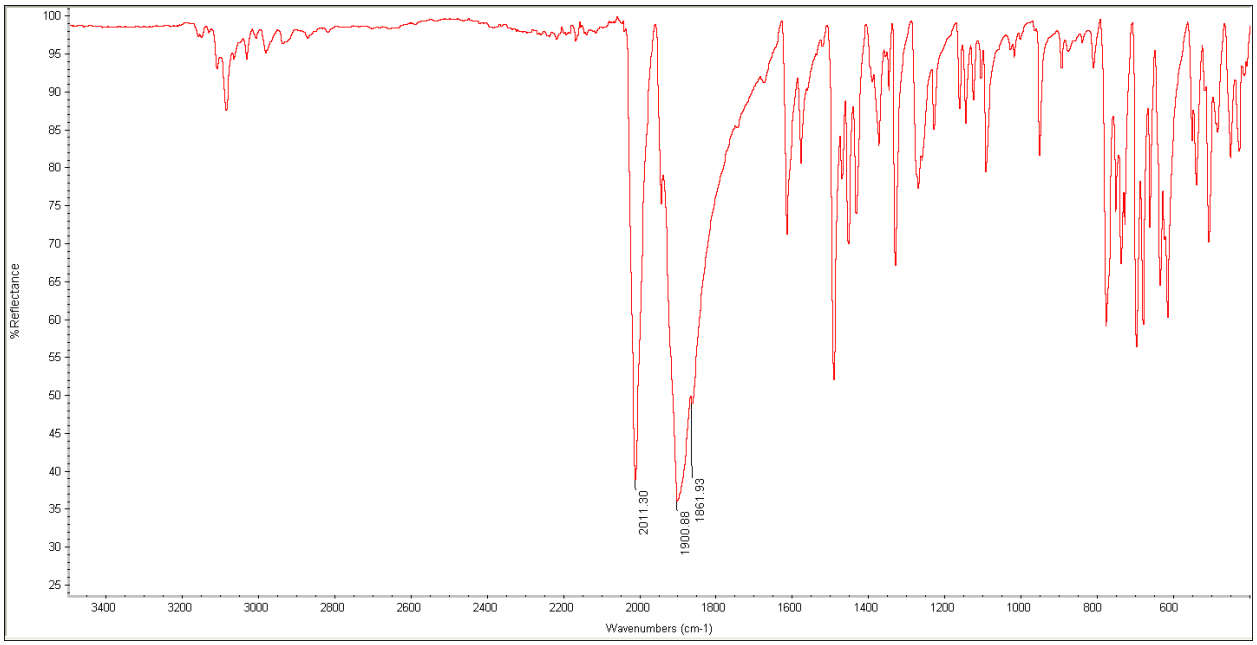

S2.1.20 UV-Vis of [MnBr(*N*-ethyl-*N*′-2-pyridylimidazol-2-ylidine)$(CO)_3$] (2.4)

Temperature: 298K
Concentration: 125μM
Solvent: MeCN

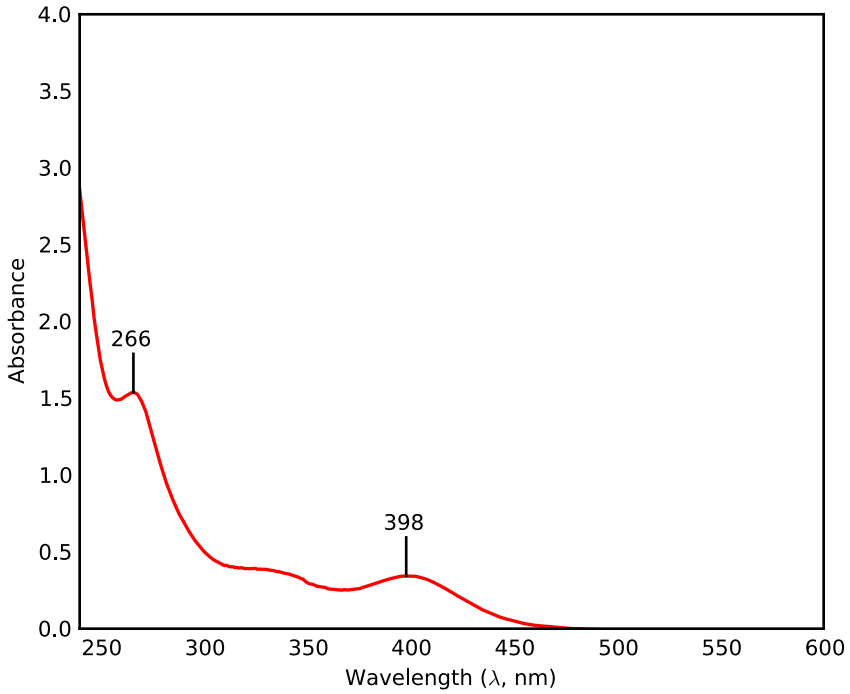

S2.1.21 ^{1}H NMR of [MnNCS(*N*-ethyl-*N*′-2-pyridylimidazol-2-ylidine)$(CO)_3$] (2.6)

Temperature: 20 ˚C
Solvent: DMSO-d_6

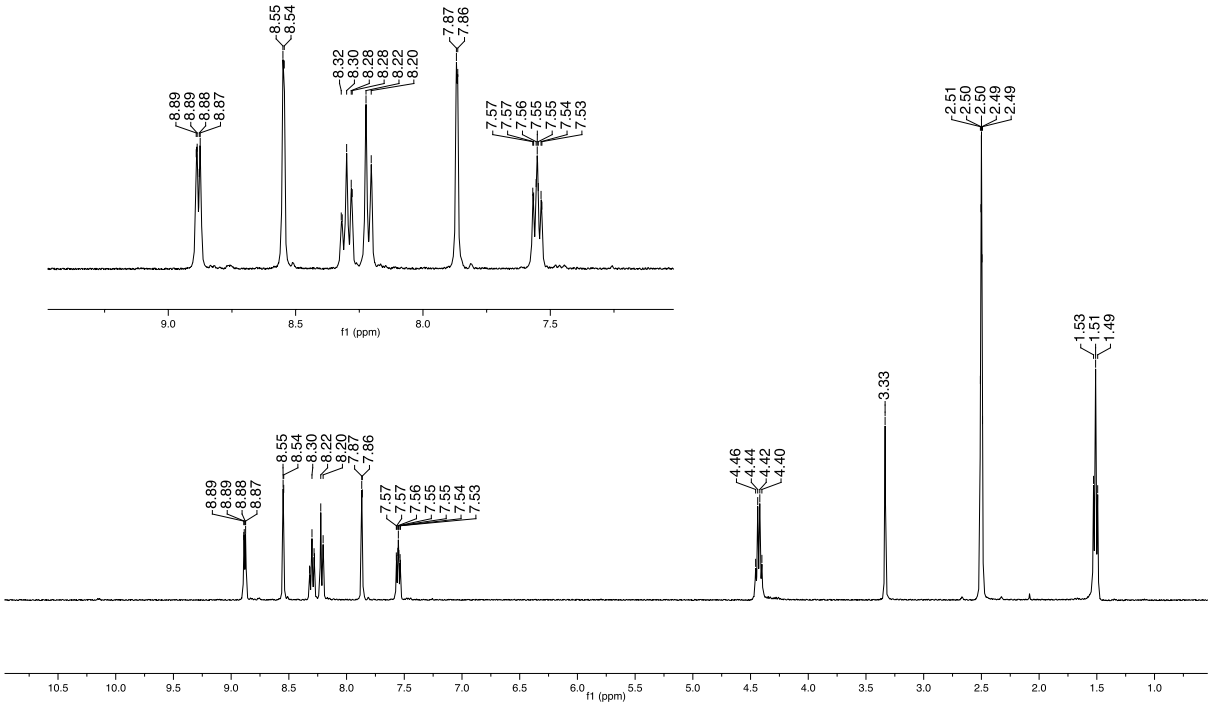

Note: The peak at 3.33 ppm is assigned to water and the peak at 2.50 ppm to dimethyl sulfoxide.

S2.1.22 ^{13}C NMR of [MnNCS(*N*-ethyl-*N*′-2-pyridylimidazol-2-ylidine)$(CO)_3$] (2.6)

Temperature: 25 ˚C
Solvent: DMSO-d_6

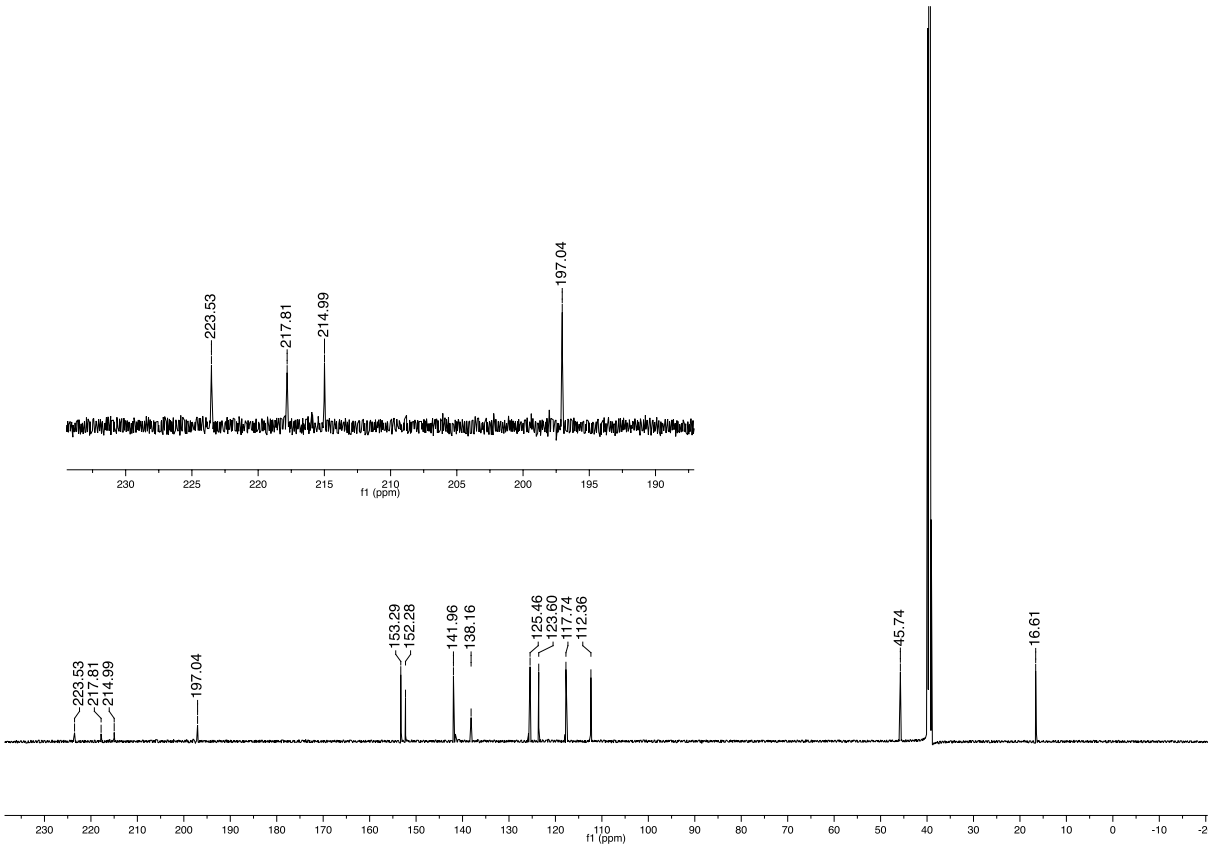

Note: The peak at 39.52 ppm is assigned to dimethyl sulfoxide.

S2.1.23 FTIR of [MnNCS(*N*-ethyl-*N*′-2-pyridylimidazol-2-ylidine)$(CO)_3$] (2.6)

Method: ATR

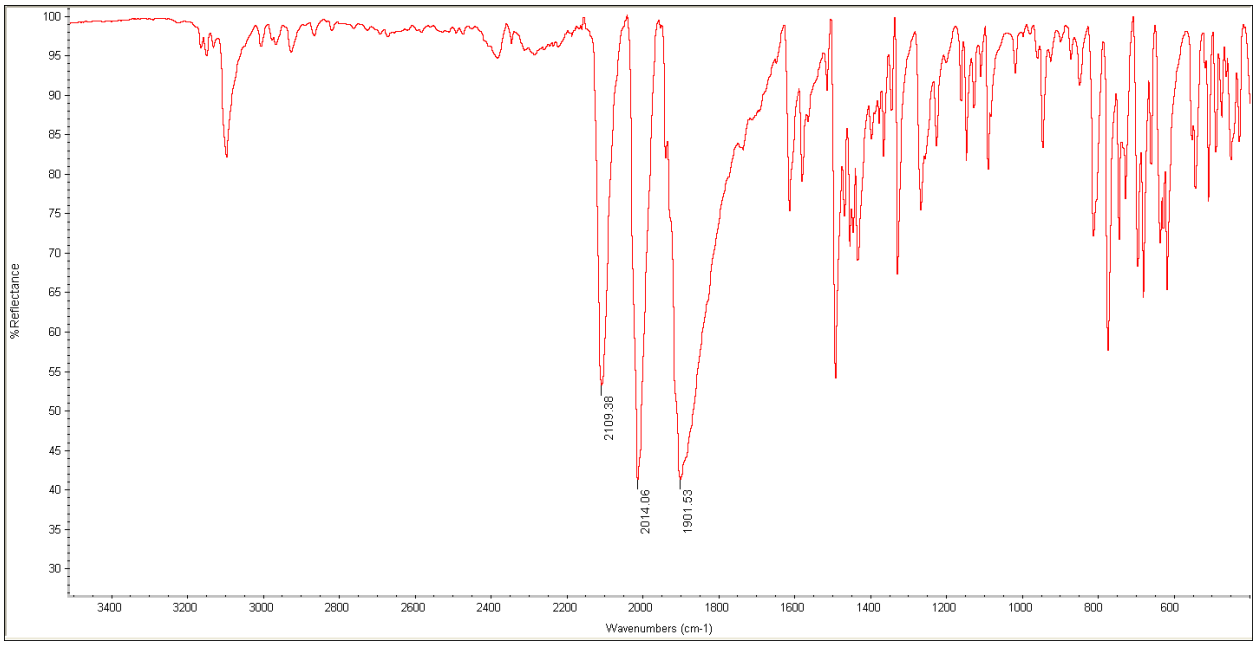

S2.1.24 UV-Vis of [MnNCS(*N*-ethyl-*N*′-2-pyridylimidazol-2-ylidine)$(CO)_3$] (2.6)

Temperature: 298K
Concentration: 125µM
Solvent: MeCN

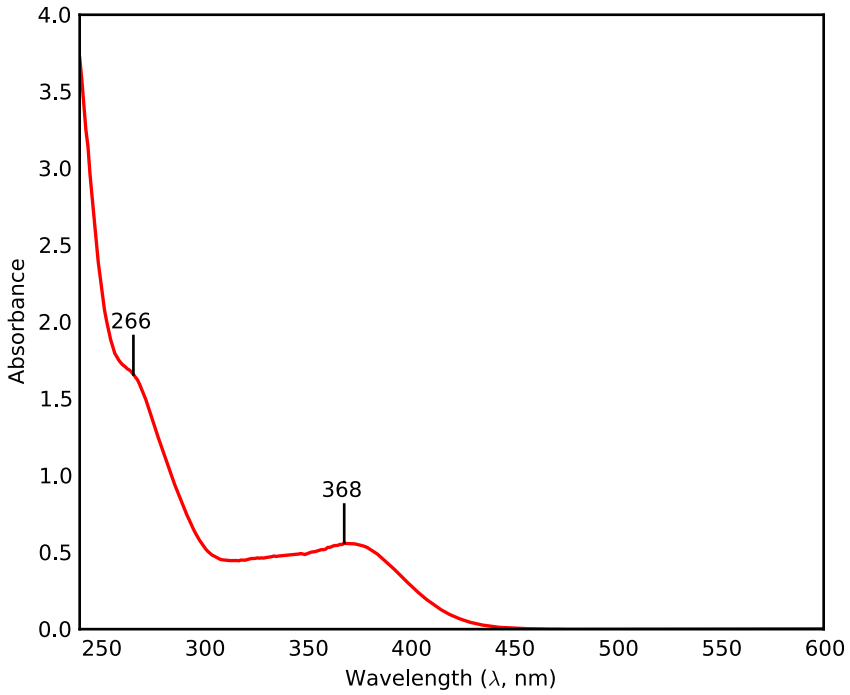

S2.1.25 ^{1}H NMR of [MnCN(*N*-ethyl-*N*′-2-pyridylimidazol-2-ylidine)$(CO)_3$] (2.7)

Temperature: 20 ˚C
Solvent: DMSO-d_6

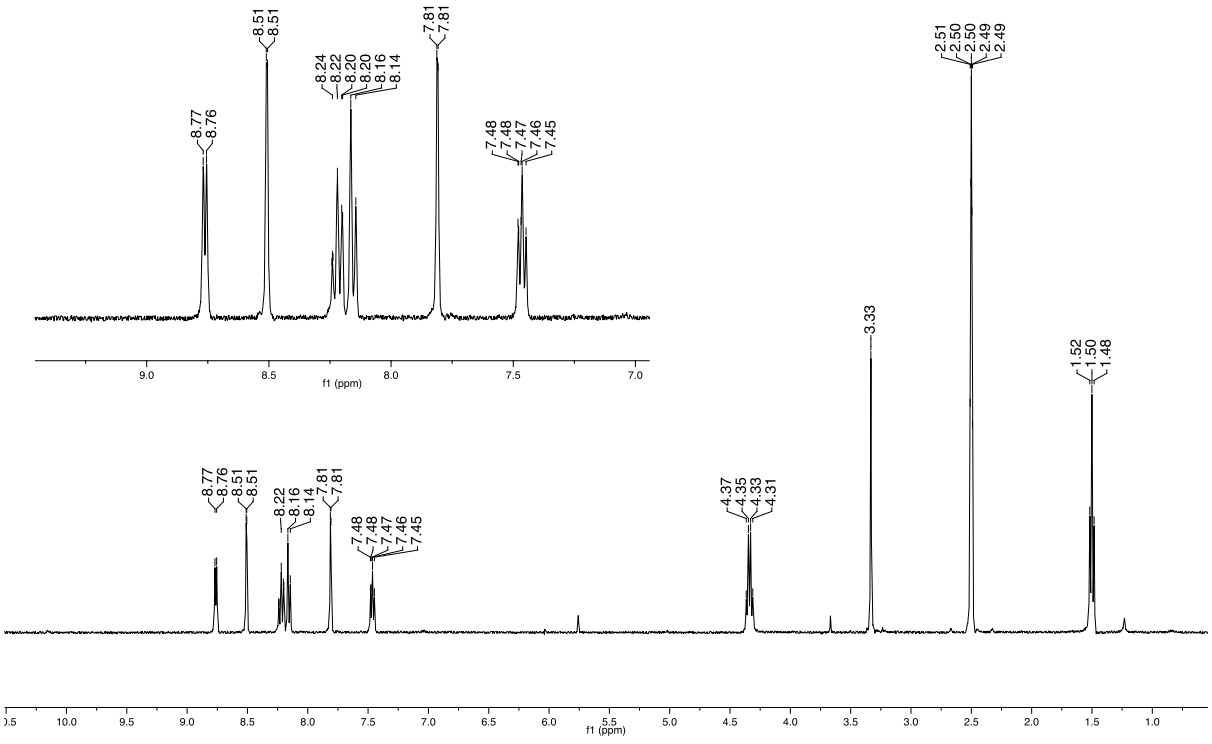

Note: The peak at 3.33 ppm is assigned to water and the peak at 2.50 ppm to dimethyl sulfoxide.

S2.1.26 ^{13}C NMR of [MnCN(*N*-ethyl-*N*′-2-pyridylimidazol-2-ylidine)$(CO)_3$] (2.7)

Temperature: 25 ˚C
Solvent: DMSO-d_6

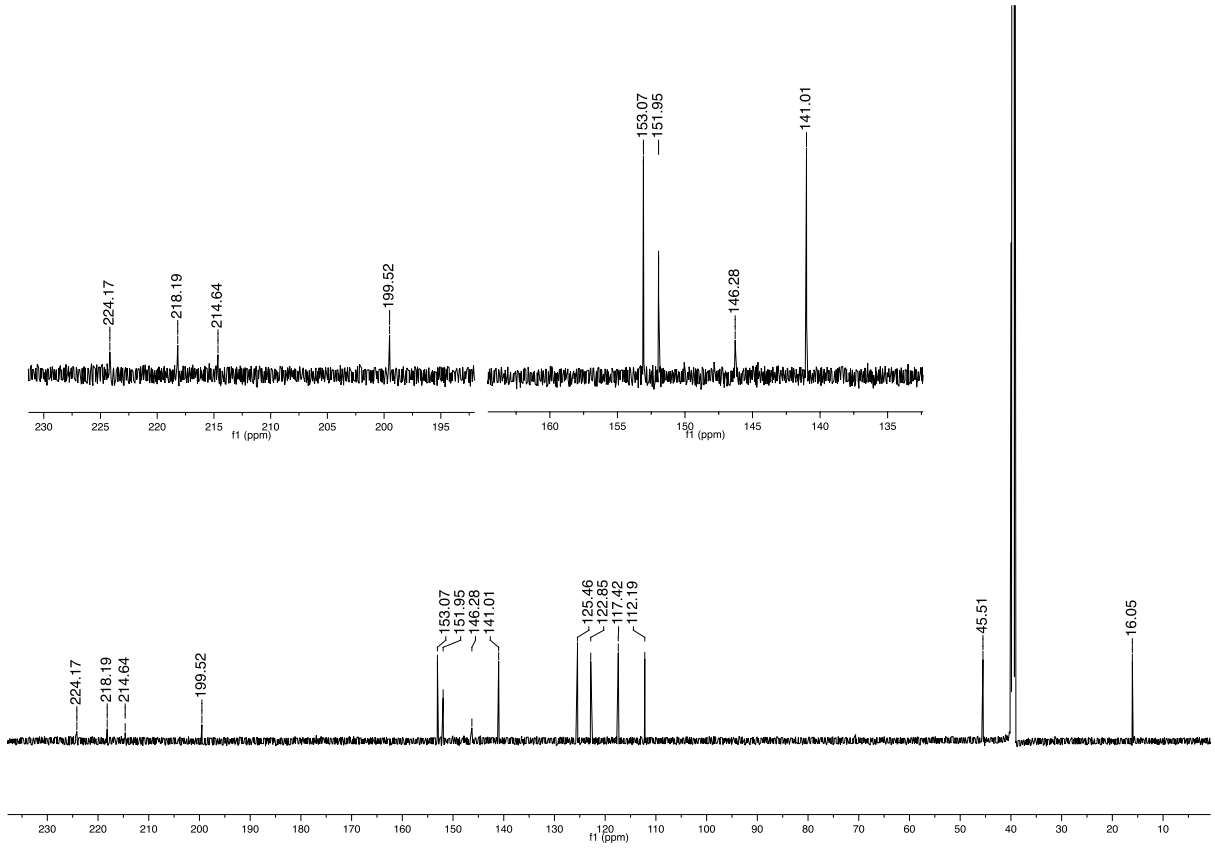

Note: The peak at 39.52 ppm is assigned to dimethyl sulfoxide.

S2.1.27 FTIR of [MnCN(*N*-ethyl-*N*′-2-pyridylimidazol-2-ylidine)$(CO)_3$] (2.7)

Method: ATR

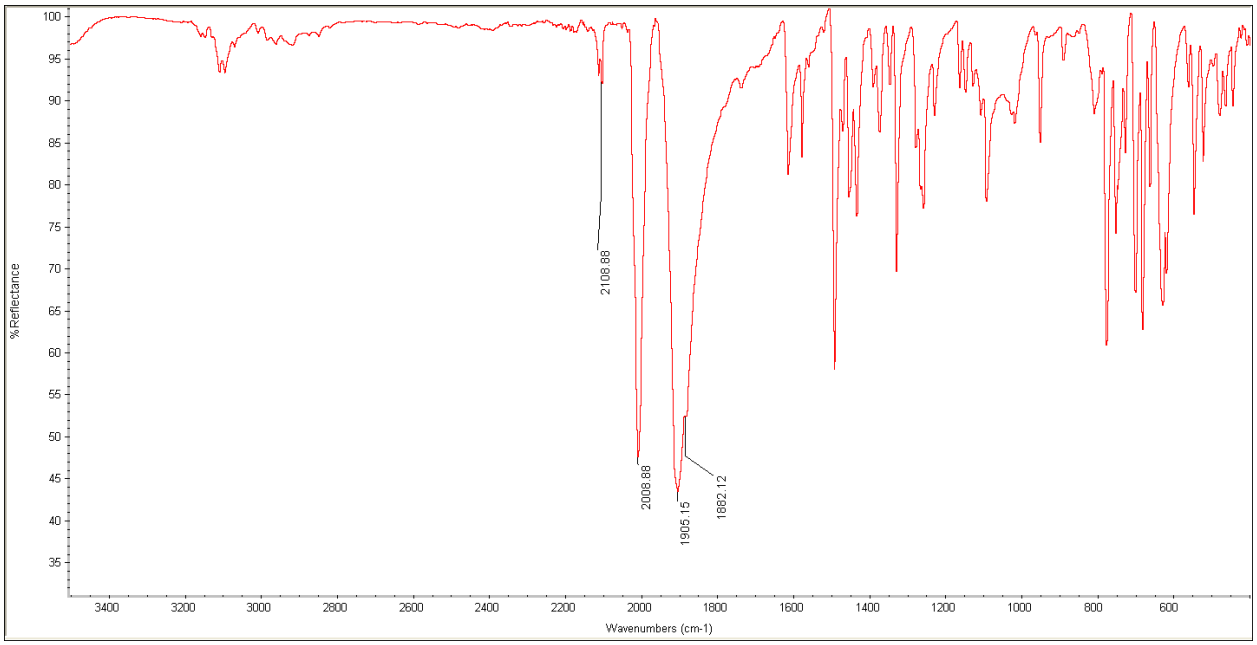

S2.1.28 UV-Vis of [MnCN(*N*-ethyl-*N*′-2-pyridylimidazol-2-ylidine)$(CO)_3$] (2.7)

Temperature: 298K
Concentration: 125µM
Solvent: MeCN

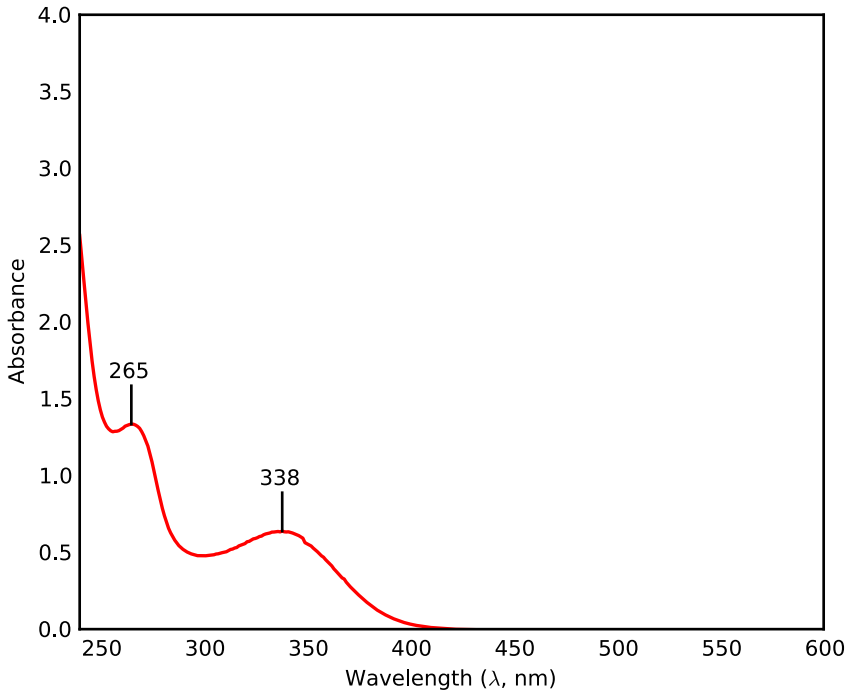

S2.1.29 ^{1}H NMR of [MnBr(*N*-ethyl-*N*′-2-pyridylbenzimidazol-2-ylidine)$(CO)_3$] (2.3)

Temperature: 20 ˚C
Solvent: DMSO-d_6

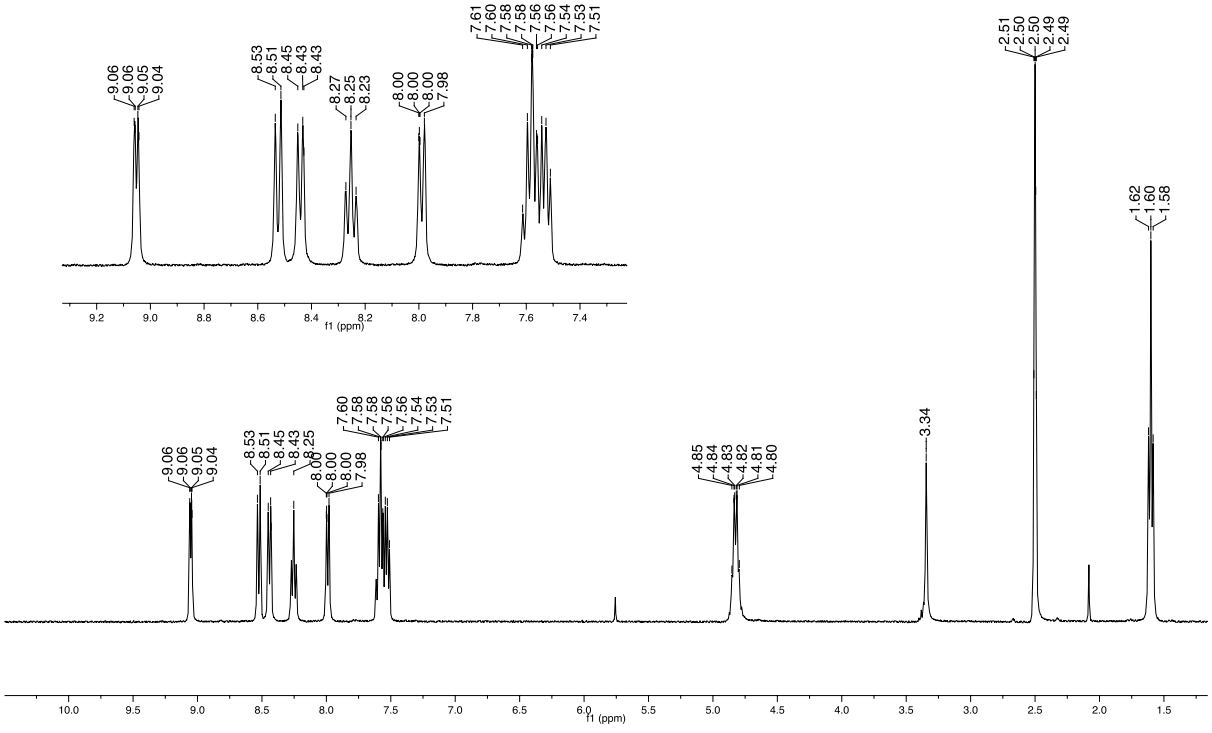

Note: The peak at roughly 5.7 ppm is assigned to residual dichloromethane, the peak at 3.34 ppm to water, and the peak at 2.50 ppm to dimethyl sulfoxide.

S2.1.30 ^{13}C NMR of [MnBr(*N*-ethyl-*N*′-2-pyridylbenzimidazol-2-ylidine)$(CO)_3$] (2.3)

Temperature: 25 ˚C
Solvent: DMSO-d_6

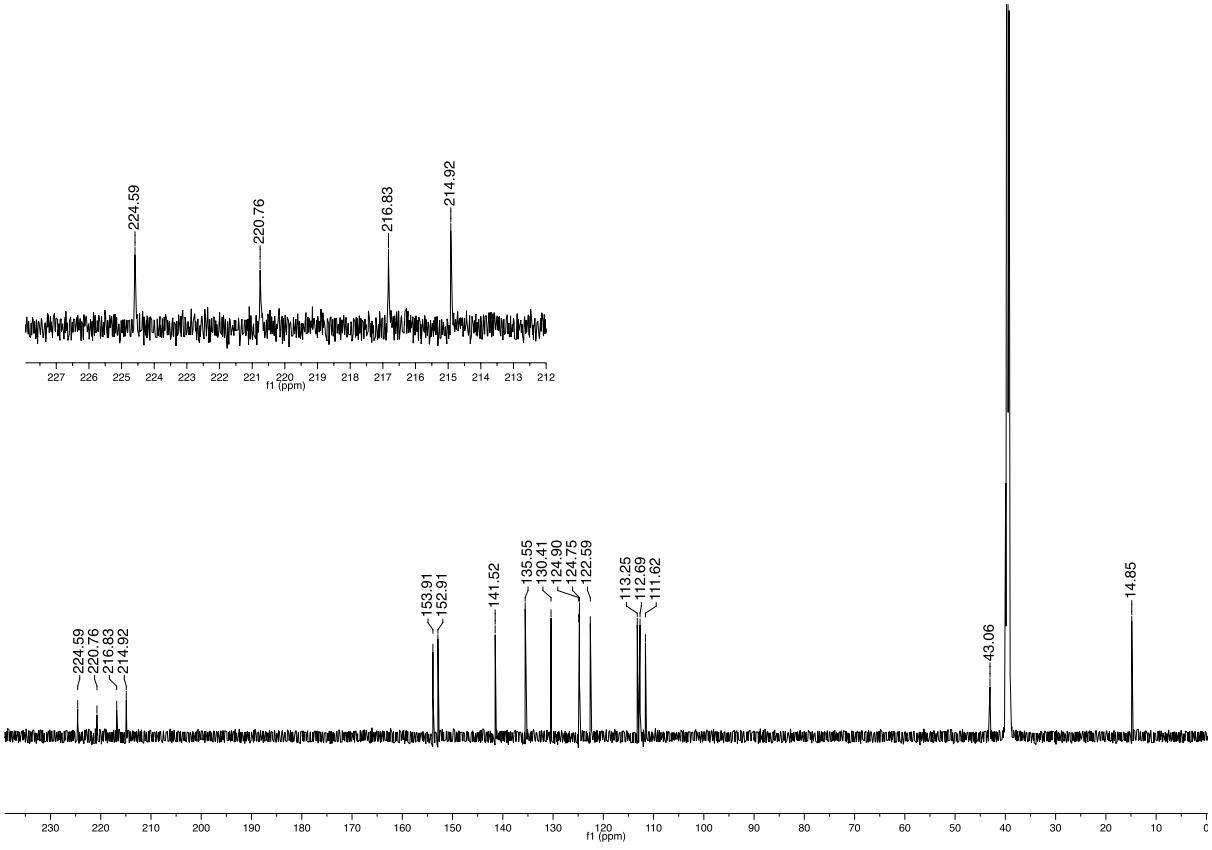

Note: The peak at 39.52 ppm is assigned to dimethyl sulfoxide.

S2.1.31 FTIR of [MnBr(*N*-ethyl-*N*′-2-pyridylbenzimidazol-2-ylidine)$(CO)_3$] (2.3)

Method: ATR

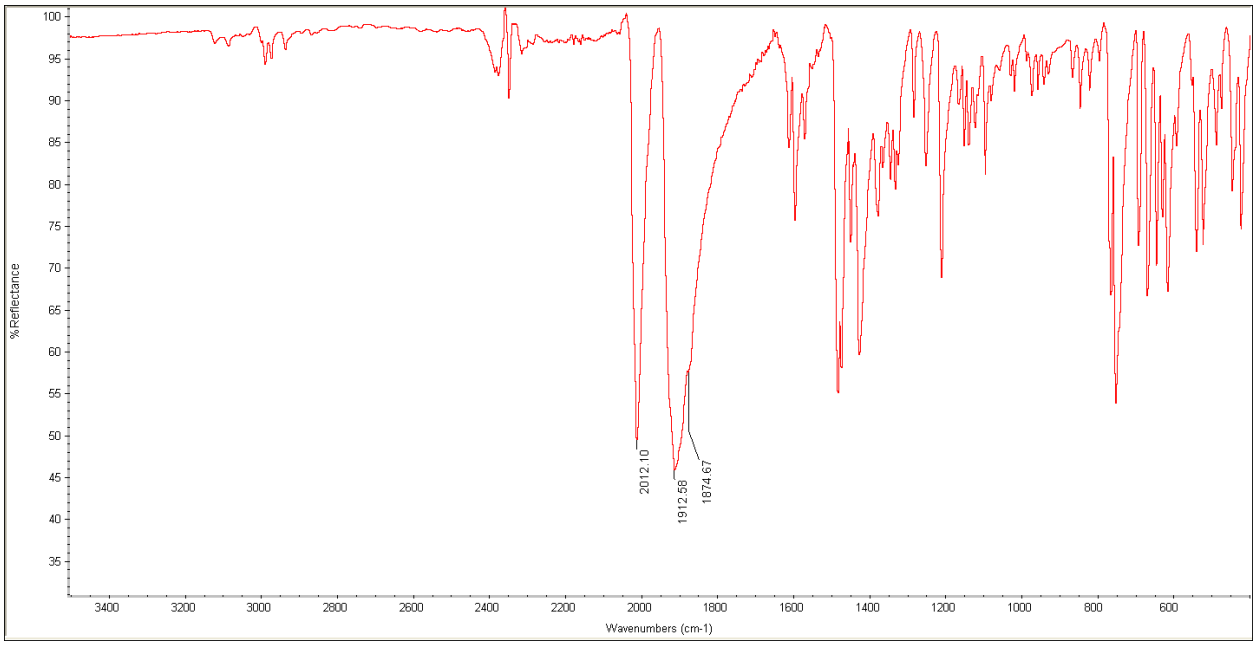

S2.1.32 UV-Vis of [MnBr(*N*-ethyl-*N*′-2-pyridylbenzimidazol-2-ylidine)$(CO)_3$] (2.3)

Temperature: 298K
Concentration: 125µM
Solvent: MeCN

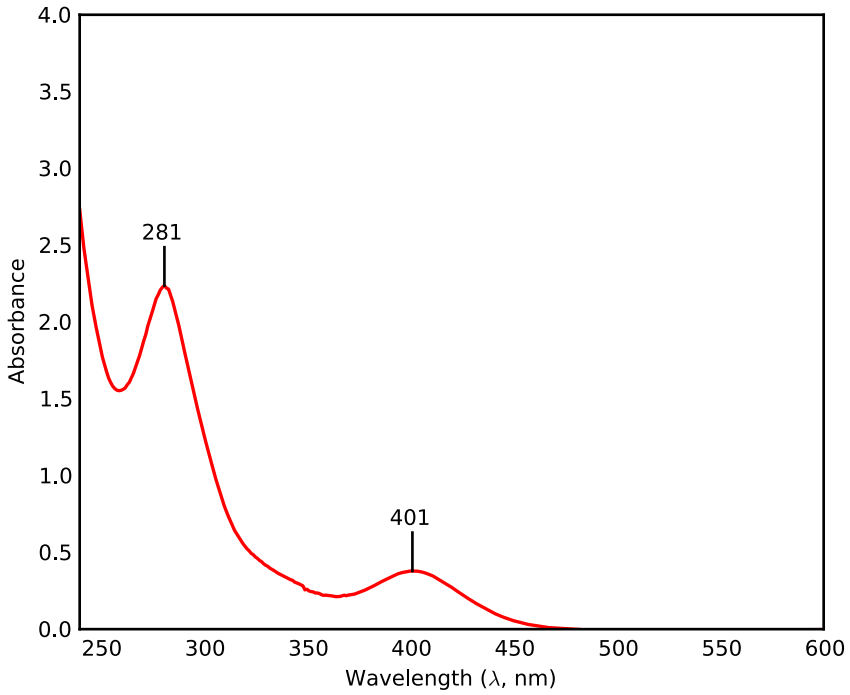

S2.1.33 ^{1}H NMR of [MnCN(*N*-ethyl-*N*′-2-pyridylbenzimidazol-2-ylidine)$(CO)_3$] (2.5)

Temperature: 20 ˚C
Solvent: DMSO-d_6

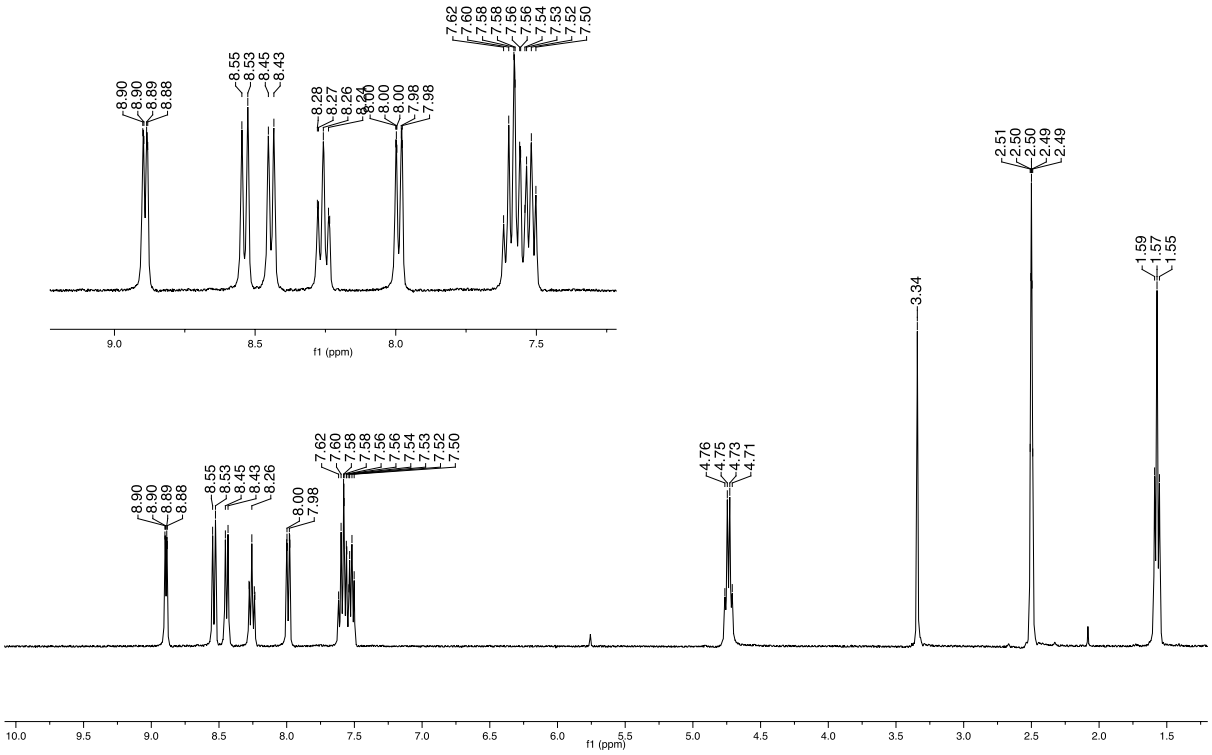

Note: The peak at roughly 5.7 ppm is assigned to residual dichloromethane, the peak at 3.34 ppm to water, the peak at 2.50 ppm to dimethyl sulfoxide, and the peak at roughly 2.1 ppm to acetone.

S2.1.34 ^{13}C NMR of [MnCN(*N*-ethyl-*N*′-2-pyridylbenzimidazol-2-ylidine)$(CO)_3$] (2.5)

Temperature: 25 ˚C
Solvent: DMSO-d_6

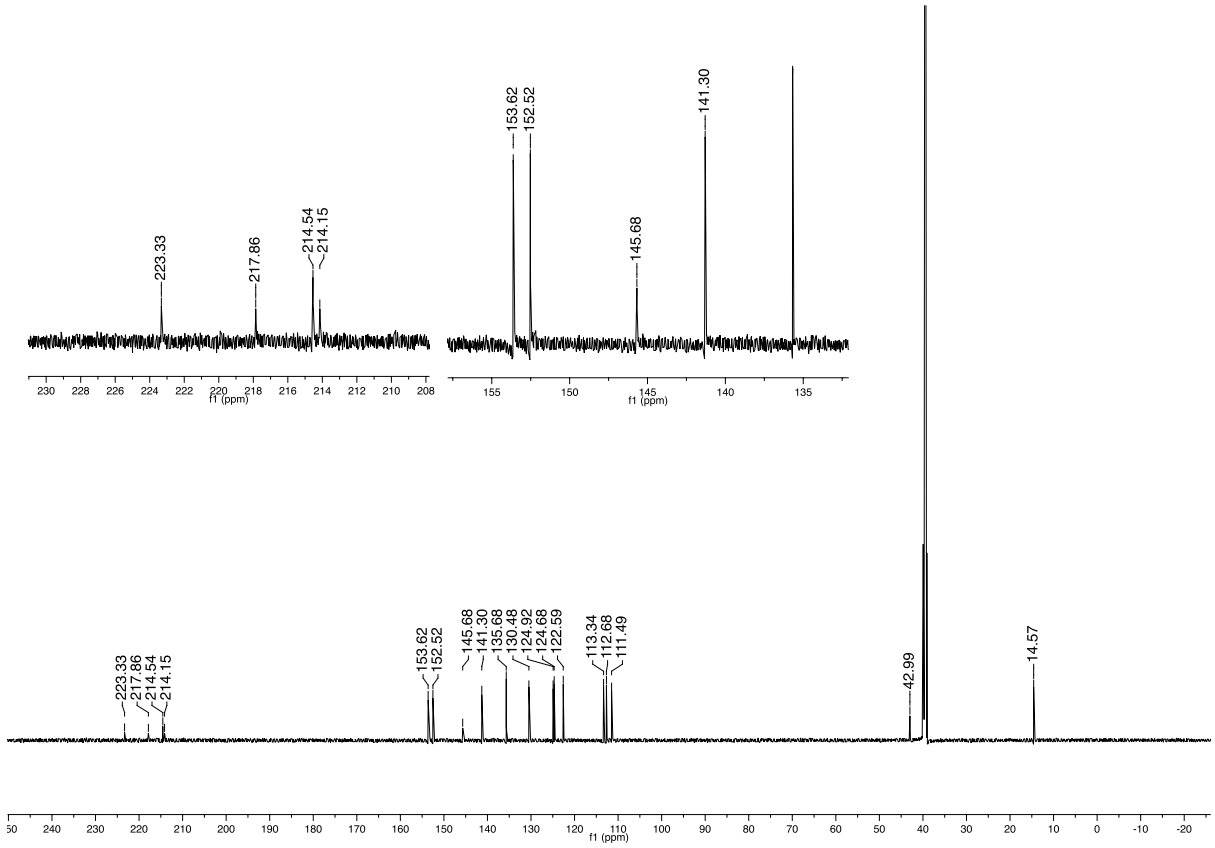

Note: The peak at 39.52 ppm is assigned to dimethyl sulfoxide.

S2.1.35 FTIR of [MnCN(*N*-ethyl-*N*′-2-pyridylbenzimidazol-2-ylidine)$(CO)_3$] (2.5)

Method: ATR

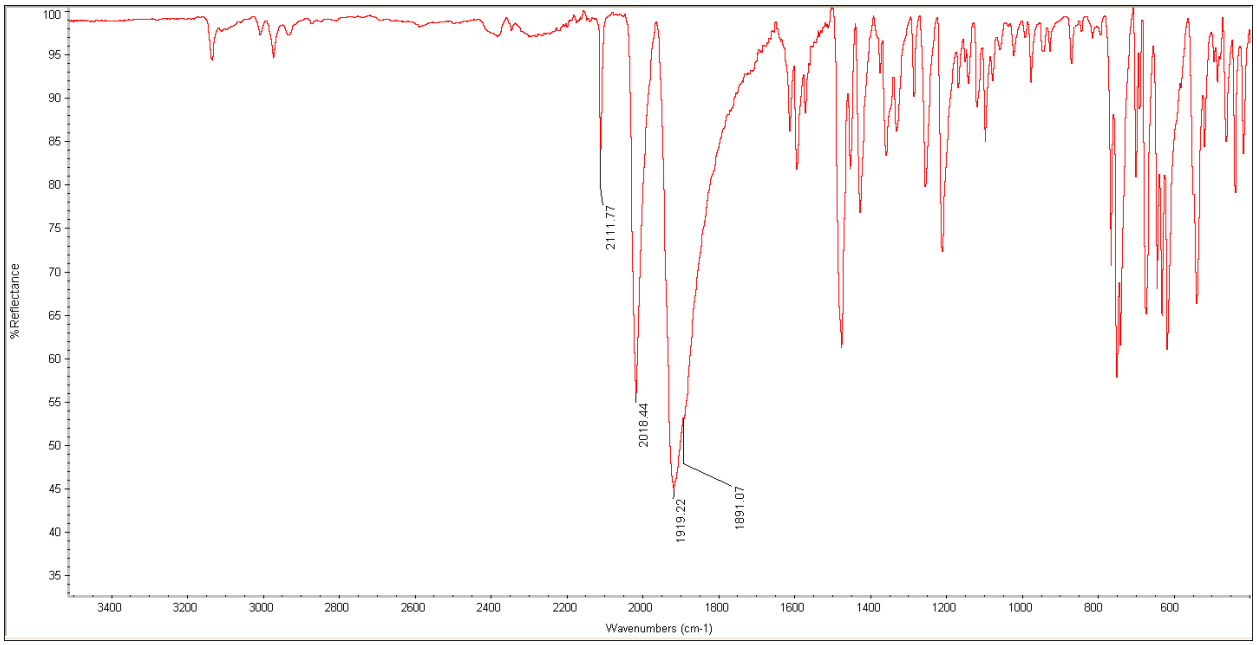

S2.1.36 UV-Vis of [MnCN(*N*-ethyl-*N*′-2-pyridylbenzimidazol-2-ylidine)$(CO)_3$] (2.5)

Temperature: 298K
Concentration: 125µM
Solvent: MeCN

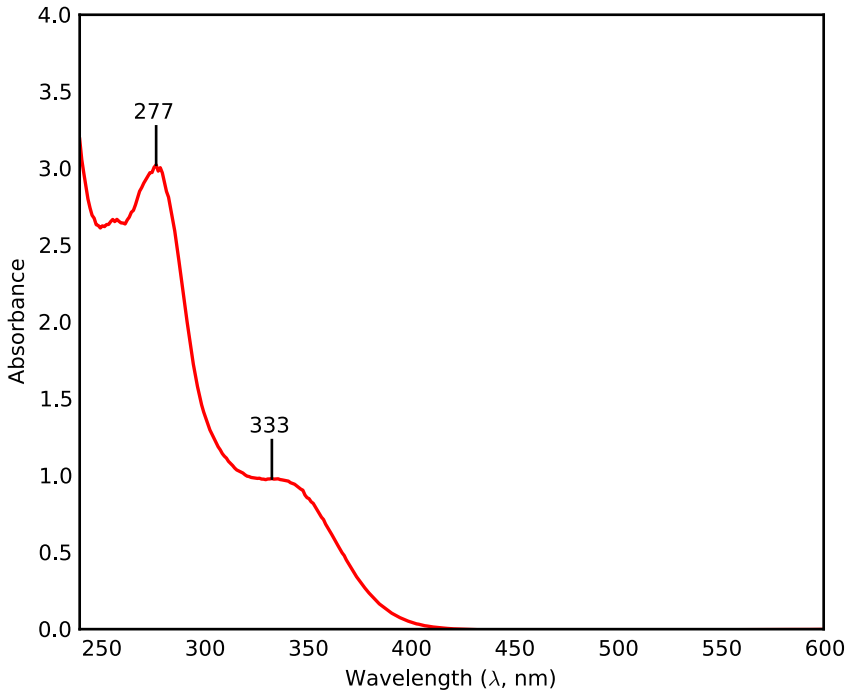

S2.1.37 ^{1}H NMR of [Mn(*N*-ethyl-*N*′-2-pyridylimidazol-2-ylidine)$(CO)_3$MeCN](PF_6) (2.8)

Temperature: 20 ˚C
Solvent: MeCN-d_3

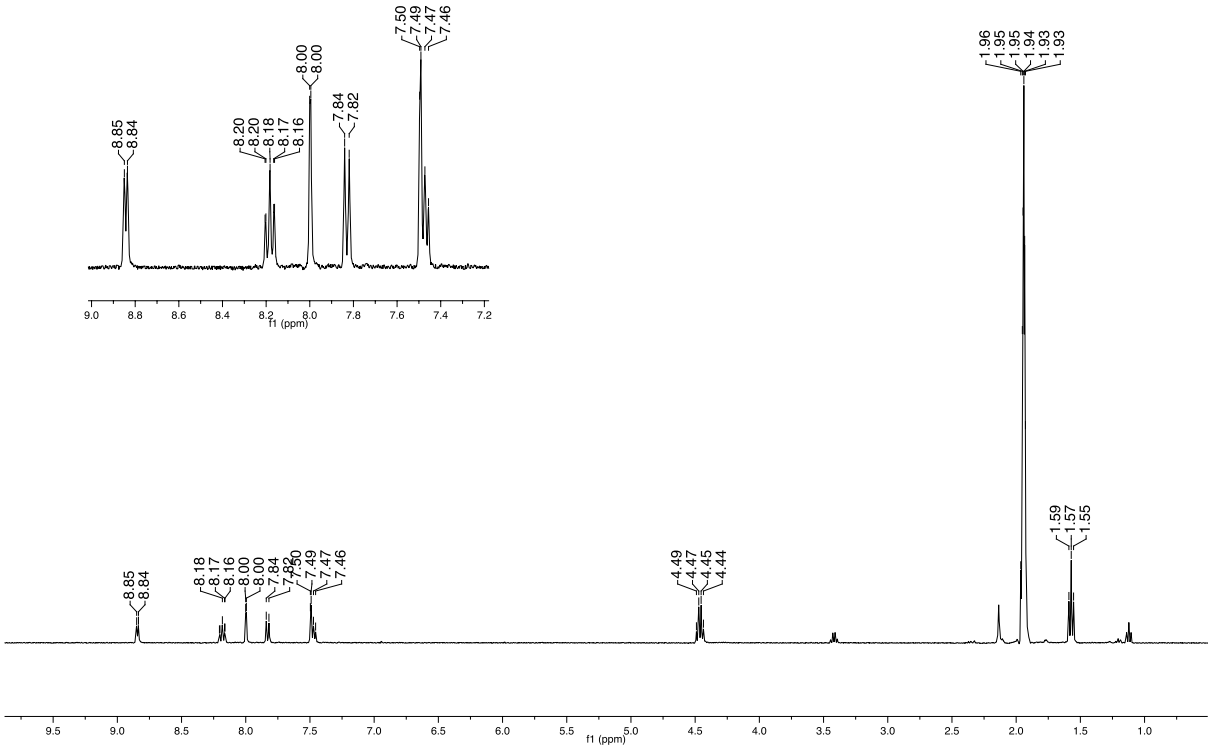

S2.1.38 FTIR of [Mn(*N*-ethyl-*N*′-2-pyridylimidazol-2-ylidine)$(CO)_3$MeCN](PF_6) (2.8)

Method: ATR

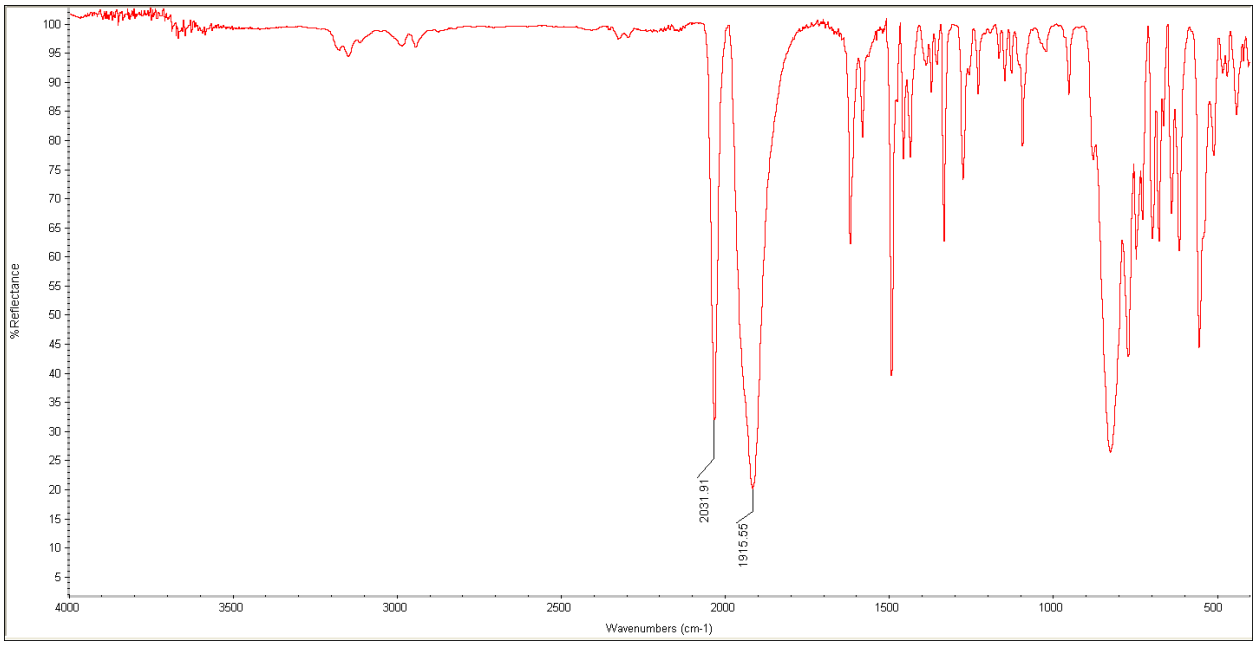

S2.1.39 UV-Vis of [Mn(*N*-ethyl-*N*′-2-pyridylimidazol-2-ylidine)$(CO)_3$MeCN](PF_6) (2.8)

Temperature: 298K
Concentration: 200µM
Solvent: MeCN

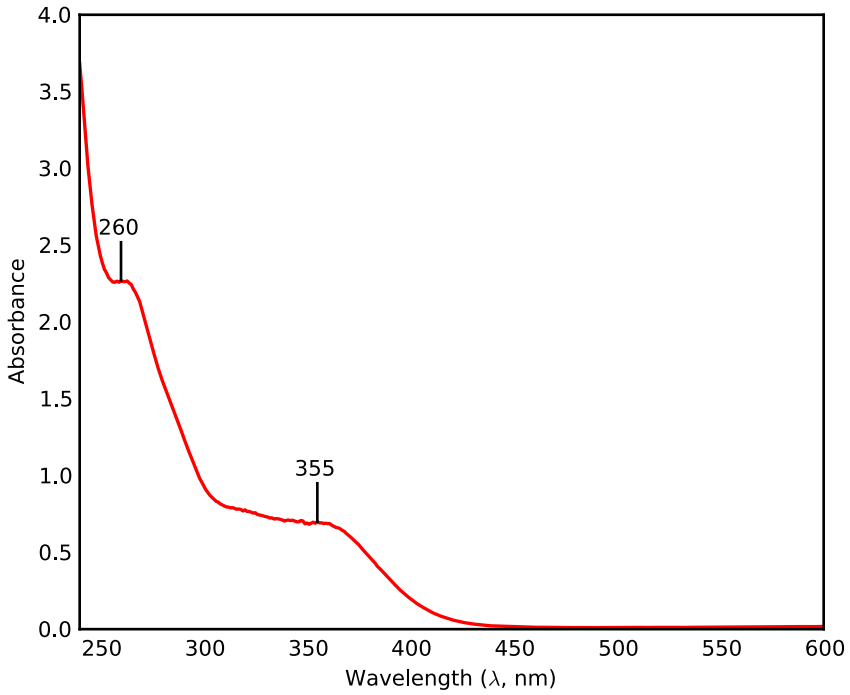

S2.1.40 Cyclic voltammetry of (2.4)

Atmosphere: Argon
Catalyst Concentration: 1 mM
Solvent: CH_3CN
Electrolyte: 0.1 M TBAP

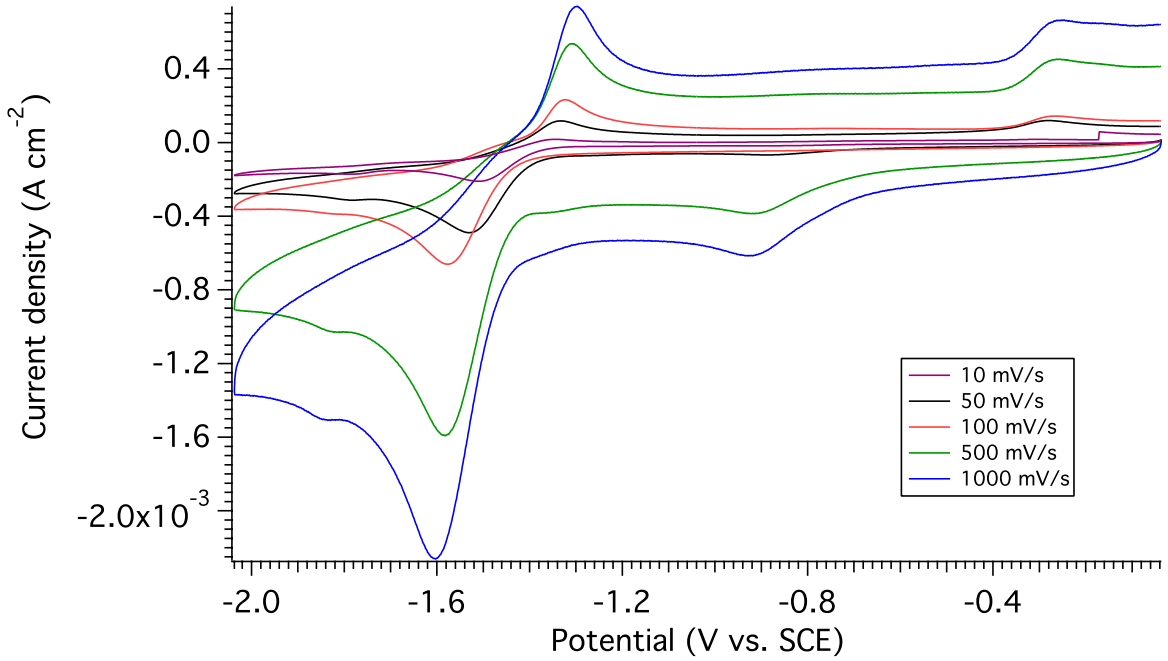

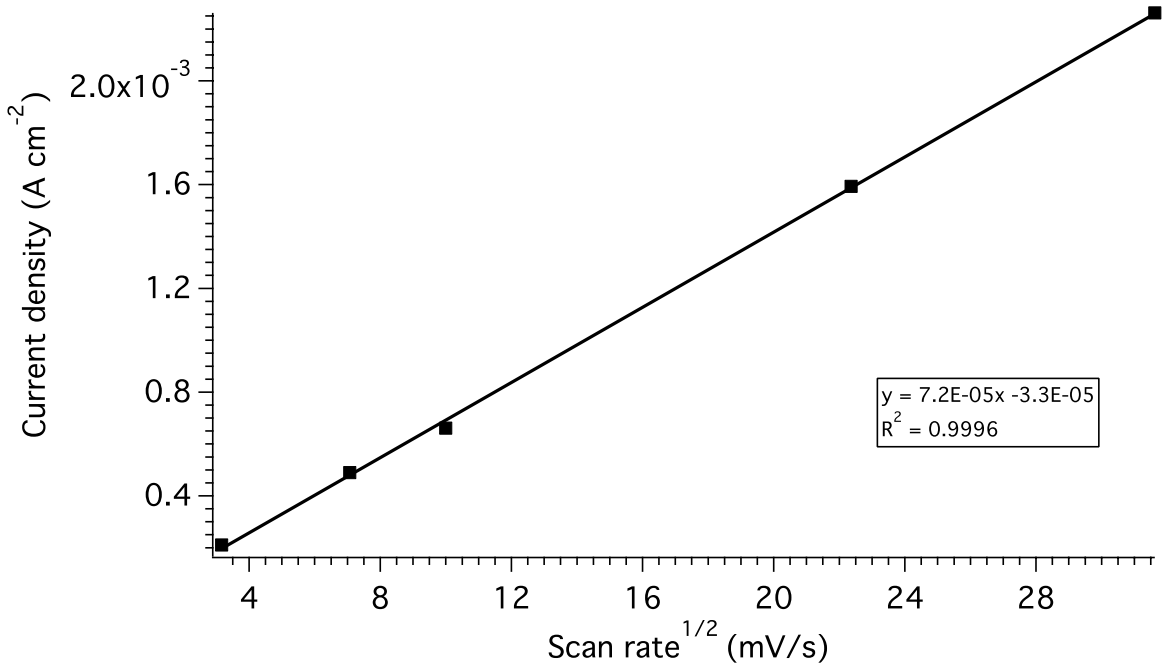

Atmosphere: Argon (black), CO_2 (red)
Catalyst Concentration: 1 mM
Solvent: CH_3CN (5 % H_2O)
Electrolyte: 0.1 M TBAP
Scanrate: 100 mV/s

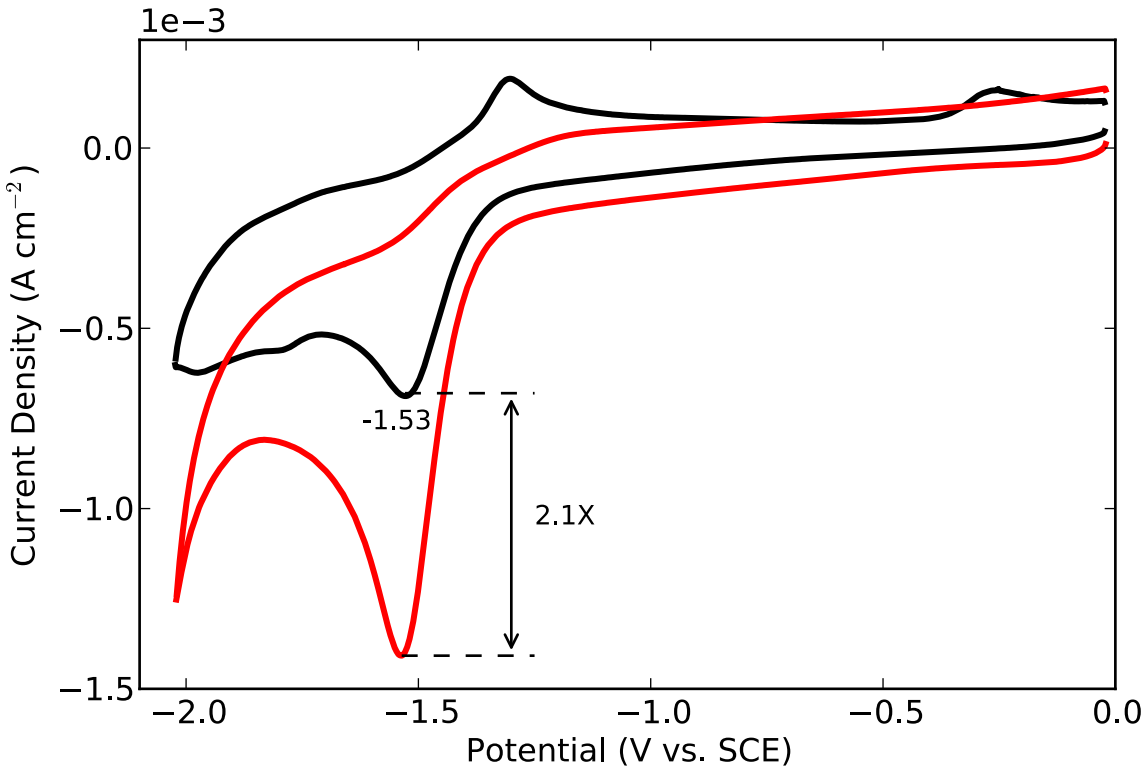

S2.1.41 Cyclic voltammetry of (2.6)

Atmosphere: Argon
Catalyst Concentration: 1 mM
Solvent: CH_3CN
Electrolyte: 0.1 M TBAP

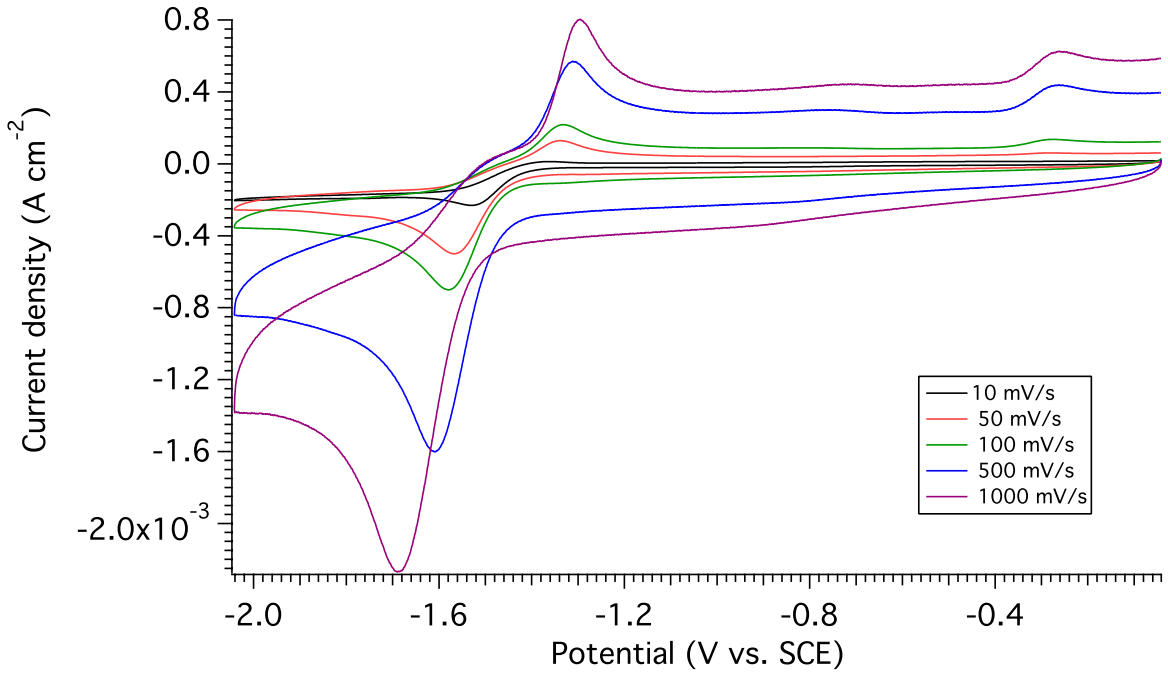

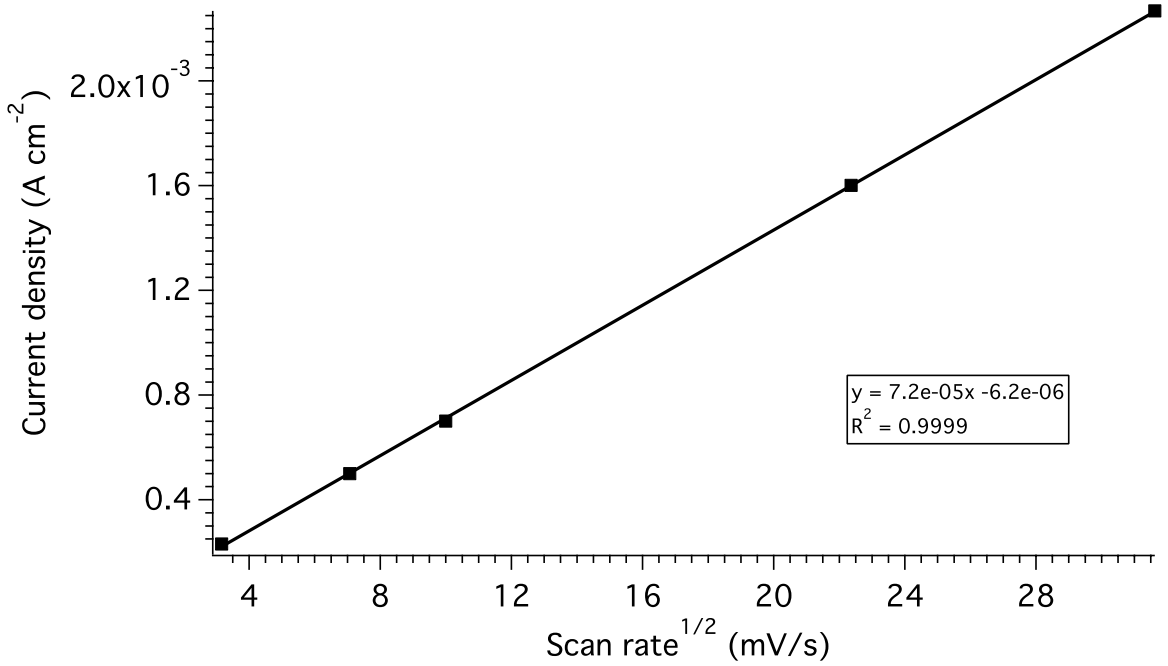

Atmosphere: Argon (black), CO_2 (red)
Catalyst Concentration: 1 mM
Solvent: CH_3CN (5 % H_2O)
Electrolyte: 0.1 M TBAP
Scanrate: 100 mV/s

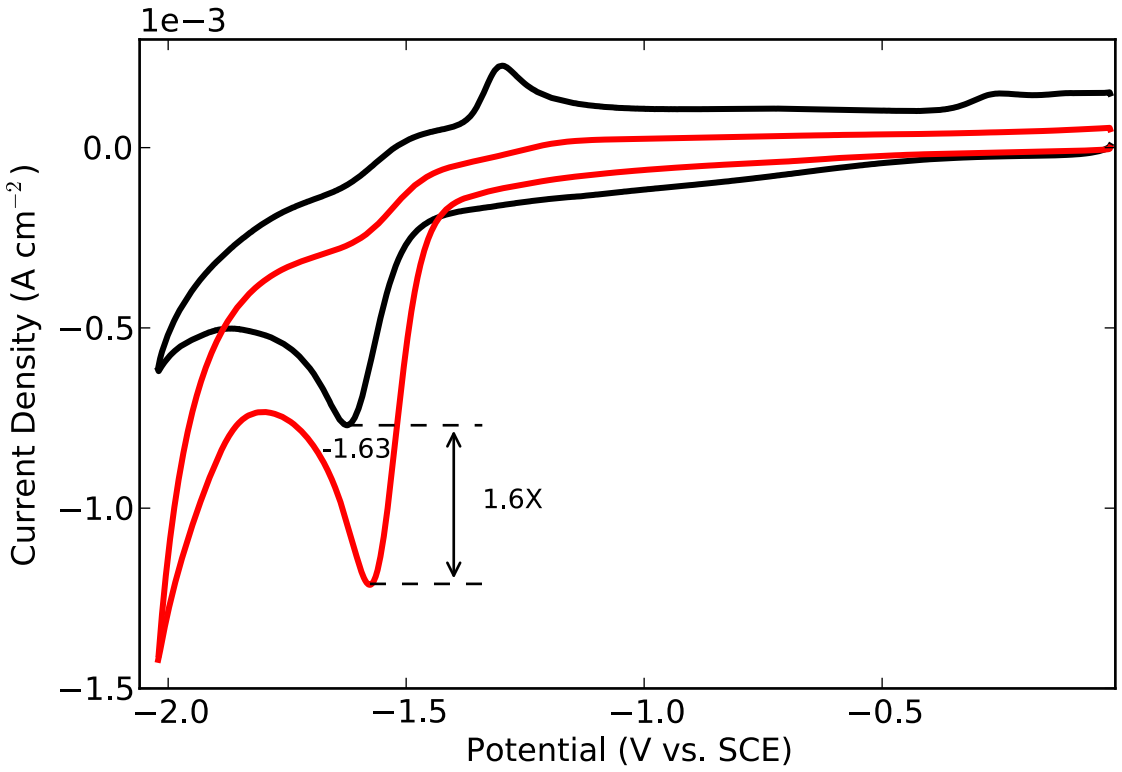

S2.1.42 Cyclic voltammetry of (2.7)

Atmosphere: Argon
Catalyst Concentration: 1 mM
Solvent: CH_3CN
Electrolyte: 0.1 M TBAP

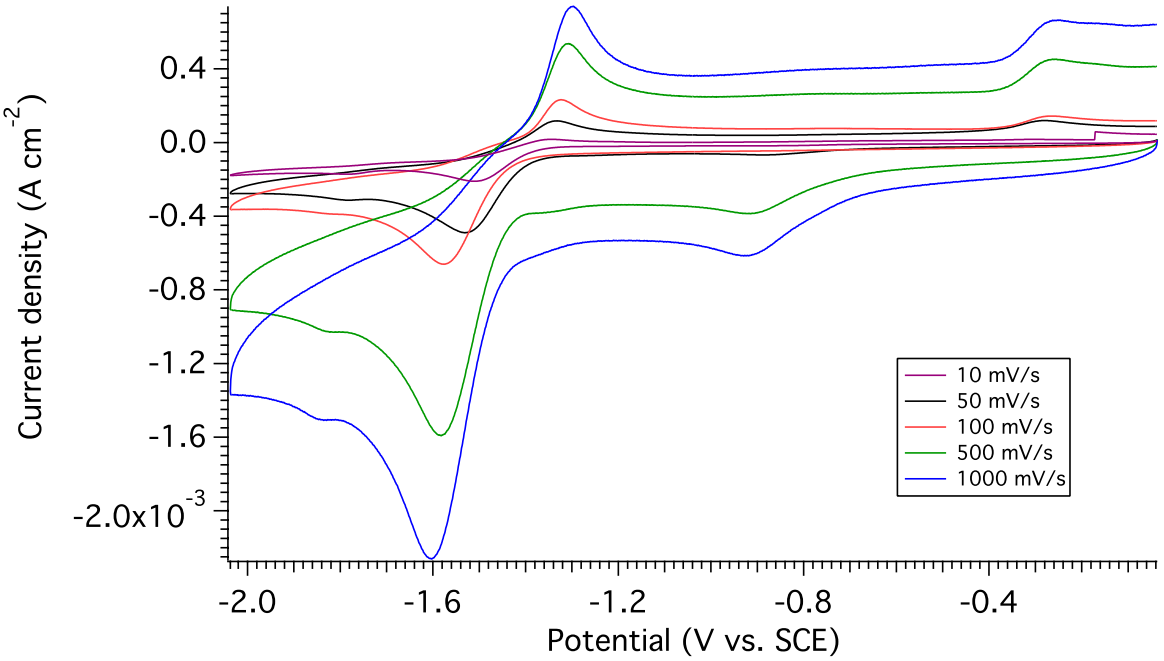

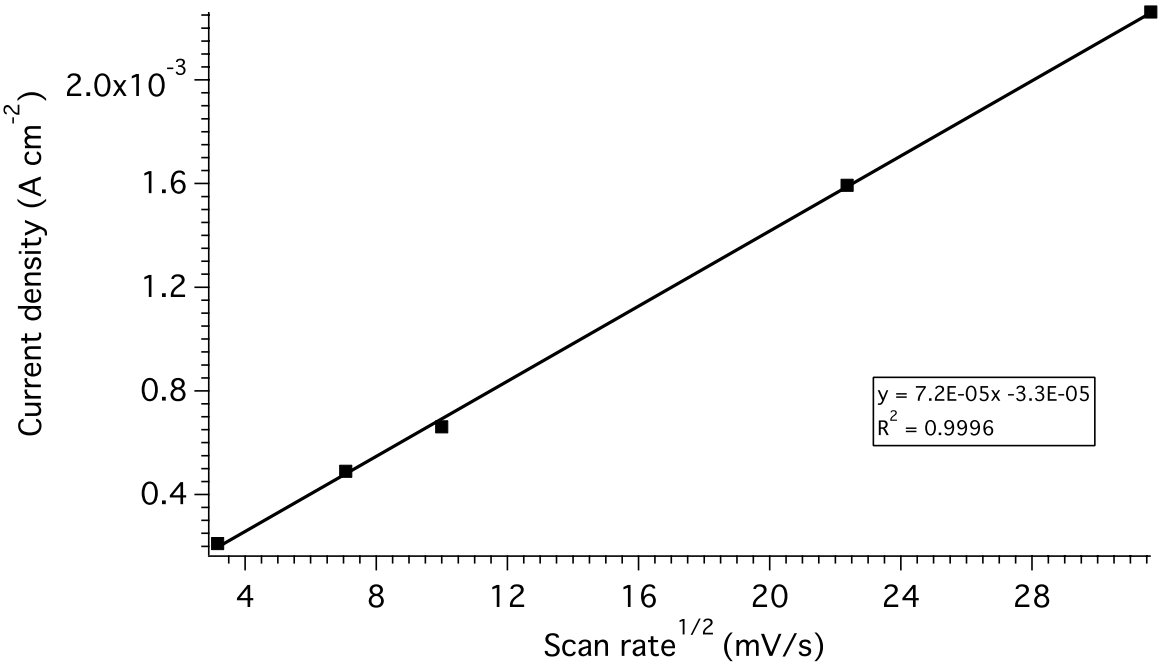

Atmosphere: Argon (black), CO_2 (red)
Catalyst Concentration: 1 mM
Solvent: CH_3CN (5 % H_2O)
Electrolyte: 0.1 M TBAP
Scanrate: 100 mV/s

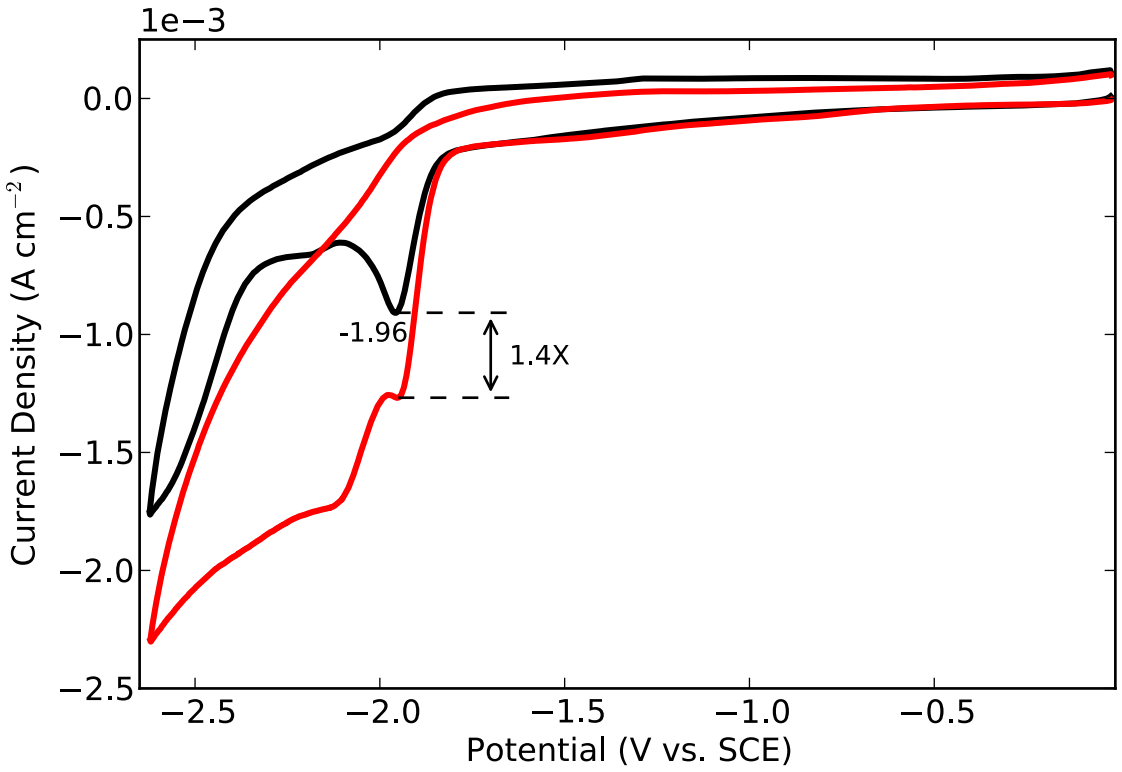

S2.1.43 Cyclic voltammetry of (2.5)

Atmosphere: Argon
Catalyst Concentration: 1 mM
Solvent: CH_3CN
Electrolyte: 0.1 M TBAP

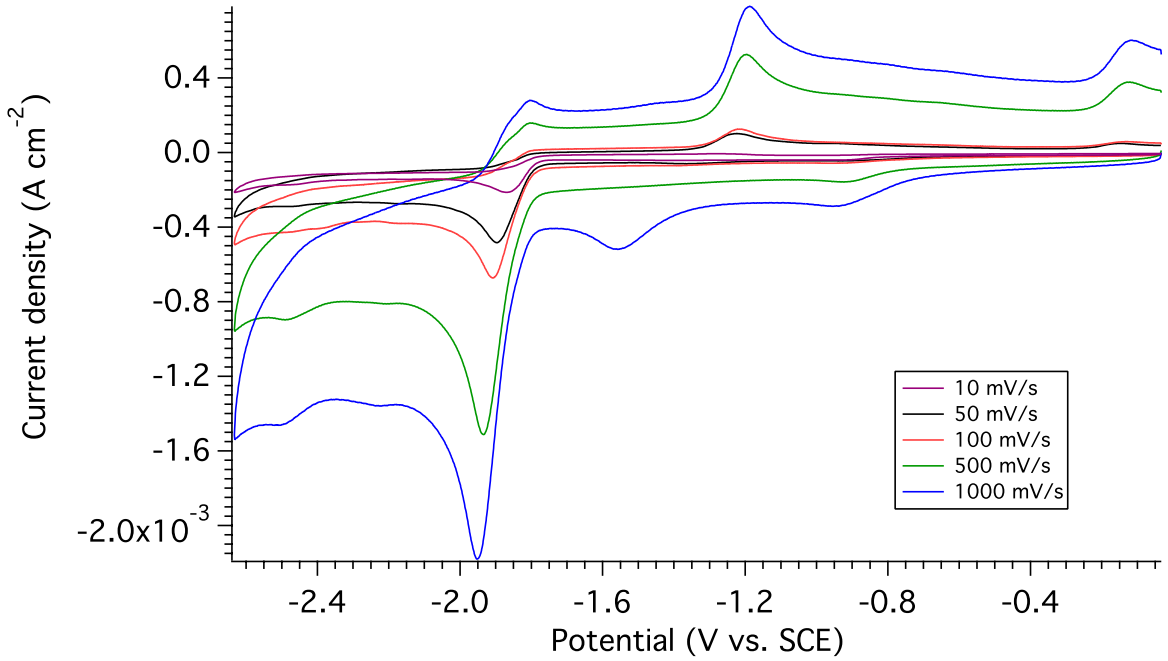

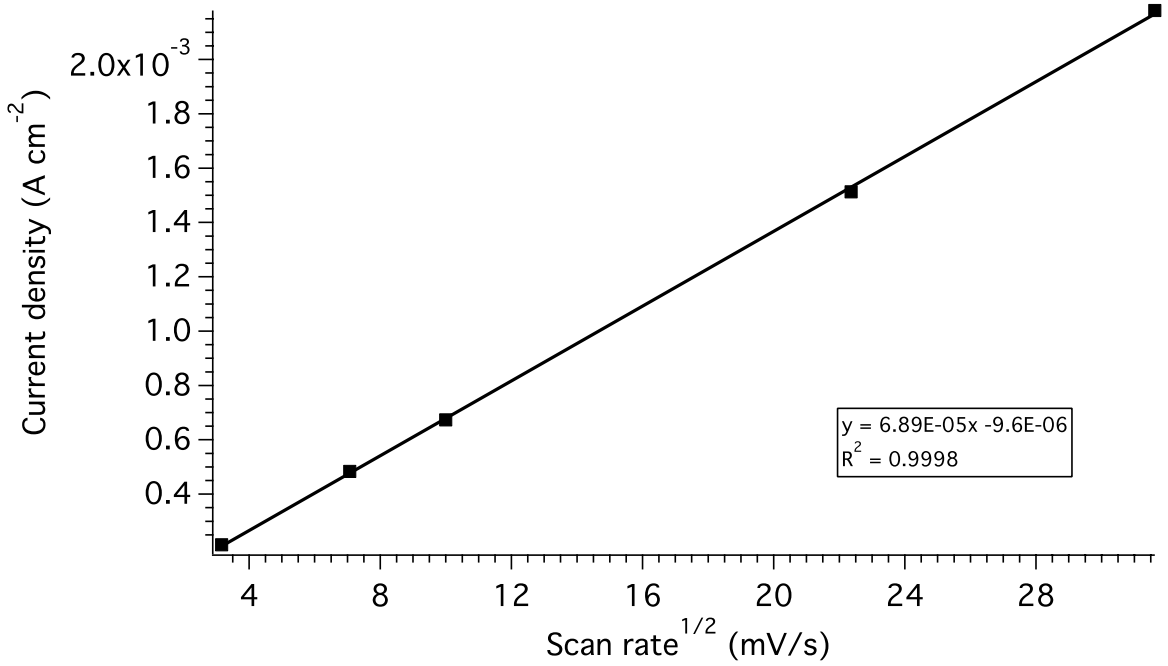

Atmosphere: Argon (black), CO_2 (red)
Catalyst Concentration: 1 mM
Solvent: CH_3CN (5 % H_2O)
Electrolyte: 0.1 M TBAP
Scanrate: 100 mV/s

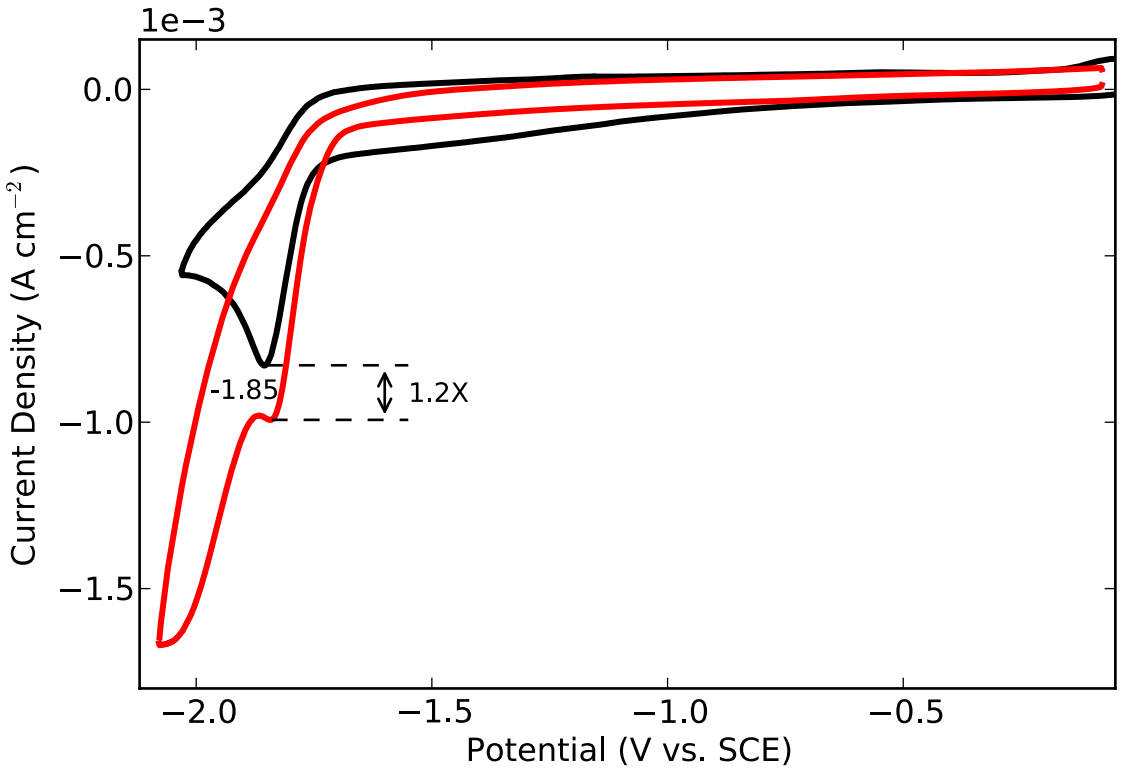

CHAPTER 3

Re(I) NHC COMPLEXES FOR ELECTROCATALYTIC CONVERSION OF CO_2[1]

[1] Stanton III, C. J.; Machan, C. W.; Vandezande, J. E.; Jin, T.; Majetich, G. F.; Schaefer III, H. F.; Kubiak, C. P.; Li, G.; Agarwal, J., Re(I) NHC Complexes for Electrocatalytic Conversion of CO_2. *Inorganic Chemistry* **2016**, *55* (6), 3136-3144.

ABSTRACT

The modular construction of ligands around an *N*-heterocyclic carbene building block represents a flexible synthetic strategy for tuning the electronic properties of metal complexes. Herein, methylbenzimidazolium-pyridine and methylbenzimidazolium-pyrimidine proligands are constructed in high yield using recently established transition-metal-free techniques. Subsequent chelation to $ReCl(CO)_5$ furnishes ReCl(*N*-methyl-*N*′-2-pyridylbenzimidazol-2-ylidine)$(CO)_3$ and ReCl(*N*-methyl-*N*′-2-pyrimidylbenzimidazol-2-ylidine)$(CO)_3$. These Re(I) NHC complexes are shown to be capable of mediating the two-electron conversion of CO_2 following one-electron reduction; the Faradaic efficiency for CO formation is observed to be >60% with minor H_2 and HCO_2H production. Data from cyclic voltammetry is presented and compared to well-studied ReCl(2,2′-bipyridine)$(CO)_3$ and MnBr(2,2′-bipyridine)$(CO)_3$ systems. Results from density functional theory computations, infrared spectroelectrochemistry, and chemical reductions are also discussed.

INTRODUCTION

Rhenium(I)–tricarbonyl complexes bearing ligands with an *N*-heterocyclic carbene (NHC) moiety were first reported in 1992.[1] Since then, tens of articles have appeared in the literature, with the majority published in the last five years, underscoring the rapid growth of this subfield.[2-25] Recent work has focused primarily on the photophysical properties of Re(I) NHC complexes, specifically on modifications of the NHC-containing ligand to modulate absorption and emission quantum yields.[26] These investigations parallel the well-studied functionalization of 2,2′-bipyridine (bpy) in ReCl(bpy)$(CO)_3$, research that dates back to the 1970s.[27, 28] By comparison, few studies have examined Re(I) NHC compounds for catalysis, as noted in a 2013 review by

Herrmann and Kühn.[29] In 2014, we investigated the first use of Mn(I) NHC complexes for the electrocatalytic reduction of CO_2 to CO.[30] The success of these compounds for mediating CO_2 conversion engenders questions regarding the efficacy and electrochemical response of valence-isoelectronic Re(I) species, especially given the well-established application of $ReCl(bpy)(CO)_3$ for both the electrocatalytic[31-36] and the photocatalytic reduction of CO_2.[37-43] Indeed, Delcamp and co-workers very recently reported successful photocatalytic CO_2 conversion using Re–pyridyl–NHC complexes.[25]

In the present research, two Re(I) NHC compounds are examined: ReCl(*N*-methyl-*N*′-2-pyridylbenzimidazol-2-ylidine)$(CO)_3$ (**3.1**) and ReCl(*N*-methyl-*N*′-2-pyrimidylbenzimidazol-2-ylidine)$(CO)_3$ (**3.2**). In either case, the bidendate, redox-active ligand is constructed from an aryl halide (either halopyridine or halopyrimidine), benzimidazole, and a haloalkane. This modular synthesis permits myriad routes for customization, e.g., benzimidazole may be exchanged for imidazole or halopyrazine for halopyrimidine. Moreover, the requisite transformations are transition-metal free and proceed in high yield.[30, 44] These compelling qualities are in contrast to a majority of bpy syntheses.[45-48]

Further comparison with bpy highlights additional advantages for employing NHC-containing ligands: (i) they allow for the possibility of π-backbonding via the low-lying empty p orbital on the carbene carbon,[49, 50] which assists in stabilizing low-valent metals, and (ii) the atoms adjacent to the coordinating carbene can be substituted, such as with sulfur or oxygen using benzothiazole or benzoxazole.[49, 51, 52] Cyclic (alkyl)(amino)carbenes (CAACs), where a carbon atom is adjacent to the carbene carbon, may also be employed.[53, 54] Taken together, NHC-containing ligands provide an accommodating framework for steric and electronic tuning[55, 56] that

has already been exploited to modulate the photophysical properties of Re(I) NHC compounds and may permit the rational construction of CO_2 conversion catalysts.

Here we demonstrate that both **3.1** and **3.2** are capable of mediating the conversion of CO_2 to both CO and HCO_2H under an applied voltage. Cyclic voltammetry data is presented and the results compared to model compounds—$ReCl(bpy)(CO)_3$ and $MnBr(bpy)(CO)_3$ [57]—in order to understand the nature of the voltammetric responses. Results from density functional theory computations, infrared spectroelectrochemistry, and chemical reductions are also employed in this regard.

RESULTS AND DISCUSSION

SYNTHESIS

Compounds **3.1** and **3.2** were constructed from $ReCl(CO)_5$ and the appropriate proligand, namely, [*N*-methyl-*N*′-2-pyridylbenzimidazolium]$^+$ PF_6- (**L3.1**) or [*N*-methyl-*N*′-2-pyrimidylbenzimidazolium]$^+$ PF_6^- (**L3.2**); see Figure 3.1. To our knowledge **3.2** has not been reported, but Chan *et al.*,[22] Li *et al.*,[16] and Casson *et al.* (butyl variant)[14] prepared **1** for photophysical examination. The former two groups utilized silver oxide to deprotonate the proligand and form the requisite carbene, reporting yields of 61%[22] and 23%,[16] respectively. Alternatively, Casson *et al.* utilized potassium carbonate in refluxing toluene to achieve an 87% yield for the chelation step,[14] and we observed an 89% yield using the same procedure. A lower yield was seen for **2** (43%).

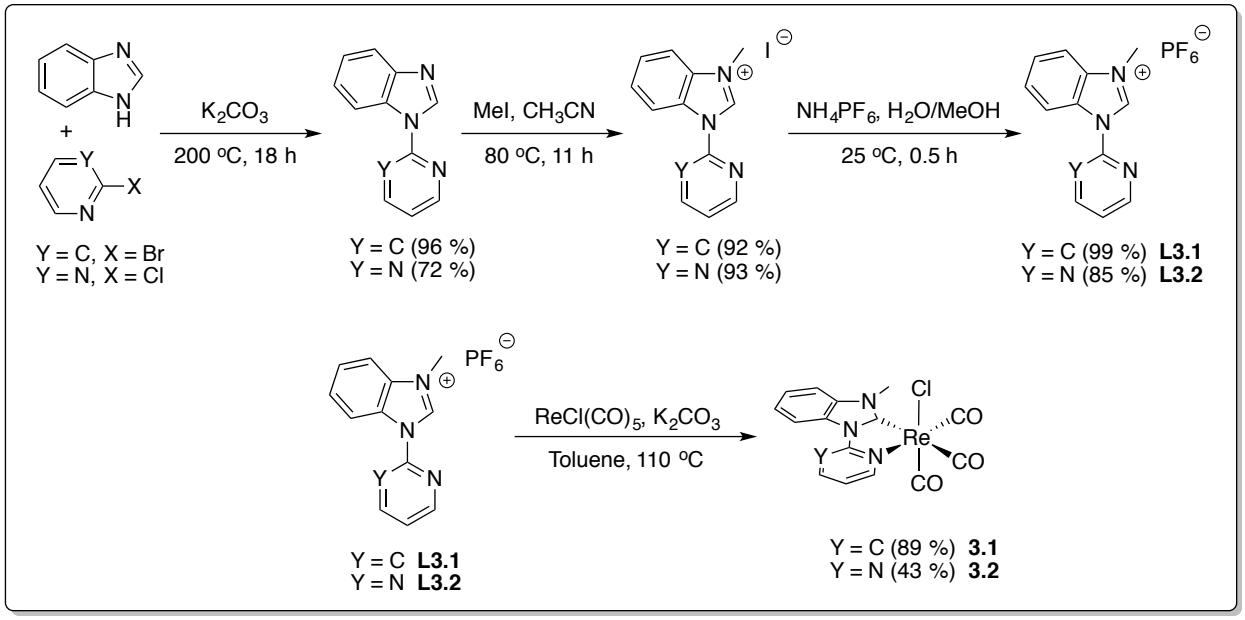

Scheme 3.1: Synthetic scheme for [*N*-methyl-*N*′-2-pyridylbenzimidazolium]$^{+}PF_6^{-}$ (**L3.1**, Y = C–H) and [*N*-methyl-*N*′-2-pyrimidylbenzimidazolium]$^{+}PF_6^{-}$ (**L3.2**, Y = N) with metalation procedure.

In two of the three reports listed above, **L3.1** was synthesized via Ullman-type coupling using copper,[58-60] while Casson *et al.* utilized a transition-metal-free transformation with refluxing DMSO and potassium hydroxide.[61, 62] Aligned with our previous work,[30, 63] the synthesis of **L3.1** and **L2** involved the transition-metal-free and solvent-free procedure reported by Hermann and Kühn,[44] which is "green" and amenable to scale-up.

Complexes **3.1** and **3.2** were characterized with ^{1}H NMR, ^{13}C ^{1}H NMR, UV–vis, and FTIR spectroscopies (see S3.SI, pp 151-156). Single crystals suitable for X-ray analysis were grown from the vapor diffusion of hexanes into a solution of **3.1** or **3.2** dissolved in DCM. The resolved X-ray structures (Figure 3.1) indicate that the NHC-aryl ligands coordinate to the Re(I) center within the equatorial plane via imine-type N atoms and carbene-type C atoms, with bite angles of 74.0° and 74.5° for **3.2** and **3.2**, respectively. In each structure, the three carbonyl ligands exist in a *facial* arrangement, as expected.

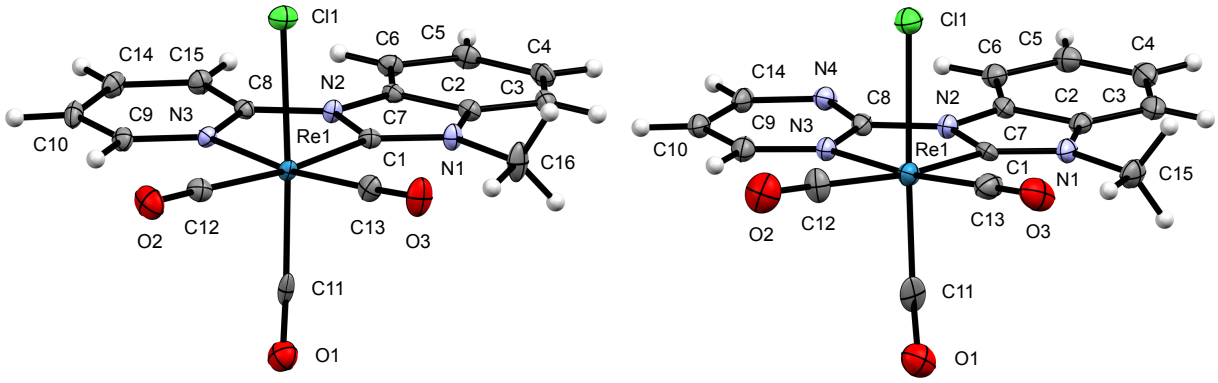

Figure 3.1: X-ray crystal structures of ReCl(*N*-methyl-*N*′-2-pyridylbenzimidazol-2-ylidine)$(CO)_3$ (**3.1**, left) and ReCl(*N*-methyl-*N*′-2-pyrimidylbenzimidazol-2-ylidine)$(CO)_3$ (**3.2**, right) with ellipsoids set at the 50% probability level.

The absorbance spectra for **3.1** and **3.2** (see Figure 3.2) include two predominant transitions: a $\pi \rightarrow \pi^*$ band below 300 nm and a lower energy band at 350 nm that was previously assigned as an admixture of metal-to-ligand charge transfer (MLCT) and ligand-to-ligand charge transfer (LLCT) excitations.[14, 19] Extinction coefficients for the MLCT/LLCT band were measured to be 5430 and 6390 L mol^{-1} cm^{-1} for **3.1** and **3.2**, respectively. Emission spectra maxima (Figure 3.2, inset) for **3.1** and **3.2** differ by 55 nm (λ_{max} = 505 and 560 nm, respectively). The red-shifted emission for **3.2** is consistent with the relative electron deficiency of the pyrimidyl unit.[18, 64-66]

Using density functional theory (see Theoretical Methods), we find that the LUMO energy of **3.2** is 6.8 kcal mol^{-1} lower than **3.1**. This energy decrease is aligned with chemical intuition regarding the electronegativity of the substituted nitrogen and may partially explain the red-shifted emission. It also suggests that the reduction potentials for **3.2** will occur at more positive potentials than **3.1**.[63] Löwdin population analyses indicate that for both **3.1** and **3.2** the HOMOs are comprised of the Re *d* orbitals (~40%), with contributions from the Cl *p* orbitals

(~14%) and orbitals localized on the carbonyl ligands (~28%). Conversely, the LUMOs are largely centered on the redox-active, NHC-aryl ligand (>80%).

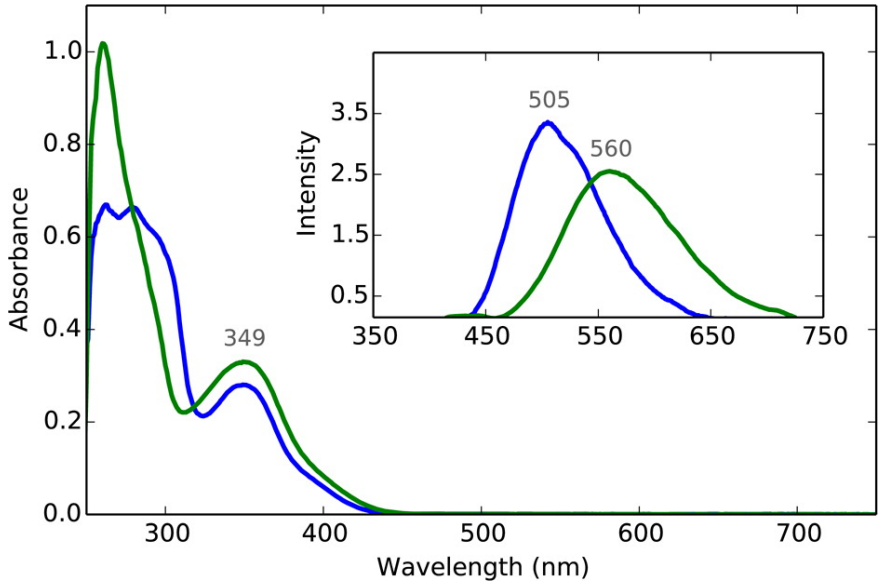

Figure 3.2: UV–vis absorption and emission (inset) spectra of **3.1** (blue) and **3.2** (green) recorded at 50 μM in CH_3CN

ELECTROCHEMISTRY

Cyclic voltammetry results for **3.1** and **3.2** are presented in Figure 3.3.A and 3.3.B, respectively, along with data obtained for the reference compounds $ReCl(bpy)(CO)_3$ (Figure 3.3.C) and $MnBr(bpy)(CO)_3$ (Figure 3.3.D). All scans were recorded under argon saturation in dry acetonitrile with 0.1 M tetrabutylammonium perchlorate (TBAP) supporting electrolyte. Compounds were loaded at a concentration of 1 mM, and the scan rate was varied from 50 to 2000 mV $s^{-1,}$ indicated by color: 50 (red), 100 (orange), 250 (green), 500 (blue), 1000 (purple), and 2000 mV s^{-1} (gray). Each figure also includes an inset, recorded at 1000 mV s^{-1}, of the voltammetric response when the switching potential is set before the second reduction. A listing of the first and second reduction potentials for the aforementioned species is shown in Table 3.1.

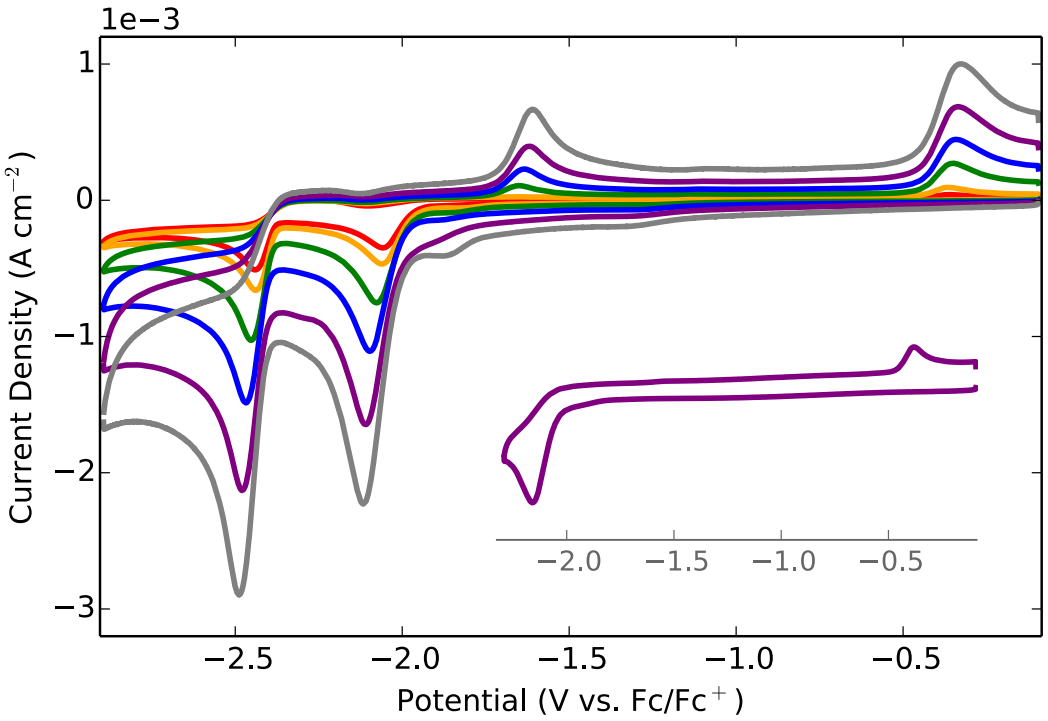

Figure 3.3.A: CV of (ReCl(*N*-methyl-*N*′-2-pyridylbenzimidazol-2-ylidine)$(CO)_3$ (**3.1**)

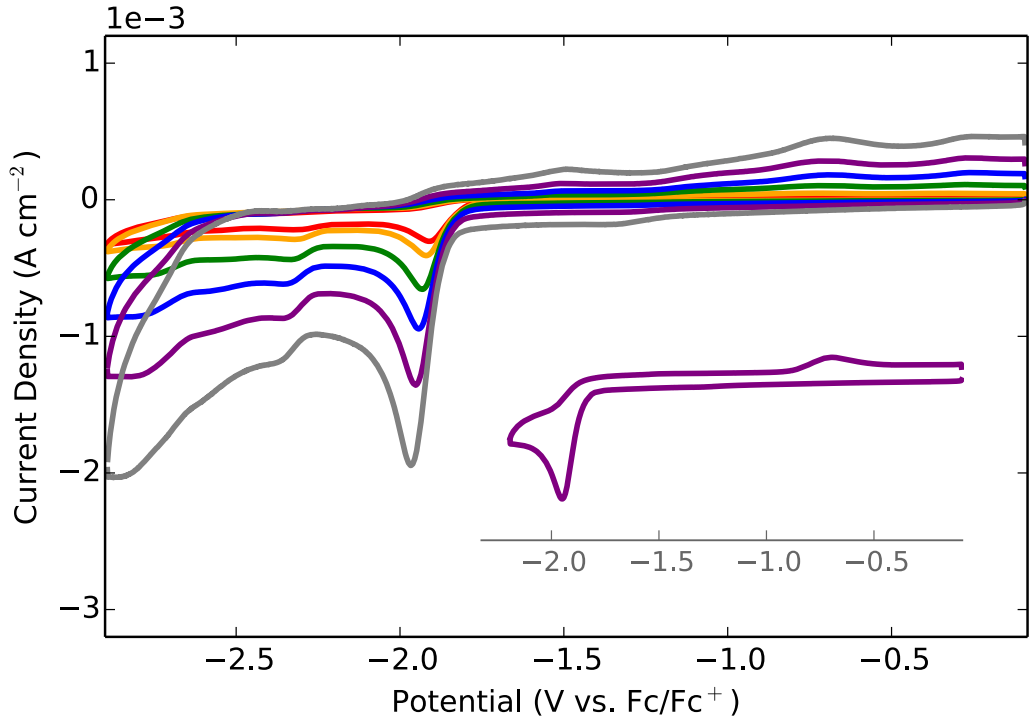

Figure 3.3.B: CV of ReCl(*N*-methyl-*N*′-2-pyrimidylbenzimidazol-2-ylidine)$(CO)_3$ (**3.2**)

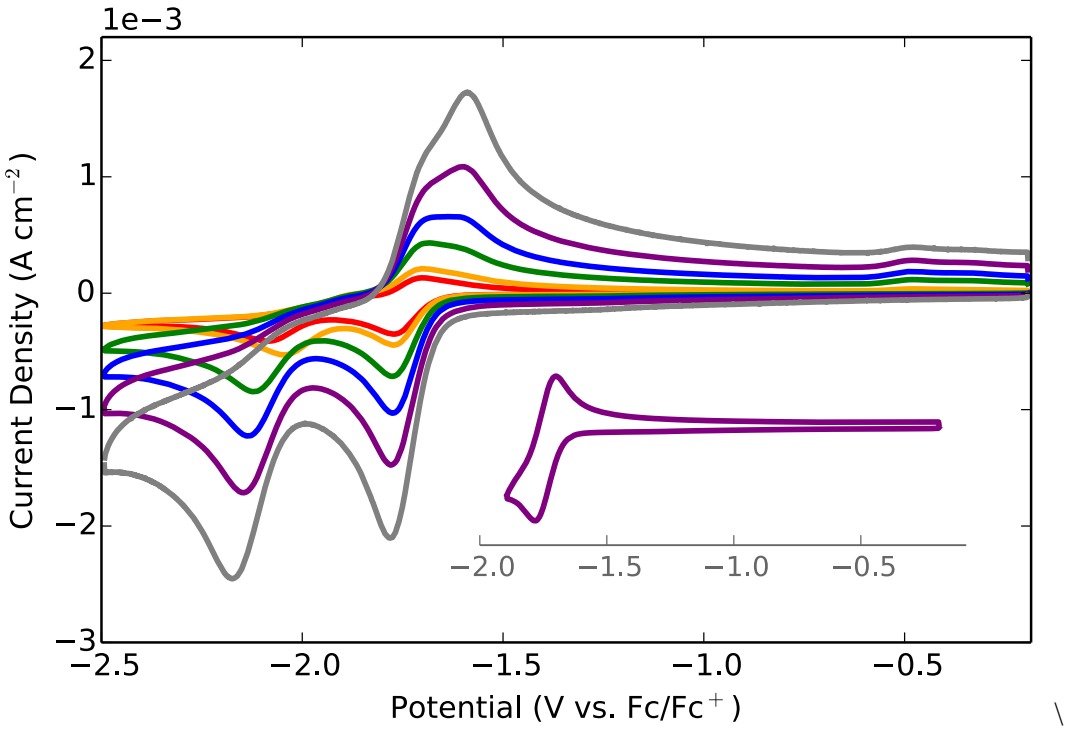

Figure 3.3.C: CV of $ReCl(bpy)(CO)_3$

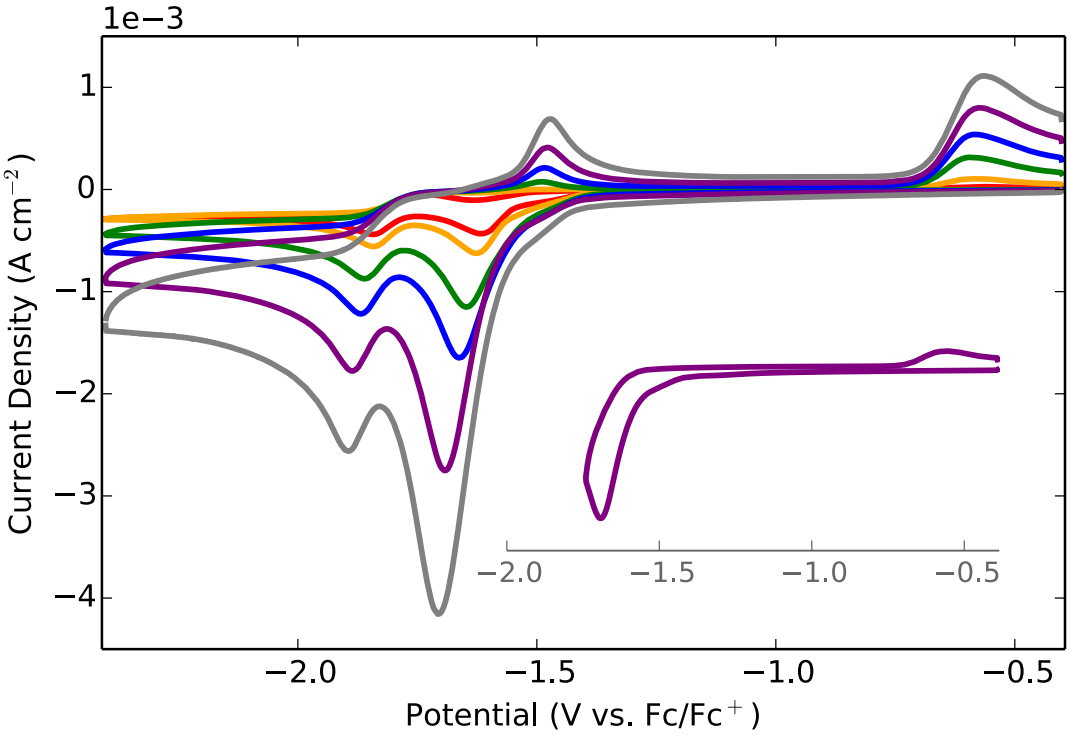

Figure 3.3.D: CV of $MnBr(bpy)(CO)_3$

Table 3.1: Comparison of First and Second Potentials (vs Fc/Fc^+) Measured in This Work[a]

Complex	First Reduction	Second Reduction
3.1	−2.06	−2.44
3.2	−1.92	−2.32
$ReCl(bpy)(CO)_3$	−1.77	−2.04
$MnBr(bpy)(CO)_3$	−1.63	−1.84

[a]Recorded under Ar at 100 mV s^{-1} in dry MeCN with 0.1 M tetrabutylammonium perchlorate (TBAP) supporting electrolyte
[b]2,2′-bipyridine
[c]Original Reports

For the parent compound, $ReCl(bpy)(CO)_3$ (Figure 3.3.C), sweeping to negative potentials at 100 mV s^{-1} yields two one-electron-reduction waves with peak currents at −1.77 and −2.04 V vs Fc/Fc^+. The first reduction is ligand based,[31, 33, 67] with the added electron residing on bpy, furnishing $[ReCl(bpy)(CO)_3]^{\bullet-}$. This process is quasireversible; the corresponding oxidation appears at −1.70 V vs Fc/Fc^+. Adding an additional electron leads to dissociation of the axial chloride to give $[Re(bpy)(CO)_3]^-$.[33] At faster scan rates, two additional waves appear on the return scan: a prominent feature at ca. −1.6 V vs Fc/Fc^+ and a slight feature at ca. −0.5 V vs Fc/Fc^+. The inset scan indicates that neither of these two waves are present when the switching potential is set before the second reduction, indicating that they are related to the formation of $[Re(bpy)(CO)_3]^-$. Indeed, the process at ca. −1.6 V vs Fc/Fc^+ may be ascribed to one-electron oxidation of $[Re(bpy)(CO)_3]^-$ to the neutral radical, $[Re(bpy)(CO)_3]^{\bullet}$. A minimal quantity of the neutral radical undergoes dimerization to form $[Re(bpy)(CO)_3]_2$;[68, 69] the slight feature at ca. −0.5 V vs Fc/Fc^+ corresponds to oxidation of this dimer.

Compound **3.1** (Figure 3.3.A) displays comparable voltammetric features to $ReCl(bpy)(CO)_3$ on the negative sweep: at 100 mV s^{-1} two waves appear at −2.06 and −2.44 V vs Fc/Fc^+, a 300 and 400 mV shift to more negative voltages, respectively, compared to the parent

compound. Unlike $ReCl(bpy)(CO)_3$, the first reduction wave for **3.1** is not quasireversible, even up to 2000 mV s^{-1}. This behavior resembles that observed for $MnBr(bpy)(CO)_3$ (Figure 3.3.D), where the first reduction is metal based and leads to the rapid dissociation of bromide.[70] Indeed, our computations predict that after one-electron reduction the Re–Cl bond in **3.1** has a bond dissociation energy (BDE) of −2.0 kcal mol^{-1}, akin to the −1.4 kcal mol^{-1} BDE for the Mn–Br bond in $[MnBr(bpy)(CO)_3]^{\bullet-}$. These values are substantially lower than the 13.1 kcal mol^{-1} BDE for the Re–Cl bond in $[ReCl(bpy)(CO)_3]^{\bullet-}$.

A consequence of preferred metal-based reduction versus ligand-based reduction is the increased proclivity for the five-coordinate neutral radical, e.g., $[M(\kappa^2\text{-L})(CO)_3]^{\bullet}$, to dimerize. This tendency yields a much larger current density for dimer oxidation in both **3.1** (at −0.36 V vs Fc/Fc^+) and $MnBr(bpy)(CO)_3$ (at −0.58 V vs Fc/Fc^+) compared to $ReCl(bpy)(CO)_3$ (at ca. −0.5 V vs Fc/Fc^+). Similar to $ReCl(bpy)(CO)_3$, **3.1** displays a new oxidative feature around −1.6 V vs Fc/Fc^+ at faster scan rates; again, the inset plot confirms that this wave corresponds to the oxidation of species formed at the second electron reduction.

For complex **3.2** (Figure 3.3.B) the two one-electron-reduction waves appear at −1.92 and −2.32 V vs Fc/Fc^+. At fast scan rates, the pattern in peak current densities for these waves, the first larger than the second, is closest to the current response observed for $MnBr(bpy)(CO)_3$, where intermediary dimer formation is the likely cause of current attenuation at the second reduction. For **3.2**, slow Re–Cl bond dissociation in the singly reduced species is more likely the limiting component. Two observations support this assertion: (i) the peak current of the second reduction is only diminished at fast scan rates (at 100 mV s^{-1} the current densities are roughly equal), and (ii) adding tetrabutylammonium chloride causes the peak current of the second reduction wave to decrease, even at 100 mV s^{-1} (see S3.SI, pp 161-162). For **3.1**, current attenuation is not observed

since the computed Re–Cl BDE is lower for the singly reduced species (−2.0 for **3.1** vs 3.0 kcal mol^{-1} for **3.2**). Indeed, for related Re–bpy systems, installation of electron-withdrawing groups on bpy (−CF_3) slows the rate of chloride loss;[71] the relative electron deficiency of the pyrimidyl unit in **3.2** may impart the same effect. On the return sweep, three oxidation waves appear at fast scan rates: ca. −0.2, ca. −0.7 V, and ca. −1.5 V vs Fc/Fc^+. The inset plot indicates that only the feature at ca. −0.7 persists when the switching potential is set before the second reduction.

As noted in the Introduction, $ReCl(bpy)(CO)_3$ is capable of mediating both photocatalytic and electrocatalytic CO_2 conversion, that is, the conversion of CO_2 at the potential of the first and second reduction, respectively. Given the promise of recent work in employing silicon substrates for photoelectrocatalysis,[39, 72-75] we were interested in the ability of **3.1** and **3.2** to convert CO_2 at the first reduction potential. To that end, we examined the voltammetric response under argon and CO_2 saturation with added Brønsted acid (0.5 M PhOH). These results are displayed in Figures 3.4.A and 3.4.B.

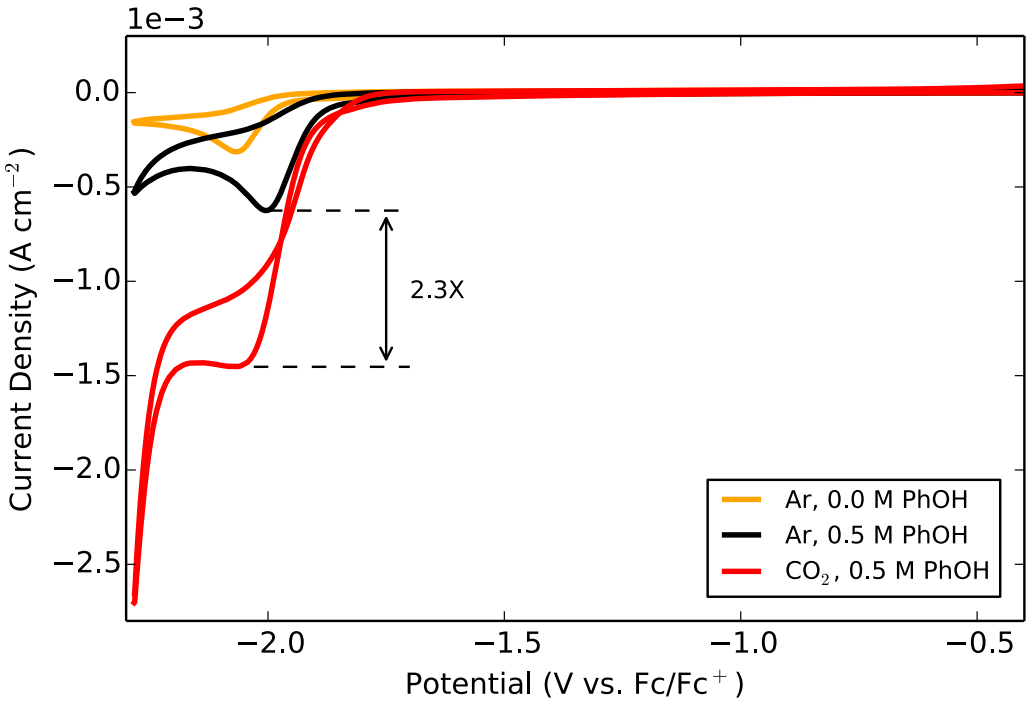

Figure 3.4.A: CV of ReCl(*N*-methyl-*N*′-2-pyridylbenzimidazol-2-ylidine)$(CO)_3$ (**3.1**) Ar and CO_2 saturation in MeCN (0.5 M PhOH) at 100 mV s^{-1} with 0.1 M tetrabutylammonium perchlorate (TBAP) supporting electrolyte.

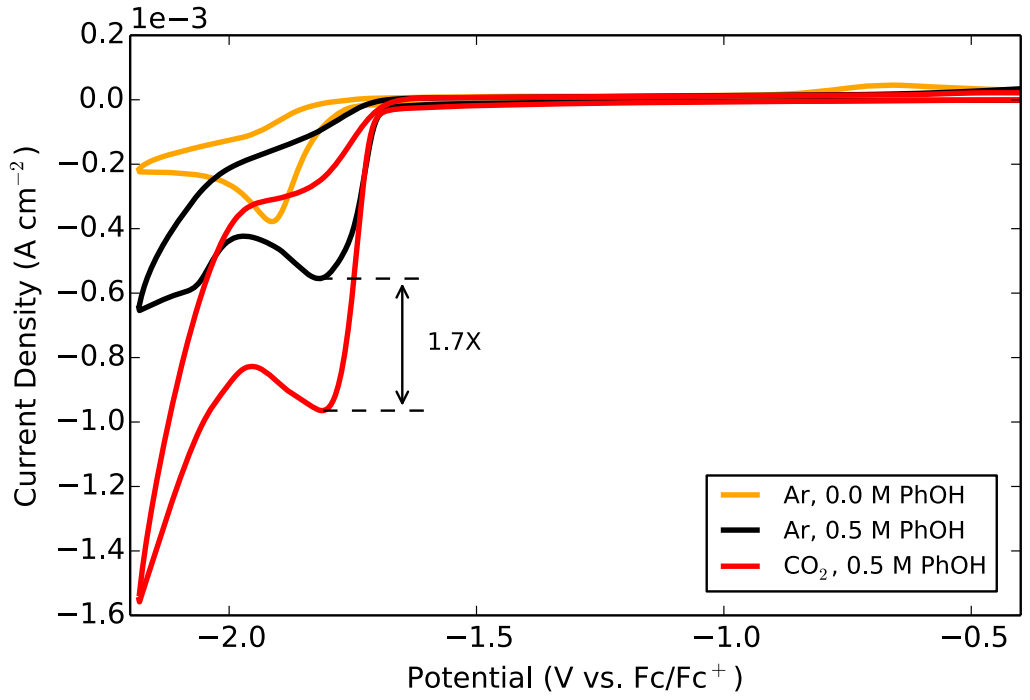

Figure 3.4.B: CV of ReCl(*N*-methyl-*N*′-2-pyrimidylbenzimidazol-2-ylidine)$(CO)_3$ (**3.2**) under Ar and CO_2 saturation in MeCN (0.5 M PhOH) at 100 mV s^{-1} with 0.1 M tetrabutylammonium perchlorate (TBAP) supporting electrolyte.

For both species, the addition of phenol under argon shifts the first reduction potential to more positive voltages: +70 mV for **3.1** and +90 mV for **3.2** (compare orange and black traces). This behavior suggests the interaction of protons with the one-electron-reduced metal center,[76] indicating that there is not strict selectivity for CO_2 (*vide infra*). After purging with CO_2 to saturation, both compounds exhibit a catalytic response. The ratio of the peak current between the catalyzed (i_{cat}) and the uncatalyzed (i_p) processes is 2.3 times for **3.1** and 1.7 times for **3.2**, noting that the turnover frequency is higher for **3.1**, but ca. 250 mV more electromotive force is required.

On the preparative scale, **3.1** and **3.2** display at least 60% Faradaic efficiency for CO production at ca. −2.2 V vs Fc/Fc^+ (see Table 3.2), which is just negative of the first reduction potentials. Some H_2 production (26% and 17%, respectively) is observed along with HCO_2H, which is consistent with the interaction of protons with the reduced metal center.[76, 77] Note that H_2 is also detected as a product for some Mn(I) NHC catalysts. Supplemental infrared spectroelectrochemical experiments suggest that H_2O is a coproduct of CO generation (see S3.SI, pp 159-160; also see ref [78]). No significant amounts of other liquid or gaseous products were observed by GC or NMR.

Table 3.2: Results from Controlled Potential Electrolyses at ca. −2.2 V vs Fc/Fc^+ with Product Analysis

Complex	Coulombs	FE_{H2}	FE_{CO}	FE_{HCO2H}
$ReCl(bpy)(CO)_3$	33 C	0%	99%	0%
3.1	32 C	26%	60%	2%
3.2	34 C	17%	62%	4%

Compounds were loaded at a concentration of approximately 1 mM in a ~45 mL solution of MeCN with 0.1 M tetrabutylammonium hexafluorophosphate ($TBAPF_6$) supporting electrolyte and 0.5 M phenol. FE is the Faradaic efficiency. CO and H_2 were quantified by GC; formic acid with ^1H NMR (see Experimental Methods).

INFRARED SPECTROELECTROCHEMISTRY

To further characterize the structures of **3.1** and **3.2** under electrochemical conditions, infrared spectra were collected at controlled potentials (see Figure 3.5.A and 3.5.B) using established infrared spectroelectrochemistry techniques.[79, 80] These results are discussed in the following paragraphs. Note that "BI-Py" and "BI-Pyrm" are used as abbreviations for the NHC-aryl ligands in compounds **3.1** and **3.2**, respectively.

For complex **3.1** (Figure 3.5.A), three infrared transitions appear in the carbonyl region at the resting potential (black spectrum): 2020, 1923, and 1894 cm^{-1}. These bands are within 10 cm^{-1} of the same transitions in $ReCl(bpy)(CO)_3$[34] and are consistent with a *facial* tricarbonyl arrangement. Adjusting the applied potential to the first reduction (ca. −2.06 V vs Fc/Fc^+, red spectrum) initially yields two sets of carbonyl stretching frequencies: 2007, 1905, and 1879 cm^{-1}, which are assigned to $[Re(BI\text{-}Py)(CO)_3]^{\bullet}$, and 1985, 1942, 1888, and 1849 cm^{-1}, which are assigned[80-83] to $[Re(BI\text{-}Py)(CO)_3]_2$. After holding this potential, the bands ascribed to $[Re(BI\text{-}Py)(CO)_3]^{\bullet}$ diminish as this species is converted to the Re–Re dimer product (green spectrum). Note that supplanting the applied potential with 1.1 equiv of a chemical reductant (KC_8) yields sharp infrared transitions corresponding to $[Re(BI\text{-}Py)(CO)_3]_2$ (see S3.SI, pp 157). Finally, at the potential of the second reduction (ca. −2.44 V vs Fc/Fc^+, blue spectrum), the bands assigned to the dimer disappear concomitant with the appearance of transitions at 1905 and 1803 cm^{-1} for $[Re(BI\text{-}Py)(CO)_3]^-$. This anionic species is also obtained with chemical reduction (see S3.SI, pp 157).

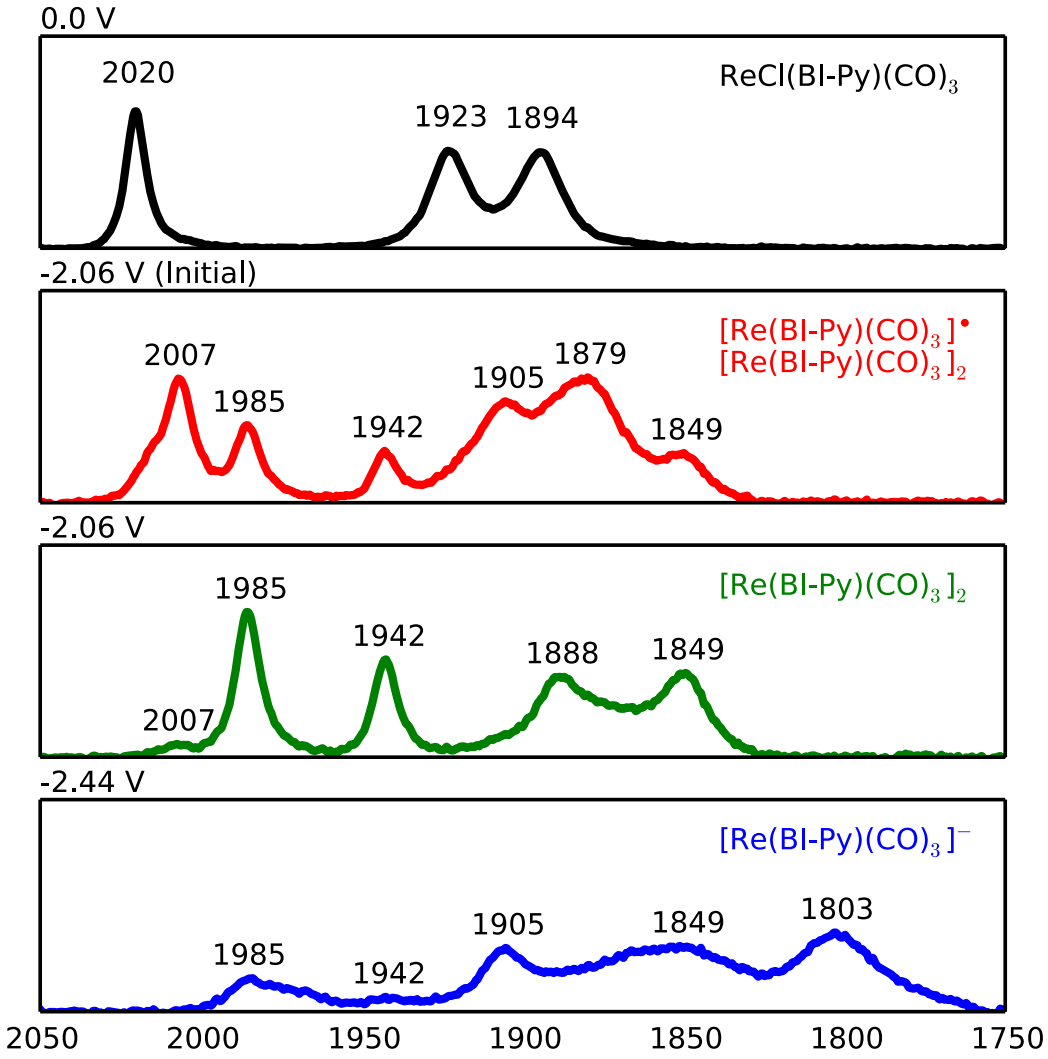

Figure 3.5.A: Infrared spectra of ReCl(*N*-methyl-*N*′-2-pyridylbenzimidazol-2-ylidine)$(CO)_3$ (**3.1**) at controlled potentials under N_2 in dry MeCN with 0.1 M tetrabutylammonium hexafluorophosphate ($TBAPF_6$) supporting electrolyte. The *x* axis is energy (cm^{-1}), and the *y* axis is absorbance.

The spectra for complex **3.2** are shown in Figure 3.6.B. At resting potential (black spectrum), three carbonyl stretching frequencies appear at 2022, 1926, and 1899 cm^{-1}. These bands are within 5 cm^{-1} of the same transitions for **1** but shifted to higher energies, which is aligned with the decrease in electron density on the metal center as a result of a more π-acidic NHC-aryl ligand. At the potential of the first reduction (ca. −1.92 V vs Fc/Fc^+, red spectrum), one set of bands appears (2002, 1898, and 1865 cm^{-1}), which are assigned to $[Re(BI\text{-}Pyrm)(CO)_3]^{\bullet}$. For complexes

3.1 and **3.2** we assign the one-electron-reduced species (red spectra) to the neutral, five-coordinate radical rather than the radical anion containing chloride, $[ReCl(BI\text{-}Pyrm)(CO)_3]^{\bullet-}$. This assignment is based on the low BDE for the Re–Cl bond in the reduced complexes, the irreversibility seen by CV under Faradaic conditions, and the observed CO_2 reduction activity at the first potential, which requires Cl loss. Using 1.1 equiv of chemical reductant instead of an applied potential furnishes no infrared transitions consistent with a dimer product (see S3.SI, pp 158). Adjusting the potential to the second reduction (ca. −0.32 V vs Fc/Fc^+, blue spectrum) yields transitions (1993, 1887, 1861 cm^{-1}) that are ascribed to $[Re(BI\text{-}Pyrm)(CO)_3]^-$.

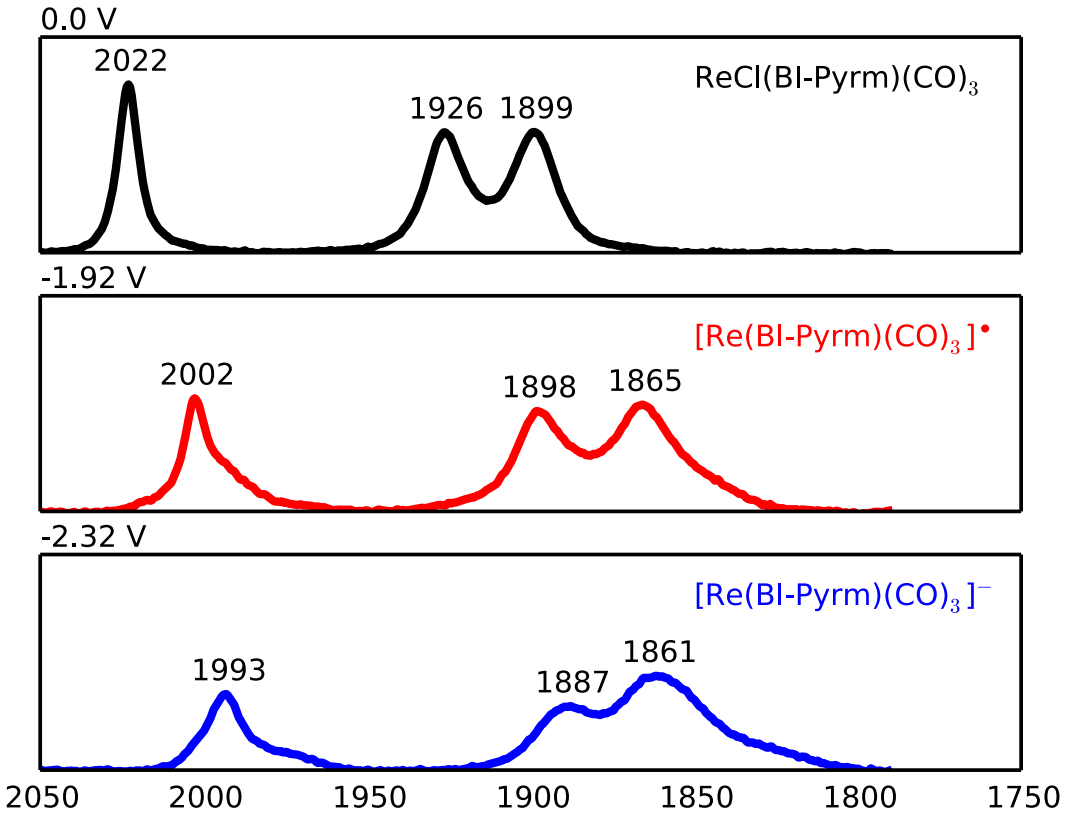

Figure 3.5.B: Infrared spectra of ReCl(*N*-methyl-*N*′-2-pyrimidylbenzimidazol-2-ylidine)$(CO)_3$ (**3.2**) at controlled potentials under N_2 in dry MeCN with 0.1 M tetrabutylammonium hexafluorophosphate ($TBAPF_6$) supporting electrolyte. The *x* axis is energy (cm^{-1}), and the *y* axis is absorbance.

CONCLUSIONS

The iterative optimization of Re(I) electrocatalysts for CO_2 conversion requires the development of ligands that are highly amenable to synthetic modification. As a proof-of-concept, two alkyl-NHC-aryl motifs based on benzimidazole coupled to either pyridine or pyrimidine were utilized as bidentate ligands within Re(I)–tricarbonyl complexes: ReCl(*N*-methyl-*N*′-2-pyridylbenzimidazol-2-ylidine)$(CO)_3$ (**1**) and ReCl(*N*-methyl-*N*′-2-pyrimidylbenzimidazol-2-ylidine)$(CO)_3$ (**2**). The increased π-acidity of the pyrimidyl unit in **2** compared to the pyridyl moiety in **1** yields a lower LUMO energy, inducing a red-shifted emission (+55 nm) and modulating the first and second reduction potentials to more positive voltages (by 140 and 120 mV, respectively).

The cyclic voltammogram of **3.1** shows similar features to ReCl(bpy)$(CO)_3$ when scanning to negative potentials, namely, two sharp one-electron-reduction waves spaced by hundreds of millivolts. Comparable features to MnBr(bpy)$(CO)_3$ are observed on the return sweep, including a substantial current density for dimer oxidation. For complex **3.2**, scanning to negative potentials yields two irreversible one-electron reduction waves, the first displaying a significantly higher current density than the second, which resembles the response of MnBr(bpy)$(CO)_3$, although no metal−metal dimer formation is observed. On the preparative scale, compounds **3.1** and **3.2** are capable of mediating CO_2 reduction to CO after loading only one electron (Faradaic efficiency > 60%). Minor H_2 (ca. 20%) and HCO_2H (<5%) production is also observed. Future work will consider ligand modifications to tune the product specificity.

EXPERIMENTAL METHODS

General

All reagents were obtained from commercial suppliers and used as received unless otherwise noted. Reactions were performed using standard Schlenk-line techniques under an atmosphere of argon. All synthetic manipulations were performed under red light to minimize photodecomposition. Toluene was dried prior to use by distilling it from Na/benzophenone. ^{1}H NMR spectra were recorded on a Varian Mercury Plus 400 MHz spectrometer, and ^{13}C NMR spectra were recorded on an Agilent DD2 600 MHz spectrometer. NMR chemical shifts were referenced to the residual protio signal of the deuterated solvent. FTIR spectra were recorded on a ThermoNicolet 6700 spectrophotometer running OMNIC software.

Cyclic Voltammetry

Cyclic voltammetry experiments were performed using a CH Instruments 601E potentiostat (Austin, TX) and recorded in a three-neck, single-compartment cell with Ace #7 joints. A 3 mm diameter glassy carbon disc (BASi) was utilized as the working electrode. The counter electrode was a platinum wire, and the reference electrode was a silver/silver chloride (Ag/AgCl) electrode separated from solution by a Teflon tip. The supporting electrolyte was composed of MeCN and 0.1 M tetrabutylammonium perchlorate (TBAP). Preparation of the electrolyte was as follows. First, HPLC-grade MeCN was dried over activated 4 Å sieves for 48 h and then stored under argon. TBAP was synthesized from the dropwise addition of perchloric acid into an equimolar amount of tetrabutylammonium bromide in water, then recrystallized three times from ethyl acetate/hexanes before drying under vacuum. After loading the TBAP into dry MeCN, the solution was passed over activated neutral alumina under argon. The electrolyte was purged with either Ar or CO_2

before CVs were recorded and stirred between successive experiments. Voltammetry was referenced to an internal ferrocene standard (Fc/Fc^+), and compounds were loaded at a concentration of 1 mM.

Bulk Electrolysis

Bulk electrolyses were performed in a custom-threaded glass jar from Chemglass fitted with a custom PEEK (polyether ether ketone) top. The top contained ports for venting, the counter electrode (Pt wire) via a fritted glass insert, the working electrode (graphite rod), pseudoreference electrode (Ag/AgCl behind CoralPor), and a septum for sampling the headspace. The system was sealed with a combination of o-rings, Teflon tape, and electrical tape and tested for airtightness before each run. For an individual run the jar was charged with a known amount of catalyst, known amount of PhOH (0.5 M), stir bar, and an electrolyte solution (0.1 M $TBAPF_6$/MeCN) before being sparged to saturation with CO_2. To prevent polymerization of PhOH on the counter electrode, 0.1 M Fc was added to the electrolyte solution as a sacrificial oxidant. After a run was completed, the headspace was sampled via airtight syringe and characterized by GC; Faradaic efficiencies were determined using a calibration curve. A turnover for this system is based on two electron equivalents being passed for every catalyst molecule in solution; for every mole of catalyst two electrons are passed to achieve one turnover. Formic acid was detected by ^1H NMR. Specifically, 5 mL of the reactant solution was removed after electrolysis and combined with 1 mL of D_2O before adding DCM to yield a biphasic solution (total volume approximately 25 mL) that was examined with ^1H NMR (400 MHz Varian; 128 scans). Formic acid standards were established by preparing MeCN solutions (5 mL; 0.1 M $TBAPF_6$) with known concentrations, followed by the

aforementioned workup. A linear fit of integrated formic acid resonances was used to determine the concentration in unknown samples.

Synthesis

Preparation of [*N*-Methyl-*N*′-2-pyridylbenzimidazolium]$^+$ PF_6^- (L3.1).

Under an atmosphere of argon, a flask was charged with benzimidazole (10.00 g, 84.6 mmol), potassium carbonate (7.79 g, 56.4 mmol), and 2-bromopyridine (2.74 mL, 28.6 mmol). The reaction mixture was stirred at 200 °C for 18 h and then allowed to cool to room temperature. The resulting solution was diluted with water (200 mL) and extracted with DCM (3 × 200 mL). The combined organic extracts were washed with saturated Na_2CO_3 (3 × 200 mL) and brine (200 mL) and then dried over anhydrous $MgSO_4$ before filtration to remove the drying agent. Concentration under reduced pressure using a rotary evaporator gave *N*,*N*′-2-pyridylbenzimidazole as a light red oil (5.45 g, 96%). This intermediate (2.70 g, 13.8 mmol) was then dissolved in 100 mL of CH_3CN under an argon atmosphere. Iodomethane (0.95 mL, 15.2 mmol) was added, and the reaction mixture was stirred at reflux overnight (11 h). After cooling to room temperature, the mixture was concentrated under reduced pressure using a rotary evaporator to afford a yellow solid. Subsequent recrystallization from CH_3CN/Et_2O gave a white solid, [*N*-methyl,*N*′-2-pyridylbenzimidazolium]$^+$ I^-, that was collected by vacuum filtration (4.30 g, 92%). Finally, the iodo salt (1.00 g, 3.0 mmol) was dissolved in 50 mL of water and stirred for 5 min before adding ammonium hexafluorophosphate (0.58 g, 3.6 mmol). The reaction mixture was stirred at room temperature for 30 min (a precipitate forms immediately). The desired product, [*N*-methyl-*N*′-2-pyridylbenzimidazolium]$^+$ PF_6^-, was collected as a white precipitate via vacuum filtration and dried in vacuo (1.05 g, 99%). ^{1}H NMR (DMSO-d_6, 20 °C): δ 10.47 (1H, s), 8.79 (1H, d, J = 4 Hz),

8.49–8.47 (1H, m), 8.30–8.28 (1H, m), 8.16–8.14 (1H, m), 8.03 (1H, d, J = 8 Hz), 7.82–7.77 (2H, m), 7.74–7.71 (1H, m), 4.20 (3H, s).

Preparation of [*N*-Methyl-*N*′-2-pyrimidylbenzimidazolium]$^+$ PF_6^- (L3.2).

Under an atmosphere of argon, a flask was charged with benzimidazole (5.00 g, 42.3 mmol), potassium carbonate (3.90 g, 28.2 mmol), and 2-chloropyrimidine (1.62 g, 14.1 mmol). The reaction mixture was stirred at 200 °C for 18 h and then allowed to cool to room temperature. The resulting solution was diluted with water (200 mL) and extracted with DCM (3 × 200 mL). The combined organic extracts were washed with saturated Na_2CO_3 (3 × 200 mL) and brine (200 mL) and then dried over anhydrous $MgSO_4$ before filtration to remove the drying agent. Concentration under reduced pressure using a rotary evaporator gave *N*,*N*′-2-pyrimidylbenzimidazole as an off-white solid (2.00 g, 72%). This intermediate (1.00 g, 5.1 mmol) was then dissolved in 50 mL of CH_3CN under an argon atmosphere. Iodomethane (1.59 mL, 25.5 mmol) was added, and the reaction mixture was stirred at reflux overnight (11 h). After cooling to room temperature, the mixture was concentrated under reduced pressure using a rotary evaporator. Subsequent recrystallization from CH_3CN/Et_2O gave a pale-yellow solid, [*N*-methyl,*N*′-2-pyrimidylbenzimidazolium]$^+$ I^-, that was collected by vacuum filtration (1.60 g, 93%). Finally, the iodo salt (1.50 g, 4.4 mmol) was dissolved in 100 mL of a 1:1 H_2O/MeOH solution and stirred for 5 min before adding ammonium hexafluorophosphate (0.87 g, 5.3 mmol). The reaction mixture was stirred at room temperature for 30 min (a precipitate forms immediately). The desired product, [*N*-methyl-*N*′-2-pyrimidylbenzimidazolium]$^+$ PF_6^-, was collected as a white precipitate via vacuum filtration and dried in vacuo (1.35 g, 85%). ^{1}H NMR (DMSO-d_6, 20 °C): δ 10.72 (1H, s), 9.15 (2H, d, J = 4 Hz), 8.85–8.83 (1H, m), 8.15–8.13 (1H, m), 7.86–7.78 (3H, m), 4.24 (3H, s).

Preparation of ReCl(*N*-methyl-*N*′-2-pyridylbenzimidazol-2-ylidine)$(CO)_3$ (3.1).

[*N*-methyl-*N*′-2-pyridylbenzimidazolium]$^+$ PF_6^- (0.40 g, 1.1 mmol), $ReCl(CO)_5$ (0.51 g, 1.4 mmol) and potassium carbonate (0.47 g, 3.4 mmol) were suspended in 25 mL of toluene and sparged with argon for 30 min. The reaction mixture was then heated to reflux under argon for 24 h. After cooling to room temperature, Et_2O (50 mL), hexanes (50 mL), and water (25 mL) were added before stirring for 30 min to afford a pale yellow precipitate, the product, which was isolated by vacuum filtration, washed with Et_2O (3 × 25 mL), and dried in vacuo (0.52 g, 89%). IR ν_{CO} (ATR, cm^{-1}): 2014 (s), 1883 (s). ^{1}H NMR (DMSO-d_6, 20 °C): δ 8.97 (1H, d, J = 4 Hz), 8.64 (1H, d, J = 8 Hz), 8.48–8.46 (1H, m), 8.38–8.34 (1H, m), 7.95–7.92 (1H, m), 7.65–7.54 (3H, m), 4.20 (3H, s). ^{13}C NMR (DMSO-d_6, 25 °C): δ 201.46, 198.78, 197.88, 188.74, 153.92, 153.22, 142.60, 135.32, 130.32, 125.44, 125.41, 123.71, 113.98, 113.10, 112.74, 34.95.

Preparation of ReCl(*N*-methyl-*N*′-2-pyrimidylbenzimidazol-2-ylidine)$(CO)_3$ (3.2).

[*N*-methyl-*N*′-2-pyrimidylbenzimidazolium]$^+$ PF_6^- (0.40 g, 1.1 mmol), $ReCl(CO)_5$ (0.51 g, 1.4 mmol), and potassium carbonate (0.47 g, 3.4 mmol) were suspended in 25 mL of toluene and sparged with argon for 30 min. The reaction mixture was then heated to reflux under argon for 24 h. After cooling to room temperature, Et_2O (50 mL), hexanes (50 mL), and water (25 mL) were added before stirring for 30 min to afford a yellow precipitate, which was isolated by vacuum filtration and washed with Et_2O (3 × 25 mL). Subsequent purification with column chromatography (silica gel, DCM:acetone, gradient 0–10%) and recrystallization from acetone/Et_2O afforded the product as a bright yellow solid (0.25 g, 43%). IR ν_{CO} (ATR, cm^{-1}): 2014 (s), 1879 (s). ^{1}H NMR (DMSO-d_6, 20 °C): δ 9.30–9.28 (1H, m), 9.23–9.22 (1H, m), 8.64–8.61 (1H, m), 7.93–7.91 (1H, m), 7.66–7.62 (3H, m), 4.20 (3H, s). ^{13}C NMR (DMSO-d_6, 25 °C): δ 199.58, 198.44, 197.18, 188.11, 162.85, 161.11, 159.14, 135.26, 130.71, 125.90, 125.67, 120.03,

THEORETICAL METHODS

Density functional theory (DFT) computations were executed with Orca 3.0.3,[84] and the B3LYP functional was utilized for all computations.[85-87] The Los Alamos LANL08 basis set was used describe all "heavy" atoms, including Mn and Re (LANL08F) along with Br and Cl (LANL08D).[88] These basis sets include an effective core potential to describe electrons close to the nucleus.[89] Conversely, the "light" atoms (H, C, N, and O) were described with the def2-TZVP basis set.[90] All computations included implicit solvent using the Conductor Like Screening Model (COSMO)[91] with the default values for acetonitrile ($\epsilon = 36.6$). Optimized structures were confirmed with vibrational analysis, and Löwdin population analysis[92] was employed to understand the nature of the optimized molecular orbitals.

REFERENCES:

1. Herrmann, W. A.; Mihalios, D.; Öfele, K.; Kiprof, P.; Belmedjahed, F., Metallcarbonyl-Synthesen, XXI. Einfache Synthese Eines Präparativ Nützlichen Alkoxy (Carbonyl) Metallats. *Chemische Berichte* **1992**, *125* (8), 1795-1799.

2. Liu, C.-Y.; Chen, D.-Y.; Lee, G.-H.; Peng, S.-M.; Liu, S.-T., Synthesis of Cyclic Diamino-Substituted Metal Carbene Complexes. *Organometallics* **1996**, *15* (3), 1055-1061.

3. Xue, W.-M.; Chan, M. C.-W.; Su, Z.-M.; Cheung, K.-K.; Liu, S.-T.; Che, C.-M., Spectroscopic and Excited-State Properties of Luminescent Rhenium(I) *N*-Heterocyclic Carbene Complexes Containing Aromatic Diimine Ligands. *Organometallics* **1998**, *17* (8), 1622-1630.

4. Huertos, M. A.; Pérez, J.; Riera, L. a.; Menéndez-Velázquez, A., From *N*-Alkylimidazole Ligands at a Rhenium Center: Ring Opening or Formation of NHC Complexes. *Journal of the American Chemical Society* **2008**, *130* (41), 13530-13531.

5. Flores-Figueroa, A.; Kaufhold, O.; Feldmann, K.-O.; Hahn, F. E., Synthesis of NHC Complexes by Template Controlled Cyclization of β-Functionalized Isocyanides. *Dalton Transactions* **2009**, (42), 9334-9342.

6. Kaufhold, O.; Stasch, A.; Pape, T.; Hepp, A.; Edwards, P. G.; Newman, P. D.; Hahn, F. E., Metal Template Controlled Formation of [11]ane-P_2C^{NHC} Macrocycles. *Journal of the American Chemical Society* **2008**, *131* (1), 306-317.

7. Hiltner, O.; Herdtweck, E.; Drees, M.; Herrmann, W. A.; Kühn, F. E., Synthesis and Characterization of Two New *fac*-Tricarbonylrhenium(I) Biscarbene Complexes. *European Journal of Inorganic Chemistry* **2009**, *2009* (13), 1825-1831.

8. Jiang, Y.; Blacque, O.; Fox, T.; Frech, C. M.; Berke, H., Development of Rhenium Catalysts for Amine Borane Dehydrocoupling and Transfer Hydrogenation of Olefins. *Organometallics* **2009**, *28* (18), 5493-5504.

9. Huertos, M. A.; Pérez, J.; Riera, L.; Díaz, J.; López, R., Effect of the Nature of the Substituent in *N*-Alkylimidazole Ligands on the Outcome of Deprotonation: Ring Opening versus the Formation of *N*-Heterocyclic Carbene Complexes. *Chemistry–A European Journal* **2010**, *16* (28), 8495-8507.

10. Huertos, M. A.; Pérez, J.; Riera, L. a.; Díaz, J.; López, R., From Bis(*N*-Alkylimidazole) to Bis(NH–NHC) in Rhenium Carbonyl Complexes. *Angewandte Chemie International Edition* **2010**, *49* (36), 6409-6412.

11. Hiltner, O.; Boch, F. J.; Brewitz, L.; Härter, P.; Drees, M.; Herdtweck, E.; Herrmann, W. A.; Kühn, F. E., Bridged *fac*-Tricarbonylrhenium(I)–Biscarbene Complexes: Synthesis, Characterization, and Molecular Dynamics. *European Journal of Inorganic Chemistry* **2010**, *2010* (33), 5284-5293.

12. Blase, V.; Pape, T.; Hahn, F. E., Template Synthesis of a Macrocycle with a Mixed NHC/Phosphine Donor Set. *Journal of Organometallic Chemistry* **2011**, *696* (21), 3337-3342.

13. Chen, C.-H.; Liu, Y.-H.; Peng, S.-M.; Chen, J.-T.; Liu, S.-T., Synthesis of *N*-Heterocyclic Carbene Rhenium(I) Carbonyl Complexes. *Dalton Transactions* **2012**, *41* (9), 2747-2754.

14. Casson, L. A.; Muzzioli, S.; Raiteri, P.; Skelton, B. W.; Stagni, S.; Massi, M.; Brown, D. H., *N*-Heterocyclic Carbenes as π*-Acceptors in Luminescent Re(I) Triscarbonyl Complexes. *Dalton Transactions* **2011**, *40* (44), 11960-11967.

15. Martin, T. A.; Ellul, C. E.; Mahon, M. F.; Warren, M. E.; Allan, D.; Whittlesey, M. K., Neutral and Cationic Mono-and Bis-*N*-heterocyclic Carbene Complexes Derived From Manganese and Rhenium Carbonyl Precursors. *Organometallics* **2011**, *30* (8), 2200-2211.

16. Li, X.-W.; Li, H.-Y.; Wang, G.-F.; Chen, F.; Li, Y.-Z.; Chen, X.-T.; Zheng, Y.-X.; Xue, Z.-L., Blue-Green Luminescent Rhenium(I) Tricarbonyl Complexes with Pyridine-Functionalized *N*-Heterocyclic Carbene Ligands. *Organometallics* **2012**, *31* (10), 3829-3835.

17. Canella, D.; Hock, S. J.; Hiltner, O.; Herdtweck, E.; Herrmann, W. A.; Kühn, F. E., Synthesis and Characterization of Propylene and Butylene Bridged *fac*-Tricarbonylrhenium(I) Biscarbene Complexes. *Dalton Transactions* **2012**, *41* (7), 2110-2121.

18. Wang, G.-F.; Liu, Y.-Z.; Chen, X.-T.; Zheng, Y.-X.; Xue, Z.-L., Synthesis, Structure and Luminescent Properties of Rhenium(I) Carbonyl Complexes Containing Pyrimidine-Functionalized *N*-Heterocyclic Carbenes. *Inorganica Chimica Acta* **2013**, *394*, 488-493.

19. Vaughan, J. G.; Reid, B. L.; Ramchandani, S.; Wright, P. J.; Muzzioli, S.; Skelton, B. W.; Raiteri, P.; Brown, D. H.; Stagni, S.; Massi, M., The Photochemistry of Rhenium(I) Tricarbonyl *N*-Heterocyclic Carbene Complexes. *Dalton Transactions* **2013**, *42* (39), 14100-14114.

20. Ng, C.-O.; Yiu, S.-M.; Ko, C.-C., Synthesis, Characterization, and Photophysical Study of Luminescent Rhenium(I) Diimine Complexes with Various Types of *N*-Heterocyclic Carbene Ligands. *Inorganic Chemistry* **2014**, *53* (6), 3022-3031.

21. Hock, S. J.; Schaper, L.-A.; Pöthig, A.; Drees, M.; Herdtweck, E.; Hiltner, O.; Herrmann, W. A.; Kühn, F. E., Synthesis and Characterisation of Chelated Cationic $Re(I)(CO)_3$bis(NHC)(WCA) Complexes. *Dalton Transactions* **2014**, *43* (5), 2259-2271.

22. Chan, C. Y.; Pellegrini, P. A.; Greguric, I.; Barnard, P. J., Rhenium and Technetium Tricarbonyl Complexes of *N*-Heterocyclic Carbene Ligands. *Inorganic Chemistry* **2014**, *53* (20), 10862-10873.

23. Vaughan, J. G.; Reid, B. L.; Wright, P. J.; Ramchandani, S.; Skelton, B. W.; Raiteri, P.; Muzzioli, S.; Brown, D. H.; Stagni, S.; Massi, M., Photophysical and Photochemical Trends in Tricarbonyl Rhenium(I) *N*-Heterocyclic Carbene Complexes. *Inorganic Chemistry* **2014**, *53* (7), 3629-3641.

24. Hille, C.; Kühn, F. E., Cationic Rhenium Complexes Ligated with *N*-Heterocyclic Carbenes–An Overview. *Dalton Transactions* **2016**, *45* (1), 15-31.

25. Huckaba, A. J.; Sharpe, E. A.; Delcamp, J. H., Photocatalytic Reduction of CO_2 with Re-Pyridyl-NHCs. *Inorganic Chemistry* **2015**, *55* (2), 682-690.

26. Visbal, R.; Gimeno, M. C., *N*-Heterocyclic Carbene Metal Complexes: Photoluminescence and Applications. *Chemical Society Reviews* **2014**, *43* (10), 3551-3574.

27. Kirgan, R. A.; Sullivan, B. P.; Rillema, D. P., Photochemistry and Photophysics of Coordination Compounds: Rhenium. In *Photochemistry and Photophysics of Coordination Compounds II*, Springer: 2007; pp 45-100.

28. Geoffroy, G. L.; Wrighton, M. S., *Organometallic Photochemistry*. Academic Press: New York, 1979.

29. Hock, S. J.; Schaper, L.-A.; Herrmann, W. A.; Kühn, F. E., Group 7 Transition Metal Complexes with *N*-Heterocyclic Carbenes. *Chemical Society Reviews* **2013**, *42* (12), 5073-5089.

30. Agarwal, J.; Shaw, T. W.; Stanton, C. J.; Majetich, G. F.; Bocarsly, A. B.; Schaefer, H. F., NHC-Containing Manganese(I) Electrocatalysts for the Two-Electron Reduction of CO_2. *Angewandte Chemie International Edition* **2014**, *126* (20), 5252-5255.

31. Grice, K. A.; Kubiak, C. P., Recent Studies of Rhenium and Manganese Bipyridine Carbonyl Catalysts for the Electrochemical Reduction of CO_2. *CO_2 Chemistry* **2013**, *66*, 163.

32. Sullivan, B. P.; Krist, K.; Guard, H., *Electrochemical and Electrocatalytic Reactions of Carbon Dioxide*. Elsevier: 2012.

33. Sullivan, B. P.; Bolinger, C. M.; Conrad, D.; Vining, W. J.; Meyer, T. J., One-and Two-Electron Pathways in the Electrocatalytic Reduction of CO_2 by *fac*-Re(bpy)$(CO)_3$Cl (bpy= 2,2′-bipyridine). *Journal of the Chemical Society, Chemical Communications* **1985**, (20), 1414-1416.

34. Smieja, J. M.; Kubiak, C. P., Re(bipy-tBu)$(CO)_3Cl^-$ Improved Catalytic Activity for Reduction of Carbon Dioxide: IR-Spectroelectrochemical and Mechanistic Studies. *Inorganic Chemistry* **2010**, *49* (20), 9283-9289.

35. Benson, E. E.; Kubiak, C. P.; Sathrum, A. J.; Smieja, J. M., Electrocatalytic and Homogeneous Approaches to Conversion of CO_2 to Liquid Fuels. *Chemical Society Reviews* **2009**, *38* (1), 89-99.

36. Blakemore, J. D.; Gupta, A.; Warren, J. J.; Brunschwig, B. S.; Gray, H. B., Noncovalent Immobilization of Electrocatalysts on Carbon Electrodes for Fuel Production. *Journal of the American Chemical Society* **2013**, *135* (49), 18288-18291.

37. Takeda, H.; Ishitani, O., Development of Efficient Photocatalytic Systems for CO_2 Reduction Using Mononuclear and Multinuclear Metal Complexes Based on Mechanistic Studies. *Coordination Chemistry Reviews* **2010**, *254* (3), 346-354.

38. Hori, H.; Johnson, F. P.; Koike, K.; Ishitani, O.; Ibusuki, T., Efficient Photocatalytic CO_2 Reduction Using $[Re(bpy)(CO)_3\{P(OEt)_3\}]^+$. *Journal of Photochemistry and Photobiology A: Chemistry* **1996**, *96* (1), 171-174.

39. Kumar, B.; Smieja, J. M.; Kubiak, C. P., Photoreduction of CO_2 on p-type Silicon Using $Re(bipy\text{-}Bu^t)(CO)_3Cl$: Photovoltages Exceeding 600 mV for the Selective Reduction of CO_2 to CO. *The Journal of Physical Chemistry C* **2010**, *114* (33), 14220-14223.

40. Fujita, E.; Brunschwig, B. S.; Ogata, T.; Yanagida, S., Toward Photochemical Carbon Dioxide Activation by Transition Metal Complexes. *Coordination Chemistry Reviews* **1994**, *132*, 195-200.

41. Fujita, E., Photochemical Carbon Dioxide Reduction with Metal Complexes. *Coordination Chemistry Reviews* **1999**, *185*, 373-384.

42. Hawecker, J.; Lehn, J. M.; Ziessel, R., Photochemical and Electrochemical Reduction of Carbon Dioxide to Carbon Monoxide Mediated by (2,2′-Bipyridine)tricarbonylchlororhenium(I) and Related Complexes as Homogeneous Catalysts. *Helvetica Chimica Acta* **1986**, *69* (8), 1990-2012.

43. Doherty, M. D.; Grills, D. C.; Fujita, E., Synthesis of Fluorinated $ReCl(4,4'\text{-}R_2\text{-}2,2'\text{-bipyridine})(CO)_3$ Complexes and Their Photophysical Characterization in CH_3CN and Supercritical CO_2. *Inorganic Chemistry* **2009**, *48* (5), 1796-1798.

44. Raba, A.; Anneser, M. R.; Jantke, D.; Cokoja, M.; Herrmann, W. A.; Kühn, F. E., Facile and Scalable Preparation of 2-Imidazolylpyridines. *Tetrahedron Letters* **2013**, *54* (26), 3384-3387.

45. Schwab, P. F.; Fleischer, F.; Michl, J., Preparation of 5-Brominated and 5,5′-Dibrominated 2,2′-Bipyridines and 2,2′-Bipyrimidines. *The Journal of Organic Chemistry* **2002**, *67* (2), 443-449.

46. Hapke, M.; Brandt, L.; Lützen, A., Versatile Tools in the Construction of Substituted 2,2′-bipyridines—Cross-Coupling Reactions with Tin, Zinc and Boron Compounds. *Chemical Society Reviews* **2008**, *37* (12), 2782-2797.

47. Newkome, G. R.; Patri, A. K.; Holder, E.; Schubert, U. S., Synthesis of 2,2′-Bipyridines: Versatile Building Blocks for Sexy Architectures and Functional Nanomaterials. *European Journal of Organic Chemistry* **2004**, *2004* (2), 235-254.

48. Verniest, G.; Wang, X.; Kimpe, N. D.; Padwa, A., Heteroaryl Cross-Coupling as an Entry Toward the Synthesis of Lavendamycin Analogues: A Model Study. *The Journal of Organic Chemistry* **2009**, *75* (2), 424-433.

49. Hopkinson, M. N.; Richter, C.; Schedler, M.; Glorius, F., An Overview of *N*-Heterocyclic Carbenes. *Nature* **2014**, *510* (7506), 485-496.

50. Nelson, D. J.; Nolan, S. P., Quantifying and Understanding the Electronic Properties of *N*-Heterocyclic Carbenes. *Chemical Society Reviews* **2013**, *42* (16), 6723-6753.

51. Bellemin-Laponnaz, S., Synthesis of *N*, *O*-Heterocyclic Carbene and Coordination to Rhodium(I) and Copper(I). *Polyhedron* **2010**, *29* (1), 30-33.

52. Ruiz, J.; Perandones, B. F., Metal-Induced Tautomerization of Oxazole and Thiazole Molecules to Heterocyclic Carbenes. *Chemical Communications* **2009**, (19), 2741-2743.

53. Soleilhavoup, M. l.; Bertrand, G., Cyclic (Alkyl)(Amino)Carbenes (CAACs): Stable Carbenes on the Rise. *Accounts of Chemical Research* **2014**, *48* (2), 256-266.

54. Lavallo, V.; Canac, Y.; Präsang, C.; Donnadieu, B.; Bertrand, G., Stable Cyclic (Alkyl)(Amino)Carbenes as Rigid or Flexible, Bulky, Electron-Rich Ligands for Transition-Metal Catalysts: A Quaternary Carbon Atom Makes the Difference. *Angewandte Chemie International Edition* **2005**, *117* (35), 5851-5855.

55. Kühl, O., *Functionalised N-Heterocyclic Carbene Complexes*. John Wiley & Sons: 2010.

56. Benhamou, L.; Chardon, E.; Lavigne, G.; Bellemin-Laponnaz, S. p.; César, V., Synthetic Routes to *N*-Heterocyclic Carbene Precursors. *Chemical reviews* **2011**, *111* (4), 2705-2733.

57. Bourrez, M.; Molton, F.; Chardon-Noblat, S.; Deronzier, A., [Mn(bipyridyl)$(CO)_3$Br]: An Abundant Metal Carbonyl Complex as Efficient Electrocatalyst for CO_2 Reduction. *Angewandte Chemie International Edition* **2011**, *123* (42), 10077-10080.

58. Zhang, H.; Cai, Q.; Ma, D., Amino Acid Promoted CuI-Catalyzed CN Bond Formation Between Aryl Halides and Amines or *N*-Containing Heterocycles. *The Journal of Organic Chemistry* **2005**, *70* (13), 5164-5173.

59. Verma, A. K.; Singh, J.; Sankar, V. K.; Chaudhary, R.; Chandra, R., Benzotriazole: An Excellent Ligand for Cu-Catalyzed *N*-Arylation of Imidazoles with Aryl and Heteroaryl Halides. *Tetrahedron Letters* **2007**, *48* (24), 4207-4210.

60. Chianese, A. R.; Bremer, P. T.; Wong, C.; Reynes, R. J., Rigid, Sterically Diverse *N*-Heterocyclic Carbene-Pyridine Chelates: Synthesis, Mild Palladation, and Palladium-Catalyzed Allylic Substitution. *Organometallics* **2009**, *28* (17), 5244-5252.

61. Cano, R.; Ramón, D. J.; Yus, M., Transition-Metal-Free *O*-, S-, and N-Arylation of Alcohols, Thiols, Amides, Amines, and Related Heterocycles. *The Journal of Organic Chemistry* **2010**, *76* (2), 654-660.

62. Yuan, Y.; Thome, I.; Kim, S. H.; Chen, D.; Beyer, A.; Bonnamour, J.; Zuidema, E.; Chang, S.; Bolm, C., Dimethyl Sulfoxide/Potassium Hydroxide: A Superbase for the Transition Metal-Free Preparation of Cross-Coupling Products. *Advanced Synthesis & Catalysis* **2010**, *352* (17), 2892-2898.

63. Agarwal, J.; Stanton III, C. J.; Shaw, T. W.; Vandezande, J. E.; Majetich, G. F.; Bocarsly, A. B.; Schaefer III, H. F., Exploring the Effect of Axial Ligand Substitution (X= Br, NCS, CN) on the Photodecomposition and Electrochemical Activity of [MnX(N–C)(CO)$_3$] Complexes. *Dalton Transactions* **2015**, *44* (5), 2122-2131.

64. Wang, Y.; Wu, J. I.-C.; Li, Q.; Schleyer, P. v. R., Aromaticity and Relative Stabilities of Azines. *Organic Letters* **2010**, *12* (21), 4824-4827.

65. Hwang, F.-M.; Chen, H.-Y.; Chen, P.-S.; Liu, C.-S.; Chi, Y.; Shu, C.-F.; Wu, F.-I.; Chou, P.-T.; Peng, S.-M.; Lee, G.-H., Iridium(III) Complexes with Orthometalated Quinoxaline Ligands: Subtle Tuning of Emission to the Saturated Red Color. *Inorganic Chemistry* **2005**, *44* (5), 1344-1353.

66. Wheeler, S. E.; Bloom, J. W., Anion–π Interactions and Positive Electrostatic Potentials of *N*-Heterocycles Arise From the Positions of the Nuclei, Not Changes in the π-Electron Distribution. *Chemical Communications* **2014**, *50* (76), 11118-11121.

67. Agarwal, J.; Fujita, E.; Schaefer III, H. F.; Muckerman, J. T., Mechanisms for CO Production From CO_2 Using Reduced Rhenium Tricarbonyl Catalysts. *Journal of the American Chemical Society* **2012**, *134* (11), 5180-5186.

68. Hayashi, Y.; Kita, S.; Brunschwig, B. S.; Fujita, E., Involvement of a Binuclear Species with the Re−C(O)O−Re Moiety in CO_2 Reduction Catalyzed by Tricarbonyl Rhenium(I) Complexes with Diimine Ligands: Strikingly Slow Formation of the Re−Re and Re−C(O)O−Re Species from Re(dmb)(CO)$_3$S (dmb= 4,4′-Dimethyl-2,2′-bipyridine), S= Solvent). *Journal of the American Chemical Society* **2003**, *125*, 11976-11987.

69. Fujita, E.; Muckerman, J. T., Why Is Re-Re Bond Formation/Cleavage in [Re(bpy)(CO)$_3$]$_2$ Different from That in [Re(CO)$_5$]$_2$? Experimental and Theoretical Studies on the Dimers and Fragments. *Inorganic Chemistry* **2004**, *43* (24), 7636-7647.

70. Riplinger, C.; Sampson, M. D.; Ritzmann, A. M.; Kubiak, C. P.; Carter, E. A., Mechanistic Contrasts Between Manganese and Rhenium Bipyridine Electrocatalysts for the Reduction of Carbon Dioxide. *Journal of the American Chemical Society* **2014**, *136* (46), 16285-16298.

71. Benson, E. E.; Grice, K. A.; Smieja, J. M.; Kubiak, C. P., Structural and Spectroscopic Studies of Reduced [Re(bpy-R)(CO)$_3$]$^{-1}$ Species Relevant to CO_2 Reduction. *Polyhedron* **2013**, *58*, 229-234.

72. White, J. L.; Baruch, M. F.; Pander III, J. E.; Hu, Y.; Fortmeyer, I. C.; Park, J. E.; Zhang, T.; Liao, K.; Gu, J.; Yan, Y., Light-Driven Heterogeneous Reduction of Carbon Dioxide: Photocatalysts and Photoelectrodes. *Chemical Reviews* **2015**, *115* (23), 12888-12935.

73. Torralba-Peñalver, E.; Luo, Y.; Compain, J.-D.; Chardon-Noblat, S.; Fabre, B., Selective Catalytic Electroreduction of CO_2 at Silicon Nanowires (SiNWs) Photocathodes Using Non-Noble Metal-Based Manganese Carbonyl Bipyridyl Molecular Catalysts in Solution and Grafted onto SiNWs. *ACS Catalysis* **2015**, *5* (10), 6138-6147.

74. Liu, R.; Stephani, C.; Tan, K. L.; Wang, D., Tuning Redox Potentials of CO_2 Reduction Catalysts for Carbon Photofixation by Si Nanowires. *Science China Materials* **2015**, *58* (7), 515-520.

75. Kumar, B.; Smieja, J. M.; Sasayama, A. F.; Kubiak, C. P., Tunable, Light-Assisted Co-Generation of CO and H_2 from CO_2 and H_2O by Re(bipy-tbu)$(CO)_3$ Cl and p-Si in Non-Aqueous Medium. *Chemical Communications* **2012**, *48* (2), 272-274.

76. Machan, C. W.; Sampson, M. D.; Kubiak, C. P., A Molecular Ruthenium Electrocatalyst for the Reduction of Carbon Dioxide to CO and Formate. *Journal of the American Chemical Society* **2015**, *137* (26), 8564-8571.

77. Agarwal, J.; Johnson, R. P.; Li, G., Reduction of CO_2 on a Tricarbonyl Rhenium(I) Complex: Modeling a Catalytic Cycle. *The Journal of Physical Chemistry A* **2011**, *115* (13), 2877-2881.

78. Machan, C. W.; Stanton III, C. J.; Vandezande, J. E.; Majetich, G. F.; Schaefer III, H. F.; Kubiak, C. P.; Agarwal, J., Electrocatalytic Reduction of Carbon Dioxide by Mn(CN)(2,2′-bipyridine)$(CO)_3$: CN Coordination Alters Mechanism. *Inorganic Chemistry* **2015**, *54* (17), 8849-8856.

79. Zavarine, I. S.; Kubiak, C. P., A Versatile Variable Temperature Thin Layer Reflectance Spectroelectrochemical Cell. *Journal of Electroanalytical Chemistry* **2001**, *495* (2), 106-109.

80. Machan, C. W.; Sampson, M. D.; Chabolla, S. A.; Dang, T.; Kubiak, C. P., Developing a Mechanistic Understanding of Molecular Electrocatalysts for CO_2 Reduction Using Infrared Spectroelectrochemistry. *Organometallics* **2014**, *33* (18), 4550-4559.

81. Christensen, P.; Hamnett, A.; Muirt, A. V.; Timney, J. A.; Higgins, S., Growth and Electrochemical Behaviour of a Poly[tricarbonyl(vinylbipyridy rhenium chloride] Film. *Journal of the Chemical Society, Faraday Transactions* **1994**, *90* (3), 459-469.

82. Stor, G. J.; Hartl, F.; van Outersterp, J. W. M.; Stufkens, D. J., Spectroelectrochemical (IR, UV/Vis) Determination of the Reduction Pathways for a Series of $[Re(CO)_3(\alpha\text{-diimine})L']^{0/+}$ (L′ = Halide, OTf$^-$, THF, MeCN, *n*-PrCN, PPh3, $P(OMe)_3$) Complexes. *Organometallics* **1995**, *14* (3), 1115-1131.

83. Johnson, F. P. A.; George, M. W.; Hartl, F.; Turner, J. J., Electrocatalytic Reduction of CO_2 Using the Complexes $[Re(bpy)(CO)_3L]^n$ (n = +1, L = $P(OEt)_3$, CH_3CN; n = 0, L = Cl^-, OTf$^-$; bpy = 2,2′-Bipyridine; OTf$^-$ = CF_3SO_3) as Catalyst Precursors: Infrared Spectroelectrochemical Investigation. *Organometallics* **1996**, *15* (15), 3374-3387.

84. Neese, F., The ORCA Program System. *Wiley Interdisciplinary Reviews: Computational Molecular Science* **2012**, *2* (1), 73-78.

85. Becke, A. D., Density-Functional Thermochemistry. III. The Role of Exact Exchange. *The Journal of Chemical Physics* **1993**, *98* (7), 5648-5652.

86. Becke, A. D., Density-Functional Thermochemistry. IV. A New Dynamical Correlation Functional and Implications for Exact-Exchange Mixing. *The Journal of Chemical Physics* **1996**, *104* (3), 1040-1046.

87. Lee, C.; Yang, W.; Parr, R. G., Development of the Colle-Salvetti Correlation-Energy Formula Into a Functional of the Electron Density. *Physical Review B* **1988**, *37* (2), 785-789.

88. Roy, L. E.; Hay, P. J.; Martin, R. L., Revised Basis Sets for the LANL Effective Core Potentials. *Journal of Chemical Theory and Computation* **2008**, *4* (7), 1029-1031.

89. Hay, P. J.; Wadt, W. R., *Ab Initio* Effective Core Potentials for Molecular Calculations. Potentials for the Transition Metal Atoms Sc to Hg. *The Journal of Chemical Physics* **1985**, *82* (1), 270-283.

90. Weigend, F.; Ahlrichs, R., Balanced Basis Sets of Split Valence, Triple Zeta Valence and Quadruple Zeta Valence Quality for H to Rn: Design and Assessment of Accuracy. *Physical Chemistry Chemical Physics* **2005**, *7* (18), 3297-3305.

91. Klamt, A.; Schuurmann, G., COSMO: A New Approach to Dielectric Screening in Solvents with Explicit Expressions for the Screening Energy and Its Gradient. *Journal of the Chemical Society, Perkin Transactions 2* **1993**, (5), 799-805.

92. Löwdin, P. O., On the Non-Orthogonality Problem Connected with the Use of Atomic Wave Functions in the Theory of Molecules and Crystals. *The Journal of Chemical Physics* **1950**, *18* (3), 365-375.

S3. SUPPORTING INFORMATION

S3.1 SELECTED SPECTRA

S3.1.1 ^{1}H NMR of [*N*-methyl-*N*′-2-pyridylbenzimidazolium]$^{+}$ PF_6^{-} (L3.1).

Temperature: 20 ˚C
Solvent: DMSO-d_6

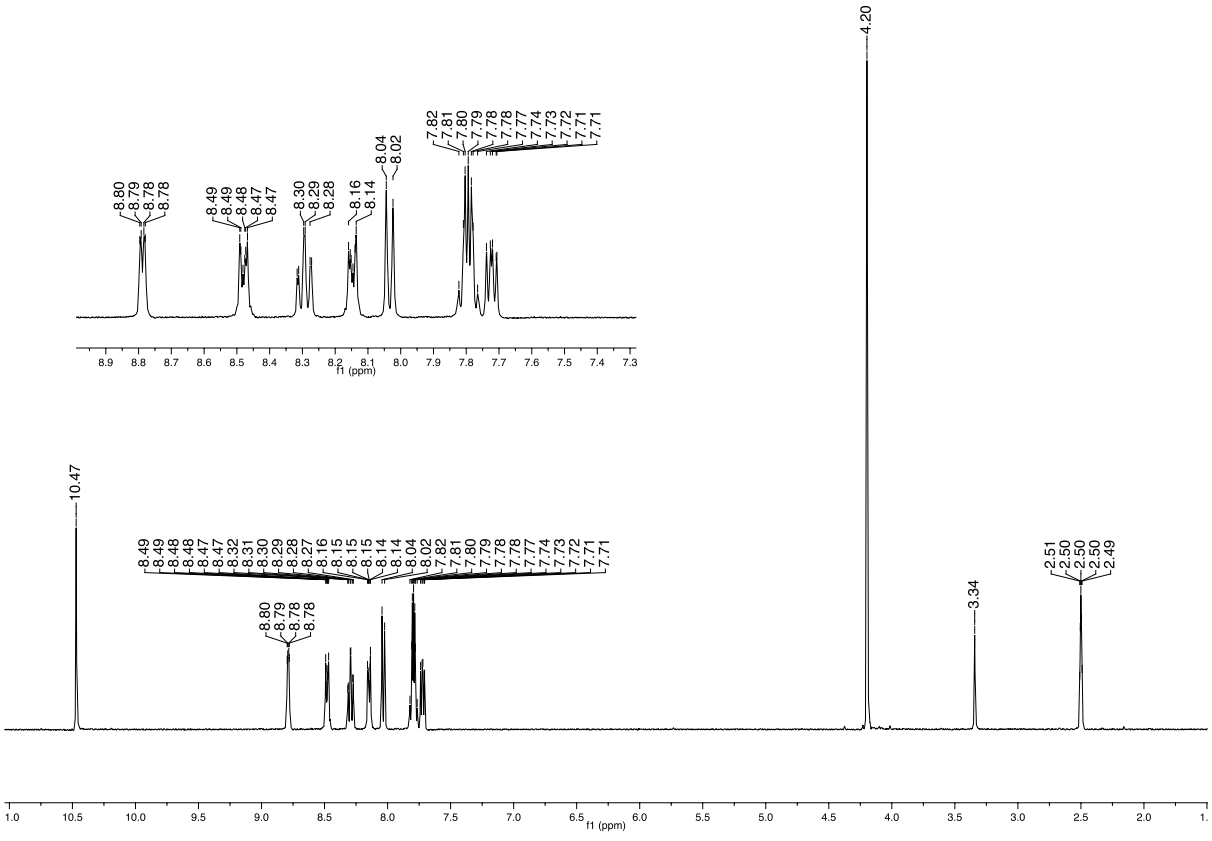

Note: The peak at 3.34 ppm is assigned to water, and the peak at 2.50 ppm to dimethyl sulfoxide.

S3.1.2 ^{1}H NMR of [*N*-methyl-*N′*-2-pyrimidylbenzimidazolium]$^{+}$ PF_6^{-} (L3.2).

Temperature: 20 ˚C
Solvent: DMSO-d_6

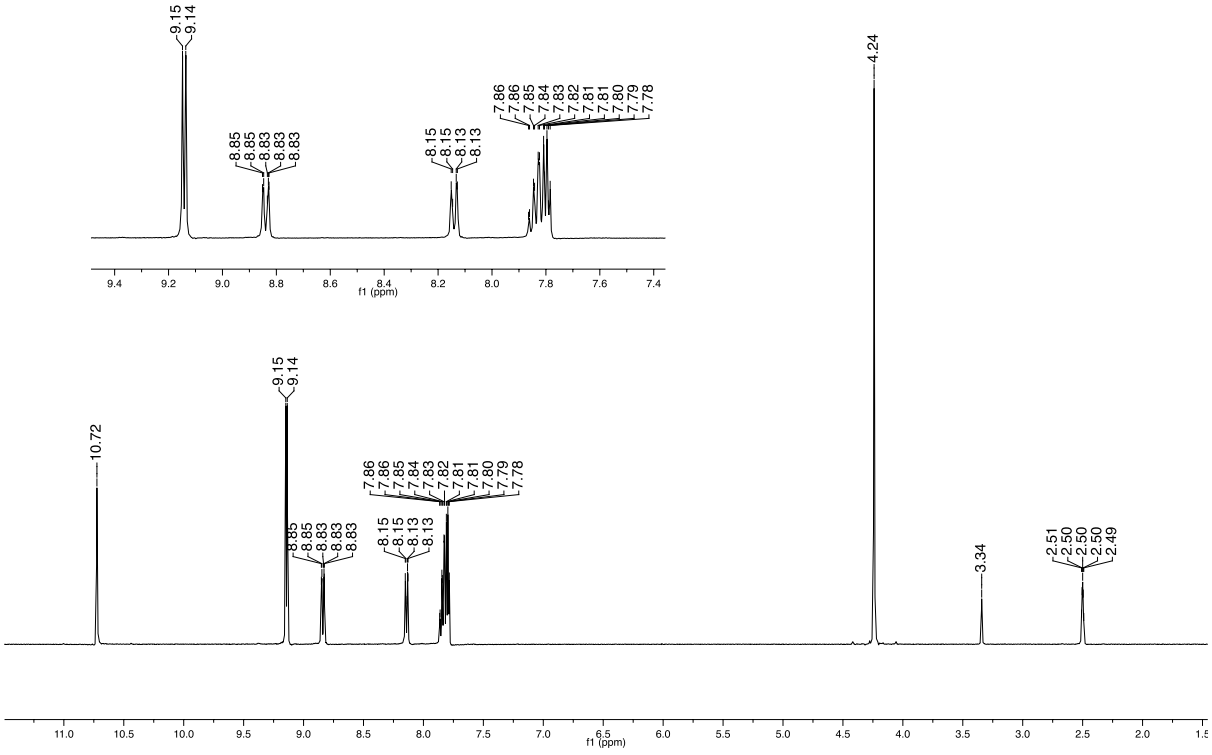

Note: The peak at 3.34 ppm is assigned to water, and the peak at 2.50 ppm to dimethyl sulfoxide.

S3.1.3 ^{1}H NMR of ReCl(*N*-methyl-*N*′-2-pyridylbenzimidazol-2-ylidine)$(CO)_3$ (3.1).

Temperature: 20 ˚C
Solvent: DMSO-d_6

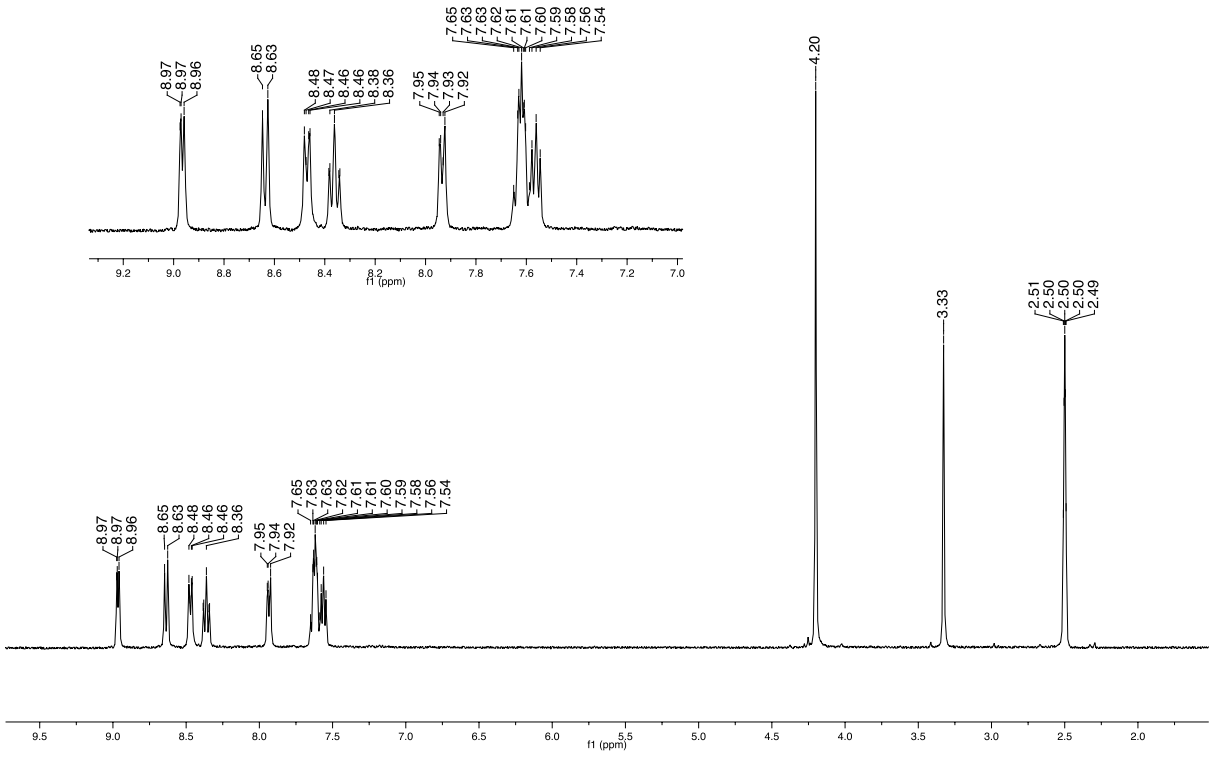

Note: The peak at 3.33 ppm is assigned to water, and the peak at 2.50 ppm to dimethyl sulfoxide.

S3.1.4 ^{13}C NMR of ReCl(*N*-methyl-*N*′-2-pyridylbenzimidazol-2-ylidine)$(CO)_3$ (3.1).

Temperature: 25 ˚C
Solvent: DMSO-d_6

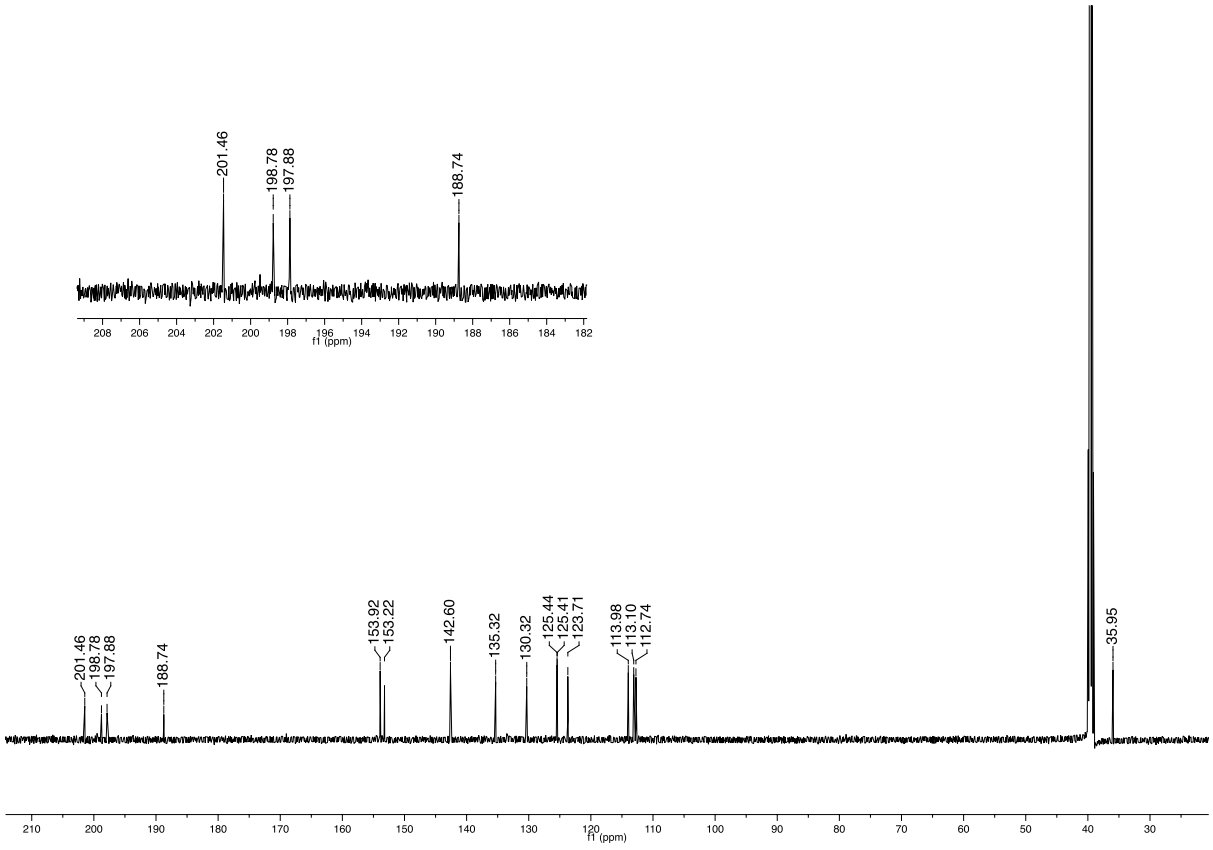

S3.1.5 FTIR of ReCl(*N*-methyl-*N*′-2-pyridylbenzimidazol-2-ylidine)$(CO)_3$ (3.1).

Method: ATR

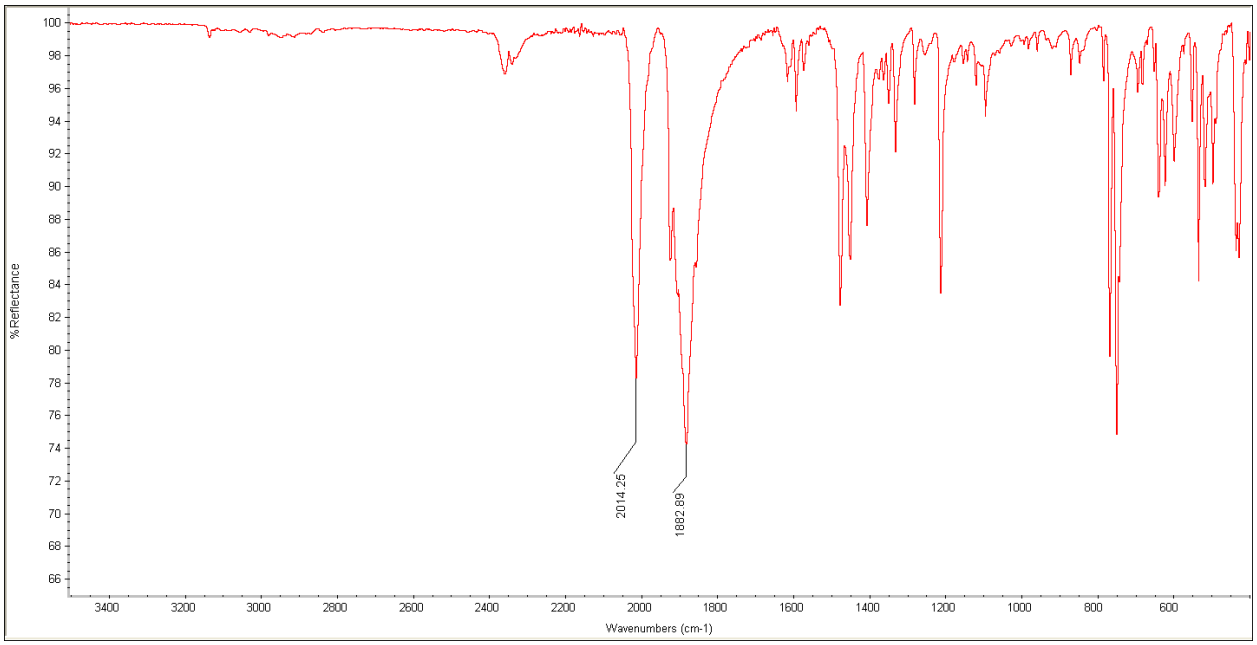

S3.1.6 ^{1}H NMR of ReCl(*N*-methyl-*N*′-2-pyrimidylbenzimidazol-2-ylidine)$(CO)_3$ (3.2).

Temperature: 20 ˚C
Solvent: DMSO-d_6

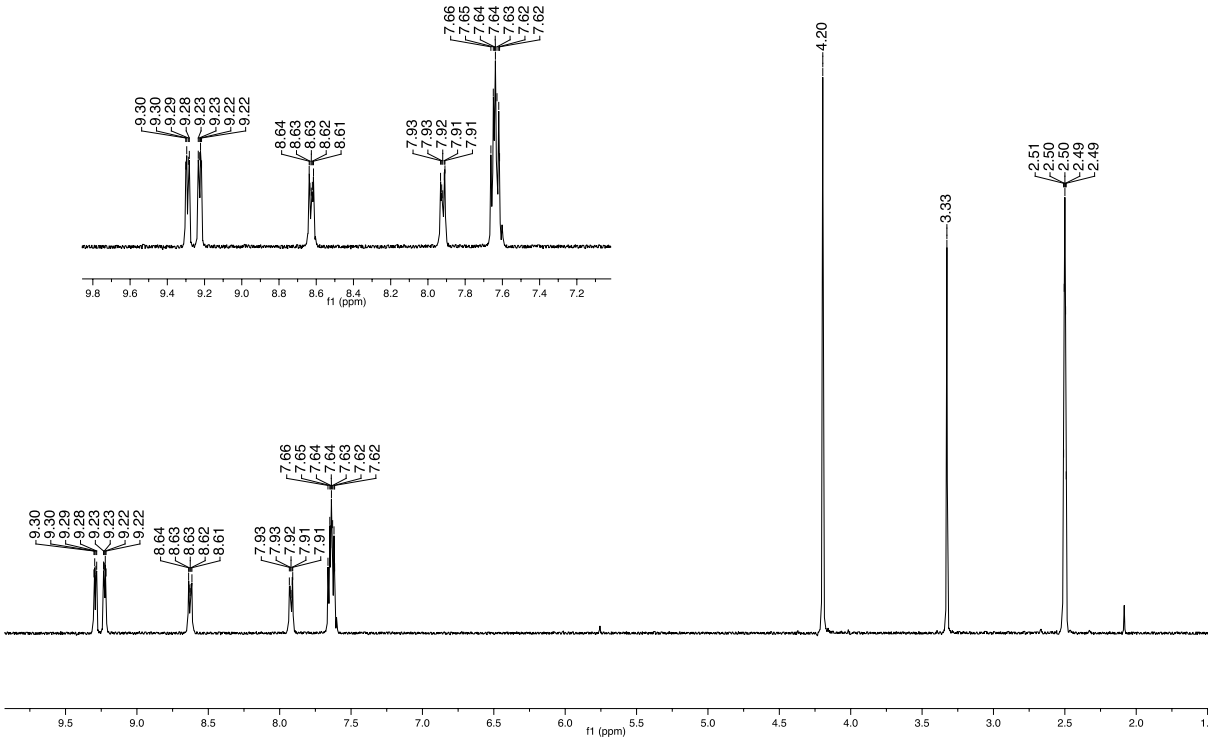

Note: The peak at 3.33 ppm is assigned to water, the peak at 2.50 ppm to dimethyl sulfoxide, and the peak at roughly 2.1 ppm to acetone.

S3.1.7 ^{13}C NMR of ReCl(*N*-methyl-*N*′-2-pyrimidylbenzimidazol-2-ylidine)$(CO)_3$ (3.1).

Temperature: 25 ˚C
Solvent: DMSO-d_6

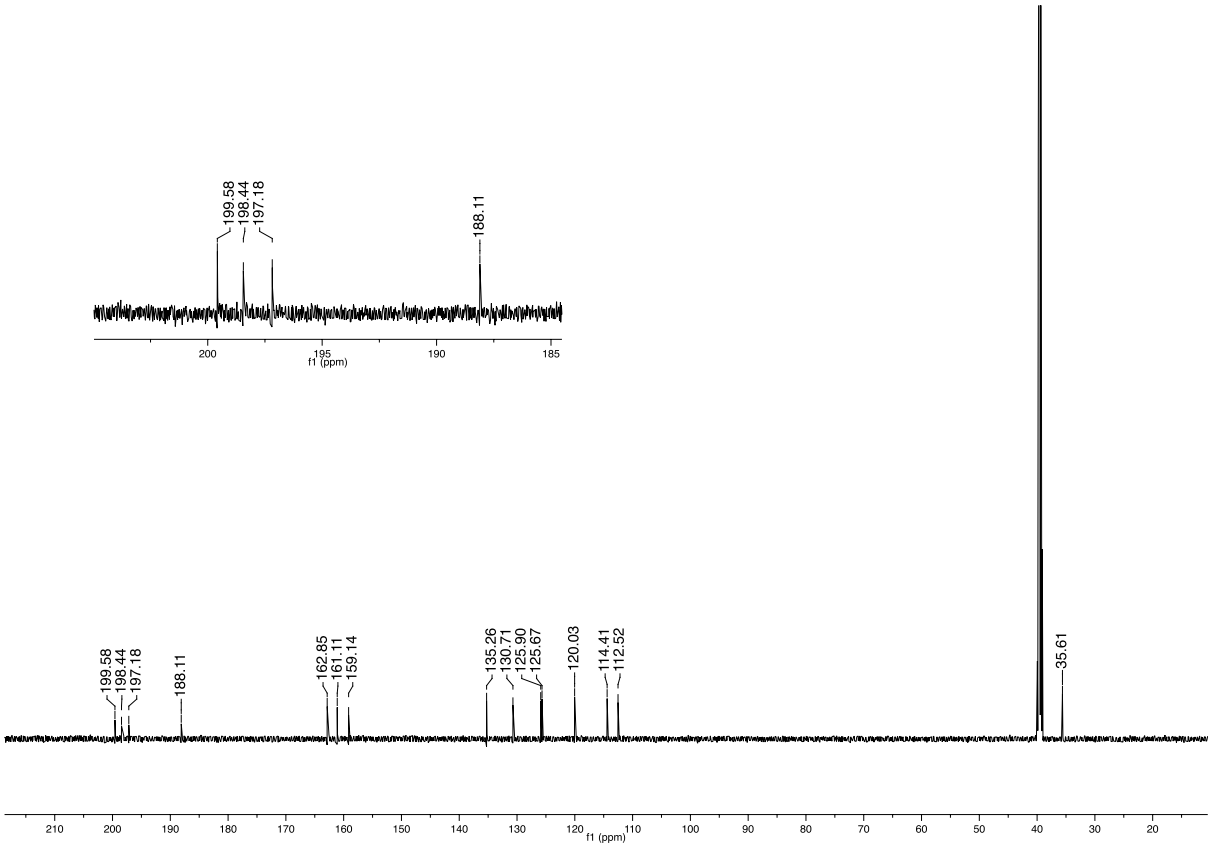

S3.1.8 FTIR of ReCl(*N*-methyl-*N*′-2-pyrimidylbenzimidazol-2-ylidine)$(CO)_3$ (3.1).

Method: ATR

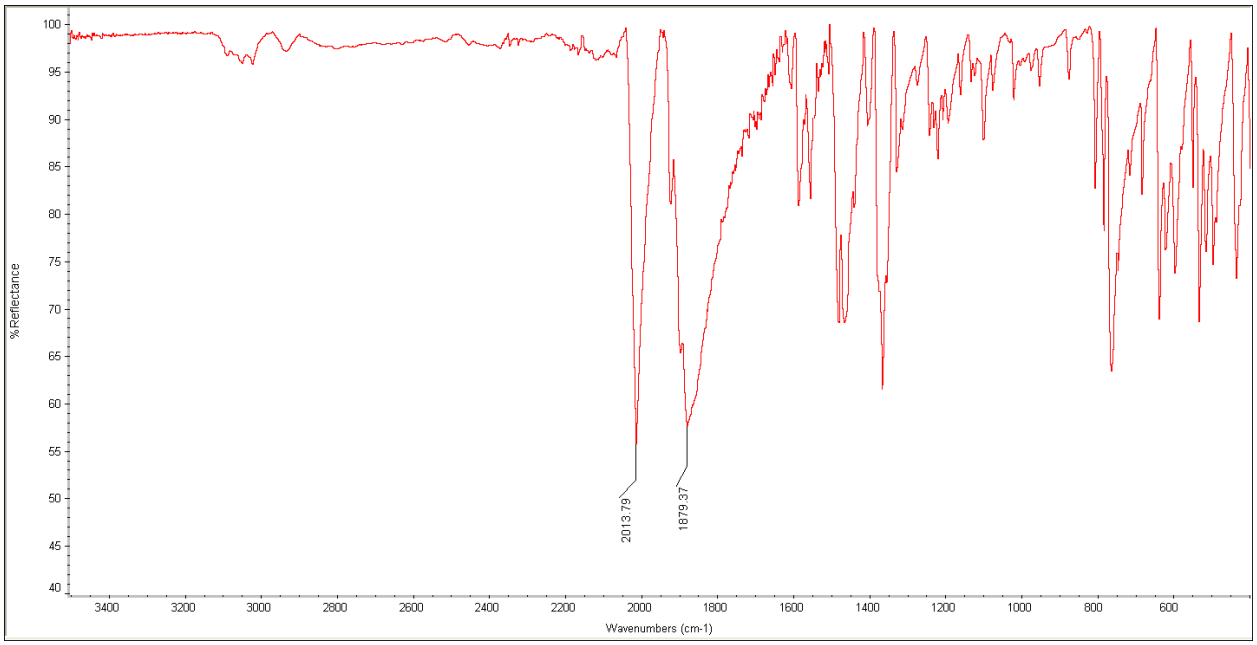

S3.2 DATA FROM CHEMICAL REDUCTION

S3.2.1 ReCl(*N*-methyl-*N*′-2-pyridylbenzimidazol-2-ylidine)$(CO)_3$ (3.1).

Atmosphere: Argon
Solvent: THF

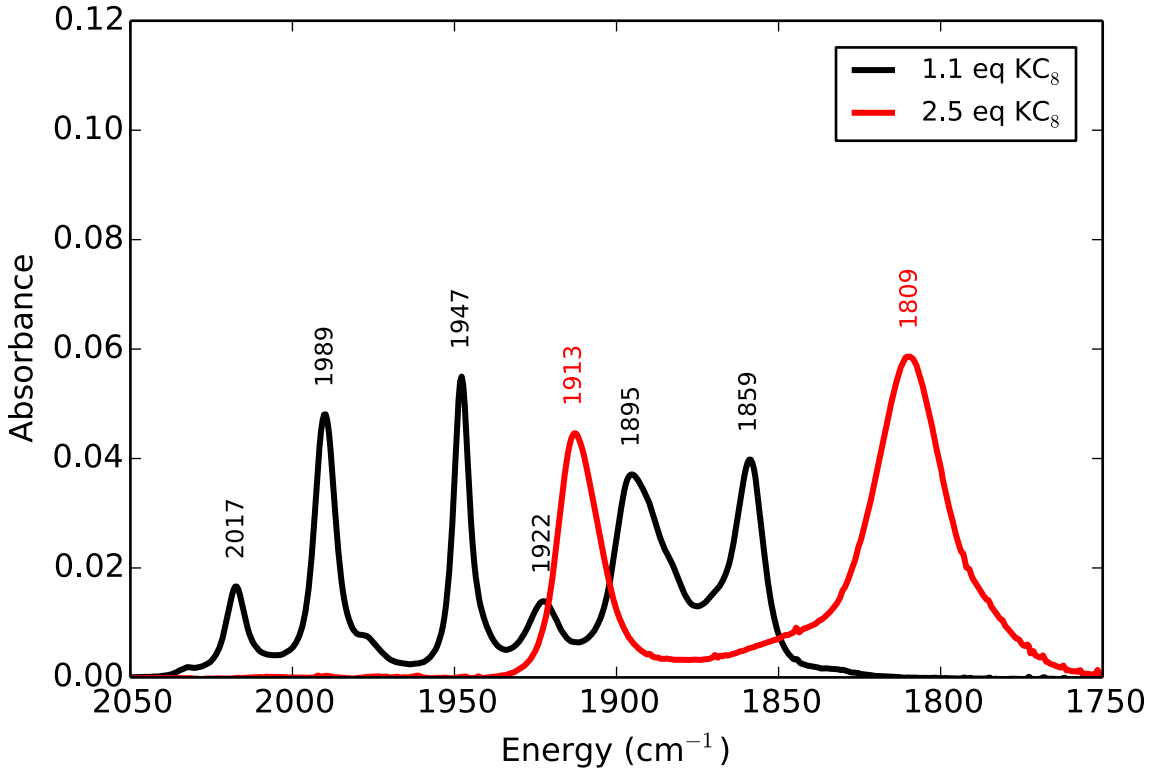

Note: A 3 mM aliquot of 18-crown-6 was added for the 2.5 eq trial.

S3.2.2 ReCl(*N*-methyl-*N*′-2-pyrimidylbenzimidazol-2-ylidine)$(CO)_3$ (3.2).

Atmosphere: Argon
Solvent: THF

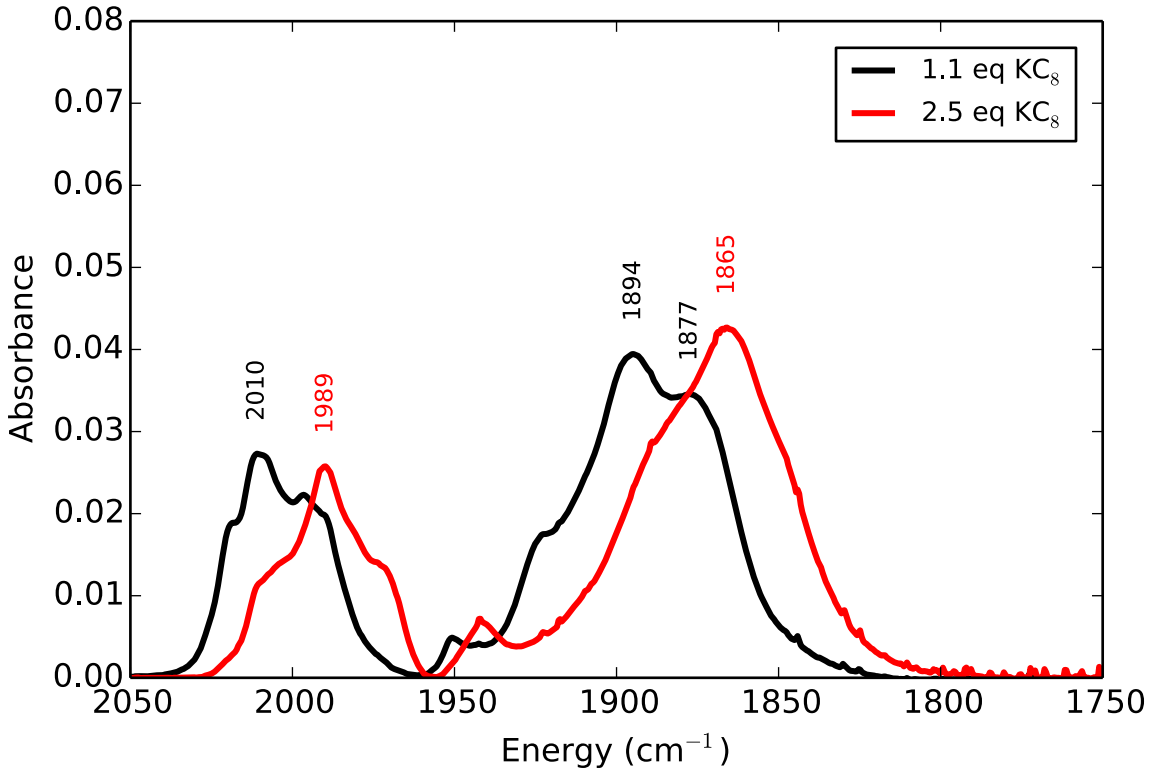

Note: A 3 mM aliquot of 18-crown-6 was added for the 2.5 eq trial.

S3.3 DATA FROM CONTROLLED-POTENTIAL INFRARED SPECTROELECTROCHEMISTRY

S3.3.1 ReCl(*N*-methyl-*N*′-2-pyridylbenzimidazol-2-ylidine)$(CO)_3$ (3.1).

Atmosphere: CO_2
Solvent: CH_3CN with 0.5 M PhOH
Electrolyte: 0.1 M $TBAPF_6$
Sample Concentration: 3.4 mmol

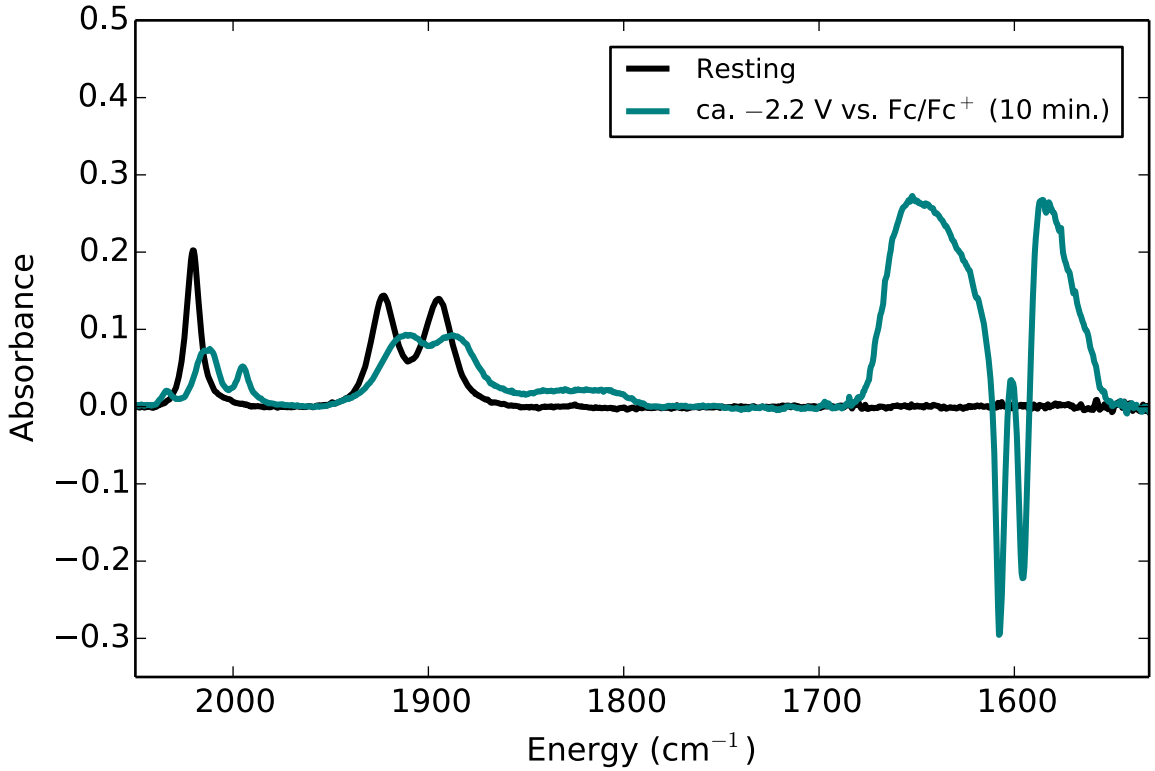

Note: Spectra are solvent subtracted such that negative absorbance indicates species consumption. PhOH (1654 and 1587 cm^{-1}); PhO (1587 cm^{-1}); and H_2O (1654 cm^{-1}). Assignments from *Inorg. Chem.* **2015**, 54, 8849-8853.

S3.3.2 ReCl(*N*-methyl-*N*′-2-pyrimidylbenzimidazol-2-ylidine)$(CO)_3$ (3.2).

Atmosphere: CO_2
Solvent: CH_3CN with 0.5 M PhOH
Electrolyte: 0.1 M $TBAPF_6$
Sample Concentration: 2.5 mmol

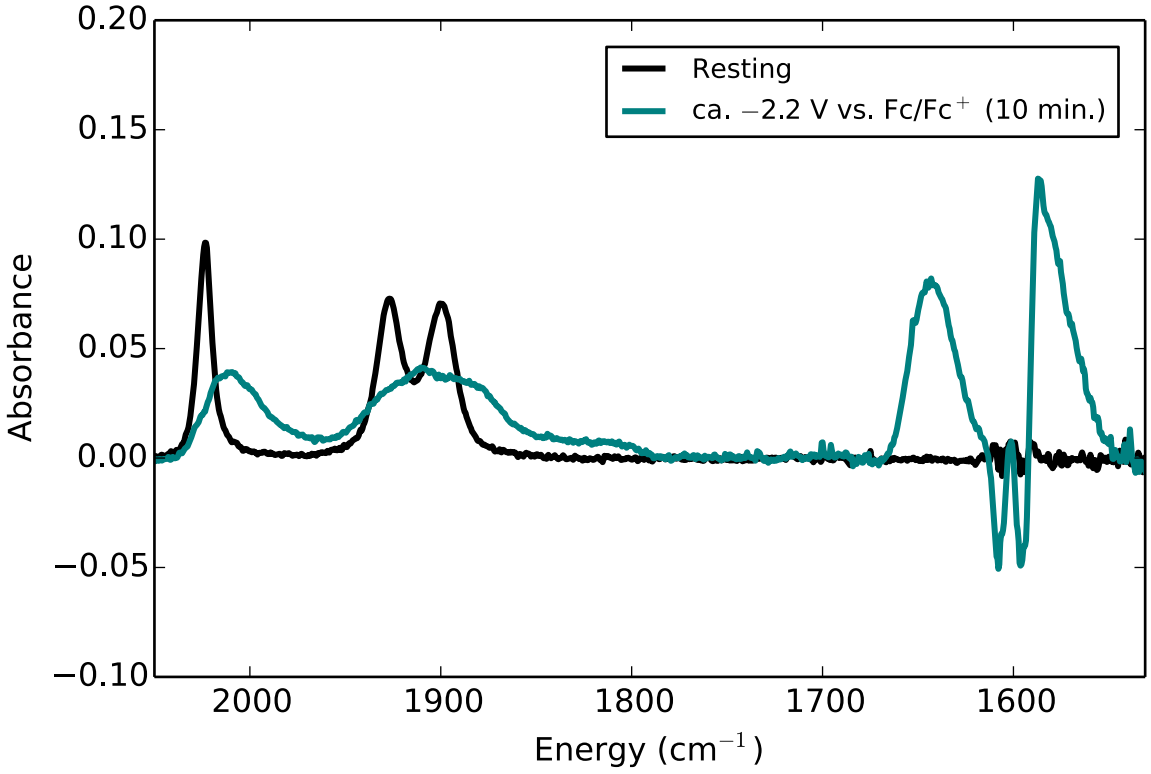

Note: Spectra are solvent subtracted such that negative absorbance indicates species consumption. PhOH (1654 and 1587 cm^{-1}); PhO (1587 cm^{-1}); and H_2O (1654 cm^{-1}). Assignments from *Inorg. Chem.* **2015**, 54, 8849-8853.

S3.4 DATA FROM TITRATIONS WITH TETRABUTYLAMMONIUM CHLORIDE (TBACl)

S3.4.1 ReCl(*N*-methyl-*N*′-2-pyridylbenzimidazol-2-ylidine)$(CO)_3$ (3.1).

Atmosphere: Ar
Solvent: CH_3CN
Electrolyte: 0.1 M $TBAPF_6$
Sample Concentration: 0.5 mmol

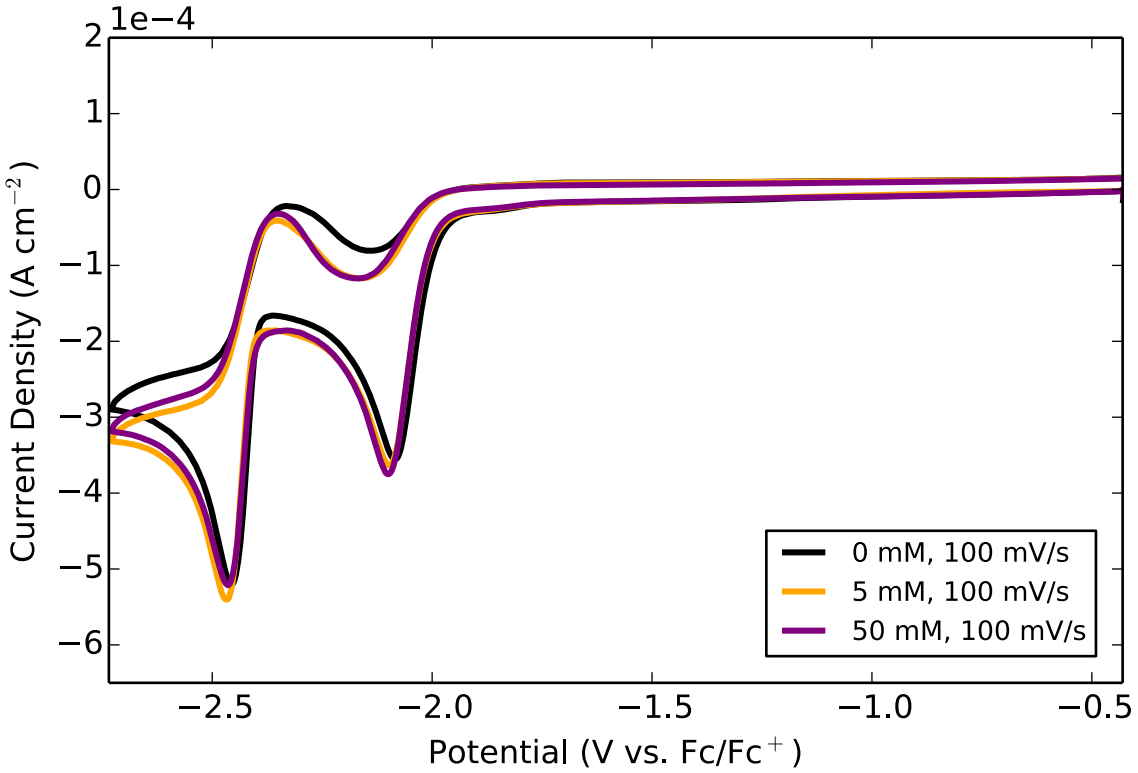

S3.4.2 ReCl(*N*-methyl-*N*′-2-pyrimidylbenzimidazol-2-ylidine)$(CO)_3$ (3.2).

Atmosphere: Ar
Solvent: CH_3CN
Electrolyte: 0.1 M $TBAPF_6$
Sample Concentration: 0.5 mmol

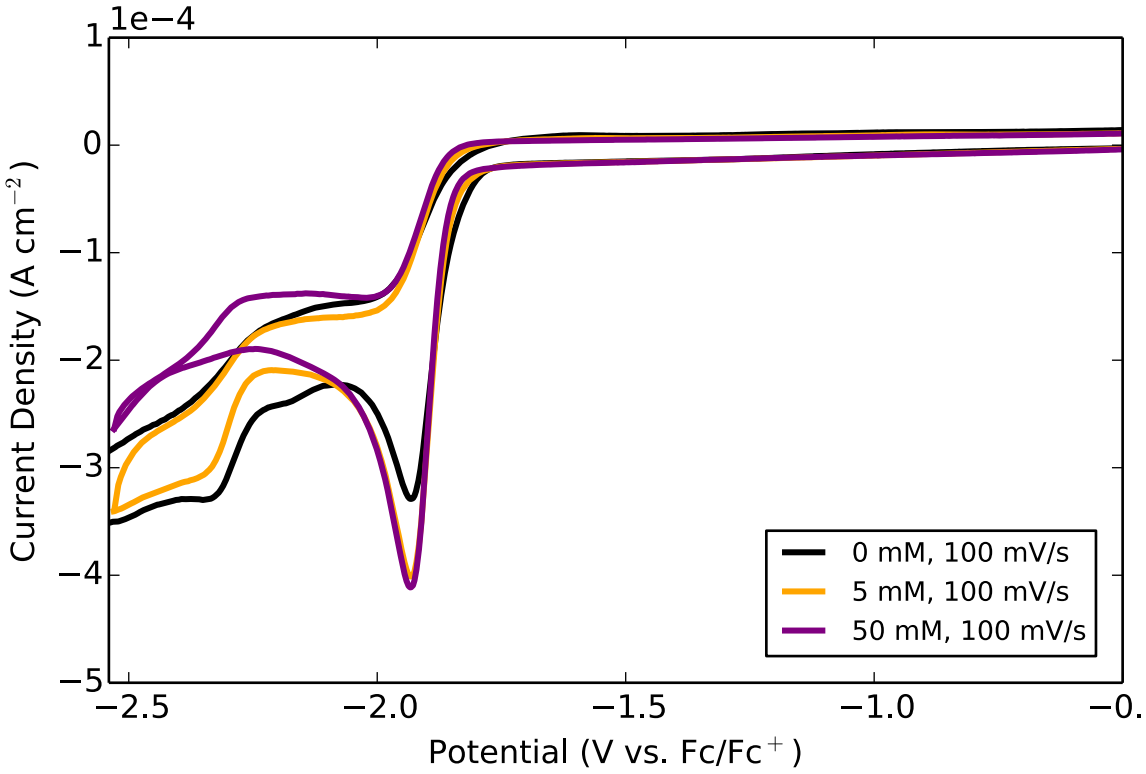

CHAPTER 4

MANGANESE(I)-NHC ELECTROCATALYSTS: INCREASING π ACIDITY LOWERS THE REDUCTION POTENTIAL AND INCREASES THE TOURNOVER FREQUNCY FOR CO_2 REDUCTION[2]

[2] Stanton III, C. J.; Vandezande, J. E.; Majetich, G. F.; Schaefer III, H. F.; Agarwal, J., Mn-NHC Electrocatalysts: Increasing π Acidity Lowers the Reduction Potential and Increases the Turnover Frequency for CO_2 Reduction. *Inorganic Chemistry* **2016**, *55* (19), 9509-9512.

ABSTRACT

A new manganese(I) *N*-heterocyclic carbene electrocatalyst containing a benzimidazole pyrimidine-based ligand is reported for the two-electron conversion of CO_2. The increased π acidity of pyrimidine shifts the two-electron reduction to −1.77 V vs Fc/Fc^+, 70 mV more positive than that for $MnBr(2,2'\text{-bipyridine})(CO)_3$; increased catalytic current enhancement is also observed (5.2× vs 2.1×). Theoretical analyses suggest that this heightened activity may follow from the preference for a reduction-first dehydroxylation mechanism.

INTRODUCTION

Manganese and rhenium tricarbonyl complexes containing NHC–aryl ligands (NHC = *N*-heterocyclic carbene) have recently emerged as capable catalysts for mediating the two-electron reduction of CO_2.[1-5] These compounds hold promise because the redox-active, NHC–aryl backbone may be built modularly, permitting iterative optimization. For example, NHC precursors (e.g., imidazole) may be combined with a myriad of commercially available heteroaryl compounds[6] to tune the electronic structure of the final complex. One strategy that has been employed by our group[1, 4] is to increase the π acidity of the NHC–aryl ligand in order to reduce the catalyst overpotential. In principle, this may be achieved by (i) extending the π framework of the NHC, such as through benzoannulation,[1, 7] (ii) utilizing π-acidic heteroaryl moieties (e.g., azines),[4, 8, 9] or, (iii) employing electron-withdrawing groups.[3, 5, 10] Indeed, the latter approach has been used to tune related iron porphyrin systems.[11-13]

From the standpoint of rational design, the merit in adjusting the π acidity follows from the electronic structure of group-VII NHC compounds. Specifically, for Re-NHC electrocatalysts, the composition of the lowest unoccupied molecular orbital (LUMO) is largely comprised of the

lowest-lying π* molecular orbital of the redox-active ligand–over 80%.[4] Lowering the energy of the LUMO directly affects the reduction potential because less electromotive force is required to move the Fermi level of the electrode above this unoccupied state.[14] As such, modulating the energy of the π* orbitals within the NHC–aryl framework translates into a change in the overpotential.

Previously, we reported two manganese(I) electrocatalysts with NHC–aryl ligands constructed from pyridine and either imidazole or benzimidazole; a decrease in the overpotential of 110 mV was realized after benzoannulation.[1] Aligned with our recent work with rhenium,[4] pyrimidine is utilized in this research. Note that, compared to pyridine, the π* molecular orbital energies of pyrimidine are reduced as a result of nitrogen-atom substitution because nitrogen is more electronegative and possesses lower-energy valence orbitals.[8, 15] This effect, relative to benzene, is illustrated in Figure 4.1. We report here that, compared to a benzimidazole–pyridine based catalyst, MnBr(*N*-ethyl-*N*′-2-pyridylbenzimidazol-2-ylidene)$(CO)_3$ (**4.1**),[2] the pyrimidine analogue, MnBr(*N*-ethyl-*N*′-2-pyrimidylbenzimidazol-2-ylidene)$(CO)_3$ (**4.2**), displays a 160 mV lower overpotential *and* a ca. 3× greater catalytic current enhancement (*vide infra*).

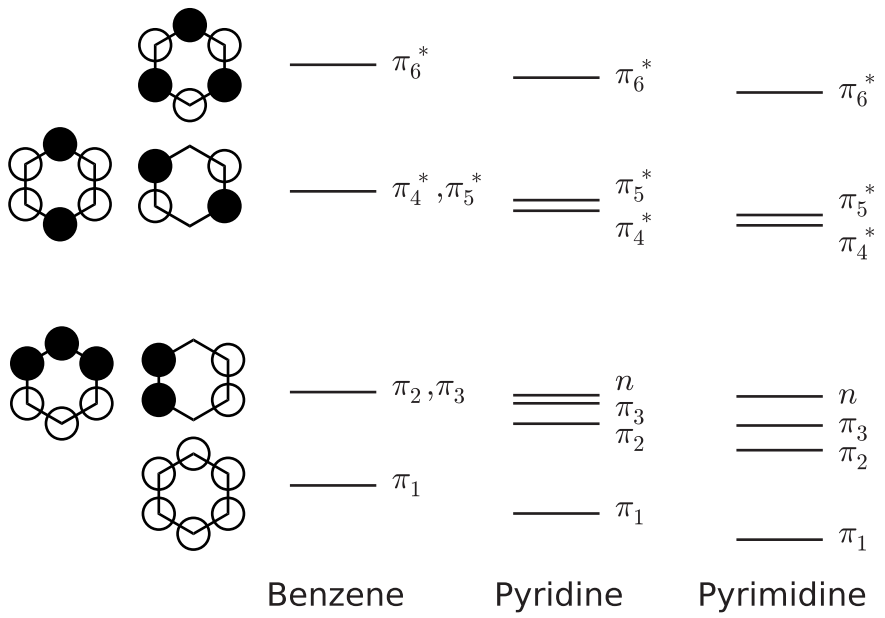

Figure 4.1: Select Molecular Orbitals (Ordered by Energy) For the Listed Compounds From B3LYP/def2-TZVP Computations.

RESULTS AND DISCUSSION

Compound **4.2** was constructed from $MnBr(CO)_5$ and *N*-ethyl-*N*′-2-pyrimidylbenzimidazol-2-ylidene (37% yield) and verified with ^{1}H and ^{13}C NMR and Fourier-transform infrared spectroscopies (see S4.SI, pp 182-185). Single crystals suitable for X-ray analysis were grown from the slow diffusion of hexanes into a solution of **2** in dichloromethane (Figure 4.2). The resolved structure shows one axial and two equatorial carbonyl ligands, consistent with the expected *facial* arrangement. Using theory (BP86/def2-TZVP), we predict that the LUMO energy of complex **4.2** lies 4.2 kcal mol^{-1} lower than that of **4.1**, aligned with the aforementioned discussion.

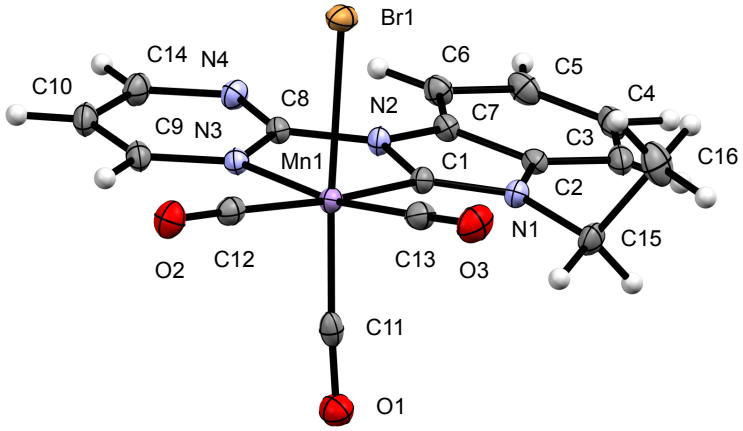

Figure 4.2: X-ray Crystal Structure of **4.2** with Ellipsoids Set at the 50% Probability Level.

Cyclic voltammograms of Mn(I)-complexes **4.1** and **4.2** recorded under argon in dry acetonitrile (MeCN) with 0.1 M tetrabutylammonium perchlorate (TBAP) supporting electrolyte are shown in figures 4.3 (complex **4.1**) and 4.4 (complex **4.2**). At 100 mV s^{-1}, **4.1** displays a single reduction wave at −1.93 V vs Fc/Fc^{+} (Fc = ferrocene) (Figure 4.3). This feature was previously assigned as a two-electron process that furnishes an anion lacking the axial bromide, $[Mn(Et\text{-}BI\text{-}Py)(CO)_3]^{-}$.[1] To confirm that two electrons are passed at this potential, we recorded additional voltammograms using a rotating-disk electrode (100–2500 rpm) and a microelectrode (r = 6.5 μm); see figure 4.5. The number of electrons (n) and diffusion coefficient (D) were calculated via the simultaneous solution of the Levich equation and the equation for limiting current (i_l) at a microelectrode.[14, 16] The values for n and D were determined to be 2.04 and 1.09×10^{-5} cm^2 s^{-1}, respectively confirming a two-electron process.

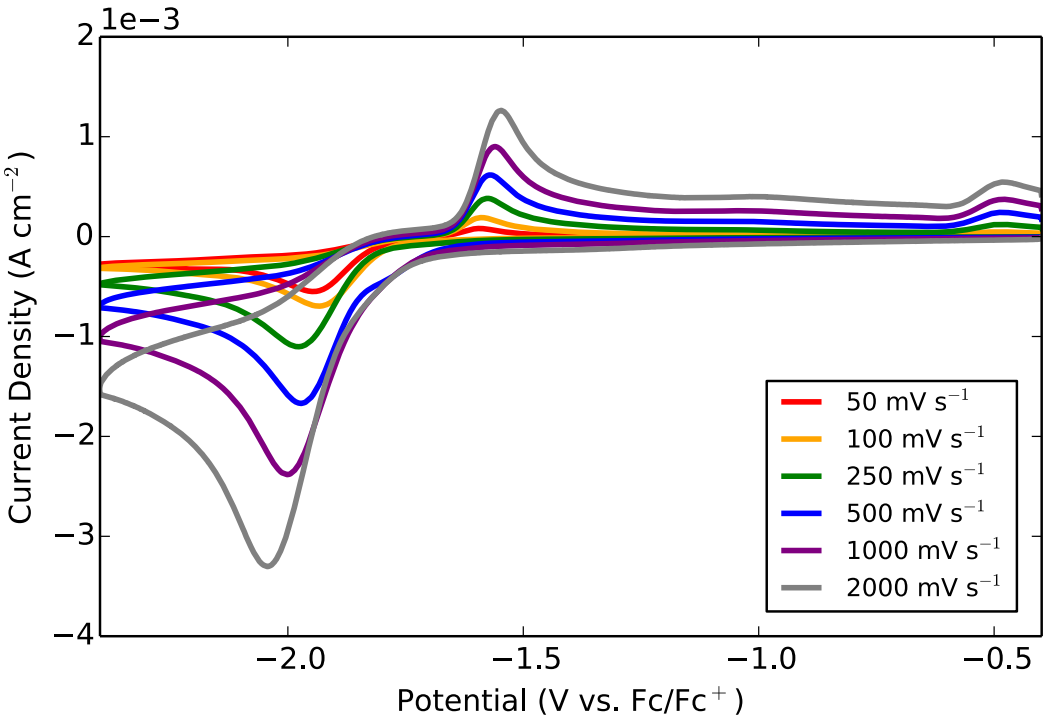

Figure 4.3: CV of 4.1 in MeCN with 0.1 M TBAP Supporting Electrolyte and Recorded Under Ar

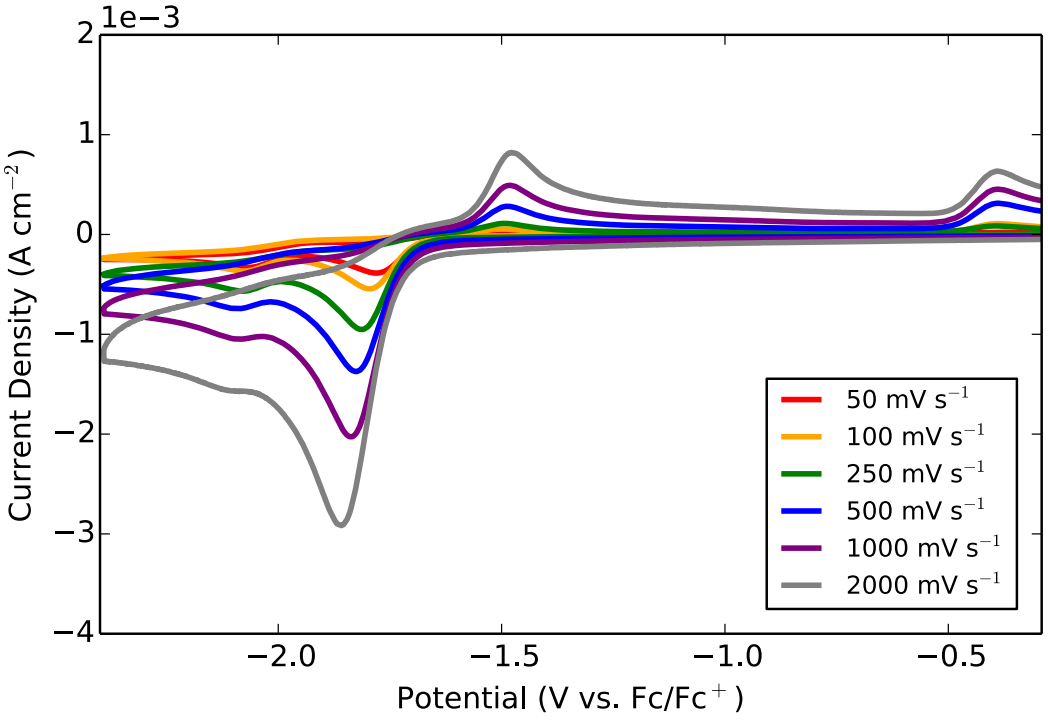

Figure 4.4: CV of **4.2** in MeCN with 0.1 M TBAP supporting electrolyte and recorded under Ar

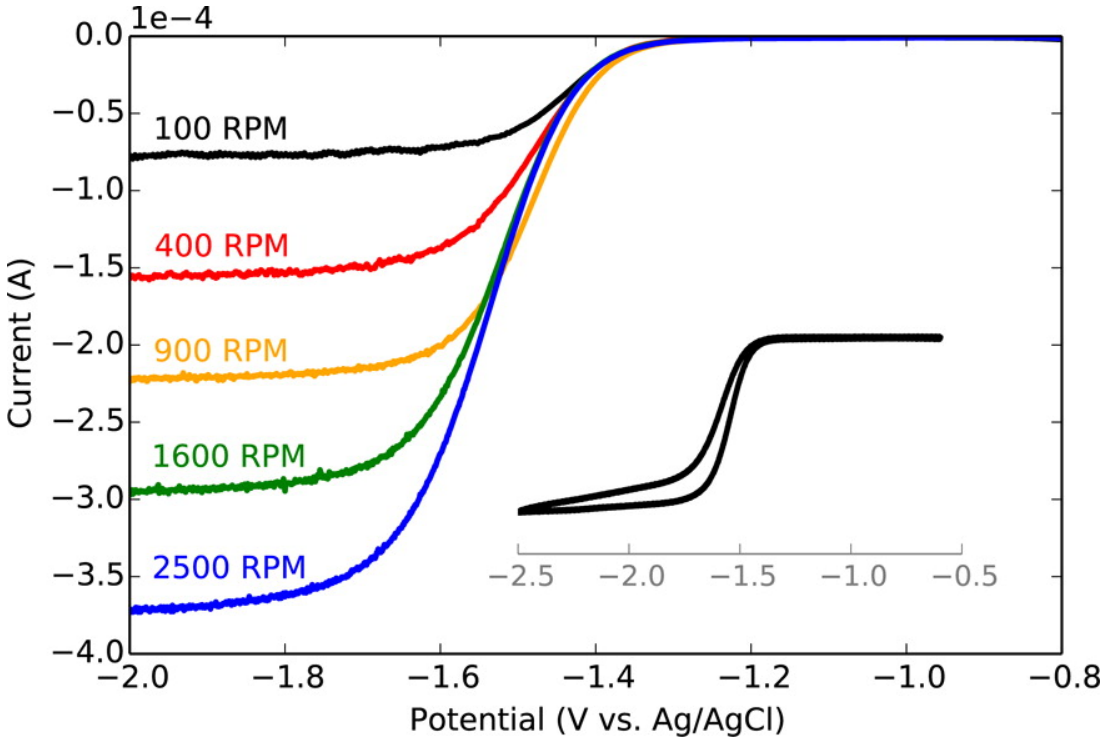

Figure 4.5: Rotating-disk voltammogram for **4.1** recorded at 10 mV s^{-1} under argon in dry MeCN with 0.1 M TBAP supporting electrolyte. Inset: Cyclic voltammogram recorded at 50 mV s^{-1} with a microelectrode (r = 6.5 μm).

On the return sweep, two oxidative waves appear: one at −1.59 V vs Fc/Fc^+, which we assign to the one-electron oxidation of $[Mn(Et\text{-}BI\text{-}Py)(CO)_3]^-$ to $[Mn(Et\text{-}BI\text{-}Py)(CO)_3]^\bullet$, and another at −0.49 V vs Fc/Fc^+, which we ascribe to the oxidation of $[Mn(Et\text{-}BI\text{-}Py)(CO)_3]_2$, a small quantity of which forms due to the dimerization of $[Mn(Et\text{-}BI\text{-}Py)(CO)_3]^\bullet$. Both of the present assignments were assisted by consideration of prior analysis.[17, 18]

Complex **4.2** displays two reduction features that appear at −1.77 and −2.08 V vs Fc/Fc^+ while scanning at 100 mV s^{-1} (Figure 4.4). Aligned with the increased π acidity of pyrimidine, the first reduction wave for **4.2** is shifted positively by 160 mV relative to **4.1** and is 70 mV more positive than the second electron reduction for $MnBr(bpy)(CO)_3$, where bpy = 2,2′-bipyridine. Similar to **4.1**, the first reduction is a two-electron feature ($D = 2.06 \times 10^{-6}$ cm^2 s^{-1}). We ascribe the second wave to the reduction of a limited quantity of dimer that forms at the first reduction.[1]

Two oxidative waves appear on the return sweep at −1.50 and −0.39 V vs Fc/Fc^+. These features are assigned as the same processes for **4.1**: one-electron oxidation of $[Mn(Et\text{-}BI\text{-}Pyrm)(CO)_3]^-$ and $[Mn(Et\text{-}BI\text{-}Pyrm)(CO)_3]_2$, respectively.

Under CO_2 saturation with added Brønsted acid (5% H_2O), **4.1** exhibits a 1.7× current enhancement at the potential of the first reduction relative to argon saturation (Figure 4.6). Compound **4.2** (Figure 4.8) displays a 5.2× enhancement under the same conditions, which is triple that of **1** and over double that observed for $MnBr(bpy)(CO)_3$ (2.1×; see S4.SI, pp 186). Using a published expression for the turnover frequency (TOF),[19, 20] we estimated TOF values for **1**, **2**, and $MnBr(bpy)(CO)_3$ as 4.5, 42.0, and 0.9 s^{-1}, respectively, noting the peak shape of the voltammograms in Figures 4.7 and 4.8.

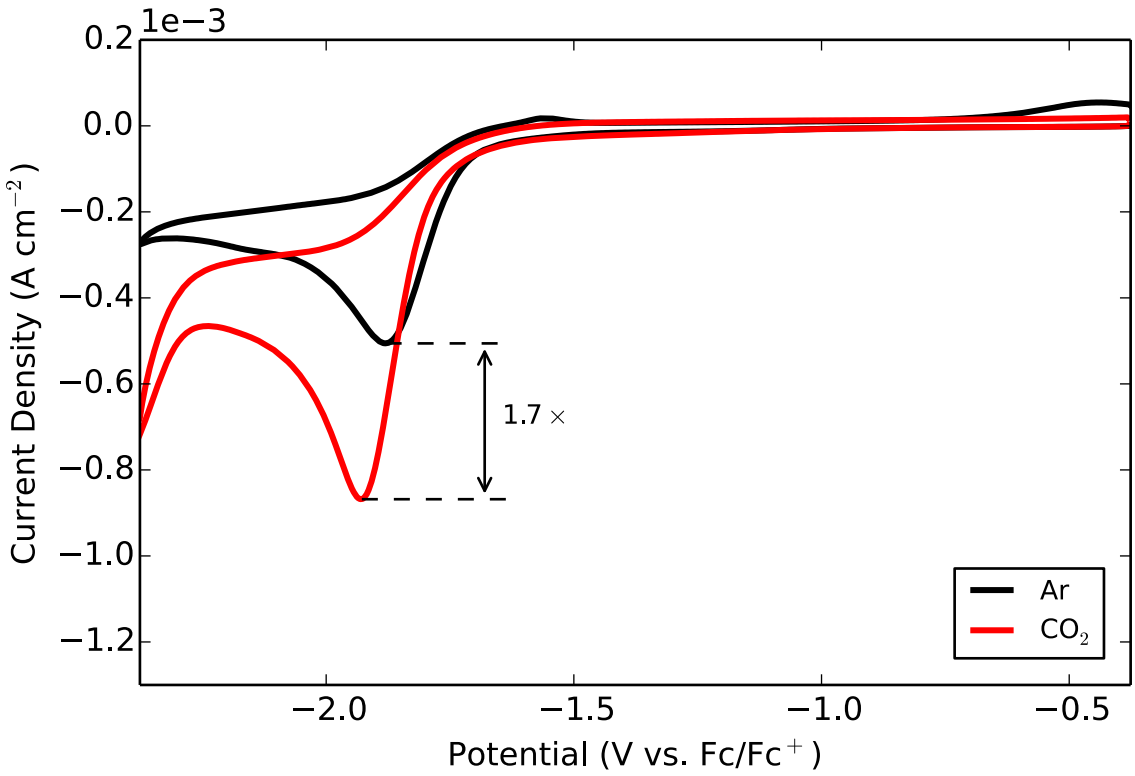

Figure 4.6: CV of **4.1** recorded at 100 mV s^{-1} under argon (black) and CO_2 (red) in wet (5% H_2O) MeCN. In the case of argon, added water was pH-adjusted to 3.7 with perchloric acid to match the pH under CO_2. Compound was loaded at a concentration of 1 mM.

On the preparative scale (Table 4.1), we find that $MnBr(bpy)(CO)_3$ displays a 73% Faradaic efficiency (FE) for CO production after passing 35 C (TON = 4) at ca. −1.75 V versus Ag/AgCl; compound **4.2** yielded an efficiency of 72%. In our laboratory, **4.1** utilized little charge beyond 20 C (FE_{CO} = 48%), but $MnBr(bpy)(CO)_3$ and **4.2** were capable of mediating catalysis beyond four turnovers with a diminishing rate of electron consumption. The quantification of H_2 was precluded by our choice of IR as a detection source, but H_2 formation could account for some of the Faradaic current. No additional carbon products were observed by NMR.

Table 4.1. Summary of Voltammetry and Electrolysis Data[a]

Complex	E_p (V)	i_{cat}/i_p	FE_{CO}	Q (C)
4.1[1]	−1.93	1.7	48%	20
4.2	−1.77	5.2	72%	35
$MnBr(bpy)(CO)_3$[17]	−1.84[4]	2.1	73%	35

[a]Potentials referenced to Fc/Fc^+; see the text for voltammetry conditions. CO production was determined by analyzing a 1 mL aliquot of the headspace after electrolysis with a long-path IR cell and then comparing it to a linear calibration curve of IR absorbances; a two-electron conversion is assumed for Faradaic efficiency calculations. Electrolyses were conducted at ca. –1.75 V vs Ag/AgCl.

To begin understanding the increased TOF observed for **4.2** relative to **4.1**, putative intermediates for both species were examined with theory. Prior theoretical work has established that, for $MnBr(bpy)(CO)_3$, heterolytic C–O bond fission in a $Mn(bpy)(CO)_3COOH$ hydroxycarbonyl intermediate is the rate-determining step for CO product formation.[9, 21-24] Bond cleavage may occur in $Mn(bpy)(CO)_3COOH$ or in the singly reduced analogue $[Mn(bpy)(CO)_3COOH]^{\bullet-}$ provided that a sufficiently negative potential is applied. Importantly, the activation energy for dehydroxylation is lower in the singly reduced intermediate.[9, 21]

With regard to **1** and **2**, relevant intermediates for the aforementioned transformations are shown in Scheme 4.1 and include a "protonation-first" pathway (**4.1-COOH** to **[4.1-CO]**$^{+}$ or **4.2-COOH** to **[4.2-CO]**$^{+}$) and a "reduction-first" pathway (**[4.1-COOH]**$^{\bullet-}$ to **[4.1-CO]**$^{\bullet}$ or **[4.2-COOH]**$^{\bullet-}$ to **[4.2-CO]**$^{\bullet}$). Lam et al. previously suggested that increasing the π acidity of bipyridine with nitrogen embedding, i.e., using bipyrimidine (bpyrm), yields a hydroxycarbonyl intermediate with a significantly diminished reduction potential. As a result, the faster, reduction-first pathway through [Mn(bpyrm)(CO)$_3$COOH]$^{\bullet-}$, may be favored, yielding an increased TOF.[9]

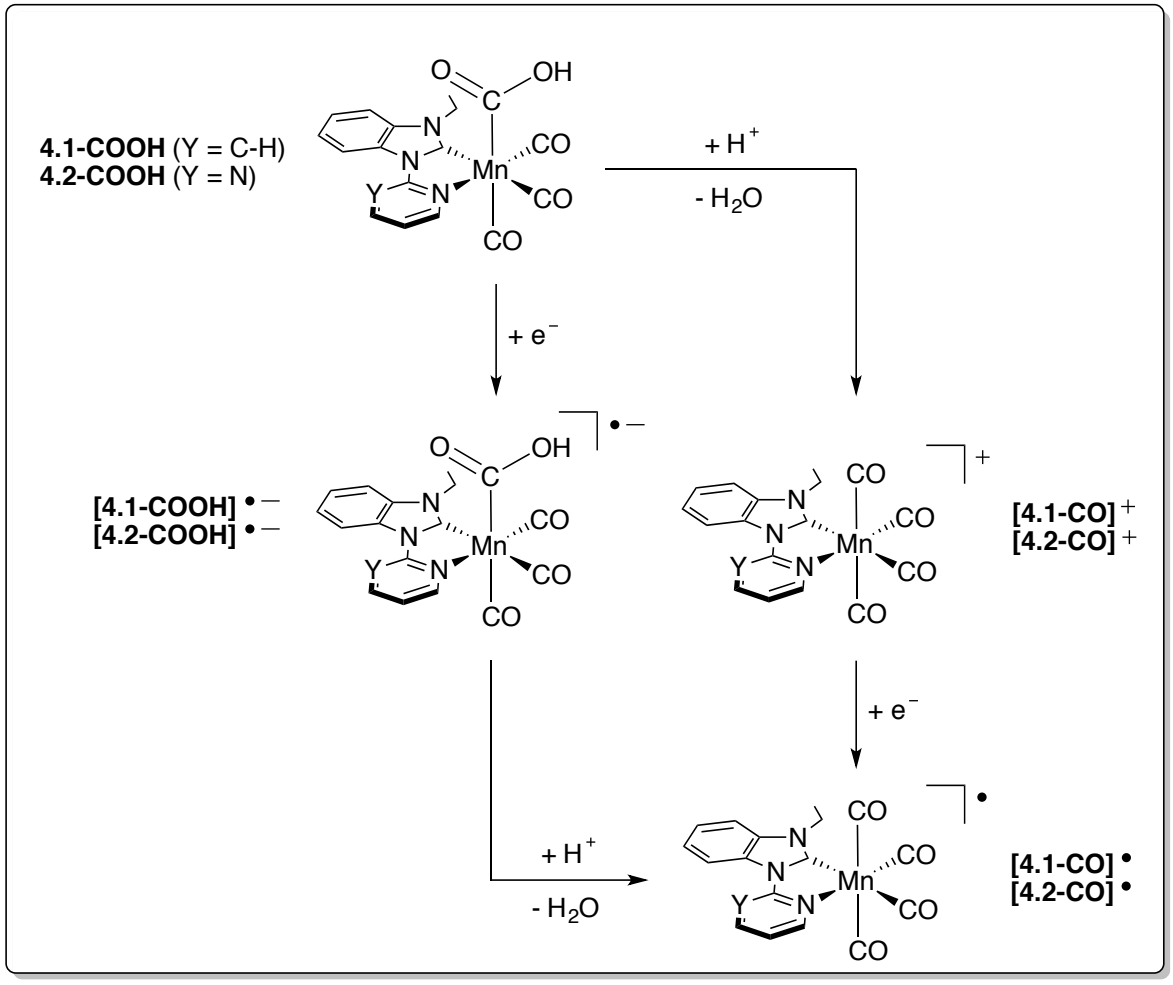

Scheme 4.1: Proposed Intermediates for C–O Bond Fission. See References 9, 21, 22

With theory, we predict that the reduction potential for **4.2-COOH** is shifted 260 mV positive relative to **4.2-COOH**. Furthermore, for **4.1** and **4.2**, the diabatic bond dissociation energies (BDEs)[25] for Mn–C(O)–OH separation are predicted to lower dramatically for the reduction-first pathway relative to the protonation-first mechanism: 71.3 and 72.4 kcal mol^{-1} for **4.1-COOH** and **4.2-COOH** vs 29.8 and 36.9 kcal mol^{-1} for **[4.1-COOH]$^{\bullet-}$** and **[4.1-COOH]$^{\bullet-}$**.

Under experimental conditions, the ability for **4.1** or **4.2** to convert CO_2 via the faster reduction first pathway depends on the reduction potential of the hydroxycarbonyl intermediate relative to the two-electron-reduction potential of the starting species. Given that the change in E_p is +160 mV (from **4.1** to **4.2**) and the predicted shift for **4.1-COOH** to **4.2-COOH** is +260 mV, **[4.2-COOH]$^{\bullet-}$** *should* form faster than **[4.1-COOH]$^{\bullet-}$** in solution. Taken together with our experimental observations, we tentatively suggest that **4.2** proceeds predominantly through the reduction-first pathway, while the rate of conversion for **4.1** is limited by the higher C–O BDE in the protonation first mechanism. Additional analyses, such as microkinetic simulations, are needed to bolster this postulation[21, 22] but are beyond the scope of this Communication.

CONCLUSIONS

In this research, we examined variation of the ligand π acidity as a tool for modulating the electronic properties of CO_2-reduction catalysts with NHC-based ligands. A new manganese(I) catalyst, **4.2**, is described that contains a NHC–aryl ligand built from benzimidazole and pyrimidine. This species possesses a lower LUMO energy relative to the previously reported pyridine analogue, shifting the two-electron reduction potential positive by 160 mV. Compared to MnBr(2,2′-bipyridine)$(CO)_3$, the reduction potential is 70 mV more positive, and over double the catalytic current enhancement is observed (5.2× vs 2.1×); nearly equal Faradaic efficiencies were

recorded on the preparative scale. Predicted reduction potentials for putative hydroxycarbonyl intermediates using theory suggest a 260 mV positive shift for pyrimidine, 100 mV more positive than the change in E_p. The improved current enhancement is tentatively suggested to result from the ability of the new pyrimidine catalyst to better access a reduction-first dihydroxylation pathway.

EXPERIMENTAL METHODS

General

All reagents were obtained from commercial suppliers and used as received unless otherwise noted. Reactions were performed using standard Schlenk-line techniques under an atmosphere of argon with minimal exposure to laboratory light. ^{1}H NMR spectra were recorded on a Varian Mercury Plus 400 MHz spectrometer and ^{13}C NMR spectra were recorded on an Agilent DD2 600 MHz spectrometer. NMR chemical shifts were referenced to the residual protio signal of the deuterated solvent. FTIR spectra were recorded on a Thermo Nicolet iS10 spectrophotometer using either a silicon ATR crystal or a 2.4-meter multi-pass gas cell.

Voltammetry

All voltammetry was performed with a CH Instruments 601E potentiostat (Austin, TX). Cyclic voltammetry measurements were recorded in a three-neck, single-compartment glass cell with Ace #7 joints. A 3 mm diameter glassy carbon electrode (BASi) was utilized as the working electrode. A 13 μm glassy carbon electrode (BASi) was employed for microelectrode experiments. For all measurements, the counter electrode was a platinum wire and the reference electrode was a silver/silver chloride (Ag/AgCl) electrode separated from solution by a Teflon tip. The supporting

electrolyte was composed of 0.1 M tetrabutylammonium perchlorate (TBAP) dissolved in dry MeCN.[4] The electrolyte was purged with either Ar or CO_2 before data were recorded. Cyclic voltammetry measurements were referenced to an internal ferrocene standard (Fc/Fc^+), and compounds were loaded at a concentration of 1 mM. Rotating disk experiments were conducted with a 3 mm diameter glassy carbon electrode (Pine) in an 100 mL three-necked with approximately 80 mL of electrolyte. For these experiments, compounds were loaded at a concentration of 2 mM.

Preparative-Scale Electrolyses

Preparative-scale electrolyses were conducted in a custom glass H-cell (approx. 80 mL) with Ace #7 and GL14 joints (Adams & Chittenden, see below).

A glassy carbon rod (6 mm diameter, Alfa Aesar) was used as the working electrode. The counter electrode was a platinum wire and the reference electrode was a silver/silver chloride (Ag/AgCl) electrode separated from solution by a Teflon tip. The supporting electrolyte was composed of

0.1M tetrabutylammonium perchlorate (TBAP) dissolved in MeCN with 5 % H_2O. All electrolyses were performed with vigorous stirring. At the completion of a run, 1 mL of headspace was sampled with a gas-tight syringe (Hamilton), diluted with CO2, then injected into an evacuated 100 mL long-path (2.4 m) infrared gas cell (Pike). Faradaic efficiencies for CO formation were subsequently calculated from a linear fit (R^2 = 0.995) of infrared absorbances from known CO volumes (see below).

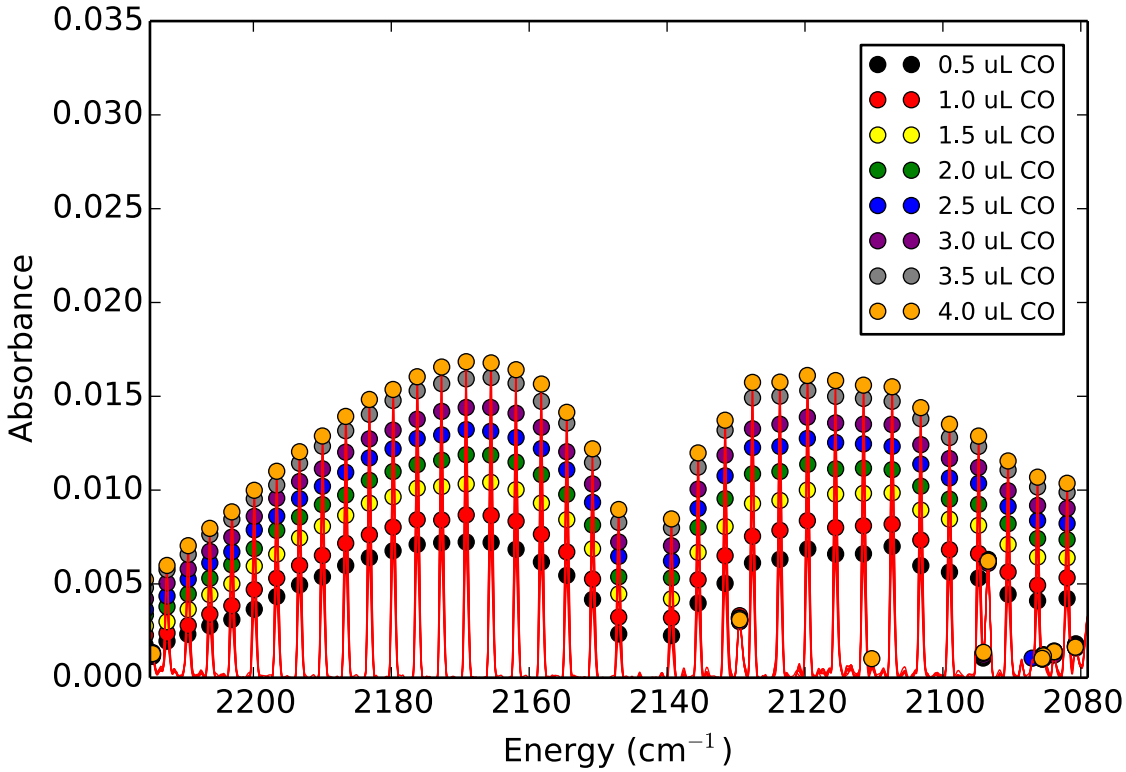

Synthesis

Preparation of [*N*-ethyl-*N′*-2-pyrimidylbenzimidazolium]$^+$ Br$^-$ (L4.2).

i. Coupling Benzimidazole and 2-Chloropyrimidine:

Under an atmosphere of argon, a ask was charged with benzimidazole (5.00 g, 42.3 mmol), potassium carbonate (3.90 g, 28.2 mmol), and 2-chloropyrimidine (1.62 g, 14.1 mmol). The

reaction mixture was stirred at 160 ºC for 18 hours, then allowed to cool to room temperature. The resulting solution was diluted with DCM (200 mL) and washed with H_2O (200 mL). The aqueous layer was then extracted with additional DCM (2 x 100 mL), and the combined organic extracts were washed with 10% NaOH until benzimidazole did not appear by TLC (3 x 100 mL). The organic extract was then washed with brine (200 mL) and dried over anhydrous MgSO4, before filtration to remove the drying agent. Concentration under reduced pressure using a rotary evaporator gave *N,N′*-2-pyrimidylbenzimidazole as an off-white solid (2.00 g, 72%).

ii. Ethylating N,N′-2-pyrimidylbenzimidazolium:

The *N,N′*-2-pyrimidylbenzimidazole (1.50 g, 7.6 mmol) intermediate was dissolved in 40.0 mL of CH_3CN under an argon atmosphere. Bromoethane (5.70 mL, 76.5 mmol) was added and the reaction was stirred at 100 ºC in a sealed tube for 48 h. After cooling to room temperature, the mixture was concentrated under reduced pressure using a rotary evaporator to afford an off-white solid. Subsequent recrystallization from CH_3CN/Et_2O gave an off-white solid, [*N*-ethyl-*N′*-2-pyrimidylbenzimidazolium]$^+$ Br^-, that was collected by vacuum filtration (2.10 g, 90%). ^{1}H NMR (DMSO-d_6, 20 ºC): δ 10.73 (1H, s), 9.16 (2H, d, J=4Hz), 8.87-8.84 (1H, m), 8.26-8.23 (1H, m), 7.85-7.80 (3H, m), 4.73 (2H, q, J=8Hz), 1.60 (3H, t, J=8Hz).

Preparation of MnBr(*N*-ethyl- *N′*-2-pyrimidylbenzimidazol-2-ylidine)$(CO)_3$ (4.2).

$MnBr(CO)_5$ (0.56 g, 2.1 mmol) and [*N*-ethyl- *N′*-2-pyrimidylbenzimidazolium]$^+Br^-$ (0.50 g, 1.6 mmol) were suspended in 25 mL of THF and sparged with argon for 30 minutes. Potassium *t*-butoxide (0.23 g, 2.1 mmol) was added to the stirring mixture, which was then heated at 60 ºC under argon for 15 h. After cooling to room temperature, THF was removed under reduced pressure using a rotary evaporator. The resulting solid residue was triturated with Et_2O to remove unreacted $MnBr(CO)_5$. Afterwards, the crude product was purified by column chromatography

(silica gel; gradient, 100% DCM to 95% DCM/5% acetone) and recrystallization (acetone/Et_2O) to afford the product as a bright yellow-orange solid (0.27 g, 37%). IR ν_{CO} (ATR, cm^{-1}): 2017, 1930, 1889. ^1H NMR (DMSO-d_6, 20 ºC): δ 9.37-9.35 (1H, m), 9.12-9.10 (1H, m), 8.58 (1H, d, J = 4Hz), 7.98 (1H, d, J = 4Hz), 7.62-7.57 (3H, m), 4.81(2H, q, J = 8Hz), 1.61 (3H, t, J = 8Hz). ^{13}C NMR (DMSO-d_6, 25 ºC): δ 225.18, 220.59, 217.08, 214.62, 163.66, 160.65, 158.99, 135.98, 131.15, 125.84, 125.50, 119.55, 114.46, 111.92, 43.35, 15.38.

REFERENCES

1. Agarwal, J.; Shaw, T. W.; Stanton, C. J.; Majetich, G. F.; Bocarsly, A. B.; Schaefer, H. F., NHC-Containing Manganese(I) Electrocatalysts for the Two-Electron Reduction of CO_2. *Angewandte Chemie International Edition* **2014**, *53* (20), 5152-5155.

2. Agarwal, J.; Stanton III, C. J.; Shaw, T. W.; Vandezande, J. E.; Majetich, G. F.; Bocarsly, A. B.; Schaefer Iii, H. F., Exploring the Effect of Axial Ligand Substitution (X = Br, NCS, CN) on the Photodecomposition and Electrochemical Activity of $[MnX(N\text{-}C)(CO)_3]$ Complexes. *Dalton Transactions* **2015**, *44* (5), 2122-2131.

3. Huckaba, A. J.; Sharpe, E. A.; Delcamp, J. H., Photocatalytic Reduction of CO_2 with Re-Pyridyl-NHCs. *Inorganic Chemistry* **2016**, *55* (2), 682-690.

4. Stanton III, C. J.; Machan, C. W.; Vandezande, J. E.; Jin, T.; Majetich, G. F.; Schaefer III, H. F.; Kubiak, C. P.; Li, G.; Agarwal, J., Re(I) NHC Complexes for Electrocatalytic Conversion of CO_2. *Inorganic Chemistry* **2016**, *55* (6), 3136-3144.

5. Liyanage, N. P.; Dulaney, H. A.; Huckaba, A. J.; Jurss, J. W.; Delcamp, J. H., Electrocatalytic Reduction of CO_2 to CO With Re-Pyridyl-NHCs: Proton Source Influence on Rates and Product Selectivities. *Inorganic Chemistry* **2016**.

6. Raba, A.; Anneser, M. R.; Jantke, D.; Cokoja, M.; Herrmann, W. A.; Kühn, F. E., Facile and Scalable Preparation of 2-Imidazolylpyridines. *Tetrahedron Letters* **2013**, *54* (26), 3384-3387.

7. Back, O.; Henry-Ellinger, M.; Martin, C. D.; Martin, D.; Bertrand, G., ^{31}P NMR Chemical Shifts of Carbene–Phosphinidene Adducts as an Indicator of the π-Accepting Properties of Carbenes. *Angewandte Chemie International Edition* **2013**, *52* (10), 2939-2943.

8. Wiberg, K. B.; Nakaji, D.; Breneman, C. M., Azines. A Theoretical Study of π-Electron Delocalization. *Journal of the American Chemical Society* **1989**, *111* (12), 4178-4190.

9. Lam, Y. C.; Nielsen, R. J.; Gray, H. B.; Goddard, W. A., A Mn Bipyrimidine Catalyst Predicted To Reduce CO_2 at Lower Overpotential. *ACS Catalysis* **2015**, *5* (4), 2521-2528.

10. Liske, A.; Verlinden, K.; Buhl, H.; Schaper, K.; Ganter, C., Determining the π-Acceptor Properties of *N*-Heterocyclic Carbenes by Measuring the ^{77}Se NMR Chemical Shifts of Their Selenium Adducts. *Organometallics* **2013**, *32* (19), 5269-5272.

11. Costentin, C.; Robert, M.; Savéant, J.-M., Current Issues in Molecular Catalysis Illustrated by Iron Porphyrins as Catalysts of the CO_2-to-CO Electrochemical Conversion. *Accounts of Chemical Research* **2015**, *48* (12), 2996-3006.

12. Costentin, C.; Passard, G.; Robert, M.; Savéant, J.-M., Pendant Acid–Base Groups in Molecular Catalysts: H-Bond Promoters or Proton Relays? Mechanisms of the Conversion of CO_2 to CO by Electrogenerated Iron(0) Porphyrins Bearing Prepositioned Phenol Functionalities. *Journal of the American Chemical Society* **2014**, *136* (33), 11821-11829.

13. Costentin, C.; Drouet, S.; Robert, M.; Savéant, J.-M., A Local Proton Source Enhances CO_2 Electroreduction to CO by a Molecular Fe Catalyst. *Science* **2012**, *338* (6103), 90-94.

14. Bard, A. J.; Faulkner, L. R., *Electrochemical Methods: Fundamentals and Applications*. John Wiley & Sons: New York, 2001.

15. Harris, D. C.; Bertolucci, M. D., *Symmetry and Spectroscopy: An Introduction to Vibrational and Electronic Spectroscopy*. Oxford University Press: New York, 1978.

16. Baur, J. E.; Wightman, R. M., Diffusion Coefficients Determined with Microelectrodes. *Journal of Electroanalytical Chemistry and Interfacial Electrochemistry* **1991**, *305* (1), 73-81.

17. Bourrez, M.; Molton, F.; Chardon-Noblat, S.; Deronzier, A., [Mn(bipyridyl)$(CO)_3$Br]: An Abundant Metal Carbonyl Complex as Efficient Electrocatalyst for CO_2 Reduction. *Angewandte Chemie International Edition* **2011**, *123* (42), 10077-10080.

18. Machan, C. W.; Stanton III, C. J.; Vandezande, J. E.; Majetich, G. F.; Schaefer III, H. F.; Kubiak, C. P.; Agarwal, J., Electrocatalytic Reduction of Carbon Dioxide by Mn(CN)(2,2′-bipyridine)$(CO)_3$: CN Coordination Alters Mechanism. *Inorganic Chemistry* **2015**, *54* (17), 8849-8856.

19. Sampson, M. D.; Kubiak, C. P., Manganese Electrocatalysts with Bulky Bipyridine Ligands: Utilizing Lewis Acids To Promote Carbon Dioxide Reduction at Low Overpotentials. *Journal of the American Chemical Society* **2016**, *138* (4), 1386-1393.

20. Smieja, J. M.; Sampson, M. D.; Grice, K. A.; Benson, E. E.; Froehlich, J. D.; Kubiak, C. P., Manganese as a Substitute for Rhenium in CO_2 Reduction Catalysts: The Importance of Acids. *Inorganic Chemistry* **2013**, *52* (5), 2484-2491.

21. Riplinger, C.; Sampson, M. D.; Ritzmann, A. M.; Kubiak, C. P.; Carter, E. A., Mechanistic Contrasts Between Manganese and Rhenium Bipyridine Electrocatalysts for the Reduction of Carbon Dioxide. *Journal of the American Chemical Society* **2014**, *136* (46), 16285-16298.

22. Riplinger, C.; Carter, E. A., Influence of Weak Brønsted Acids on Electrocatalytic CO_2 Reduction by Manganese and Rhenium Bipyridine Catalysts. *ACS Catalysis* **2015**, *5* (2), 900-908.

23. Agarwal, J.; Shaw, T. W.; Schaefer III, H. F.; Bocarsly, A. B., Design of a Catalytic Active Site for Electrochemical CO_2 Reduction with Mn(I)-Tricarbonyl Species. *Inorganic Chemistry* **2015**, *54* (11), 5285-5294.

24. Rawat, K. S.; Mahata, A.; Choudhuri, I.; Pathak, B., *N*-Heterocylic Carbene-Based Mn Electrocatalyst for Two-Electron CO_2 Reduction over Proton Reduction. *The Journal of Physical Chemistry C* **2016**, *120* (16), 8821-8831.

25. Grant, D. J.; Matus, M. H.; Switzer, J. R.; Dixon, D. A.; Francisco, J. S.; Christe, K. O., Bond Dissociation Energies in Second-Row Compounds. *The Journal of Physical Chemistry A* **2008**, *112* (14), 3145-3156.

S4. SUPPORTING INFORMATION

S4.1 SELECTED SPECTRA

S4.1.1 ^{1}H NMR of [*N*-ethyl-*N*′-2-pyrimidylbenzimidazolium]$^{+}$ Br^{-} (L4.2).

Temperature: 20 ˚C
Solvent: DMSO-d_6

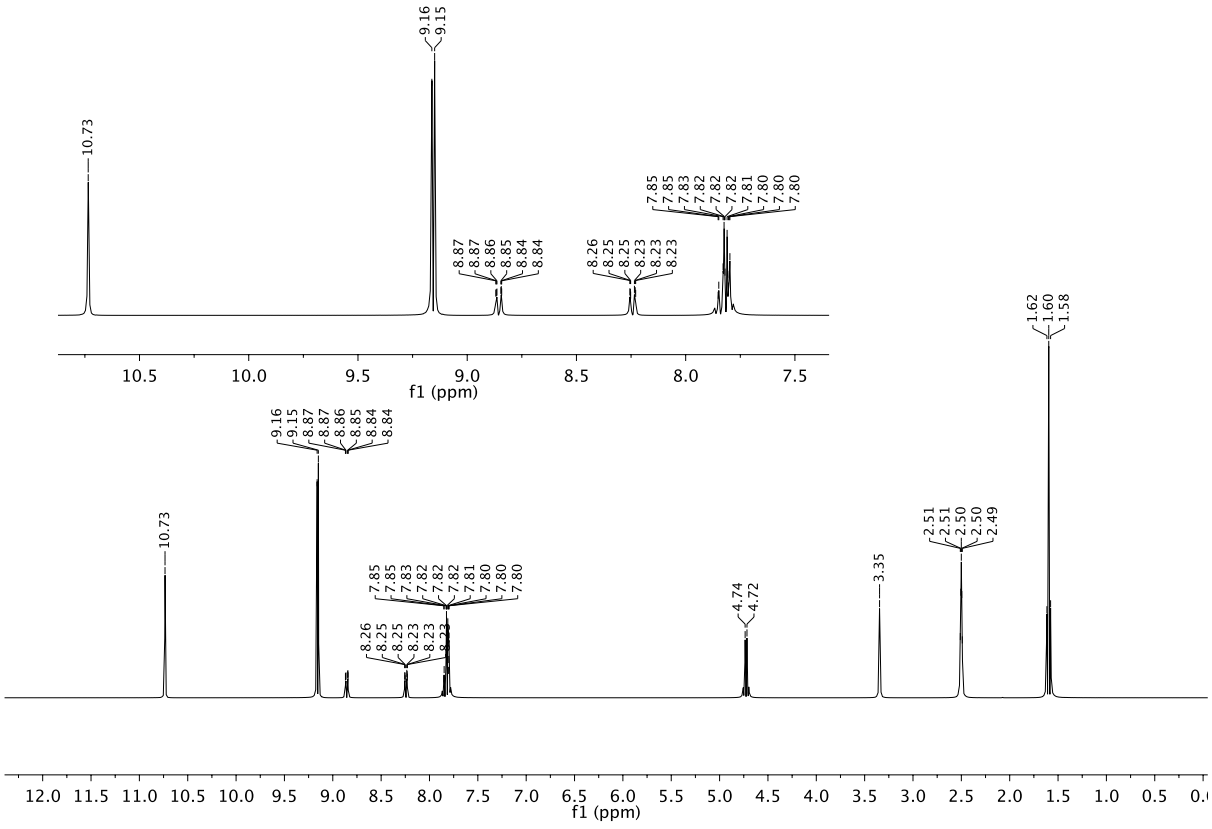

Note: The peak at 3.35 ppm is assigned to water, and the peak at 2.50 ppm to dimethyl sulfoxide.

S4.1.2 ^{1}H NMR of MnBr(*N*-ethyl- *N′*-2-pyrimidylbenzimidazol-2-ylidine)$(CO)_3$ (4.2).

Temperature: 20 ˚C
Solvent: DMSO-d_6

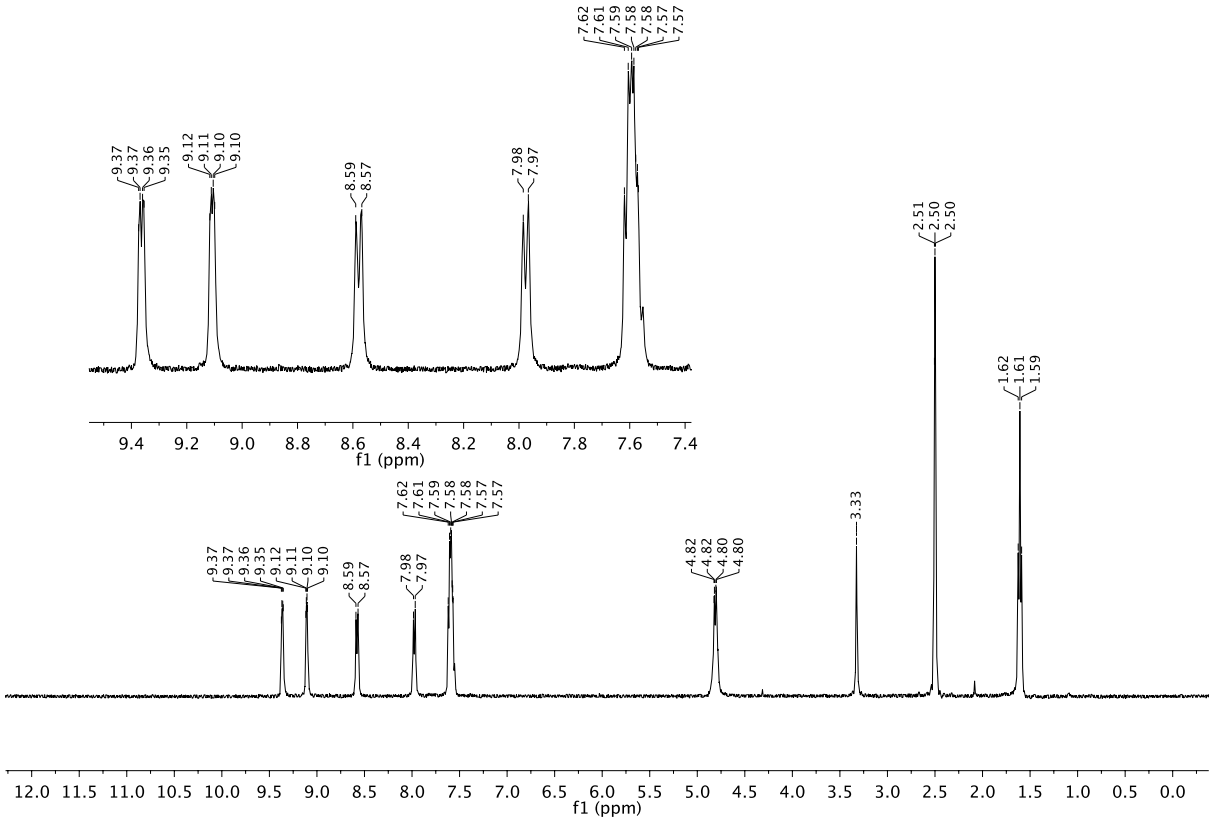

Note: The peak at 3.33 ppm is assigned to water, and the peak at 2.50 ppm to dimethyl sulfoxide.

S4.1.3 ^{13}C NMR of MnBr(*N*-ethyl- *N′*-2-pyrimidylbenzimidazol-2-ylidine)$(CO)_3$ (4.2).

Temperature: 25 ˚C
Solvent: DMSO-d_6

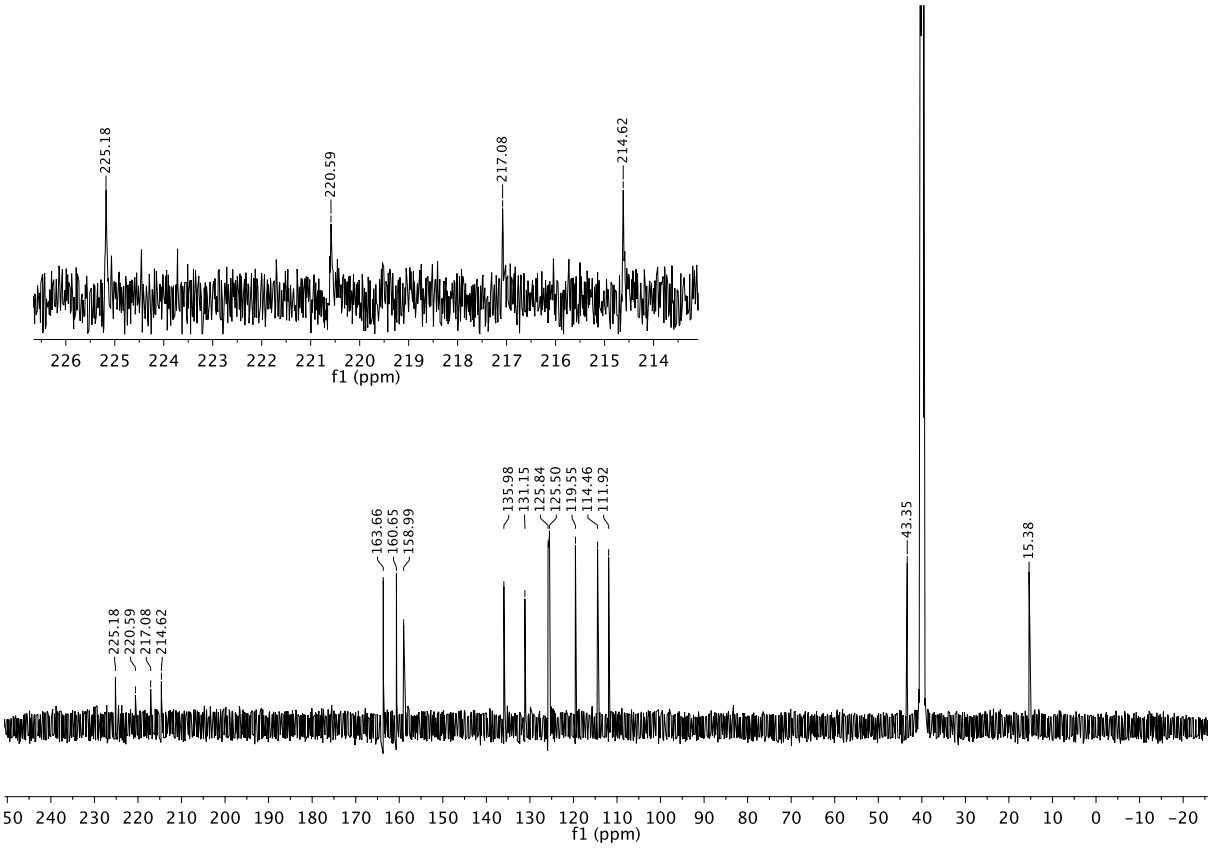

S4.1.4 FTIR of MnBr(*N*-ethyl- *N'*-2-pyrimidylbenzimidazol-2-ylidine)$(CO)_3$ (4.2).

Method: ATR (Silicon Crystal)

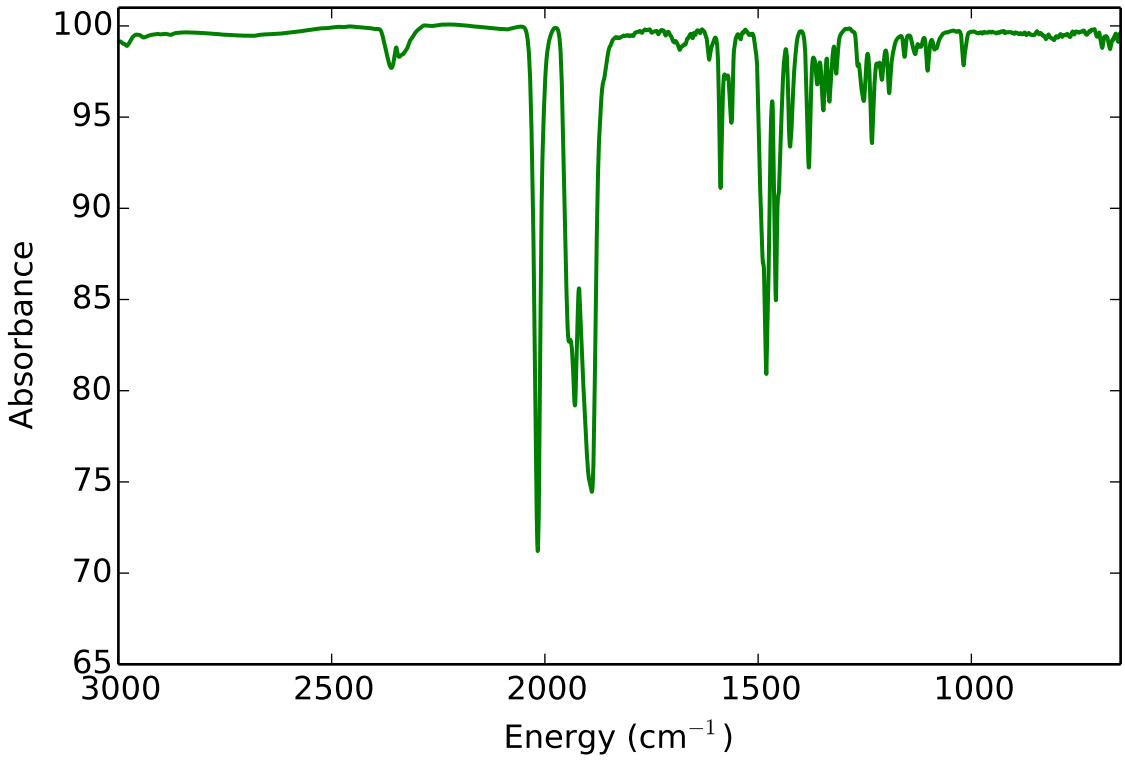

S4.2 CYCLIC VOLTAMMETRY

S4.2.1 MnBr(2,2′-bipyridine)$(CO)_3$

Solvent: CH_3CN with 5% H2O
Electrolyte: 0.1 M TBAP
Sample Concentration: 1 mM

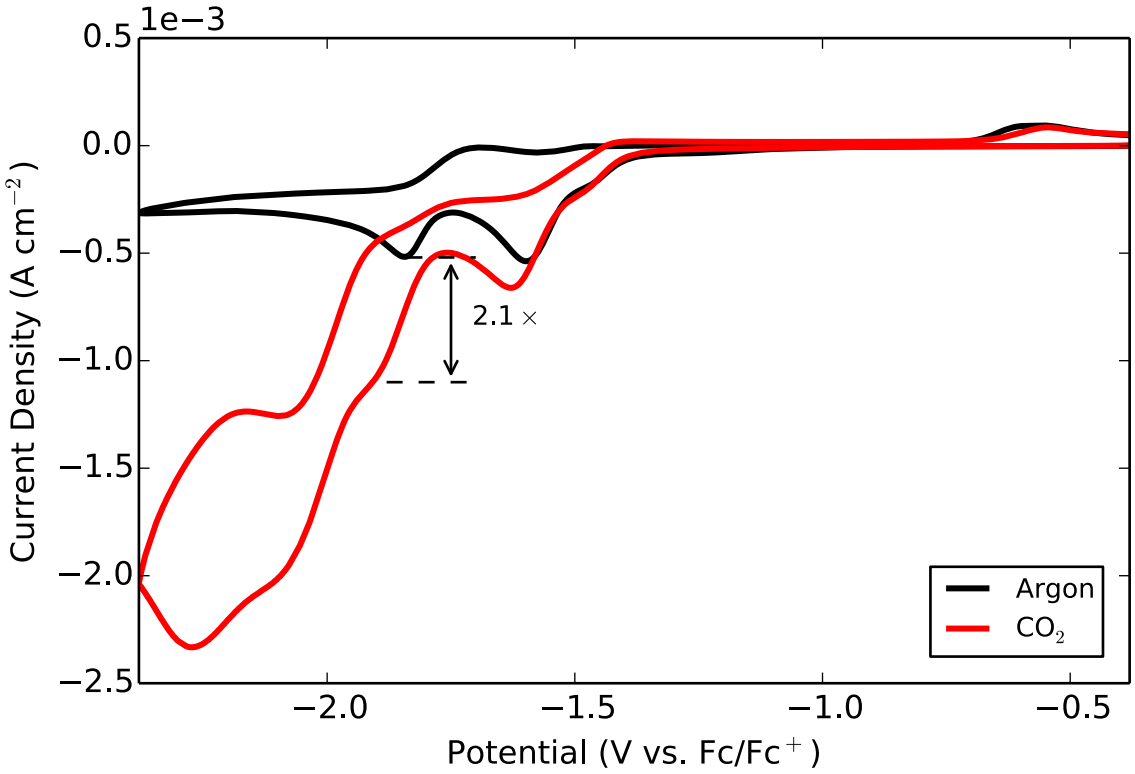

CHAPTER 5

ELECTROCATALYTIC REDUCTION OF CARBON DIOXIDE BY Mn(CN)(2, 2′-BIPYRIDINE)$(CO)_3$: CN COORDINATION ALTERS MECHANISM[3]

[3] Machan, C. W.; Stanton III, C. J.; Vandezande, J. E.; Majetich, G. F.; Schaefer III, H. F.; Kubiak, C. P.; Agarwal, J., Electrocatalytic Reduction of Carbon Dioxide by Mn(CN)(2,2′-bipyridine)$(CO)_3$: CN Coordination Alters Mechanism. *Inorganic Chemistry* **2015**, *54* (17), 8849-8856.

ABSTRACT

MnBr(2,2′-bipyridine)$(CO)_3$ is an efficient and selective electrocatalyst for the conversion of CO_2 to CO. Herein, substitution of the axial bromide for a pseudohalogen (CN) is investigated, yielding Mn(CN)(2,2′-bipyridine)$(CO)_3$. This replacement shifts the first and second reductions to more negative potentials (−1.94 and −2.51 V vs Fc/Fc^+, respectively), but imparts quasi-reversibility at the first feature. The two-electron, two-proton reduction of CO_2 to CO and H_2O is observed at the potential of the first reduction. Data from IR spectroelectrochemistry, cyclic voltammetry, and controlled potential electrolysis indicate that this behavior arises from the disproportionation of two one-electron-reduced species to generate the catalytically active species. Computations using density functional theory are also presented in support of this new mechanism.

INTRODUCTION

In 2010, ~33.5×10^9 t of carbon dioxide (CO_2) were emitted from fossil fuel combustion and cement manufacture globally,[1] up 8.8×10^9 t from the end of the previous decade. This elevated level of anthropogenic CO_2 emission continues to effect climate change,[2, 3] underscoring the need for CO_2 recovery prior to atmospheric release and the development of utilization technology that harnesses CO_2 as a raw material.[4] To realize the latter objective, new processes must be identified for large-scale conversion that require minimal energy input along with cheap and abundant reagents. In this context, the electrocatalytic conversion of CO_2 to carbon monoxide (CO) using renewable energy and water is an intriguing solution.[5] Coupling this conversion with industrial Fischer–Tropsch chemistry could represent an efficient energy cycle that connects an abundant combustion byproduct to the generation of liquid fuels.

Prior research has established that a variety of materials are capable of binding and reducing CO_2 under an applied voltage, including metal electrodes,[6-12] surface-modified electrodes,[13-16] and homogeneous transition-metal catalysts.[5, 17-24] This investigation is concerned with the latter: the use of soluble molecular electrocatalysts to shuttle redox equivalents from an electrode surface to CO_2 to effect selective reduction with minimal overpotential. Specifically, our interest is in manganese(I) tricarbonyl compounds, which have been shown to be effective mediators for the two-electron, two-proton reduction of CO_2 to CO in nonaqueous media with added Brønsted acids.[25-33] Notably, these species display high Faradaic efficiencies for CO—usually 85% to 100%—at relatively low overpotentials (~500 mV).[25, 26, 28, 33, 34] (Compared to the standard potential, $E_{CO2/CO,CH3CN}^{0} = -0.650$ V vs NHE)[34] In recent work, manganese(I) catalysts have also been utilized to mediate photochemical CO_2 reduction to formate.[35, 36]

The most widely investigated manganese catalyst is $MnBr(bpy)(CO)_3$ where bpy = 2,2′-bipyridine. Some variation of the supporting bidentate ligand has been reported, including the extension of bpy with *tert*-butyl,[26] mesityl,[27] and phenol moieties.[31, 37] Additionally, bpy has been replaced with an *N*-heterocyclic carbene (NHC)-pyridine framework[28, 33] along with functionalized 1,4-diazobutadienes.[29, 32] In any case, the proposed active species is a doubly reduced anion that possesses a vacant axial site for CO_2 coordination: $[Mn(\kappa^2\text{-L})(CO)_3]^-$ (Scheme 1, intermediate **c**). Theoretical[38] and experimental[39, 40] investigations of the mechanism suggest that one-electron reduction of the metal center causes the axial ligand, usually a bromide ion, to dissociate. Subsequently, the neutral radical monomer dimerizes to give $[Mn(\kappa^2\text{-L})(CO)_3]_2$ (intermediate **b**). The metal–metal bond within this species cleaves after loading two additional electrons, yielding two monomers of the anionic, five-coordinate active species (intermediate **c**). Subsequent CO_2 coordination is rapid and irreversible. The resulting oxoanion is readily protonated, furnishing a

Mn–COOH intermediate (intermediate **d**). The desired product (CO) is liberated from a proposed tetracarbonyl species, $[Mn(\kappa^2\text{-L})(CO)_4]^+$ (intermediate **e**), after carbon–oxygen bond cleavage within the hydroxycarbonyl moiety,[38] yielding a vacant site for the next cycle.

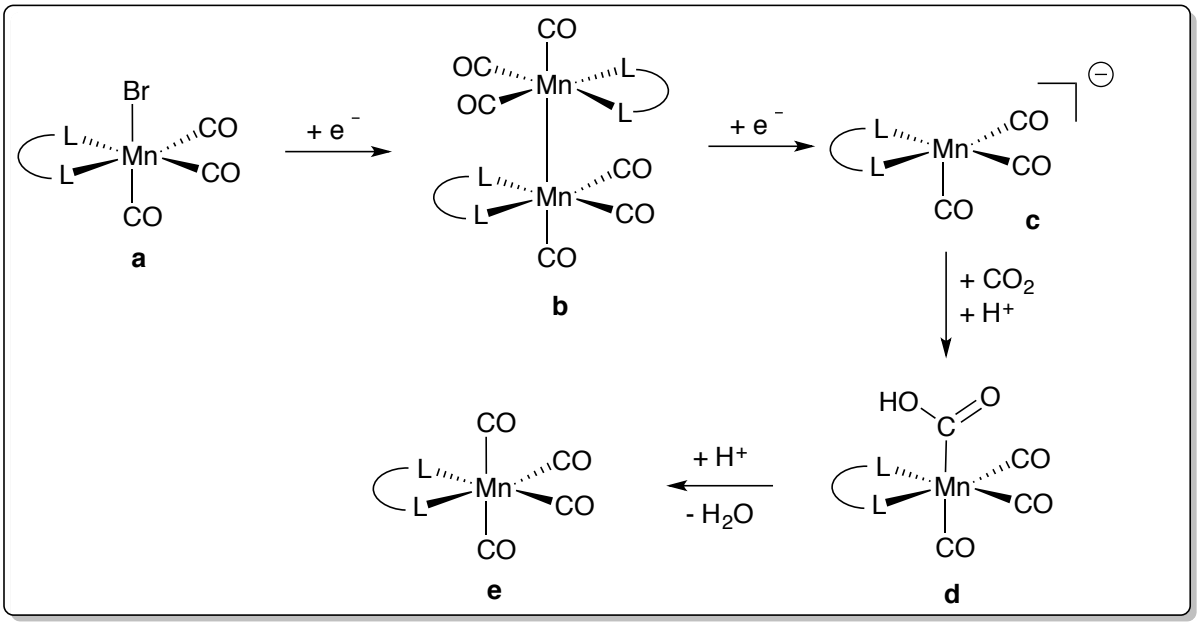

Scheme 5.1: Summary of the Proposed Mechanism for $Mn(\kappa^2\text{-L})(CO)_3$ Electroctalysts, where κ^2-L is a Bidentate Ligand Such as 2,2′-bipyridine

A requisite component of the catalytic process described is the availability of a coordination site to allow for CO_2 binding; bromide initially dissociates to yield the necessary vacancy, while liberation of the CO product in cycles thereafter allows for additional turnover. Bromide may also be substituted by other, labile ligands such as formate, and the same mechanism persists.[40] When bromine is replaced with a pseudohalogen such as NCS or CN, however, the Faradaic efficiency for CO production is diminished, concomitant with the formation of H_2 for NHC-pyridine based compounds.[33] The mechanism in this case is unclear: must the tricarbonyl core be retained for efficient catalysis, requiring dissociation of the pseudohalogen or may CO

dissociate to provide a site for CO_2 coordination? Here, we explore the mechanism of CO_2 reduction using $Mn(CN)(bpy)(CO)_3$. Cyclic voltammetry, IR spectroelectrochemistry (IR-SEC), and computations are provided to support a disproportionation mechanism whereby the interaction of two one-electron-reduced complexes yields the catalytically active species: a two-electron-reduced complex lacking the axial CN ligand.

RESULTS AND DISCUSSION

Synthesis and Characterization

A genuine sample of $Mn(CN)(bpy)(CO)_3$ (**5.1**) was prepared via metathesis,[33] using $MnBr(bpy)(CO)_3$ and excess KCN. After workup, **5.1** was obtained in 93% yield and fully characterized using UV–vis, NMR, and FT-IR spectroscopies (see S5.SI, pp 215-218). Crystals suitable for single-crystal X-ray analysis were obtained from the slow diffusion of pentanes into a solution of **1** dissolved in tetrahydrofuran (Figure 1). The crystal structure confirms the expected octahedral geometry and *facial* arrangement of the tricarbonyl core.

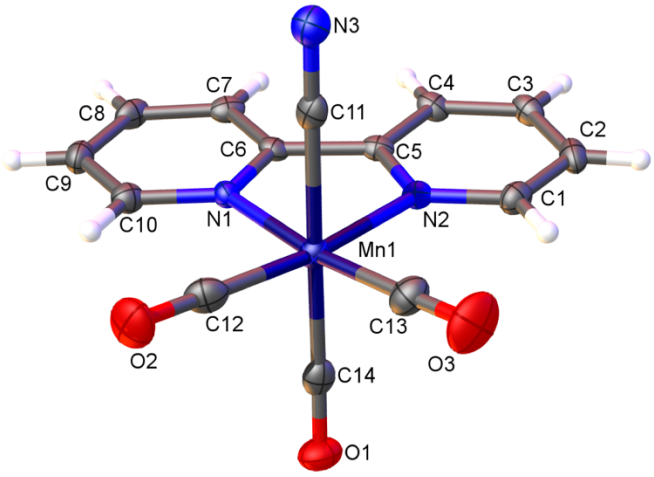

Figure 5.1: Molecular structure of $Mn(CN)(bpy)(CO)_3$ (**5.1**) obtained from X-ray diffraction (Z' = 2) with ellipsoids set at the 50% probability level. THF and H_2O molecules have been omitted for clarity.

Relative to the parent compound $MnBr(bpy)(CO)_3$, the UV–vis spectrum of **1** displays a blue-shifted metal-to-ligand charge transfer (MLCT) band (377 nm vs 416 nm[25]), which is aligned with the strong-field nature of CN^- compared to Br^-. Density functional theory (DFT) computations predict a 5 kcal mol^{-1} increase in the highest occupied molecular orbital–lowest unoccupied molecular orbital gap energy as a result of cyanide substitution, which is consistent with the observed shift in MLCT band origin. The ^{13}C NMR spectrum of **1** shows two resonances in the carbonyl region—one at 213 ppm and another at 221 ppm—indicating a vibrationally averaged C_s structure. These features are assigned to the sole axial carbonyl ligand and two equatorial carbonyl ligands, respectively. The carbon atom of cyanide resonates at 149 ppm.

Not surprisingly, the ^{13}C NMR spectrum of $MnBr(bpy)(CO)_3$ closely matches that of **1**; corresponding resonances agree to within 1 ppm with the exception of a new peak for CN and a dramatic (8 ppm) upfield shift for the peak corresponding to C14 within the axial carbonyl (Figure 5.1). Traditional bonding concepts fail to explain this disparity: an upfield shift generally indicates increased shielding from additional electron density around the nucleus, but substituting a π-donating ligand (Br; M ← L) for a π-accepting ligand (CN; M → L) should decrease back bonding to C14 as a result of a reduced charge on the Mn center. Indeed, natural bond orbital (NBO)[41] computations suggest diminished electron density on C14 as a result of substitution, including reduced occupation of the C14–O1 σ* and π* orbitals. Mayer bond analysis[42] also indicates an increased C14–O1 bond order. However, the computed ^{13}C NMR chemical shifts for **1** correctly predict the upfield shift of C14 relative to the same atom in $MnBr(bpy)(CO)_3$. This suggests that another effect may be involved, such as shielding due to ring currents within the CN π orbitals,[43] but further investigation is required to develop an adequate understanding of the underlying electronic structure.

Cyclic Voltammetry

The cyclic voltammetry of **5.1** is presented in Figures 5.2A and 5.2B. Scans were recorded under argon (Ar) in dry acetonitrile (MeCN) with 0.1 M tetrabutylammonium perchlorate (TBAP) supporting electrolyte at scan rates ranging from 10 to 2000 mV s^{-1}. Scanning to negative potentials at 100 mV s^{-1}, the first redox feature is observed at −1.94 V vs Fc/Fc^+ ($E_{1/2}$ = −1.91 V vs Fc/Fc^+). This is a one-electron, quasi-reversible process with peak-to-peak separation (ΔE_p) of 60 mV. At more negative potentials, a second, irreversible feature is observed at −2.51 V vs Fc/Fc^+ (Figure 5.2B). Both processes are diffusion-limited, as indicated by a linearly dependent relationship between the peak current and square root of the scan rate (see S5.SI, pp 219). The return scan from the second redox wave shows two new oxidative processes: one at −1.51 V vs Fc/Fc^+ and another at −0.61 V vs Fc/Fc^+. As shown in the plot of Figure 5.2A, these irreversible oxidations are absent if the switching potential is before the second reduction.

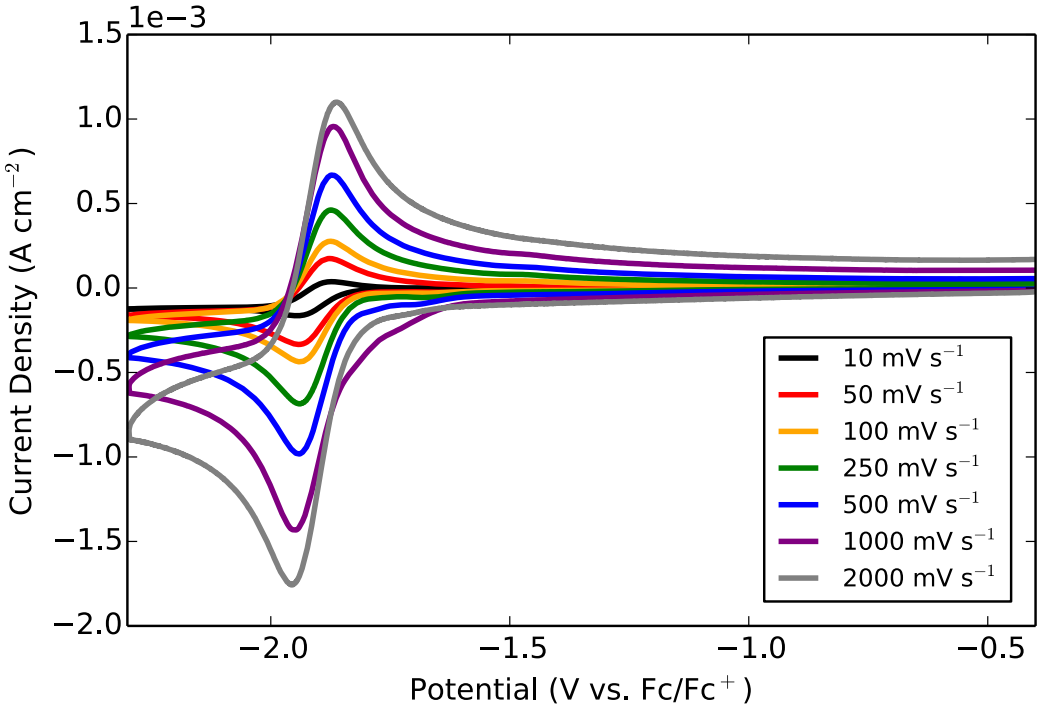

Figure 5.2A: CV of $Mn(CN)(bpy)(CO)_3$ (**5.1**, 1 mM) under Ar in dry MeCN with 0.1 M TBAP supporting electrolyte. The switching potential was set to −2.2 V vs Fc/Fc^+.

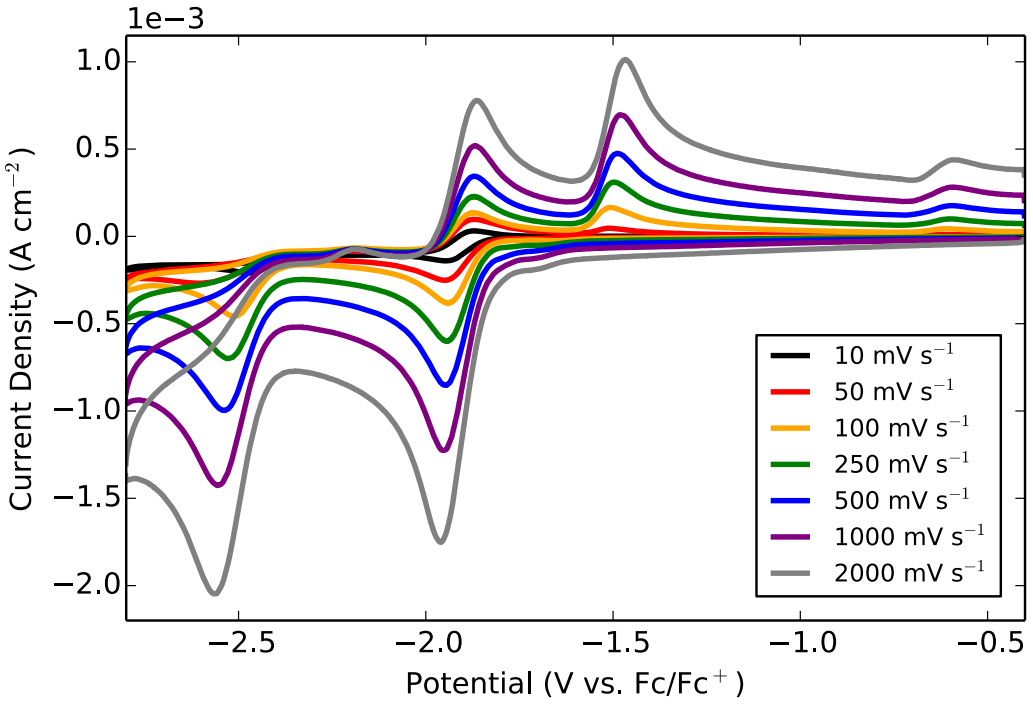

Figure 5.2B: CV of Mn(CN)(bpy)(CO)$_3$ (**5.1**, 1 mM) under Ar in dry MeCN with 0.1 M TBAP supporting electrolyte. The switching potential was set to −2.8 V vs Fc/Fc$^+$.

We ascribe the first reduction process at −1.94 V vs Fc/Fc$^+$ to a ligand-based reduction (Figure 5.3, species **D**); NBO computations indicate that 90% of the added charge resides on atoms within the bpy framework. Aligned with the reversibility observed in Figure 5.2A, the optimized structure of [Mn(CN)(bpy)(CO)$_3$]$^{\bullet-}$ does not favor dissociation—the bond dissociation energies (BDE) for the axial CO and CN ligands are considerable at 31 and 23 kcal mol^{-1}, respectively. This stands in contrast to the behavior of [MnBr(bpy)(CO)$_3$]$^{\bullet-}$, which is observed to liberate Br$^-$.[38-40]

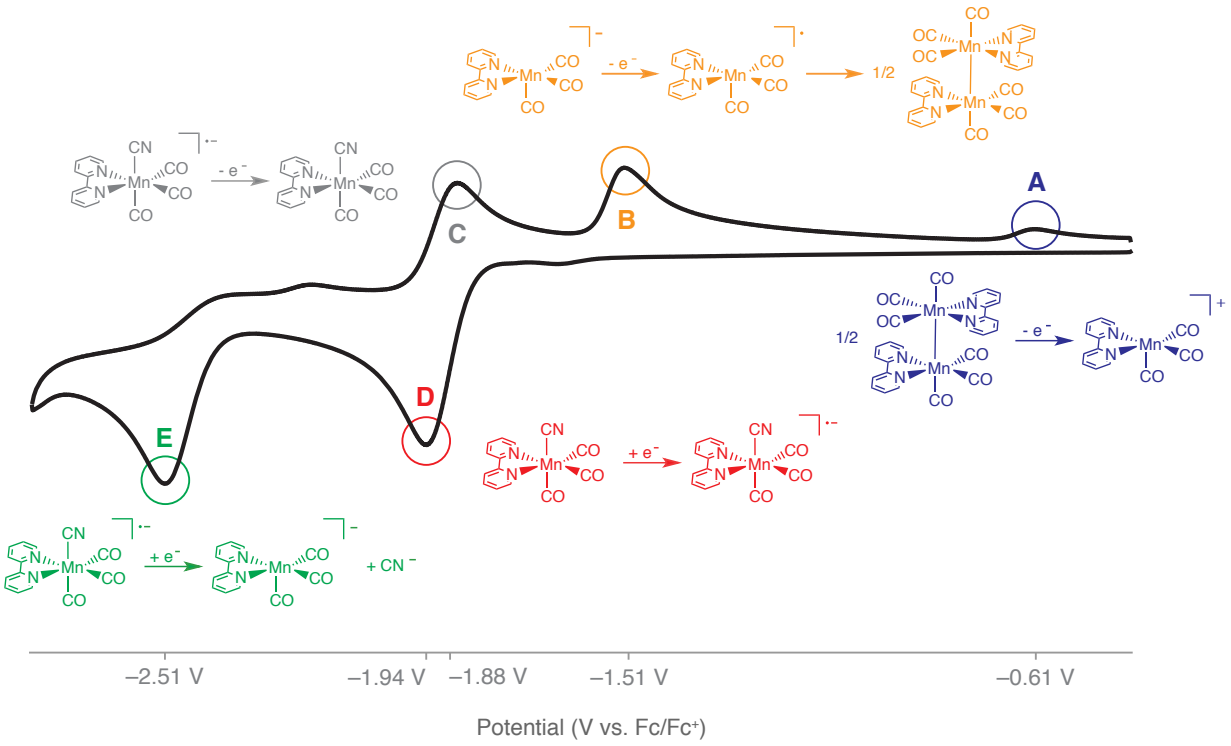

Figure 5.3: CV of $Mn(CN)(bpy)(CO)_3$ (**5.1**, 1 mM) under Ar in dry MeCN with 0.1 M TBAP supporting electrolyte at 100 mV s^{-1}. See text for descriptions of the redox features.

The second reduction wave at −2.51 V vs Fc/Fc^+ (Figure 5.3, species **E**) is also ligand-based. Here, NBO computations suggest that 89% of the added charge is localized to bpy. In the optimized structure of $[Mn(CN)(bpy)(CO)_3]^{2-}$, the axial CO BDE remains significant (22 kcal mol^{-1}), but CN coordination is considerably weaker at 4 kcal mol^{-1}. Under experimental conditions, CN loss is nearly certain, which is supported by the observed irreversibility. Even increasing the scan rate to 2000 mV s^{-1} does not impart quasi-reversibility, indicating that the chemical change is very rapid on this time scale.

The oxidative processes at −0.61 V (Figure 5.3, species **A**) and −1.51 V vs Fc/Fc^+ (Figure 5.3, species **B**) may be assigned on the basis of previous literature reports. We designate process **A** as the oxidation of $[Mn(bpy)(CO)_3]_2$. Previously, the oxidation of several Mn–Mn dimers were observed in this region of the voltammogram: $[Mn(4,4'$-*tert*-butyl-bpy$)(CO)_3]_2$ at −0.68 V vs

Fc/Fc^+,[26] [Mn(*N*-methyl-*N*′-2-pyridylimidazol-2-ylidine)$(CO)_3]_2$ at −0.63 V vs Fc/Fc^+,[33]and $[Mn(bpy)(CO)_3]_2$ at −0.60 V vs Fc/Fc^+.[25] (Values reported vs the saturated calomel electrode (SCE) and vs 10 mM Ag/Ag^+ were converted to vs Fc/Fc^+ by adding −0.380[44] and −0.087[45] V, respectively.) Presumably, axial CO loss in **5.1** could also yield the requisite vacancy for Mn–Mn bonding, but we eliminate this possibility on the grounds that (i) the computed BDE for the axial CO is roughly 5 times that of CN, (ii) optimization of $[Mn(CN)(bpy)(CO)_2]_2^{2-}$ fails due to dissociation, and (iii) the addition of tetrabutylammonium cyanide (TBACN) to the electrolyte solution completely suppresses this feature (see S5.SI, pp 220).

The remaining feature at −1.51 V vs Fc/Fc^+ (Figure 5.3, species **B**) is ascribed to the oxidation of $[Mn(bpy)(CO)_3]^-$. Bourrez *et al.* previously recorded the oxidation of $[Mn(bpy)(CO)_3]^-$ at −1.48 V vs Fc/Fc^+, which was assigned based on UV–vis spectroscopy.[25] Moreover, a similar wave appears in the CV of MnBr(4,4′-*t*-butyl-bpy)$(CO)_3$ at ca. −1.6 V vs Fc/Fc^+ following two-electron reduction.[26] In these reports, where Br^- is available, the peak current for the oxidation of $[Mn(\kappa^2\text{-L})(CO)_3]^-$ is less than the peak current for oxidizing available Mn–Mn dimer. Here we observe the opposite pattern in peak current, suggesting that $[Mn(bpy)(CO)_3]^\bullet$ is captured by free CN^- before Mn–Mn bonding can occur, which is supported by the addition of TBACN as previously described. No evidence for an acetonitrile bound complex was observed (vide infra); in solution, CN^- is likely to outcompete MeCN for available coordination sites.

To gauge the ability for **5.1** to mediate CO_2 reduction, additional voltammograms were recorded under a CO_2 atmosphere in the presence of a Brønsted acid, either water (Figure 5.4) or phenol (Figure 5.5). With 5% added water, a slight current enhancement (1.2×) occurs at the peak current of the first reduction wave (ca. −1.94 V vs Fc/Fc^+) under CO_2 (red). At the potential of the second reduction (ca. −2.51 V vs Fc/Fc^+), a significant current enhancement (5.7×) is observed.

We assign the majority of this enhancement to the catalytic reduction of CO_2 by a $[Mn(bpy)(CO)_3]^-$ active species, but caution that some reduction of water by glassy carbon is observed in control experiments at this very negative potential. The oxidation of $[Mn(bpy)(CO)_3]^-$ at ca. −1.51 V vs Fc/Fc^+ is absent from the return wave under CO_2, suggesting that this species is consumed.

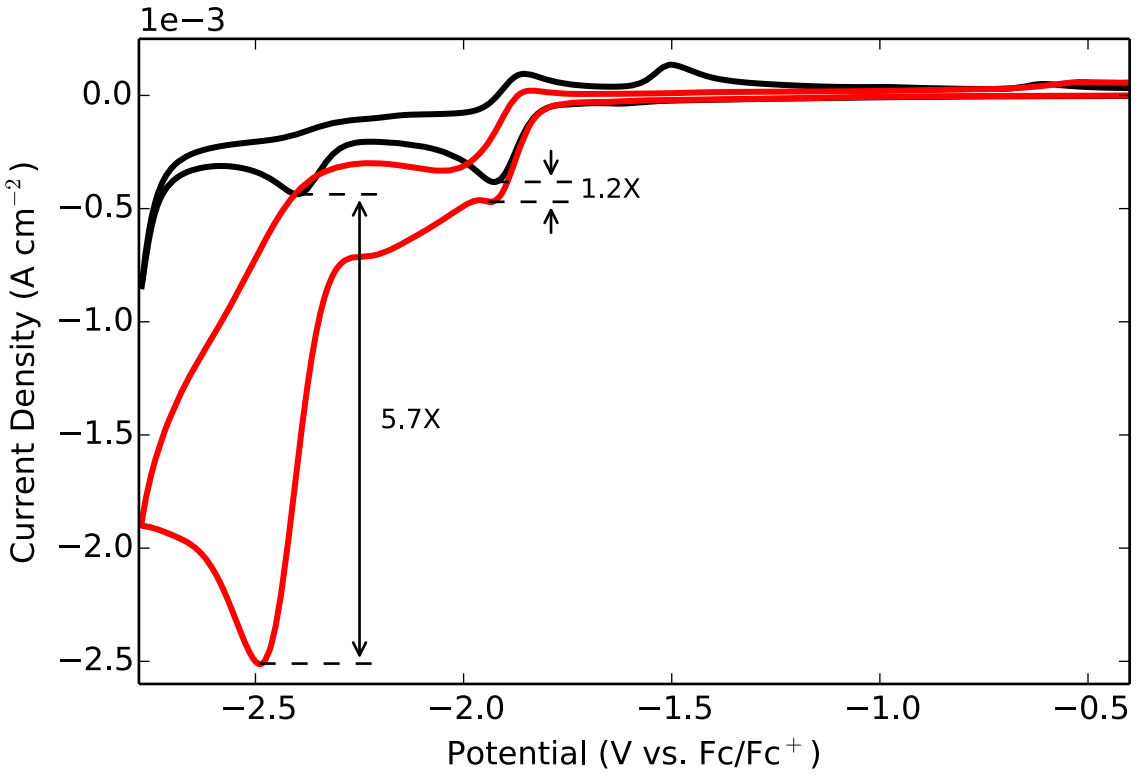

Figure 5.4 CV of $Mn(CN)(bpy)(CO)_3$ (**5.1**, 1 mM) under Ar (black) or CO_2 (red) in MeCN (5% H_2O) with 0.1 M TBAP supporting electrolyte at 100 mV s^{-1}. In the case of Ar, added water was pH adjusted to 3.7 to match the pH under CO_2.

When phenol is substituted for water as the Brønsted acid in solution (Figure 5.5), the voltammetry window shrinks (see S5.SI, pp 224),[46] allowing only for the current enhancement at the first reduction to be probed. Note that in the absence of phenol no current enhancement is observed; the scan under CO_2 (red) matches that under Ar (black). As phenol is titrated into the

electrolyte solution, current enhancement appears at the potential of the first reduction, from a 4.6× enhancement using 0.5 M phenol to a 7.2× enhancement using 1.5 M phenol. This superior activity when using phenol relative to water is aligned with previous reports of manganese catalysts.[38, 47] Phenol is employed as a Brønsted acid in the remainder of this work.

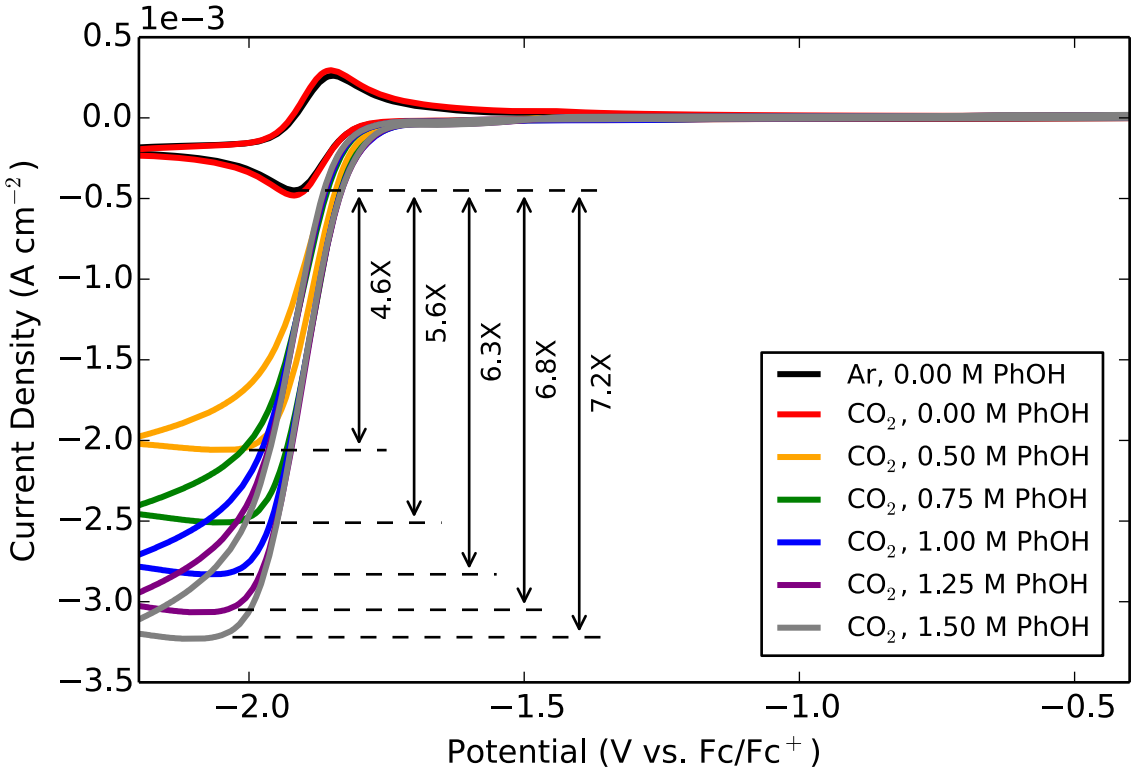

Figure 5.5: CV of Mn(CN)(bpy)$(CO)_3$ (**5.1**, 1 mM) under CO_2 in MeCN with added phenol (PhOH) and 0.1 M TBAP supporting electrolyte at 100 mV s^{-1}. A scan under Ar with no phenol (black) is shown for reference.

Infared Spectroelectrochemistry

IR-SEC allows for the direct interrogation of electrochemical reactions as a function of time and potential using IR spectroscopy.[39, 48] In an effort to understand the behavior of **1** in the region of the first reduction—the lowest potential where catalytic current enhancement is observed—we recorded the IR spectrum at the resting potential and at the potential of the first

reduction under an atmosphere of N_2 (Figure 5.6). At the resting potential (black), four IR bands are observed at 2115 (CN), 2029 (CO), 1942 (CO), and 1928 cm^{-1} (CO). The computed IR spectrum of **5.1**, scaled by 0.978 61 to account for the anharmonicity of the potential energy surface, qualitatively agrees with the observed transitions: the C–N stretch is predicted to appear at 2152 cm^{-1}, while the lone symmetric and two asymmetric stretches of the tricarbonyl group are predicted to appear at 2033, 1939, and 1930 cm^{-1}, respectively.

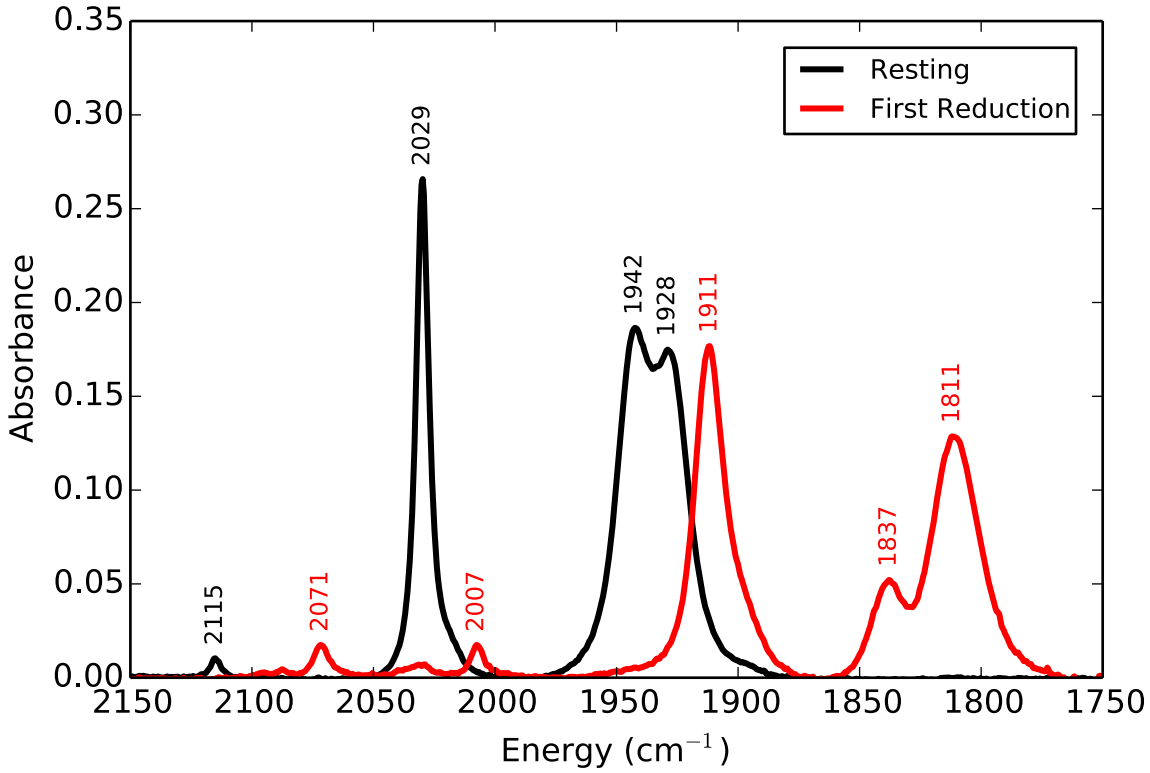

Figure 5.6: Infrared spectra of Mn(CN)(bpy)$(CO)_3$ (**5.1**) at controlled potentials under an atmosphere of N_2. **5.1** (6.2 mM) was added to dry MeCN with 0.1 M $TBAPF_6$ supporting electrolyte.

When the potential of the IR-SEC cell is stepwise shifted from resting to that of the first reduction (red; ca. −1.94 V vs Fc/Fc^+), five new bands appear at lower frequencies concomitant with the disappearance of the original spectrum. This red shift is expected: additional electron

density should partially occupy the π* orbitals of the CN and CO ligands, reducing their stretching frequencies. Curiously, the observed CO transitions (1911, 1837, and 1811 cm^{-1}) align best with the predicted frequencies for $[Mn(bpy)(CO)_3]^-$, a *two*-electron-reduced compound. The low-intensity band at 2007 cm^{-1} matches the computed symmetric CO stretch of $[Mn(CN)(bpy)(CO)_3]^{\bullet-}$ (2010 cm^{-1}), suggesting that the one-electron-reduced species is a minor product. The two remaining CO stretches for this compound (1909 and 1895 cm^{-1}) are predicted to have lower intensities than the symmetric stretch and would be concealed by the broad band at 1911 cm^{-1}. These data would suggest the possible disproportionation of two one-electron-reduced species, $[Mn(CN)(bpy)(CO)_3]^{\bullet-}$, formed at the potential of the first reduction.

To support this hypothesis we supplanted the applied voltage with a chemical reductant, $CoCp^*_2$, which possesses a redox potential of −1.91 V vs Fc/Fc^+.[44] Indeed, the same shift and spectral pattern is observed as before (Figure 5.7). The intensities of the new bands in the CO stretching region (1911, 1837, and 1811 cm^{-1}) continue to rise after 1 equiv of $CoCp^*_2$ is added, supporting the formation of a two-electron product. Furthermore, the UV–vis spectrum of the product after adding 2.1 equiv of $CoCp^*_2$ shows new transitions at 352 and 559 nm (see S5.SI, pp 220), which agrees with previous assignments for $[Mn(bpy)(CO)_3]^-$.[25] The presence of an intermediary compound—such as $[Mn(bpy)(CO)_3]^{\bullet}$, which could form from the slow dissociation of CN^- after one-electron reduction—is not observed. Spectra collected following the addition of substoichiometric equivalents of $CoCp^*_2$ (i.e., from 0 → 1 equiv) indicate only two compounds are present: the starting species $Mn(CN)(bpy)(CO)_3$ and the two-electon-reduced species $[Mn(bpy)(CO)_3]^-$.

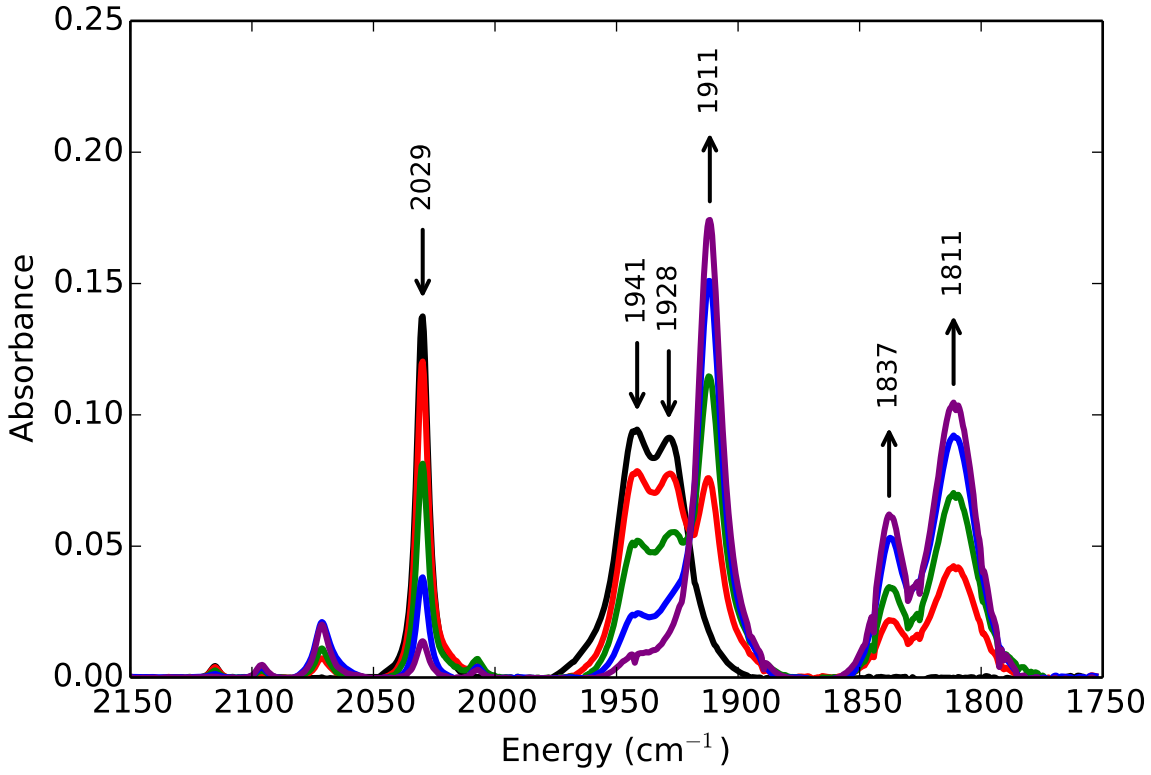

Figure 5.7: Infrared spectra of Mn(CN)(bpy)(CO)$_3$ (**5.1**) with added chemical reductant under an atmosphere of N_2. **5.1** (3 mM) was added to dry MeCN **1** (3 mM) was added to dry MeCN and titrated with CoCp*$_2$ (black → purple; 0 → 2.1 equiv). Also see **SI ppXX** for comparison with computational predictions.

In the cyclic voltammetry discussed above, Figure 5.2.A shows no oxidative features for [Mn(bpy)(CO)$_3$]$^-$ (−1.51 V vs Fc/Fc$^+$) if the switching potential is before the second reduction, which is not aligned with a disproportionation mechanism unless the timescale is too short for appreciable formation of a two-electron species. To probe this, we electrolyzed **5.1** at the potential of the first reduction, then swept oxidatively to 0.0 V. After holding the voltage at −1.94 V vs Fc/Fc$^+$ for 120 s we observed a new peak consistent with the oxidation of [Mn(bpy)(CO)$_3$]$^-$ (see S5.SI, pp 222), consistent with a disproportionation reaction. From these data, we propose the mechanism shown in Scheme 2. Density functional theory computations predict the overall free energy (ΔG) of disproportionation to be −1 kcal mol^{-1}, though this near-equilibrium process should be driven by the loss of CN and the continuously applied potential. Under catalytic conditions, the

thermodynamically favorable interaction of $[Mn(bpy)(CO)_3]^-$ with CO_2 in the presence of a Brønsted acid[38] should further accelerate disproportionation.

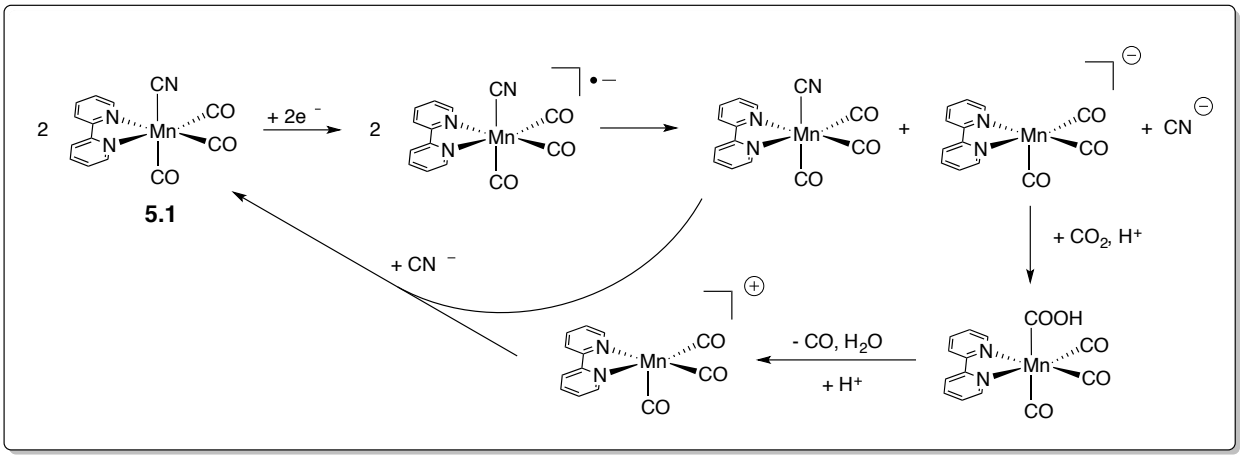

Scheme 5.2: Proposed Disproportionation Mechanism Following One-Electron-Reduction, and Subsequent CO_2 Conversion to CO

Controlled Potential Electrolysis

To understand the behavior of **5.1** under catalytic conditions, controlled potential electrolyses were performed both at the preparative scale in an IR-SEC cell and at the bulk scale with headspace analysis. To begin, the IR spectrum of **5.1** was recorded in MeCN with 0.1 M tetrabutylammonium hexafluorophosphate ($TBAPF_6$) and 0.5 M phenol in an IR-SEC cell. The expected transitions for the starting compound (**1**) were observed: [2119 (CN), 2031 (CO), 1943 (CO), and 1930 cm^{-1} (CO)], see Figure 5.8.A. After sparging with CO_2 for 10 s, the potential of the IR-SEC cell was then set to the first reduction (ca. −1.9 V vs Fc/Fc^+), and sequential IR spectra were recorded roughly every minute for 5 min. Over time, the sharp bands assigned to phenol (1607 and 1596 cm^{-1}) decrease in intensity—note that all spectra were solvent-subtracted such that the depletion of PhOH is reflected as negative absorbance values—and two broad bands appear at 1654 and 1587 cm^{-1}. We assign the latter transition to phenoxide (PhO^-) from

control experiments using NaOPh (see S5.SI, pp 226), while the band at 1654 cm^{-1} is assigned to water that is produced during the conversion of $CO_2 + 2H^+ + 2e^- \rightarrow CO + H_2O$. In the C–O stretching region only bands assigned to **1** are evident throughout the experiment, indicating that available $[Mn(bpy)(CO)_3]^-$ is rapidly consumed.

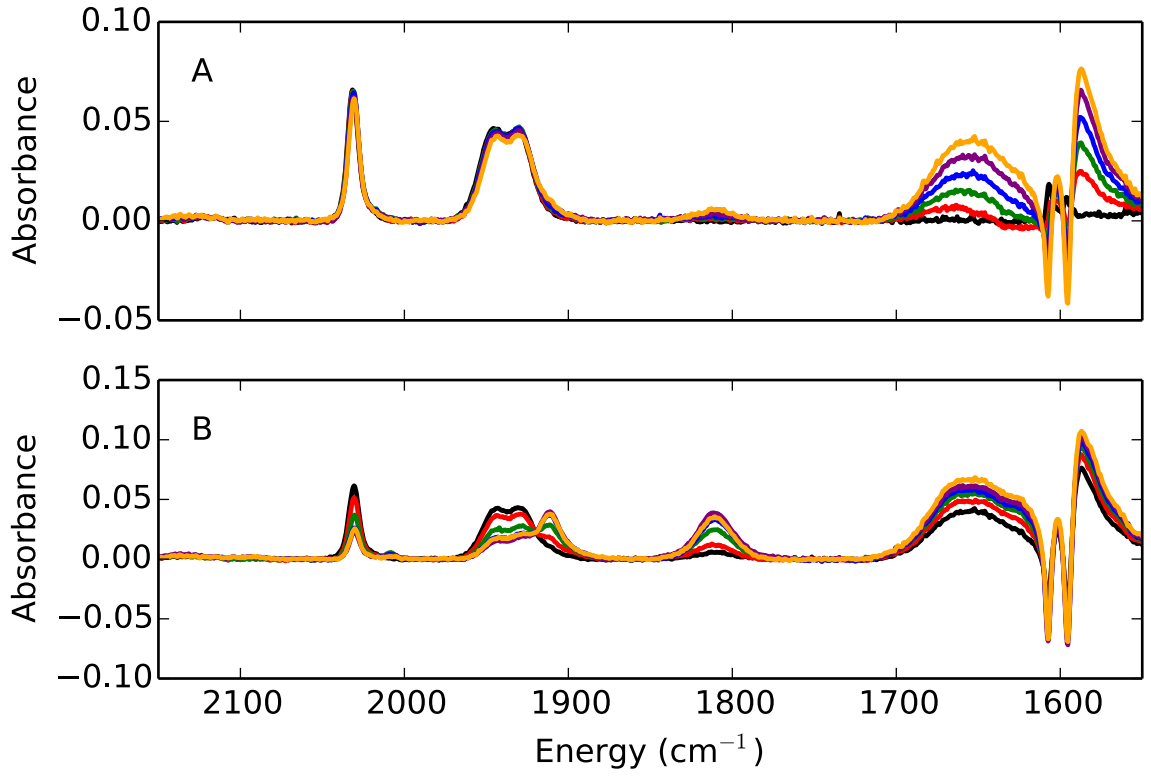

Figure 5.8: Infrared spectra of $Mn(CN)(bpy)(CO)_3$ (**5.1**, 7.9 mM) at ca. −1.9 V vs Fc/Fc^+ (**A**) then ca. −2.1 V vs Fc/Fc^+ (**B**) under an atmosphere of CO_2 in MeCN with 0.1 M $TBAPF_6$ supporting electrolyte and 0.5 M phenol. Scans were recorded roughly every minute (black → orange).

The potential of the IR-SEC cell was then increased to ca. −2.1 V vs Fc/Fc^+, and additional scans were recorded (Figure 5.8.B). The continued consumption of phenol is evidenced by the decrease in intensity at 1607 and 1596 cm^{-1} along with an increase in intensity at 1587 cm^{-1}. Infrared transitions corresponding to the active species, $[Mn(bpy)(CO)_3]^-$, (1909

and 1805 cm^{-1}) begin to appear, since the rate of reduction of **1** should be faster at this potential and the available substrate diminishes over the time scale of the experiment.

Further analysis was performed at the bulk scale in a 70 mL custom reaction vessel with a graphite working electrode, platinum counter electrode, and Ag/AgCl pseudoreference electrode. These results are listed in Table 1. Across three trials at ca. −2.2 V vs Fc/Fc^+, analysis of the headspace with gas chromatography shows the presence of between 160 and 180 μmol of CO from ~40 μmol of **5.1**, yielding an average Faradaic efficiency of 98% [average turnover number (TON) = 4]. Some H_2 is observed in each trial, but the average Faradaic efficiency is 1%, indicating excellent selectivity for CO_2 over available protons.

Table 5.1: Results from Three Controlled Potential Electrolyses at ca. −2.2 V vs Fc/Fc^+ with Analysis of the Headspace Using Gas Chromatography[a]

Trial	Charge Passed	mol CO[b]	mol H_2[b]
1	3.40 C	1.70×10^{-4} (96%)	2.65×10^{-6} (2%)
2	3.20 C	1.60×10^{-4} (97%)	2.47×10^{-6} (1%)
3	3.40 C	1.79×10^{-4} (102%)	2.19×10^{-6} (1%)

[a]Compound 5.1 was loaded at a concentration of ~0.9 mM in a 45 mL solution of dry MeCN with 0.1 M $TBAPF_6$ supporting electrolyte and 0.5 M phenol
[b]Faradaic efficiencies shown in parentheses

Conclusions

Literature reports of Mn(I) electrocatalysts have grown to encompass many derivatives of $MnBr(\kappa^2\text{-L})(CO)_3$, where κ^2-L can be functionalized or nonfunctionalized 2,2′-bipyridine, 1,4-diazobutadiene, or a pyridine-NHC construct. In this report, we have examined the replacement of Br for CN, yielding Mn(CN)(2,2′-bipyridine)$(CO)_3$. This substitution maintains the C_s symmetric, octahedral structure of the parent compound, but has a significant effect on the voltammetric response. Specifically, the first and second reduction potentials are shifted negative to −1.94 and

−2.51 V vs Fc/Fc^+, respectively. The strong-field nature of CN imparts quasi-reversibility at the first feature, limiting the formation of $[Mn(bpy)(CO)_3]_2$. Indeed, the addition of tetrabutylammonium cyanide is found to completely surpress Mn–Mn bonding. At the second-reduction potential, CN dissociates to yield the catalytically active species $[Mn(bpy)(CO)_3]^-$.

From theoretical computations, chemical reductions, and IR SEC, we find that $[Mn(bpy)(CO)_3]^-$ may also be generated via the disproportionation of two one-electron-reduced compounds, allowing for the two-electron, two-proton reduction of CO_2 to CO and H_2O to nominally occur at the potential of the first reduction, −1.94 V vs Fc/Fc^+. Controlled potential electrolyses (three trials) performed at the potential of the first reduction (ca. −2.2 V vs Fc/Fc^+) with 0.5 M phenol yields average Faradaic efficiences of FE_{CO} = 98% and FE_{H2} = 1% over four turnovers, demonstrating the excellent selectivity of Mn(CN)(2,2′-bipyridine)$(CO)_3$ for reducing CO_2 over available protons, and further supporting the disproportionation mechanism. Future work will examine how the blue-shifted absorbance of this CN-substituted compound affects its lifetime under visible-light conditions.

EXPERIMENTAL METHODS

General

All reagents were obtained from commercial suppliers and used as received unless otherwise noted. Reactions were performed using standard Schlenk-line techniques under an atmosphere of argon. Methanol was dried prior to use by distilling it from CaH_2. ^1H NMR spectra were recorded on a Varian Mercury Plus 400 MHz spectrometer, and ^{13}C NMR spectra were recorded on an Agilent DD2 600 MHz spectrometer. NMR chemical shifts were referenced to the residual protio signal of the deuterated solvent. Fourier transform infrared (FTIR) spectra were recorded on a

ThermoNicolet 6700 spectrophotometer running OMNIC software. Absorption spectra were recorded on a CARY 300 Bio UV–vis spectrophotometer with a quartz cuvette (1 cm path length). MnBr(2,2′-bipyridine)$(CO)_3$ was prepared according to standard methods.[25]

Electrochemistry

Electrochemical experiments were performed using either a CH Instruments 601E or BAS Epsilon potentiostat. For all experiments, a single compartment cell was employed. A 3 mm diameter glassy carbon (GC) electrode (BASi or CH Instruments) was utilized as the working electrode (WE). The counter electrode (CE) was a platinum (Pt) wire, and the reference electrode (RE) was a silver/silver chloride (Ag/AgCl) electrode separated from solution by a Vycor or Teflon tip. Experiments were run with and without an added internal reference of ferrocene. Electrolyte solutions were composed of dry MeCN, containing 1 mM of catalyst and 0.1 M $TBAPF_6$ or 0.1 M TBAP supporting electrolyte, unless otherwise noted. The electrolyte was purged with Ar, N_2, or CO_2 before cyclic voltammograms were recorded and stirred between successive experiments. All voltammetry was referenced to an internal ferrocene standard, except for bulk electrolysis experiments where a pseudo-RE Ag/AgCl reference was employed.

Infrared Spectroelectrochemistry

The reader is referred to previous literature on IR-SEC from our laboratory for the cell design and setup.[39, 48] A Pine Instrument Company model AFCBP1 bipotentiostat was employed for all measurements. During potential sweeps, thin layer bulk electrolysis was monitored by Fourier-transform reflectance IR off the electrode surface. All experiments were conducted in 0.1 M $TBAPF_6$/MeCN solutions and prepared with the catalyst under a nitrogen atmosphere. The IR-

SEC cells include GC, Ag, and Pt electrodes for the WE, RE, and CE, respectively. As such, all potentials are referenced to a pseudo-RE, Ag/Ag^+ (silver wire; roughly +200 mV from the Fc/Fc^+ couple).

Controlled Potential Electrolysis

Trials were performed using a custom flask from Chemglass affixed with a custom PEEK lid with ports for three electrodes, purging, and sampling. A graphite WE, platinum CE, and Ag/AgCl pseudo-RE were employed. The system was sealed and tested for air-tightness before each run. In a typical trial, the flask was charged with a known amount of catalyst, 0.5 M phenol, stir bar, and electrolyte (0.1 M $TBAPF_6$ in MeCN) before being sparged to saturation with CO_2. To prevent the polymerization of PhOH on the counter electrode, 0.1 M Fc was added to the electrolyte solution as a sacrificial oxidant. After a completed run, the headspace was sampled via airtight syringe and characterized with gas chromatography. Each turnover for this system is based on two electron equivalents being passed for every catalyst molecule in solution.

Synthesis

Preparation of Mn(CN)(2,2′-Bipyridine)$(CO)_3$ (5.1).

MnBr(2,2′-Bipyridine)$(CO)_3$ (1.75 g, 4.7 mmol) and KCN (15.17g, 233.0 mmol) were suspended in 100 mL of MeOH and stirred at 60 °C under argon for 15 h. After it cooled to room temperature, the reaction mixture was diluted with H_2O (100 mL) and extracted with dichloromethane (3 × 100 mL). The combined organic extracts were washed with H_2O (100 mL) and brine (100 mL) and then dried over anhydrous $MgSO_4$ before filtration to remove the drying agent. Concentration under reduced pressure using a rotary evaporator gave the desired product as a light yellow solid

(1.40 g, 93%). IR (ATR, cm^{-1}) ν_{CO}: 2022 (s), 1909 (s), 1887 (sh); ν_{CN}: 2108 (m). ^{1}H NMR (DMSO-d_6), 20 °C: δ 9.06 (2H, d, J = 4 Hz), 8.69 (2H, d, J = 8 Hz), 8.28–8.23 (2H, m), 7.75–7.72 (2H, m). ^{13}C NMR (DMSO-d_6, 25 °C): δ 221.07, 213.13, 154.66, 153.28, 149.29, 139.14, 127.09, 123.42.

THEORECTICAL METHODS

Computations were performed with DFT using the B3LYP functional[49-51] as implemented in Orca 3.0.1.[52] Optimized geometric parameters and harmonic vibrational frequencies were obtained with the inclusion of an implicit solvent model using the conductor like screening model (COSMO)[53] with the default values for acetonitrile (ϵ = 36.6). The def2-TZVP basis set[54] was used to describe all "light" atoms. Mn and Br were described with the LANL08(f)[55] and LANL2DZ[56, 57] basis sets, respectively, and their corresponding effective core potentials. Vibrational analysis was used to confirm the nature of the stationary points as true minima. All structures were computed with tight convergence criteria (RMS force < 1×10^{-6} Hartree/bohr), and vibrational frequencies were scaled by 0.978 61 to account for the anharmonicity of the potential energy surface.

Natural bond orbital computations were performed with NBO5.[41] NMR computations were performed using the IGLO method[58, 59] with the origin placed at the center of electronic charge and orbitals localized using Pipek–Mezey approach.[60] Previous studies indicate DFT-IGLO computations using this localization adequately describe the nuclei within ligands bound to transition metals.[61, 62] Chemical shifts were first computed relative to DMSO, then converted relative to tetramethylsilane by adding 39.5 ppm.[63]

REFERENCES

1. Le Quéré, C.; Moriarty, R.; Andrew, R.; Peters, G.; Ciais, P.; Friedlingstein, P.; Jones, S.; Sitch, S.; Tans, P.; Arneth, A., Global Carbon Budget 2014. *Earth System Science Data Discussions* **2014**, *7* (2), 521-610.

2. Members, P. P., Making Sense of Palaeoclimate Sensitivity. *Nature* **2012**, *491* (7426), 683-691.

3. Song, C., Global Challenges and Strategies for Control, Conversion and Utilization of CO_2 for Sustainable Development Involving Energy, Catalysis, Adsorption and Chemical Processing. *Catalysis Today* **2006**, *115* (1), 2-32.

4. Leitner, W., Carbon Dioxide as a Raw Material: The Synthesis of Formic Acid and Its Derivatives from CO_2. *Angewandte Chemie International Edition* **1995**, *34* (20), 2207-2221.

5. Costentin, C.; Robert, M.; Savéant, J.-M., Catalysis of the Electrochemical Reduction of Carbon Dioxide. *Chemical Society Reviews* **2013**, *42* (6), 2423-2436.

6. Medina-Ramos, J.; DiMeglio, J. L.; Rosenthal, J., Efficient Reduction of CO_2 to CO with High Current Density Using in Situ or ex Situ Prepared Bi-Based Materials. *Journal of the American Chemical Society* **2014**, *136* (23), 8361-8367.

7. Hara, K.; Kudo, A.; Sakata, T., Electrochemical Reduction of Carbon Dioxide Under High Pressure on Various Electrodes in an Aqueous Electrolyte. *Journal of Electroanalytical Chemistry* **1995**, *391* (1), 141-147.

8. Chen, Y.; Li, C. W.; Kanan, M. W., Aqueous CO_2 Reduction at Very Low Overpotential on Oxide-Derived Au Nanoparticles. *Journal of the American Chemical Society* **2012**, *134* (49), 19969-19972.

9. Gattrell, M.; Gupta, N.; Co, A., A Review of the Aqueous Electrochemical Reduction of CO_2 to Hydrocarbons at Copper. *Journal of Electroanalytical Chemistry* **2006**, *594* (1), 1-19.

10. Kuhl, K. P.; Cave, E. R.; Abram, D. N.; Jaramillo, T. F., New Insights Into the Electrochemical Reduction of Carbon Dioxide on Metallic Copper Surfaces. *Energy & Environmental Science* **2012**, *5* (5), 7050-7059.

11. Kuhl, K. P.; Hatsukade, T.; Cave, E. R.; Abram, D. N.; Kibsgaard, J.; Jaramillo, T. F., Electrocatalytic Conversion of Carbon Dioxide to Methane and Methanol on Transition Metal Surfaces. *Journal of the American Chemical Society* **2014**, *136* (40), 14107-14113.

12. Hori, Y., Electrochemical CO_2 Reduction on Metal Electrodes. In *Modern Aspects of Electrochemistry*, Vayenas, C. G.; White, R. E.; Gamboa-Aldeco, M. E., Eds. Springer New York: New York, NY, 2008; pp 89-189.

13. Abruña, H. D., Coordination Chemistry in Two Dimensions: Chemically Modified Electrodes. *Coordination Chemistry Reviews* **1988**, *86*, 135-189.

14. Ramos Sende, J. A.; Arana, C. R.; Hernandez, L.; Potts, K. T.; Keshevarz-K, M.; Abruna, H. D., Electrocatalysis of CO_2 Reduction in Aqueous Media at Electrodes Modified with Electropolymerized Films of Vinylterpyridine Complexes of Transition Metals. *Inorganic Chemistry* **1995**, *34* (12), 3339-3348.

15. O'Toole, T. R.; Margerum, L. D.; Westmoreland, T. D.; Vining, W. J.; Murray, R. W.; Meyer, T. J., Electrocatalytic Reduction of CO_2 at a Chemically Modified Electrode. *Journal of the Chemical Society, Chemical Communications* **1985**, (20), 1416-1417.

16. Christensen, P.; Hamnett, A.; Muir, A. V. G.; Timney, J. A.; Higgins, S., Growth and Electrochemical Behaviour of a Poly[tricarbonyl(vinylbipyridyl)rhenium Chloride] Film. Heterogeneous Reduction of CO_2. *Journal of the Chemical Society, Faraday Transactions* **1994**, *90* (3), 459-469.

17. Grice, K. A.; Kubiak, C. P., Recent Studies of Rhenium and Manganese Bipyridine Carbonyl Catalysts for the Electrochemical Reduction of CO_2. In *Advances in Inorganic Chemistry*, Michele, A.; Rudi van, E., Eds. Academic Press: 2014; Vol. Volume 66, pp 163-188.

18. Schneider, J.; Jia, H.; Muckerman, J. T.; Fujita, E., Thermodynamics and Kinetics of CO_2, CO, and H^+ Binding to the Metal Centre of CO_2 Reduction Catalysts. *Chemical Society Reviews* **2012**, *41* (6), 2036-2051.

19. Collin, J. P.; Sauvage, J. P., Electrochemical Reduction of Carbon Dioxide Mediated by Molecular Catalysts. *Coordination Chemistry Reviews* **1989**, *93* (2), 245-268.

20. Sullivan, B. P.; Bolinger, C. M.; Conrad, D.; Vining, W. J.; Meyer, T. J., One- and Two-Electron Pathways in the Electrocatalytic Reduction of CO_2 by *fac*-Re(bpy)$(CO)_3$Cl (bpy = 2,2′-bipyridine). *Journal of the Chemical Society, Chemical Communications* **1985**, (20), 1414-1416.

21. Keene, F. R.; Sullivan, B. P., In *Electrochemical and Electrocatalytic Reactions of Carbon Dioxide*, Sullivan, B. P.; Krist, K.; Guard, H., Eds. Elsevier: Amsterdam, 1993; pp 1-18.

22. Bruce, M. R. M.; Megehee, E.; Sullivan, B. P.; Thorp, H. H.; O'Toole, T. R.; Downard, A.; Pugh, J. R.; Meyer, T. J., Electrocatalytic Reduction of Carbon Dioxide Based on 2,2′-Bipyridyl Complexes of Osmium. *Inorganic Chemistry* **1992**, *31* (23), 4864-4873.

23. Ishida, H.; Tanaka, K.; Tanaka, T., Electrochemical CO_2 Reduction Catalyzed by Ruthenium Complexes $[Ru(bpy)_2(CO)_2]^{2+}$ and $[Ru(bpy)_2(CO)Cl]^+$. The Effect of pH on the Formation of CO and $HCOO^-$. *Organometallics* **1987**, *6* (1), 181-186.

24. Clark, M. L.; Grice, K. A.; Moore, C. E.; Rheingold, A. L.; Kubiak, C. P., Electrocatalytic CO_2 Reduction by M(bpy-R)$(CO)_4$ (M = Mo, W; R = H, *t*Bu) Complexes. Electrochemical, Spectroscopic, and Computational Studies and Comparison with Group 7 Catalysts. *Chemical Science* **2014**, *5* (5), 1894-1900.

25. Bourrez, M.; Molton, F.; Chardon-Noblat, S.; Deronzier, A., [Mn(bipyridyl)$(CO)_3$Br]: An Abundant Metal Carbonyl Complex as Efficient Electrocatalyst for CO_2 Reduction. *Angewandte Chemie International Edition* **2011**, *50* (42), 9903-9906.

26. Smieja, J. M.; Sampson, M. D.; Grice, K. A.; Benson, E. E.; Froehlich, J. D.; Kubiak, C. P., Manganese as a Substitute for Rhenium in CO_2 Reduction Catalysts: The Importance of Acids. *Inorganic Chemistry* **2013**, *52* (5), 2484-2491.

27. Sampson, M. D.; Nguyen, A. D.; Grice, K. A.; Moore, C. E.; Rheingold, A. L.; Kubiak, C. P., Manganese Catalysts with Bulky Bipyridine Ligands for the Electrocatalytic Reduction of Carbon Dioxide: Eliminating Dimerization and Altering Catalysis. *Journal of the American Chemical Society* **2014**, *136* (14), 5460-5471.

28. Agarwal, J.; Shaw, T. W.; Stanton, C. J.; Majetich, G. F.; Bocarsly, A. B.; Schaefer, H. F., NHC-Containing Manganese(I) Electrocatalysts for the Two-Electron Reduction of CO_2. *Angewandte Chemie International Edition* **2014**, *53* (20), 5252-5255.

29. Zeng, Q.; Tory, J.; Hartl, F., Electrocatalytic Reduction of Carbon Dioxide with a Manganese(I) Tricarbonyl Complex Containing a Nonaromatic α-Diimine Ligand. *Organometallics* **2014**, *33* (18), 5002-5008.

30. Walsh, J. J.; Smith, C. L.; Neri, G.; Whitehead, G. F.; Robertson, C. M.; Cowan, A. J., Improving the Efficiency of Electrochemical CO_2 Reduction Using Immobilized Manganese Complexes. *Faraday Discussions* **2015**, *183*, 147-160.

31. Franco, F.; Cometto, C.; Vallana, F. F.; Sordello, F.; Priola, E.; Minero, C.; Nervi, C.; Gobetto, R., A Local Proton Source in a [Mn(bpy-R)$(CO)_3$Br]-Type Redox Catalyst Enables CO_2 Reduction Even in the Absence of Brønsted Acids. *Chemical Communications* **2014**, *50* (93), 14670-14673.

32. Vollmer, M. V.; Machan, C. W.; Clark, M. L.; Antholine, W. E.; Agarwal, J.; Schaefer, H. F.; Kubiak, C. P.; Walensky, J. R., Synthesis, Spectroscopy, and Electrochemistry of (α-Diimine)M$(CO)_3$Br, M = Mn, Re, Complexes: Ligands Isoelectronic to Bipyridyl Show Differences in CO_2 Reduction. *Organometallics* **2015**, *34* (1), 3-12.

33. Agarwal, J.; Stanton III, C. J.; Shaw, T. W.; Vandezande, J. E.; Majetich, G. F.; Bocarsly, A. B.; Schaefer III, H. F., Exploring the Effect of Axial Ligand Substitution (X= Br, NCS, CN) on the Photodecomposition and Electrochemical Activity of [MnX(N–C)$(CO)_3$] Complexes. *Dalton Transactions* **2015**, *44* (5), 2122-2131.

34. Costentin, C.; Drouet, S.; Robert, M.; Savéant, J.-M., A Local Proton Source Enhances CO_2 Electroreduction to CO by a Molecular Fe Catalyst. *Science* **2012**, *338* (6103), 90-94.

35. Takeda, H.; Koizumi, H.; Okamoto, K.; Ishitani, O., Photocatalytic CO_2 Reduction Using a Mn Complex as a Catalyst. *Chemical Communications* **2014**, *50* (12), 1491-1493.

36. Fei, H.; Sampson, M. D.; Lee, Y.; Kubiak, C. P.; Cohen, S. M., Photocatalytic CO_2 Reduction to Formate Using a Mn(I) Molecular Catalyst in a Robust Metal–Organic Framework. *Inorganic Chemistry* **2015**, *54* (14), 6821-6828.

37. Agarwal, J.; Shaw, T. W.; Schaefer III, H. F.; Bocarsly, A. B., Design of a Catalytic Active Site for Electrochemical CO_2 Reduction with Mn(I)-Tricarbonyl Species. *Inorganic Chemistry* **2015**, *54* (11), 5285-5294.

38. Riplinger, C.; Sampson, M. D.; Ritzmann, A. M.; Kubiak, C. P.; Carter, E. A., Mechanistic Contrasts Between Manganese and Rhenium Bipyridine Electrocatalysts for the Reduction of Carbon Dioxide. *Journal of the American Chemical Society* **2014**, *136* (46), 16285-16298.

39. Machan, C. W.; Sampson, M. D.; Chabolla, S. A.; Dang, T.; Kubiak, C. P., Developing a Mechanistic Understanding of Molecular Electrocatalysts for CO_2 Reduction using Infrared Spectroelectrochemistry. *Organometallics* **2014**, *33* (18), 4550-4559.

40. Grills, D. C.; Farrington, J. A.; Layne, B. H.; Lymar, S. V.; Mello, B. A.; Preses, J. M.; Wishart, J. F., Mechanism of the Formation of a Mn-Based CO_2 Reduction Catalyst Revealed by Pulse Radiolysis with Time-Resolved Infrared Detection. *Journal of the American Chemical Society* **2014**, *136* (15), 5563-5566.

41. Glendening, E.; Badenhoop, J.; Reed, A.; Carpenter, J.; Bohmann, J.; Morales, C.; Weinhold, F., *NBO 5.0 Program* **2001**, Theoretical Chemistry Institute, University of Wisconsin: Madison, WI, USA.

42. Mayer, I., Bond Order and Valence: Relations to Mulliken's Population Analysis. *International Journal of Quantum Chemistry* **1984**, *26* (1), 151-154.

43. Friebolin, H., *Basic One-and Two-Dimensional NMR Spectroscopy*. Wiley-VCH Verlag GmbH & Co. KGaA: Wienheim, Germany, 2011.

44. Connelly, N. G.; Geiger, W. E., Chemical Redox Agents for Organometallic Chemistry. *Chemical Reviews* **1996**, *96* (2), 877-910.

45. Pavlishchuk, V. V.; Addison, A. W., Conversion Constants for Redox Potentials Measured Versus Different Reference Electrodes in Acetonitrile Solutions at 25°C. *Inorganica Chimica Acta* **2000**, *298* (1), 97-102.

46. McCarthy, B. D.; Martin, D. J.; Rountree, E. S.; Ullman, A. C.; Dempsey, J. L., Electrochemical Reduction of Brønsted Acids by Glassy Carbon in Acetonitrile—Implications for Electrocatalytic Hydrogen Evolution. *Inorganic Chemistry* **2014**, *53* (16), 8350-8361.

47. Riplinger, C.; Carter, E. A., Influence of Weak Brønsted Acids on Electrocatalytic CO_2 Reduction by Manganese and Rhenium Bipyridine Catalysts. *ACS Catalysis* **2015**, *5* (2), 900-908.

48. Zavarine, I. S.; Kubiak, C. P., A Versatile Variable Temperature Thin Layer Reflectance Spectroelectrochemical Cell. *Journal of Electroanalytical Chemistry* **2001**, *495* (2), 106-109.

49. Becke, A. D., Density-Functional Thermochemistry. III. The Role of Exact Exchange. *The Journal of Chemical Physics* **1993**, *98* (7), 5648-5652.

50. Becke, A. D., Density-Functional Thermochemistry. IV. A New Dynamical Correlation Functional and Implications for Exact-Exchange Mixing. *The Journal of Chemical Physics* **1996**, *104* (3), 1040-1046.

51. Lee, C.; Yang, W.; Parr, R. G., Development of the Colle-Salvetti Correlation-Energy Formula into a Functional of the Electron Density. *Physical Review B* **1988**, *37* (2), 785-789.

52. Neese, F., The ORCA Program System. *Wiley Interdisciplinary Reviews: Computational Molecular Science* **2012**, *2* (1), 73-78.

53. Klamt, A.; Schuurmann, G., COSMO: A New Approach to Dielectric Screening in Solvents with Explicit Expressions for the Screening Energy and its Gradient. *Journal of the Chemical Society, Perkin Transactions 2* **1993**, (5), 799-805.

54. Weigend, F.; Ahlrichs, R., Balanced Basis Sets of Split Valence, Triple Zeta Valence and Quadruple Zeta Valence Quality for H to Rn: Design and Assessment of Accuracy. *Physical Chemistry Chemical Physics* **2005**, *7* (18), 3297-3305.

55. Roy, L. E.; Hay, P. J.; Martin, R. L., Revised Basis Sets for the LANL Effective Core Potentials. *Journal of Chemical Theory and Computation* **2008**, *4* (7), 1029-1031.

56. Ehlers, A. W.; Böhme, M.; Dapprich, S.; Gobbi, A.; Höllwarth, A.; Jonas, V.; Köhler, K. F.; Stegmann, R.; Veldkamp, A.; Frenking, G., A Set of f-Polarization Functions for Pseudo-Potential Basis Sets of the Transition Metals Sc–Cu, Y–Ag and La–Au. *Chemical Physics Letters* **1993**, *208* (1), 111-114.

57. Hay, P. J.; Wadt, W. R., Ab *Initio* Effective Core Potentials for Molecular Calculations. Potentials for the Transition Metal Atoms Sc to Hg. *The Journal of Chemical Physics* **1985**, *82* (1), 270-283.

58. Kutzelnigg, W., Theory of Magnetic Susceptibilities and NMR Chemical Shifts in Terms of Localized Quantities. *Israel Journal of Chemistry* **1980**, *19* (1-4), 193-200.

59. Schindler, M.; Kutzelnigg, W., Theory of Magnetic Susceptibilities and NMR Chemical Shifts in Terms of Localized Quantities. II. Application to Some Simple Molecules. *The Journal of Chemical Physics* **1982**, *76* (4), 1919-1933.

60. Pipek, J.; Mezey, P. G., A Fast Intrinsic Localization Procedure Applicable for *Ab Initio* and Semiempirical Linear Combination of Atomic Orbital Wave Functions. *The Journal of Chemical Physics* **1989**, *90* (9), 4916-4926.

61. Kaupp, M., NMR Chemical-Shift Anomaly and Bonding in Piano-Stool Carbonyl and Related Complexes–an *Ab Initio* ECP/DFT Study. *Chemistry – A European Journal* **1996**, *2* (3), 348-358.

62. Kaupp, M.; Malkina, O. L.; Malkin, V. G., The Calculation of ^{17}O Chemical Shielding in Transition Metal Oxo Complexes. I. Comparison of DFT and Ab Initio Approaches, and

Mechanisms of Relativity-Induced Shielding. *The Journal of Chemical Physics* **1997**, *106* (22), 9201-9212.

63. Gottlieb, H. E.; Kotlyar, V.; Nudelman, A., NMR Chemical Shifts of Common Laboratory Solvents as Trace Impurities. *The Journal of Organic Chemistry* **1997**, *62* (21), 7512-7515.

S5. SUPPORTING INFORMATION

S5.1 SELECTED SPECTRA

S5.1.1 ^{1}H NMR of Mn(CN)(2,2′-Bipyridine)(CO)$_3$ (5.1)

Temperature: 20 ˚C
Solvent: DMSO-d_6

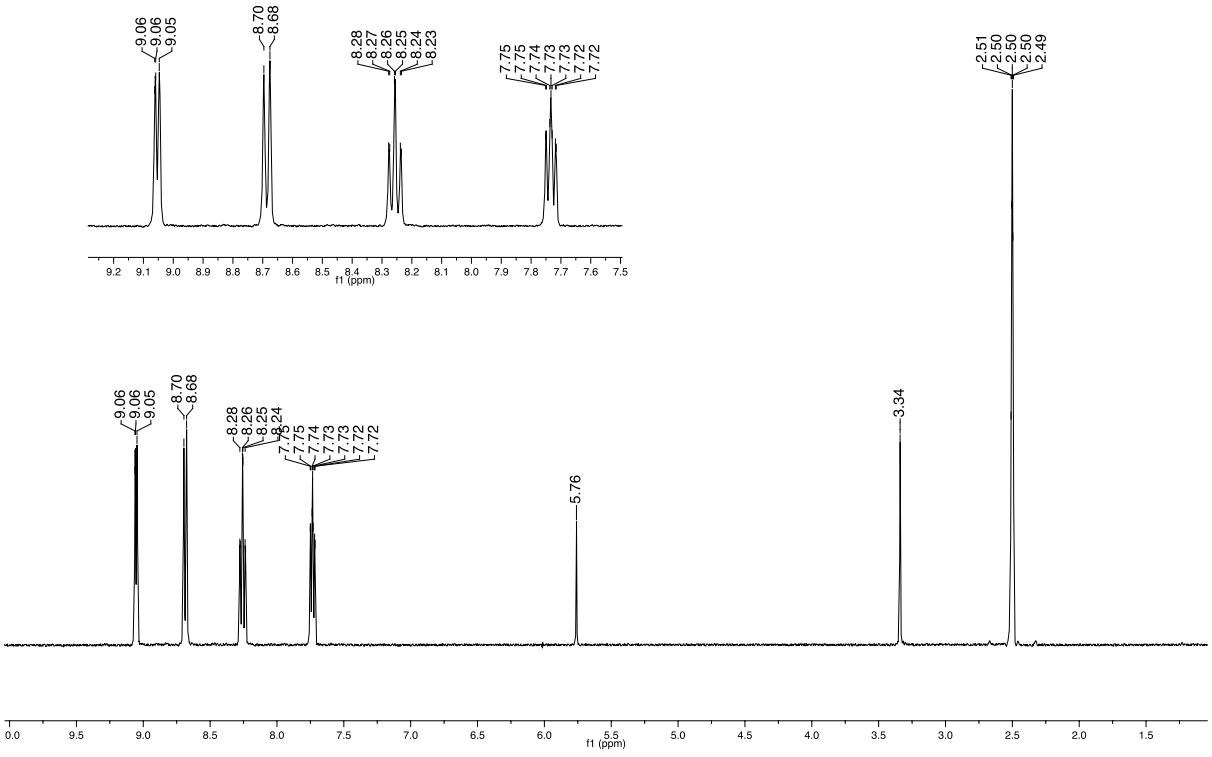

Note: The peak at 5.76 ppm is assigned to dichloromethane, the peak at 3.34 ppm is assigned to water, and the peak at 2.50 ppm to dimethyl sulfoxide.

S5.1.2 ^{13}C NMR of Mn(CN)(2,2′-Bipyridine)(CO)$_3$ (5.1)

Temperature: 25 ˚C
Solvent: DMSO-d_6

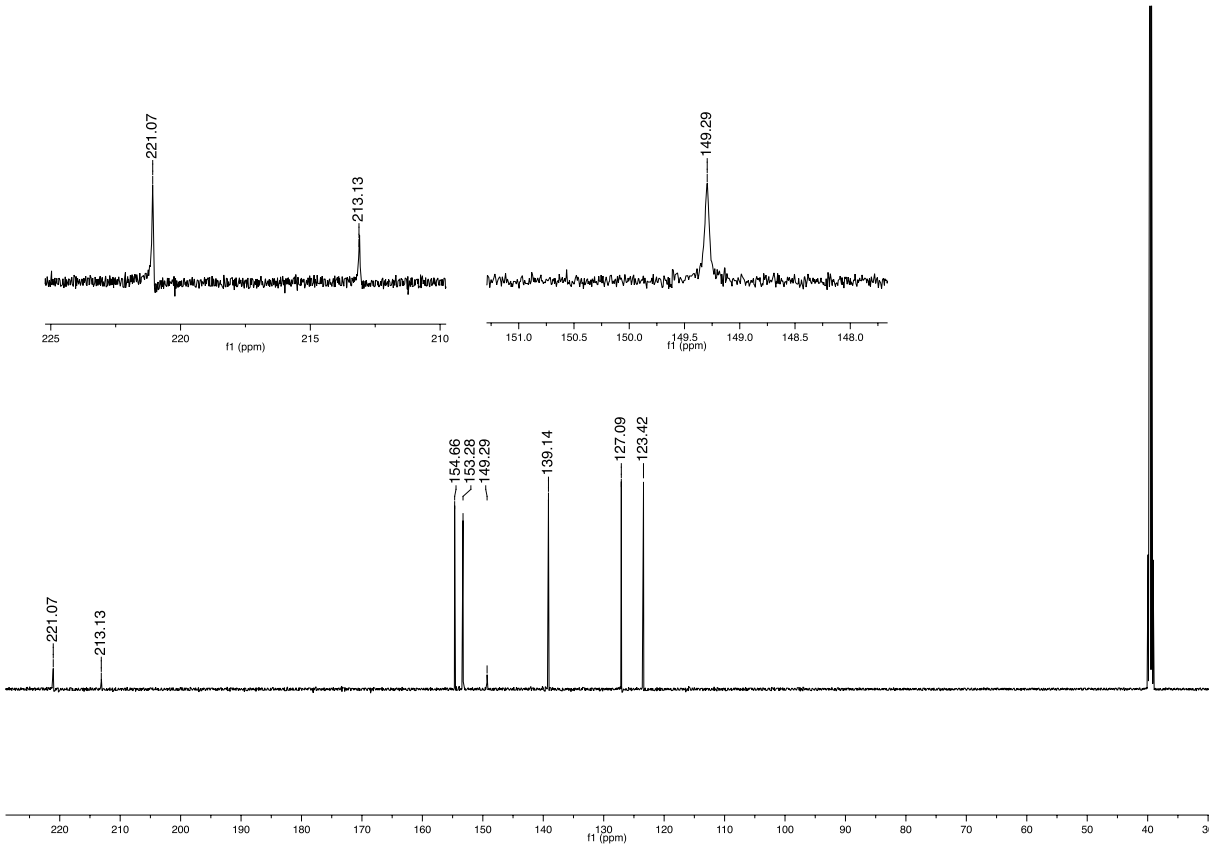

S5.1.3 FTIR of Mn(CN)(2,2′-Bipyridine)$(CO)_3$ (5.1)

Method: ATR

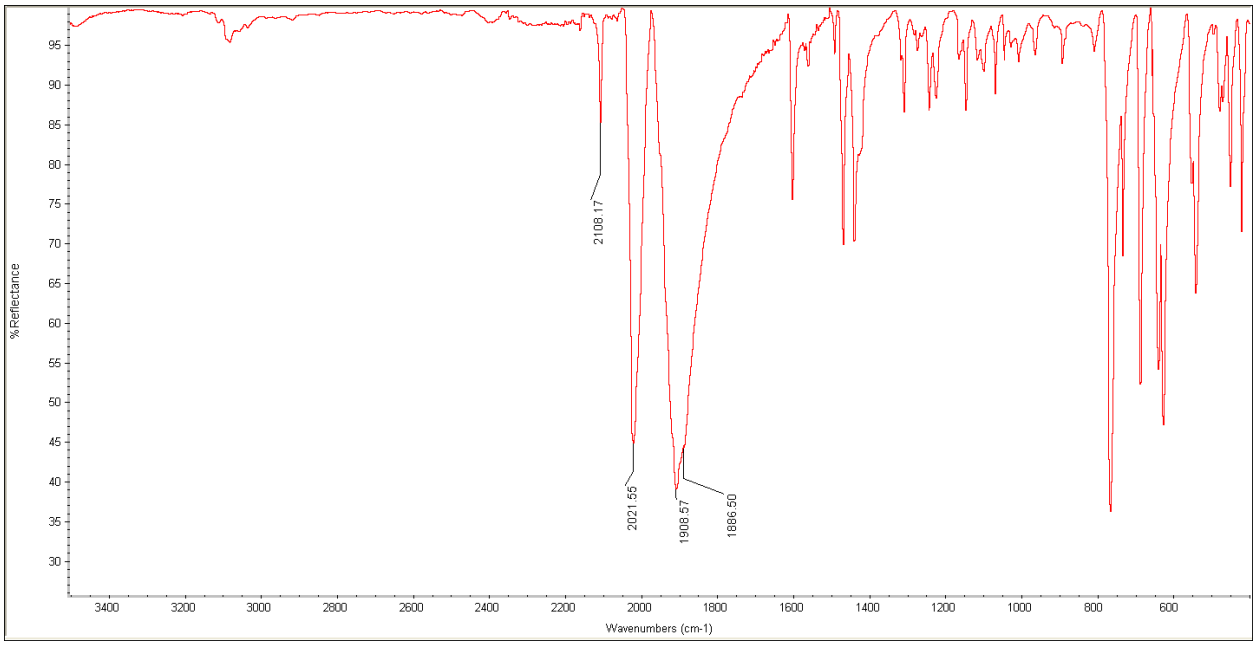

S5.1.4 UV-Vis of Mn(CN)(2,2′-Bipyridine)$(CO)_3$ (5.1)

Solvent: MeCN
Temperature: 298 K

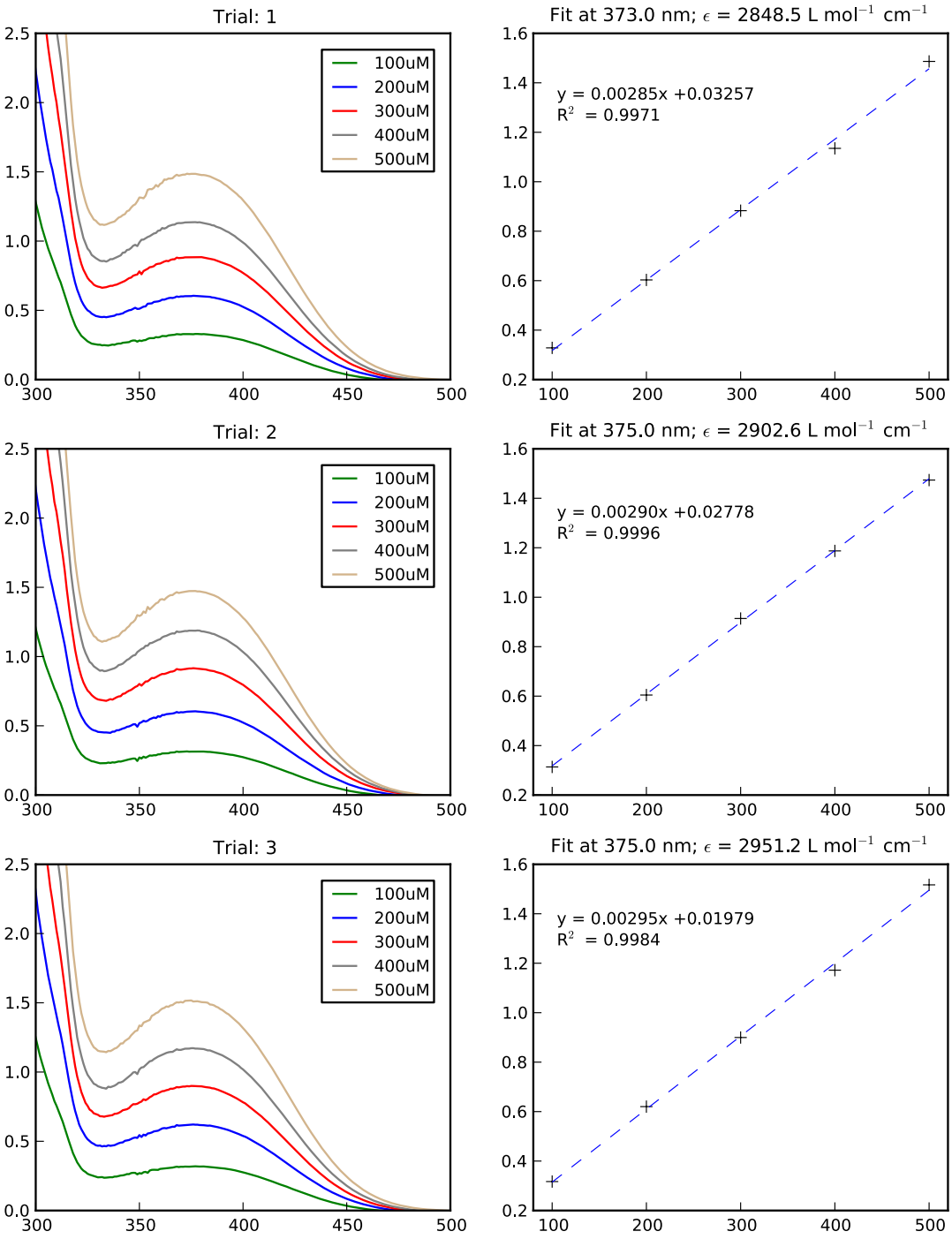

S5.2 MISCELLANEOUS DATA

S5.2.1 Scan Rate Dependence Data for Mn(CN)(2,2′-Bipyridine)$(CO)_3$ (5.1)

Atmosphere: Argon
Sample Concentration: 1 mM
Solvent: CH_3CN
Electrolyte: 0.1 M TBAP

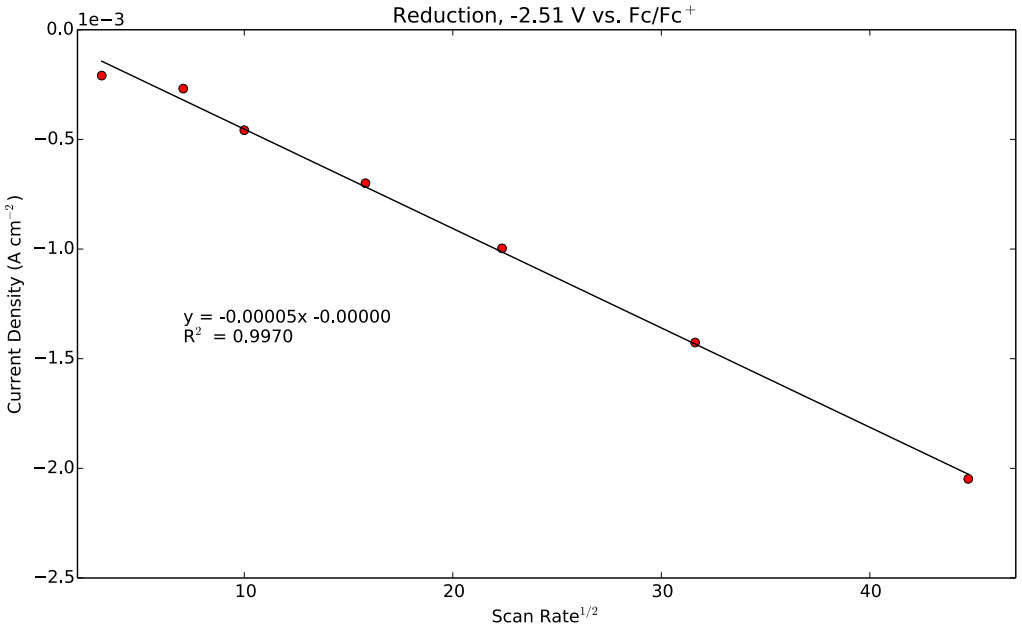

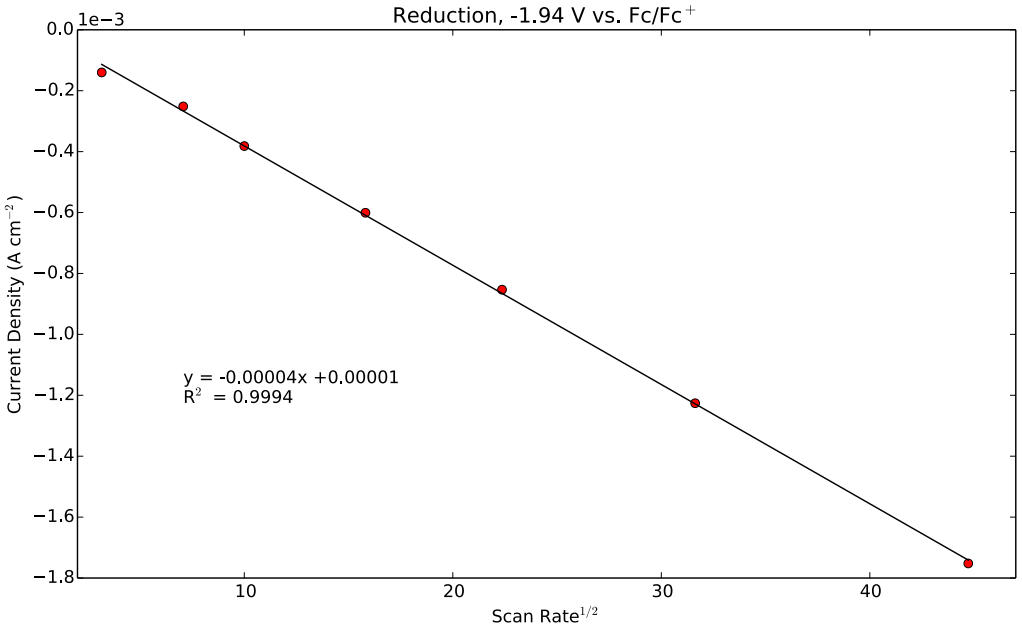

S5.2.2 Cyclic Voltammetry with added TBACN

Atmosphere: Argon
Sample Concentration: 1 mM
Solvent: CH_3CN
Electrolyte: 0.1 M TBAP
Scan Rate: 100 mV s^{-1}

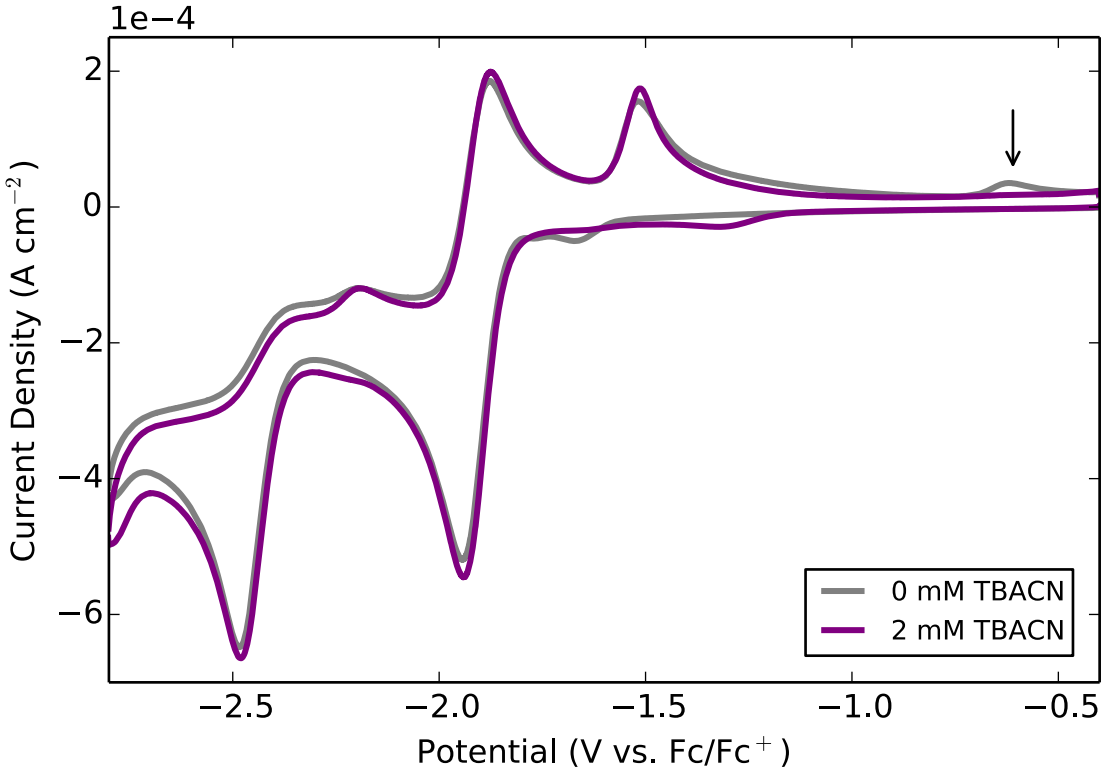

S5.2.3 Chemical Reductions (CoCp*2) with UV-Vis Recording

Atmosphere: Argon
Sample Concentration: 3 mM
Solvent: CH_3CN

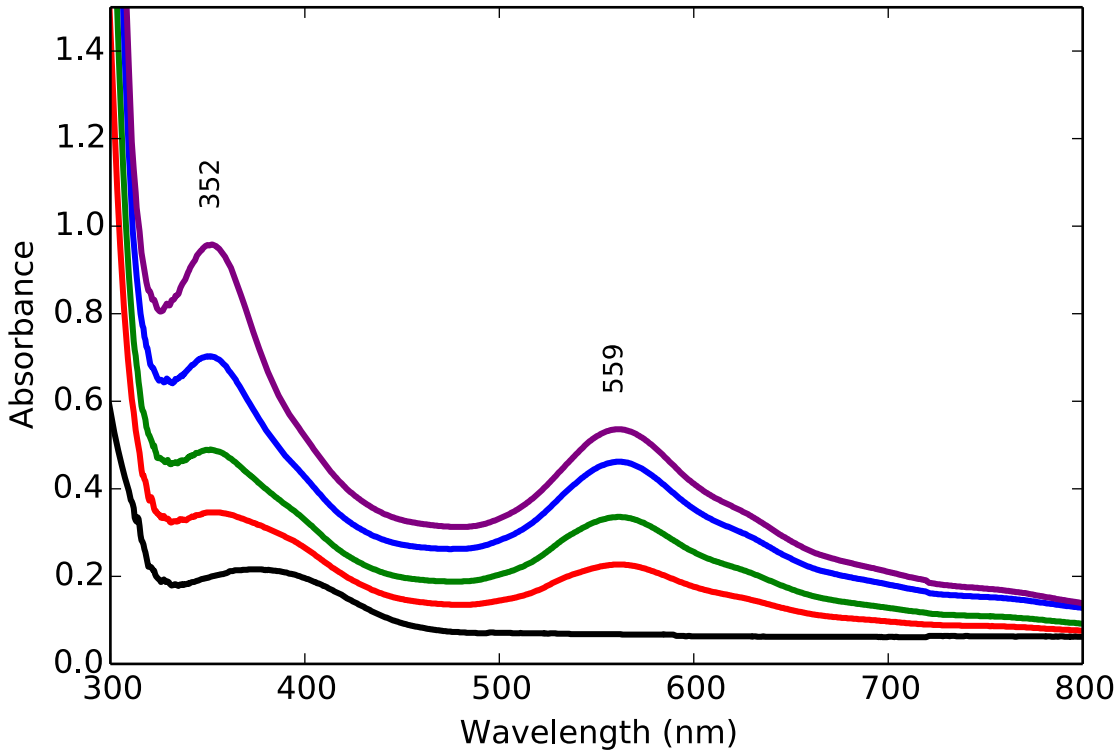

Note: UV-Vis spectrum recorded during titration with $CoCp^*_2$ (black → purple; 0 → 2.1 eq.) CaF_2 windows were employed with a 0.1 mm pathlength.

S5.2.4 Electrolysis at the First Reduction Followed by an Oxidative Sweep

Atmosphere: Argon
Sample Concentration: 3 mM
Solvent: CH_3CN
Electrolyte: 0.1 M TBAP
Scan Rate: 100 mV s^{-1}

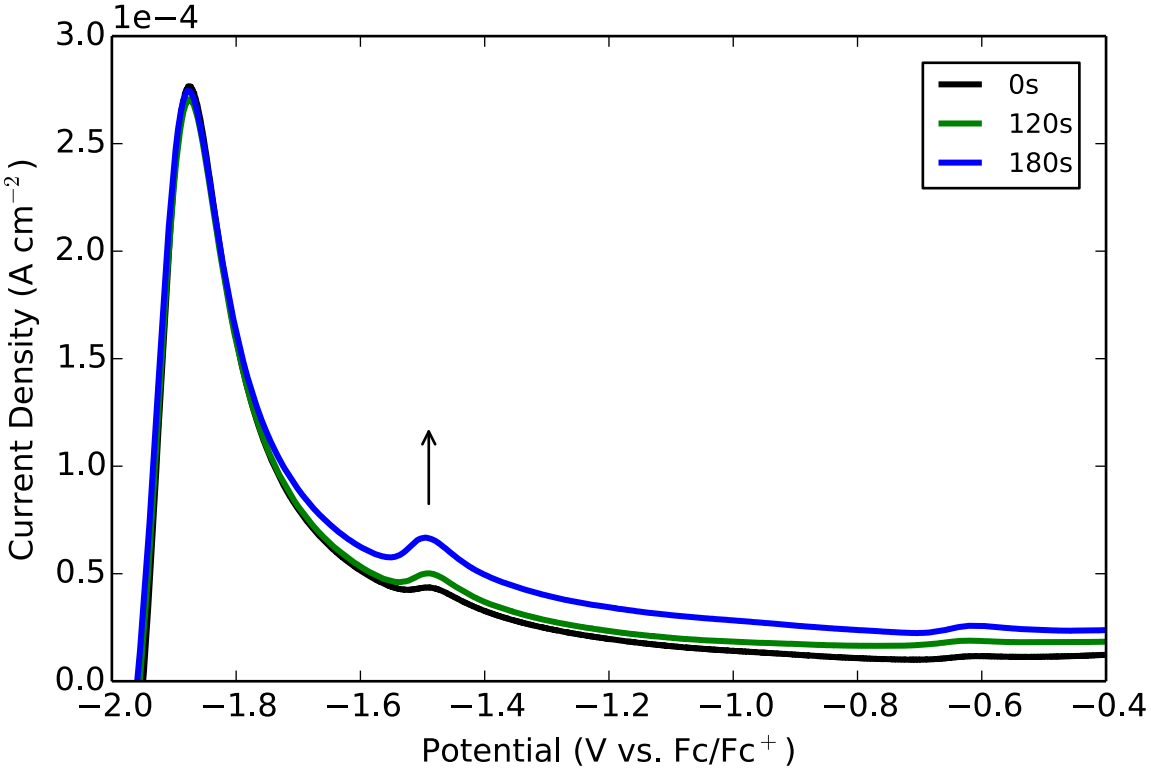

S5.2.5 Comparison of Observed and Predicted CO Stretching Frequencies

Black Diamonds: $Mn(CN)(bpy)(CO)_3$ (2033, 1939, 1930 cm^{-1})
Green Diamonds: $[Mn(CN)(bpy)(CO)_3]$ (2010, 1909, 1895 cm^{-1})
Red Diamonds: $[Mn(bpy)(CO)_3]$ (1878, 1789, 1772 cm^{-1})

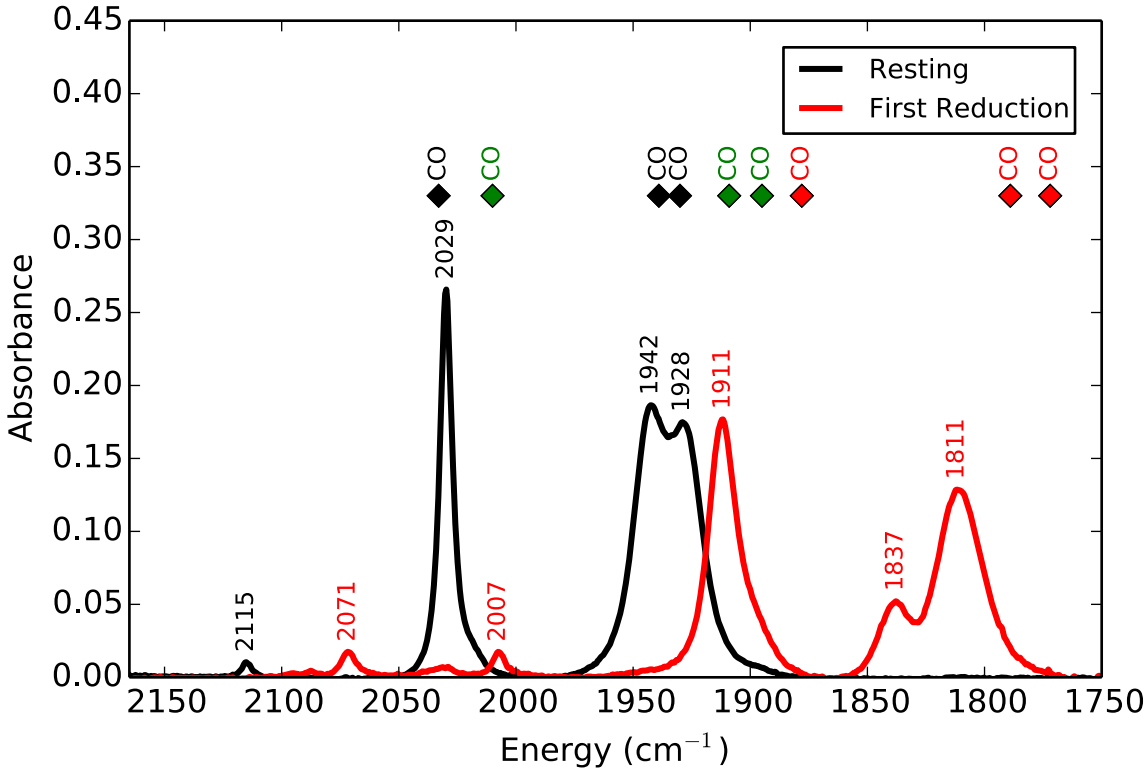

Note: Infrared spectra of $Mn(CN)(bpy)(CO)_3$ (6.2 mM) at controlled potentials under an atmosphere of N_2 with dry MeCN and 0.1 M tetrabutylammonium hexafluorophosphate ($TBAPF_6$) supporting electrolyte.

S5.2.6 Voltammetry Window with Phenol

Atmosphere: Argon
Solvent: CH_3CN
Electrolyte: 0.1 M TBAP
Scan Rate: 100 mV s^{-1}

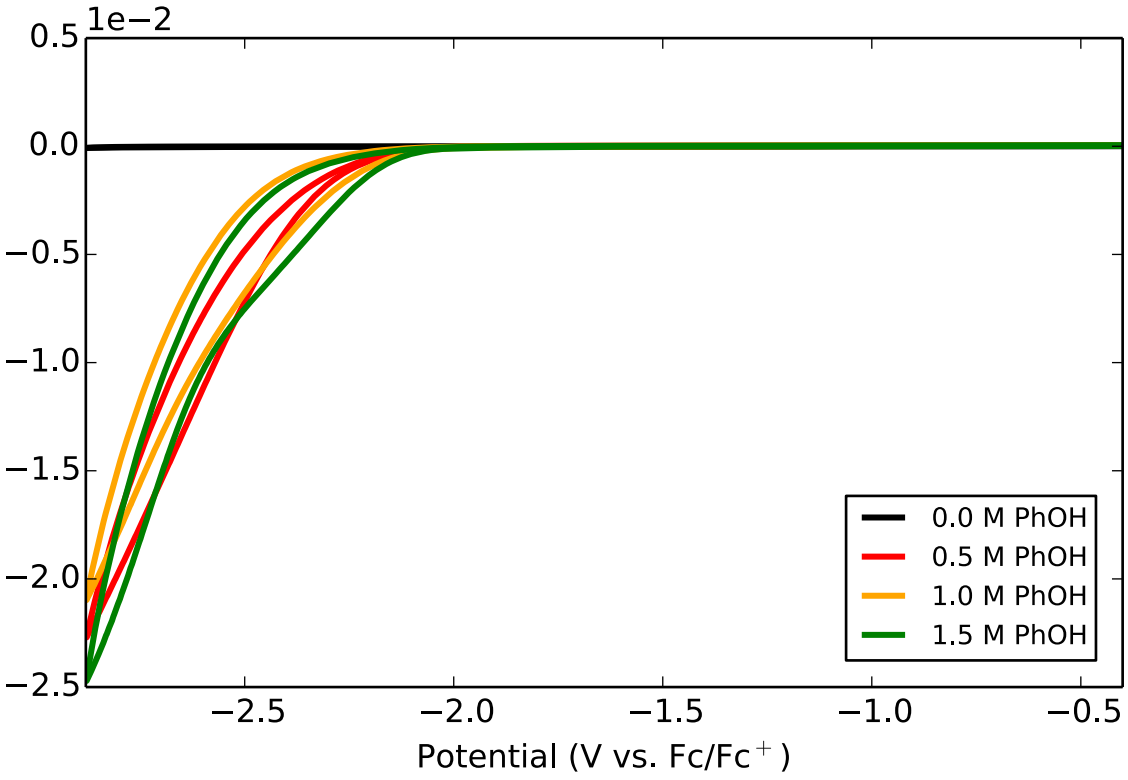

S5.2.7 Voltammetry Window with Phenol and Complex 5.1

Atmosphere: Argon
Sample Concentration: 1 mM
Solvent: CH_3CN
Electrolyte: 0.1 M TBAP
Scan Rate: 100 mV s^{-1}

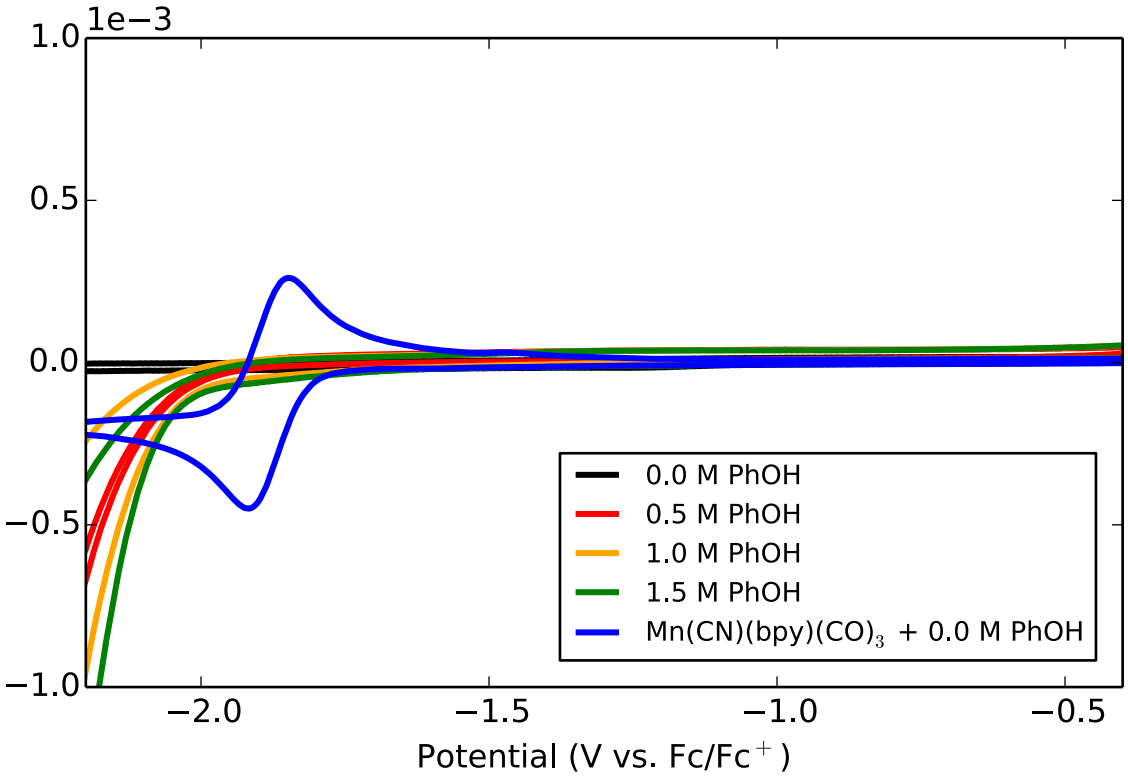

S5.2.8 Infrared Spectrum of HOPh and NaOPh

Atmosphere: Nitrogen
Solvent: CH_3CN

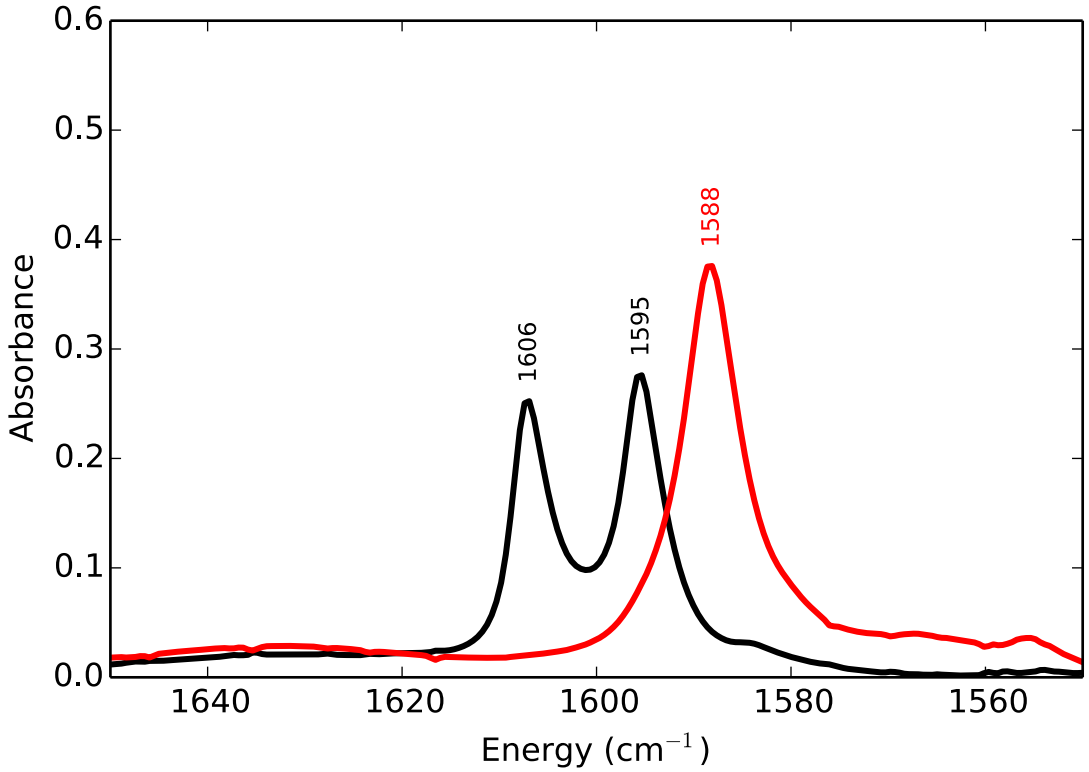

Note: HOPh is shown in black; NaOPh is shown in red.

CHAPTER 6

CONCLUSIONS AND FUTURE OUTLOOK

Lehn's pioneering work with *fac*-ReCl(bpy)$(CO)_3$, laid the groundwork for electrochemical CO_2 reduction with molecular catalysts centered around group VII-metals. For thirty years, catalysts derived from ReCl(bpy)$(CO)_3$ have been extensively explored, and several studies have shown that the performance of these catalysts can be improved by structural modification of the supporting ligand around the metal center. In an effort to find a cheaper, more abundant metal that could mediate the electrochemical reduction of CO_2, Bourrez *et al.* explored valence isoelectronic manganese compounds. In 2011, they identified MnBr(bpy)$(CO)_3$ was identified as an efficient and selective electrocatalyst for CO_2 reduction. Initial studies showed that manganese catalysts were capable of reducing CO_2 to CO at a significantly lower overpotential while retaining a similar selectivity and Faradaic efficiency when compared to rhenium analogs. In addition, manganese catalysts were shown to be quite selective for CO_2 reduction over proton reduction, even in presence of a variety of acids. Several improvements to the MnBr(bpy)$(CO)_3$ have been discussed in Chapter 1, with the bulk of the reported catalysts having a bipyridyl supporting ligand around the manganese center.

Our group has focused on the design and synthesis of novel redox-active ligands that contain *N*-heterocyclic carbenes (NHCs). We have established an efficient, green, and modular construction of these ligands based around a benzimidazole or imidazole core. In 2014, we reported the use of NHC-aryl frameworks to support Mn(I) carbonyl systems for electrocatalytic

conversion of CO_2 to CO. These compounds demonstrated comparable turnover frequency to $MnBr(bpy)(CO)_3$, where bpy = 2,2'-bipyridine. Increasing the π-acidity of the NHC-aryl ligand (i.e., moving from imidazole to benzimidazole) reduced the overpotential by 110 mV. Our group's synthetic approach allows for a facile and straightforward tuning of steric and electronic properties for Mn(I) catalyst systems. In 2015, a new series of $[MnX(N\text{-}C)(CO)_3]$-type CO_2 complexes were synthesized and characterized. Catalytic CO production was observed for all compounds. However, when X = CN or NCS, substantial H_2 production was also observed. UV studies indicate that all compounds undergo photodecomposition under 350 nm and 420 nm light, but CN-substituted complexes decomposed more slowly under 420 nm light, with five times longer lifetimes. The data from these studies indicate that Mn(I)-NHC based catalysts can be tuned by ligand substitution, either by structural modifications of the NHC or axial ligand substitution.

The success of these compounds motivated us to examine valence-isoelectronic Re(I)-NHC systems. There, benzimidazole was either mated to pyridine, or pyrimidine, in order to investigate a systematic increase in π-acidity. Both compounds were capable of mediating the two-electron conversion of CO_2 following a one-electron reduction; for the pyrimidyl system, a 140 mV and 120 mV decrease in overpotential were observed at the first and second reduction potentials, respectively. The Faradaic efficiency for CO formation was ≥60%, with minor H_2 and HCO_2H production. Recently, the benzimidazole-pyrimidine based ligand has been coupled to a Mn(I) tricarbonyl system. As a result of this modification, 70 mV and 160 mV decreases in overpotential were observed when compared to $MnBr(bpy)(CO)_3$ and our original Mn(I) NHC-pyridyl catalyst, respectively. In addition, this NHC-pyrimidyl catalyst showed over double the catalytic current enhancement (5.2× vs 2.1×) when compared to Bourrez's catalyst, $MnBr(bpy)(CO)_3$.

Future improvements for our Mn(I)-NHC catalysts may be realized by the addition of either non-innocent functional groups (i.e., phenol) or additional electron−deficient *N*-aryl groups (i.e., $PhCF_3$) in the second coordination sphere. By incorporating a phenolic group on our Mn(I)-NHC catalysts, we should observe increased current enhancement at the potential of CO_2 reduction, as shown by Savéant, Agarwal and Franco. In order to efficiently build these ligands, our laboratory has developed a general and high yielding *N*-arylation method for our benzimidazole based ligands utilizing non-symmetric diaryliodonium salts. To that end, we have recently assembled electron–deficient Mn(I)-NHC complexes which are currently being explored for both electrocatalytic and photocatalytic reduction of CO_2.

To date, our most succesful Mn(I)-NHC catalyst systems are based around a benzimidazole core. We should be able to incorporate other NHC cores in our catalysts, including benzoxazole, benzothiazole or a cyclic(alkyl)(amino)carbene cores. It can also be envisioned that our Mn(I)-NHC catalyst systems can be coupled to a TiO_2 (or other oxide) surface, as reported by Rosser. As our Mn(I)-NHC catalyst systems have already been shown to outperform $MnBr(bpy)(CO)_3$, the proposed TiO_2|Mn(I)-NHC-P cathode should also be a viable (and improved) catalyst system. In addition, further ligand modifications can be made to the TiO_2|Mn(I)-NHC-P cathode, perhaps increasing the photo stability of the Mn(I) system or minimizing Mn-Mn dimer formation, thus bringing molecular electrocatalytic CO_2 reduction closer to a full artificial photosynthetic system.